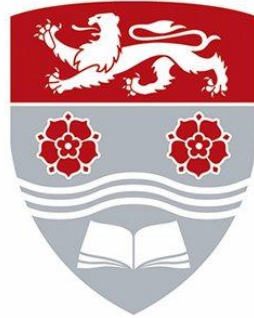


The University of Lancaster
Biomedical and Life Sciences



Characterisation of non-essential genes required for survival
under conditions of DNA stress

Hassan Ahmed Ezzat Soliman

Supervisor: Clive Price

July 2017

Author's declaration of originality

I, Hassan Ahmed Ezzat Soliman, confirm that the work presented in this thesis is my own and has not been submitted in substantially the same form for the award of a higher degree elsewhere. Any sections of the thesis which have been published or submitted for a higher degree elsewhere have been clearly identified by me and indicated in the thesis.

.....

Submitted in part fulfilment of the requirements for the degree of Doctor of Philosophy

Contents

Table of Contents	1
List of Figures	8
List of Tables	16
Table of abbreviations	18
Acknowledgements	24
Abstract	25
Chapter 1: Introduction	27
1.1 Cancer as a genetic disease	27
1.2 Cancer and Genomic instability	29
1.3 The Cell Cycle	31
1.4 DNA replication	34
1.5 DNA replication stress	41
1.6 DNA checkpoint response	44
1.7 DNA damage checkpoint	48
1.8 TopBP1 structure	50
1.9 The role of TopBP1 in the DNA replication checkpoint	52
1.10 TopBP1 role in ATR Activation	55
1.11 The role of TopBP1 in DNA Repair	56
1.12 The role of TopBP1 in the Initiation of DNA Replication	57

1.13 The role of TopBP1 in the Regulation of Transcription	59
1.14 The role of TopBP1 in Disease	61
1.15 Rad4	62
1.16 The Temperature Sensitive Mutant	63
1.17 Fission Yeast Morphology	64
1.18 Fission Yeast as a model	67
1.19 Synthetic Genetic Array Analysis	69
1.20 Hip1	71
1.21 Swi1 and Swi3	72
1.22 Mrc1	74
1.23 Aims	75
Chapter 2: Materials and Methods	76
2.1.1 Yeast Strains	76
2.1.2 Plasmids	80
2.2.1 Media	81
2.2.2 Buffers and Solutions	82
2.3 <i>Schizosaccharomyces pombe</i> Methods	84
2.3.1 <i>S.pombe</i> Strain Construction	84
2.3.2 Spore microdissection	88
2.3.3 Random Spore Analysis	89

2.3.4 Statistics	90
2.3.5 <i>S. pombe</i> Standard Chromosomal DNA preparation	91
2.3.6 Lithium Acetate Yeast Transformation	92
2.3.7 Hydroxyurea Block and Release	94
2.3.8 Fluorescence Microscopy	94
2.3.9 Immunofluorescence	95
2.4.1 Polymerase Chain Reaction (PCR)	96
2.4.2 Cloning and Transformation of plasmids into <i>E.coli</i>	98
2.4.3 Purification of plasmid DNA	100
2.4.4 Restriction Digests	100
2.4.5 DNA ligation with T4 DNA Ligase	101
2.4.6 Agarose Gel Electrophoresis	102
2.4.7 Gel Extraction	102
2.4.8 RNA Extraction	102
2.4.9 Reverse transcriptase Real-time PCR	104
2.5.1 Protein Extraction	107
2.5.2 Protein Quantification	107
2.5.3 SDS-PAGE	107
2.5.4 Coomassie Staining of Gels	110
2.5.5 Western Blotting	110

2.5.6 Incubation of PVDF membrane with antibodies	111
2.5.7 Enhanced Chemi-Luminescence (ECL)	112
2.5.8 Flow Cytometry	112

Chapter 3:

The Genetic Analysis of the interaction between <i>hip1</i> and <i>rad4-116</i>	113
3.1 Introduction	114
3.1.1 Synthetic Lethality on Agar	115
3.1.2 <i>hip1</i> Δ causes synthetic lethality when combined with <i>rad4-116</i>	118
3.2 The DNA replication stalled fork profile of <i>hip1</i> Δ	119
3.3 The Phenotypic characterisation of the <i>hip1-V5</i> strains	132
3.3.1 The depletion of <i>hip1-V5</i> expression by RT-QPCR	134
3.3.2 The depletion of Hip1-V5 expression by Western Blotting	137
3.3.3 Phenotypic Characterisation of <i>hip1-V5</i> strains by microscopy	142
3.3.4 The effect of thiamine addition on SPSC 1103 cell length	146
3.3.5 The viability profile of <i>hip1</i> Δ <i>hip1-V5</i> <i>rad4-116</i>	152
3.3.6 Phenotypic Characterisation of <i>hip1-V5</i> strains by FACS	154
3.4 Hip1 Chapter Discussion	157

Chapter 4:

The Genetic Analysis of the interaction between the Swi complex members and <i>rad4-116</i>	164
--	------------

4.1 Introduction	165
4.1.1 Synthetic Lethality on Agar	166
4.1.2 <i>swi1Δ</i> causes synthetic lethality when combined with <i>rad4-116</i>	169
4.2 The DNA replication stalled fork profile of <i>swi1Δ</i>	170
4.3 The Phenotypic characterisation of the <i>swi1-V5</i> strains	178
4.3.1 The depletion of <i>swi1-V5</i> expression by RT-QPCR	180
4.3.2 The depletion of Swi1-V5 expression by Western Blotting	183
4.3.3 Phenotypic Characterisation of <i>swi1-V5</i> strains by microscopy	188
4.3.4 The effect of thiamine addition on the cell length of <i>swi1-V5</i> strains	192
4.3.5 The viability profile of <i>swi1Δ swi1-V5 rad4-116</i>	195
4.3.6 Phenotypic Characterisation of <i>swi1-V5</i> strains by FACS	197
4.4.1 Synthetic Lethality on Agar	200
4.4.2 <i>swi3Δ</i> causes synthetic lethality when combined with <i>rad4-116</i>	203
4.5 The DNA replication stalled fork profile of <i>swi3Δ</i>	204
4.6 The Phenotypic characterisation of the <i>swi3-V5</i> strains	212
4.6.1 The depletion of <i>swi3-V5</i> expression by RT-QPCR	214
4.6.2 The depletion of Swi3-V5 expression by Western Blotting	217
4.6.3 Phenotypic Characterisation of <i>swi3-V5</i> strains by microscopy	222
4.6.4 The effect of thiamine addition on SPSC 1102 cell length	226

4.6.5 The viability profile of <i>swi3Δ swi3-V5 rad4-116</i>	232
4.6.6 Phenotypic Characterisation of <i>swi3-V5</i> strains by FACS	234
4.7 The Swi complex members chapter discussion	237
Chapter 5:	
The Genetic Analysis of the interaction between <i>mrc1</i> and <i>rad4-116</i>	244
5.1 Introduction	245
5.1.1 Synthetic Lethality on Agar	246
5.1.2 <i>mrc1Δ</i> causes synthetic lethality when combined with <i>rad4-116</i>	249
5.2 The DNA replication stalled fork profile of <i>mrc1Δ</i>	250
5.3 The Phenotypic characterisation of the <i>mrc1-V5</i> strains	258
5.3.1 The depletion of <i>mrc1-V5</i> expression by RT-QPCR	260
5.3.2 The depletion of Mrc1-V5 expression by Western Blotting	263
5.3.3 Phenotypic Characterisation of <i>mrc1-V5</i> strains by microscopy	268
5.3.4 The effect of thiamine addition on the cell length of <i>mrc1-V5</i> strains	272
5.3.5 The viability profile of <i>mrc1Δ mrc1-V5 rad4-116</i>	275
5.3.6 Phenotypic Characterisation of <i>mrc1-V5</i> strains by FACS	277
5.4 Characterisation of the <i>rad4-116 mrc1Δ mrc1-V5 rad52-GFP</i> strain	280
5.4.1 The depletion of <i>mrc1-V5</i> expression by RT-QPCR	282
5.4.2 The depletion of Mrc1-V5 expression by Western Blotting	284
5.4.3 The effect of thiamine addition on the SPSC 1117 cell morphology	286

5.4.4 The effect of thiamine addition on SPSC 1117 viability	290
5.4.5 Phenotypic Characterisation of SPSC 1117 by FACS	291
5.5 Mrc1 Chapter Discussion	294
Chapter 6: Discussion	300
Bibliography	309

List of Figures

Figure 1-1. The formation of initiation complex in <i>S.pombe</i>	40
Figure 1-2. The TopBP1-ATR activation at the stalled replication fork	42
Figure 1-3. The structure conservation of TopBP1	51
Figure 1-4. The cell cycle in the fission yeast	65
Figure 3-1. The growth of individual spores to colonies of the <i>rad4-116</i> strain cross with <i>hip1Δ</i> strain	116
Figure 3-2 . Merged image of Rad52-GFP foci of the <i>hip1Δ</i> strain	122
Figure 3-3 . Rad52-GFP foci of the <i>hip1Δ</i> strain at its peak	123
Figure 3-4. Viability counts for the <i>rad4⁺</i> , <i>rad4-116</i> and <i>hip1Δ</i> strains carrying the <i>rad52-GFP</i> gene	124
Figure 3-5. The Rad52-GFP profile of the <i>hip1Δ</i> strain	125
Figure 3-6 . Merged image of Rad52-GFP foci of the <i>rad4⁺</i> strain	126
Figure 3-7 . The Rad52-GFP profile of the <i>rad4⁺</i> strain	127
Figure 3-8 . Merged image of Rad52-GFP foci of the <i>rad4-116</i> strain	128
Figure 3-9. The Rad52-GFP profile of the <i>rad4-116</i> strain	129
Figure 3-10. A comparison of the Rad52-GFP profiles of the <i>rad4-116</i> , <i>rad4⁺</i> and <i>hip1Δ</i> strains	130
Figure 3-11. The adjusted relative quantity of RNA measured by RT-QPCR for the <i>hip1-V5</i> strain SPSC 1095	135
Figure 3-12. The adjusted relative quantity of RNA measured by RT-QPCR for the <i>hip1Δ hip1-V5</i> strain SPSC 1100	135

Figure 3-13 . The adjusted relative quantity of RNA measured by RT-QPCR for the <i>hip1Δ hip1-V5 rad4-116</i> strain SPSC 1103	136
Figure 3-14. The comparison the adjusted relative quantity of RNA of strains carrying the <i>hip1-V5</i> allele	136
Figure 3-15. Expression of V5 tag in the base <i>hip1-V5</i> strain SPSC 1095 after the addition of thiamine	138
Figure 3-16 .Depletion of V5 tag in the base <i>hip1-V5</i> strain SPSC 1095 after the addition of thiamine	139
Figure 3-17.Depletion of V5 tag in the <i>hip1-V5 hip1Δ</i> strain SPSC 1100 after the addition of thiamine	140
Figure 3-18.Depletion of V5 tag in the <i>hip1-V5 hip1Δ rad4-116</i> strain SPSC 1103 after the addition of thiamine	141
Figure 3-19. The cell morphology of the <i>hip1-V5</i> strain SPSC 1095 at 60X magnification across 24 hours after thiamine induction	143
Figure 3-20. The cell morphology of the <i>hip1Δ hip1-V5</i> strain SPSC 1100 at 60X magnification across 24 hours after thiamine induction	144
Figure 3-21. The cell morphology of the <i>hip1Δ hip1-V5 rad4-116</i> strain SPSC 1103 at 60X magnification across 24 hours after thiamine induction	145
Figure 3-22. The population of SPSC 1103 divided by cell length at the 0 hour timepoint after thiamine addition.	146
Figure 3-23. The population of SPSC 1103 divided by cell length at the 4 hour timepoint after thiamine addition.	147
Figure 3-24. The population of SPSC 1103 divided by cell length at the 8 hour timepoint after thiamine addition.	147

Figure 3-25. The population of SPSC 1103 divided by cell length at the 12 hour timepoint after thiamine addition.	148
Figure 3-26. The population of SPSC 1103 divided by cell length at the 24 hour timepoint after thiamine addition.	148
Figure 3-27. The average cell length of the strains carrying the <i>hip1-V5</i> allele	149
Figure 3-28. The viability comparison of strains carrying the <i>hip1-V5</i> allele against the control <i>rad4-116</i> strain	153
Figure 3-29. SPSC 1095 and SPSC 1100 cell population as investigated through FACS	155
Figure 3-30. SPSC 1103 cell population as investigated through FACS	156
Figure 4-1. The growth of individual spores to colonies of the <i>rad4-116</i> strain cross with <i>swi1Δ</i> strain	167
Figure 4-2 . Merged image of Rad52-GFP foci of the <i>swi1Δ</i> strain	172
Figure 4-3. Rad52-GFP foci of the <i>swi1Δ</i> strain at its peak	173
Figure 4-4. Viability counts for the <i>rad4⁺</i> , <i>rad4-116</i> and <i>swi1Δ</i> strains carrying the <i>rad52-GFP</i> gene	174
Figure 4-5. The Rad52-GFP profile of the <i>swi1Δ</i> strain	175
Figure 4-6. A comparison of the Rad52-GFP profiles of the <i>rad4-116</i> , <i>rad4⁺</i> and <i>swi1Δ</i> strains	176
Figure 4-7. The adjusted relative quantity of RNA measured by RT-QPCR for the <i>swi1-V5</i> strain SPSC 1096	180
Figure 4-8. The adjusted relative quantity of RNA measured by RT-QPCR for the <i>swi1Δ swi1-V5</i> strain SPSC 1098	181

Figure 4-9. The adjusted relative quantity of RNA measured by RT-QPCR for the <i>swi1Δ swi1-V5 rad4-116</i> strain SPSC 1099	181
Figure 4-10. The comparison the adjusted relative quantity of RNA of strains carrying the <i>swi1-V5</i> allele	182
Figure 4-11. Expression of V5 tag in the base <i>swi1-V5</i> strain SPSC 1096 after the addition of thiamine	184
Figure 4-12. Depletion of V5 tag in the base <i>swi1-V5</i> strain SPSC 1096 after the addition of thiamine	185
Figure 4-13. Depletion of V5 tag in the <i>swi1-V5 swi1Δ</i> strain SPSC 1098 after the addition of thiamine	186
Figure 4-14. Depletion of V5 tag in the <i>swi1-V5 swi1Δ rad4-116</i> strain SPSC 1099 after the addition of thiamine	187
Figure 4-15. The cell morphology of the <i>swi1-V5</i> strain SPSC 1096 at 100X magnification across 24 hours after thiamine induction	189
Figure 4-16. The cell morphology of the <i>swi1Δ swi1-V5</i> strain SPSC 1098 at 60X magnification across 24 hours after thiamine induction	190
Figure 4-17. The cell morphology of the <i>swi1Δ swi1-V5 rad4-116</i> strain SPSC 1099 at 100X magnification across 24 hours after thiamine induction	191
Figure 4-18. The average cell length of strains carrying the <i>swi1-V5</i> allele	192
Figure 4-19. The viability comparison of strains carrying the <i>swi1-V5</i> allele against the control <i>rad4-116</i> strain	196
Figure 4-20. SPSC 1096 and SPSC 1098 cell population as investigated through FACS	198
Figure 4-21. SPSC 1099 cell population as investigated through FACS	199

Figure 4-22. The growth of individual spores to colonies of the <i>rad4-116</i> strain cross with <i>swi3Δ</i> strain	201
Figure 4-23 . Merged image of Rad52-GFP foci of the <i>swi1Δ</i> strain	206
Figure 4-24. Rad52-GFP foci of the <i>swi3Δ</i> strain at its peak	207
Figure 4-25. Viability counts for the <i>rad4⁺</i> , <i>rad4-116</i> and <i>swi3Δ</i> strains carrying the <i>rad52-GFP</i> gene	208
Figure 4-26. The Rad52-GFP profile of the <i>swi3Δ</i> strain	209
Figure 4-27. A comparison of the Rad52-GFP profiles of the <i>rad4-116</i> , <i>rad4⁺</i> and <i>swi3Δ</i> strains	210
Figure 4-28. The adjusted relative quantity of RNA measured by RT-QPCR for the <i>hip1-V5</i> strain SPSC 1097	214
Figure 4-29. The adjusted relative quantity of RNA measured by RT-QPCR for the <i>swi3Δ swi3-V5</i> strain SPSC 1101	215
Figure 4-30. The adjusted relative quantity of RNA measured by RT-QPCR for the <i>swi3Δ swi3-V5 rad4-116</i> strain SPSC 1102	215
Figure 4-31. The comparison the adjusted relative quantity of RNA of strains carrying the <i>swi3-V5</i> allele	216
Figure 4-32 .Expression of V5 tag in the base <i>swi3-V5</i> strain SPSC 1097 after the addition of thiamine	218
Figure 4-33. Depletion of V5 tag in the <i>swi3-V5</i> strain SPSC 1097 after the addition of thiamine	218
Figure 4-34. Depletion of V5 tag in the <i>swi3-V5 swi3Δ</i> strain SPSC 1101 after the addition of thiamine	220
Figure 4-35. Depletion of V5 tag in the <i>swi3-V5 swi3Δ rad4-116</i> strain SPSC 1102 after the addition of thiamine	221

Figure 4-36. The cell morphology of the <i>swi3-V5</i> strain SPSC 1097 across 24 hours after thiamine induction	223
Figure 4-37. The cell morphology of the <i>swi3Δ swi3-V5</i> strain SPSC 1101 at 60X magnification across 24 hours after thiamine induction	224
Figure 4-38. The cell morphology of the <i>swi3Δ swi3-V5 rad4-116</i> strain SPSC 1102 at 100X magnification across 24 hours after thiamine induction	225
Figure 4-39. The population of SPSC 1102 divided by cell length at the 0 hour timepoint after thiamine addition.	226
Figure 4-40. The population of SPSC 1102 divided by cell length at the 4 hour timepoint after thiamine addition.	227
Figure 4-41. The population of SPSC 1102 divided by cell length at the 8 hour timepoint after thiamine addition.	227
Figure 4-42. The population of SPSC 1102 divided by cell length at the 12 hour timepoint after thiamine addition.	228
Figure 4-43. The population of SPSC 1102 divided by cell length at the 24 hour timepoint after thiamine addition.	228
Figure 4-44. The average cell length of the strains carrying the <i>swi3-V5</i> allele	229
Figure 4-45. The viability comparison of strains carrying the <i>swi3-V5</i> allele against the control <i>rad4-116</i> strain.	233
Figure 4-46. SPSC 1097 and SPSC 1101 cell population as investigated through FACS	235
Figure 4-47. SPSC 1102 cell population as investigated through FACS	236

Figure 5-1. The growth of individual spores to colonies of the <i>rad4-116</i> strain cross with <i>mrc1Δ</i> strain	247
Figure 5-2 . Merged image of Rad52-GFP foci of the <i>mrc1Δ</i> strain	252
Figure 5-3. Rad52-GFP foci of the <i>mrc1Δ</i> strain at its peak	253
Figure 5-4. Viability counts for the <i>rad4⁺</i> , <i>rad4-116</i> and <i>mrc1Δ</i> strains carrying the <i>rad52-GFP</i> gene	254
Figure 5-5. The Rad52-GFP profile of the <i>mrc1Δ</i> strain	255
Figure 5-6. A comparison of the Rad52-GFP profiles of the <i>rad4-116</i> , <i>rad4⁺</i> and <i>mrc1Δ</i> strains	256
Figure 5-7. The adjusted relative quantity of RNA measured by RT-QPCR for the <i>mrc1-V5</i> strain SPSC 1114	260
Figure 5-8. The adjusted relative quantity of RNA measured by RT-QPCR for the <i>mrc1Δ mrc1-V5</i> strain SPSC 1115	261
Figure 5-9. The adjusted relative quantity of RNA measured by RT-QPCR for the <i>mrc1Δ mrc1-V5 rad4-116</i> strain SPSC 1116	261
Figure 5-10. The comparison the adjusted relative quantity of RNA of strains carrying the <i>mrc1-V5</i> allele	262
Figure 5-11. Expression of V5 tag in the base <i>mrc1-V5</i> strain SPSC 1114 after the addition of thiamine	264
Figure 5-12. Depletion of V5 tag in the <i>mrc1-V5</i> base strain SPSC 1114 after the addition of thiamine	265
Figure 5-13. Depletion of V5 tag in the <i>mrc1-V5 mrc1Δ</i> strain SPSC 1115 after the addition of thiamine	266
Figure 5-14. Depletion of V5 tag in the <i>mrc1-V5 mrc1Δ rad4-116</i> strain SPSC 1116 after the addition of thiamine	267

Figure 5-15. The cell morphology of the <i>mrc1-V5</i> strain SPSC 1114 at 60X magnification across 24 hours after thiamine induction	269
Figure 5-16. The cell morphology of the <i>mrc1Δ mrc1-V5</i> strain SPSC 1115 at 60X magnification across 24 hours after thiamine induction	270
Figure 5-17. The cell morphology of the <i>mrc1Δ mrc1-V5 rad4-116</i> strain SPSC 1116 at 100X magnification across 24 hours after thiamine induction	271
Figure 5-18. The average cell length of the strains carrying the <i>mrc1-V5</i> allele	272
Figure 5-19. The viability comparison of strains carrying the <i>mrc1-V5</i> allele against the control <i>rad4-116</i> strain	276
Figure 5-20. SPSC 1114 and SPSC 1115 cell population FACS analysis	278
Figure 5-21. SPSC 1116 cell population as investigated through FACS	279
Figure 5-22. The adjusted relative quantity of RNA measured by RT-QPCR for the <i>mrc1Δ mrc1-V5 rad4-116 rad52-GFP</i> strain SPSC 1117	283
Figure 5-23. Depletion of V5 tag in the <i>mrc1-V5 mrc1Δ rad4-116</i> strain carrying Rad52-GFP SPSC 1117 after the addition of thiamine	285
Figure 5-24. Rad52-GFP foci of the <i>mrc1-V5 mrc1Δ rad4-116 rad52-GFP</i> strain at 100 X magnification at timepoint 0	286
Figure 5-25 . Merged image of Rad52-GFP foci of the <i>mrc1-V5 mrc1Δ rad4-116 rad52-GFP</i> strain	287
Figure 5-26. Rad52-GFP foci of the <i>mrc1-V5 mrc1Δ rad4-116 rad52-GFP</i> strain at 60X magnification at timepoint 24	288
Figure 5-27. The Rad52-GFP profile of SPSC 1117 across the 24 hour timepoint	289
Figure 5-28. The viability change in SPSC 1117 across the 24 hour timepoint	290
Figure 5-29. SPSC 1117 cell population as investigated through FACS	291

List of Tables

Table 2.1 The <i>S. pombe</i> strains	79
Table 2.2 The plasmids	80
Table 2.3 The media recipes	81
Table 2.4 The recipes for buffers and solutions	82
Table 2.5. The combinations for primers used in gene deletion testing	85
Table 2.6. The sequences for primers used in gene deletion testing	85
Table 2.7. The Primers used in the cloning of genes into the <i>pINTL</i> plasmid for V5 tagging	87
Table 2.8. The Primers used in the testing of transformed strains after the integration of V5 tagged alleles	87
Table 2.9 The components of the PCR reaction	96
Table 2.10 The cycle conditions of the PCR reaction	97
Table 2.11 The components of the TOPO® Cloning reaction	98
Table 2.12 The components of the ligation reaction	101
Table 2.13 The components of the RT-QPCR reaction	104
Table 2.14 showing the cycle conditions of the RT-QPCR reaction	105

Table 2.15. The combinations for primers used in gene expression quantification corresponding to the gene being tested	106
Table 2.16. The sequences for primers used in RT-QPCR	106
Table 2.17 The recipe for 10% and 12% resolving gels used in Polyacrylamide Gel Electrophoresis	109
Table 2.18 The recipe for 6% stacking gels used in Polyacrylamide Gel Electrophoresis	109
Table 2.19 The list of antibodies used in the Western Blotting	111
Table 3-A The cross between the <i>rad4-116</i> strain and <i>hip1Δ</i>	117
Table 4-A The cross between the <i>rad4-116</i> strain and <i>swi1Δ</i>	168
Table 4-B The cross between the <i>rad4-116</i> strain and <i>swi3Δ</i>	202
Table 5-A The cross between the <i>rad4-116</i> strain and <i>mrc1Δ</i>	248

Table of abbreviations:

53BP1	p53 binding protein
9-1-1	Rad9-Rad1-Hus1
A	Adenine
a.a.	Amino Acid
Amp	Ampicillin
APS	Ammonium persulfate
AT	Ataxia-telangiectesia
ATM	Ataxia telangeictesia mutated
ATP	Adenosine triphosphate
ATR	ATM and Rad3 related
ATRIP	ATR-interacting protein
BER	Base excision repair
Bp	Base pair
BRCA	Breast cancer
BRCT	BRCA1 C-terminal domain
BrdU	5'-bromo-2'-deoxyuridine
BSA	Bovine serum albumin
<i>C. elegans</i>	<i>Caenorhabditis elegans</i>
Cdc	Cell division cycle
CDK	Cyclin-Dependent Kinase
CDKI	Cyclin dependent kinase Inhibitor
CHK1	Checkpoint 1
cDNA	Complementary DNA

<i>D. melanogaster</i>	<i>Drosophilla melanogaster</i>
DAPI	4',6-Diamino-2-Phenyl-Indole
dd H ₂ O	Double distilled water
DDK	Dbf4p-dependent kinase
DMSO	Dimethyl sulfoxide
DNA	Deoxyribonucleic acid
dNTP	Deoxyribonucleotide triphosphate
DSB	Double strand break
dsDNA	double-stranded DNA
DTT	Dithiothreitol
<i>E. coli</i>	<i>Escherichia coli</i>
ECL	Enhanced chemi-luminescence
EDTA	Ethylenediaminetetraacetic acid
EMM	Edinburgh minimal medium
EtOH	Ethanol
FACS	Fluorescent-activated cell sorting
G	Guanine
G1	Gap/growth phase 1
G2	Gap/growth phase 2
G2/M	The growth phase 2/mitosis boundary of the cell cycle
G418	Geneticin
GFP	Green Fluorescent Protein
h	Hours

<i>H. sapiens</i>	<i>Homo sapiens</i>
HIRA	Histone cell cycle regulation defective homolog A
HR	Homologous recombination
HRP	Horse-radish peroxidase
HSPs	Heat Shock Proteins
HU	Hydroxyurea
IR	Ionising radiation
Kan	Kanamycin
Kb	Kilobases
kDa	Kilodaltons
LB	Luria Bertani medium
Leu	Leucine
M phase	Mitosis
MCM	Mini-chromosome maintenance
MCS	Multi-cloning site
min	Minutes
MMR	Mismatch repair
MRN	Mre11-Rad40-Nbs1
mRNA	messenger Ribonucleic acid
NaOH	Sodium hydroxide
NAT	Nourseothricin
NEB	New England Biolabs
NER	Nucleotide excision repair

NHEJ	Non-homologous end joining
OD	Optical density measured
ORF	Open reading frame
ORI	Origins of replication
ORC	Origin recognition complex
PARP	Poly-(ADP-ribose) polymerase
PBS	Phosphate buffered saline
PBST	Phosphate buffered saline plus tween
PCNA	Proliferating cell nuclear antigen
PCR	Polymerase chain reaction
PEG	Polyethylene glycol
PIC	Preinitiation complex
PIK	Phosphoinositid-3-kinase
PIPES	2-[4-(2-Sulfoethyl)Piperazin-1-yl]ethanesulfonic Acid
Pol	Polymerase
Pre-RC	Pre-replication complex
PVDF	Polyvinylidene difluoride
Rad	Radiation
RB	Retinoblastoma
rDNA	Ribosomal DNA
RFC	Replication factor complex
RNA	Ribonucleic acid
ROS	Reactive oxygen species

RPA	Replication protein A
RT-QPCR	Reverse transcriptase quantitative PCR
s	Seconds
<i>S. cerevisiae</i>	<i>Saccharomyces cerevisiae</i>
<i>S. pombe</i>	<i>Schizosaccharomyces pombe</i>
S-phase	Synthesis phase
SDS	Sodium dodecyl sulphate
SDS-PAGE	Sodium dodecyl sulphate polyacrylamide gel electrophoresis
ssDNA	single strand DNA
SWI/SNF	SWItch/Sucrose NonFermentable
T	Thymine
TE	Tris EDTA
TAE	Tris acetic acid EDTA
TBS	Tris Buffered Saline
TBST	Tris buffer saline plus Tween
TCA	Trichloroacetic acid
TEMED	Tetramethylethylenediamine
Top	Topoisomerase
Tris	Tris(hydroxymethyl)aminomethane
Ura	Uracil
<i>ura4</i>	Gene encoding dihydroorotase (involved in the <i>de novo</i> biosynthesis of pyrimidines)

UV	Ultraviolet
v/v	Volume for volume
w/o	Without
w/v	Weight for volume
wt	Wild-type
YE	Yeast extract
YES	Yeast extract with supplements

Acknowledgments

My sincerest thanks to Dr. Clive Price for giving me the opportunity and privilege to learn and work under his tutelage and showing patience while teaching me. Special thanks to Dr. Edward Parkin and Dr. Paul McKean for their guidance and help. I would also like to express my gratitude and appreciation to the members of the lab and staff in the department for the technical support. I would like to thank my family for everything they have done for me during my project. Finally, I would like to thank the North West Cancer Research Fund for funding my PhD research.

Abstract

Genomic instability is a hallmark of cancer. Cancer progression depends on the development and amplification of mutations that alter the cellular response to threats to the genome. This can lead to DNA replication stress and the potential loss of genetic integrity of the newly formed cells. The study of the sophisticated systems of DNA replication has been an attractive area for research in human and cancer, yet, the results do not fully provide a clear understanding. This could be due to sheer complexity of these systems in *Homo sapiens* as some key elements in these processes have evolved to be multifunctional to several pathways rather than one. This project utilises fission yeast to map the interactions occurring in some of the most crucial pathways in both DNA replication and checkpoint monitoring. One particularly interesting protein that fits the multifunctional description, is TopBP1. Rad4 is the *Schizosaccharomyces pombe* (*S. pombe*) TopBP1 homologue that is essential for the initiation of DNA replication, DNA repair as well as the activation of DNA damage checkpoint signalling. We have modelled conditions of replication stress in the genetically tractable fission yeast, *S. pombe* using the hypomorphic *rad4-116* allele. Synthetic genetic analysis was used to identify processes required for cell survival under conditions of DNA replication stress. With the aim of mapping the genetic interactions of *rad4* and its mutant allele, *rad4-116*, several genes that could have an interaction with *rad4* during replication stress have emerged as attractive. Interactions with genes involved in chromatin remodelling, such as *hip1*, and replication fork stalling resolution, such as *mrc1*, *swi1* and *swi3* were explored. Results from these studies will provide a clear view of the *rad4* interactions, the association of Rad4 with the replisome which in turn should provide a more robust

understanding of the pathways associated. Ultimately, this will serve as a platform for targeting these pathways for anti-cancer drug development.

Chapter 1: Introduction

1.1 Cancer as a genetic disease

Due to increased life expectancies in the modern world, cancer prevalence has also followed the same pattern of increase. As such, the WHO (World Health Organisation) expects a 70% increase in cancer-related deaths over the span of the next 20 years (WHO, 2015). The incidence of cancer worldwide was estimated to be over 14 million new cases in 2012, with deaths related to cancer estimated to be over 8 million (Cancer Research UK). Cancer itself is not a single disease as falsely perceived, but a collection of diseases sharing typical common features among them. It is well recognised that oncogenesis is a multi-step process with a wide variety of genetic and epigenetic changes occurring in cells that eventually lead to the generation of cancer.

The most common types of cancer include breast, prostate and lung cancer. Since the 1950s, understanding the biochemical mechanisms involved in the development of cancer has been a priority in the battle against the disease. Indeed, due to the attention afforded to cancer research, certain types of cancers such as lymphomas, leukaemias, and testicular carcinomas have been well studied and are now easily treatable. However, the treatment of many of the common cancers such as lung, colorectal and prostate is mostly only palliative at best. The prime reason for this contrast is that the majority of treatment strategies rely on non-specific cytotoxic anti-proliferative drugs. These drugs carry inherent toxicity to all the cells meaning that most of the time it is not possible to administer high enough doses to effectively treat the cancer, effectively limiting their success in the clinic. This problem is common across most of the cytotoxic drugs and thus a solution to improve the drugs'

therapeutic index is desperately needed. Logically, the treatment of cancer would be vastly improved by the development of more specific drugs that relied on the identified dysfunctional molecular pathways in tumourigenesis to only target cancer cells.

It was originally suggested that tumours result from aberrant cell growth (Haggard, 1938). This revolutionary idea launched the basis for cancer research aiming to underline and contrast the differences between cancer and normal cells. Research on cancer has highlighted that, basically, cancer is a mass of cells resulting from the uncontrolled cellular proliferation. As a summation of the first 70 years of cancer research, six distinctive common features, termed as “hallmarks of cancer”, have been proposed (Hanahan and Weinberg, 2000). These hallmarks were the first characteristics that were common across all cancer types and are involved in the mechanisms of cancer development and maintenance. The six hallmarks are limitless proliferative potential, evasion of programmed cell death (apoptosis), self-sufficiency in growth signals, sustained angiogenesis, insensitivity to growth-inhibitory signals, evasion of programmed cell death and finally, tissue invasion.

However, since then, several features which fall under the description of the hallmarks were also discovered and studied. These features were later known as the emerging hallmarks of cancer and are energy metabolism and evading immune destruction. Furthermore, a common feature that enabled the hallmarks is genomic instability, which was identified as the driving force of cancer development (Negrini *et al.*, 2010; Hanahan and Weinberg, 2011). The hallmarks described by Hanahan and Weinberg provide a blueprint encompassing the path to study cancer leading to enhanced and refined treatment and diagnostic options.

1.2 Cancer and Genomic instability

Generally, genomic instability can result in a wide range of genetic alterations, but, these can be categorised into two groups. The two groups are gross chromosomal rearrangements, which are conformational changes that can be detected by microscopy and small DNA mutations, which include base substitutions, deletions and insertions which can be detected by sequencing but not by microscopy.

Chromosomal rearrangements can be associated with failures in the mitotic spindle checkpoint which prevents dividing cells from segregating their chromosomes accurately. This can also occur as a result of telomere fusion from erroneous repair of double strand breaks near the telomeres (Muraki *et al.*, 2012). For the second category, mutations within DNA sequences generally arise with errors during the replication process and aberrant DNA repair (Gonzalez-Aguilera *et al.*, 2008).

For example, genomic instability can result in errors within the genome which can eventually cause the loss of cellular control of the regulation of cell replication and growth. The rise of genomic instability could be due to the increased mutation rates caused by the loss of functionality in genes that are integral in the preservation of genomic integrity. However, cancerous growth does not start after the mutation of one gene. A hypothesis proposed, by Knudson, called the “two hit-hypothesis” suggested that at least two mutations, or hits, in both copies of a gene defining tumour suppressor loci are required for cancer to develop (Knudson, 1971). These mutations could be in vital genes that play major roles in the biochemical processes of the hallmarks of cancer. Above all, errors or defects in genes which play a role in DNA replication, DNA repair or checkpoint response have been highlighted to play a

key role in the predisposition to cancer (Eyfjord and Bodvarsdottir, 2005; Negrini *et al.*, 2010).

Generally, there are two classes of genes that mutate in cancer, the first being proto-oncogenes which mutate into oncogenes to drive the cancer cell progression and the other class being tumour suppressor genes whose normal function is stop the development and progression of mutant cells (Croce, 2008; Sun and Yang, 2010). An example of the of the proto-oncogenes is Ras that when mutated leads to an increase in cell signalling leading to DNA replication stress (Maya-Mendoza *et al.*, 2015). The mutation of proto-oncogenes into oncogenes that drive the increased activation of transcriptional pathways that control cellular proliferation including cyclin proteins, which activate cell cycle promoting cyclin dependent kinases (CDKs) (Nevins, 2001, Musgrove *et al.*, 2011). As a regular event occurring in the cancer, replication stress can be identified as the stalling or slowing of replication forks causing any alteration in the regular replication process such as the unwinding of DNA through decoupling of replicative helicases and polymerases (Ciccio and Elledge, 2010). It can be viewed as an important event that is common across all cancer types to the point that it has been proposed as a hallmark of cancer (Macheret and Halazonetis, 2015). The focus of this study within that framework is the hallmark of cancer of genomic DNA replication stress and instability.

1.3 The Cell cycle

Across all cell types, from the simplest bacteria to the most complex multicellular organisms, precise coordination of DNA replication with chromosome segregation during the cell division cycle is essential to ensure that both daughter cells inherit a complete and intact complement of genetic material. Due its importance, DNA molecules, which are conserved across all organisms, are long polymeric chains of adenine, thymine, guanine and cytosine deoxyribonucleotides. These chains are arranged as a double helix in an anti-parallel manner, with the bases towards the inside of the helix and the phosphate groups towards the outside of the helix (Watson and Crick, 1953). According to the completed human genome project, human cells contain nearly 3 billion base pairs of DNA that constitute all 46 chromosomes. The relatively large genomes of eukaryotic cells are replicated from multiple replication origins on multiple chromosomes. Further highlighting its importance, the cell division cycle process has been linked to a wide variety of physiologic such as embryonic development and cell growth and pathologic processes such as cancer and Alzheimer's disease (Zhivotovsky and Orrenius, 2010).

Similar to the other eukaryotes, the mitotic cycle of *Schizosaccharomyces pombe* can be divided into two major phases known as interphase and mitotic phase. The interphase is the stage when cells grow, replicate their DNA and prepare to undergo mitosis. Interphase can be further divided into 3 stages G1, S, G2 and mitosis into 5 stages prophase, prometaphase, metaphase, anaphase and telophase followed by cytokinesis (Morgan, 2007). In the S phase the replication of the entire genome occurs. This process varies in time, as it occurs in about 30 minutes in *S. cerevisiae*

and nearly ten hours in mammalian cells (Brewer *et al.*, 1984). The cells then prepare for mitosis in the G2 phase in which the DNA is surveyed for mismatches and mistakes and the molecular machinery needed for mitosis is assembled. Then, chromosomes segregate in mitosis throughout the 5 phases of prophase, prometaphase, metaphase, anaphase and telophase in which cells divide (Schafer, 1998). The cells undergo nuclear division and divide their duplicated organelles and cytoplasmic components into their identical daughter cells. The cells then separate their cytoplasm into newly formed cells in a process called cytokinesis and they are now ready to enter a new cycle (Tyson and Novak, 2008). Exit from the cell cycle can occur before the S phase. Cells that exit the cell cycle, enter quiescence, which is known as G0 (Malumbres and Barbacid, 2009; Duronio and Xiong, 2013). G0 is where some differentiated cells enter quiescence never leave G0 until they need to undergo replication again. Most commonly, cells enter G0 in response to acute nutrient starvation or contact inhibition (Coverley *et al.*, 2002).

The main regulators controlling the cellular progression of the cell cycle are the Cyclin Dependent Kinases (CDKs) which were first discovered through the Nobel Prize-winning research by Tim Hunt, Paul Nurse and Leland H. Hartwell in different organisms. Alongside CDKs, cyclins, CDK inhibitors, CDK-activating kinases and phosphatases form a network of proteins and biochemical molecules that drives the cell cycle through the time-dependent accumulation, inhibition and proteolysis of its components (Schafer, 1998). The combination of increased CDK activation and oncogenic mutation and transcription causes an increase in DNA stress which leads to further genome instability. This positive feedback loop causes an exponential progression of tumorigenesis (Gaillard *et al.*, 2015).

CDKs are a family of kinases which act by phosphorylating downstream targets that drive the progression through the cell cycle in only one direction. Typically, CDKs are inactive if they do not dimerise with a cyclin protein. Mammals contain approximately 20 CDKs with varying roles in cell cycle guidance and progression as well as the regulation of transcription some (Malumbres *et al.*, 2009; Malumbres 2014). On the other hand, there are approximately 30 identified cyclins in mammals. Similar to CDKs, cyclin proteins play various roles in cell cycle regulation and in transcriptional control (Lee and Sicinski, 2006; Malumbres *et al.*, 2009; 2014). While several CDKs exist in higher eukaryotes, in *S. pombe* only one CDK called Cdk1 or Cdc2. The Cdc2 protein level is constant across the phases of the cell cycle but changes in its activity do occur (Moser and Russell, 2000). The activity of Cdc2 is regulated by its association with the different cyclins, Cig1, Cig2, Puc1 and Cdc13. The cyclin Cig2 is required for S-phase progression while Cdc13 is essential for the initiation of mitosis (Booher *et al.*, 1989; Mondesert *et al.*, 1996).

Cdc2 has the ability to drive both the G1/S and the G2/M transitions using the four cyclins, Puc1, Cig1, Cig2 and Cdc13 (Nurse *et al.*, 1976). Cdc2 binds to Puc1 to drive mitosis and entry into G1 (Forsburg and Nurse, 1994). Then, Cdc2 binds to Cig1 to drive the G1/S transition and then to Cig2 during the S phase for DNA replication initiation and cytokinesis (Connolly and Beach, 1994 ; Mondesert *et al.*, 1996). The binding of Cdc2 to Cdc13 during the G2/M inhibits the re-initiation of DNA synthesis and to drive the cells into the M phase (Fisher and Nurse, 1996). Cdc13 is then degraded by APC-ubiquitin-driven proteolysis and Puc1 levels rise again through the M phase. This causes the segregation of the sister chromatids to allow the entry into the G1 phase and be ready for a new cell cycle (Martín-Castellanos *et al.*, 2000). There exists a point of no return during the G1 phase

called START; at which DNA synthesis occurs with no regard to growth signals as the cells commit to the cell cycle (Simanis *et al.*, 1987).

1.4 DNA Replication

The evolution of a system for controlling multiple replication origins is such that they are all activated precisely once during each S phase is undoubtedly an important step because it removed a major constraint on genome size in the form of the amount of DNA that can be replicated from a single replication origin. More impressively, bacterial and eukaryotic cells have the remarkable ability to duplicate their entire genomes accurately when events such as DNA damage occur. The cellular DNA is normally under a considerable amount of threat from extracellular mutagens such as ultraviolet light (UV) or ionising radiation (IR) or intracellular mutagens such as reactive oxygen species (ROS) (Lindahl, 1993).

Relative to mammalian cells bacteria have much smaller genomes, *E. coli* strain K-12 has a single chromosome encoding more than 4000 genes as a 4.6 million base pair circular chromosome (Blattner *et al.*, 1997). *E. coli* tend to replicate their whole genomic DNA from a single site on the DNA most commonly referred to as an origin of replication (*OriC*). This origin of replication is a specific sequence that is attached to a protein known as DnaA. The role of DnaA is to recruit and gather proteins that unwind the DNA strands to load and recruit DNA primase, DNA polymerase III holoenzyme and other replication factors (Kaguni, 2011; Robinson and Van Oijen, 2013). Once the DNA replication starts, the process proceeds in a bi-directional manner from *OriC* until the replication process is completed with decatenation when the linked daughter chromosomes are separated by topoisomerase IV (Drlica and Zhao, 1997).

Conversely, in eukaryotes, the large genomes are arranged into multiple linear chromosomes and require more sophisticated machinery and controls to ensure the timely and precise replication of the whole genome (Yekezare *et al.*, 2013). For example, the genome *Saccharomyces cerevisiae* is approximately 3 times larger compared to that of *E. coli* whilst also having a much slower replication fork speed (Raghuraman *et al.*, 2001). Similar to *E. coli*, replication initiation is determined by a specific sequence of DNA called autonomously replicating sequences (ARS) instead of *OriC*, at which DNA replication begins (Liachko and Dunham, 2014). However, in contrast to the single replication origin found in *E. coli*, *S. cerevisiae* has nearly 400 origin sites distributed in its genome with varying levels of usage frequency during replication (Nieduszynski *et al.*, 2006; Muller *et al.*, 2014). Logically, as the organism and genome complexity rises, the sophistication of the origin and origin identifying and binding machinery rises. This trend is continued in mammalian DNA replication, in which origins are more complex as mammalian genomes do not utilise ARSs.

Mammalian cells alternatively use epigenetic mechanisms to determine location of the origin, usually, in the form of GC rich sequence elements such as CpG islands (Delgado *et al.*, 1998). Impressively, in *homo sapiens* between 30,000 and 50,000 origins have been reported to fire during DNA replication with about half of the same origins firing in consecutive S phases (Tuduri *et al.*, 2010; Leonard and Méchali, 2013). Less than one tenth of all origins fire in each cell during replication with many dormant origins which are ready to be used in case any DNA damage or replicative stress occur (McIntosh and Blow, 2012). This is especially important as the suppression of these dormant origins is required to provide resistance to DNA fork

stalling agents such as Hydroxyurea which induces replication stress (Ge *et al.*, 2007). Replication origins do not fire in a synchronous pattern during the replication of the whole genome. Depending on the order of the origin firing, they can be divided into the higher density early firing origins and lower density late firing replication origins. (Cayrou *et al.*, 2011). In a spatial manner, the firing of one origin in *S. cerevisiae* at a single ARS acts to inhibit the firing of neighbouring origins and that control mechanism is conserved in mammalian cells (Brewer and Fangman, 1993; Lebofsky *et al.*, 2006). During the S phase in mammals, nearly 5000 replication centres or foci activate to copy DNA at sites that are present in a close proximity within a 3D area by formatting the DNA loop structures (Chagin *et al.*, 2016). To avoid overlapping of origin firing and to prevent the misfiring of origins, eukaryotic cells have developed a molecular switch which, when turned on, acts to promote just a single initiation event from each origin (Zegerman and Diffley, 2003; 2009; Burrows and Elledge, 2008 ; Cimprich and Cortez, 2008).

Even though *S.pombe* origins of replications do not have a general recognisable sequence motif, they are typically 500 basepairs to 1000 basepairs with AT-rich regions and are normally present within the intergenic regions of the DNA. Using the analysis of genome-wide bioinformatics, at least 384 potential origins have been identified in *S.pombe* with some being identified as early and late origins depending on the timing of their firing during the cell cycle (Segurado *et al.*, 2003; Heichinger *et al.*, 2006). Fission yeast do not utilise a hereditary temporal initiation programme for their origins and their origins that have fired during a specific cell cycle are not required to fire at the exact same time in subsequent cell cycles, if at all. (Kim and Huberman, 2001; Legouras *et al.*, 2006; Mantiero *et al.*, 2011). There also seems to be a correlation between the chromatin status and the respective epigenetics on one

side and the replication timing on the other side, as euchromatin appear to be replicated earlier than the heterochromatic regions of the genome (Sclafani and Holzen,2007; Maric and Prioleau, 2010).

DNA replication can be divided into 3 phases in the initiation of replication, the elongation of DNA strands and the termination of the process. The initiation step is started at the replication origin or origins depending on the organism. The step is regulated such that no overlap of origins occur within a 3D space (Chagin *et al.*, 2016). The elongation step involves the progression of replication by the replicative polymerases in a bidirectional manner. A step known as origin licensing occurs from the anaphase step to the G1 phase of the cell cycle to ensure that DNA replication is carried out only one time per single cell cycle. A variety of proteins and factors are loaded onto the origins that are licensed for replication to form the pre-replication complex (preRC).

During DNA replication, the DNA template is unwound as its double strands separate at the sites of replication initiation aided by the helicase activity of the Mcm2-7 (minichromosome maintenance). DNA replication polymerases initiate the replication process in a bidirectional manner from the replication fork in the 5 prime - 3 prime direction. The replication of the leading strand proceeds in a continuous linear fashion, but due to the energetic requirements of 5 prime - 3 prime direction DNA synthesis, the lagging strand DNA is synthesised by the formation of short discontinuous fragments of DNA called Okazaki fragments (Ge and Blow 2009).

To be able to pinpoint the origins, origins are bound by the origin recognition complex (ORC) which is a heterohexamer constituted of subunits named ORC 1, 2, 3, 4 5 and 6 with ORC1 binding being an early event in the regulation of replication

(Shackleton and Peltier, 1992; Dhar *et al.*, 2001). ORC1 and ORC6 bind relatively loosely to the origin while ORCs 2 to 5 bind strongly to the origin. The ORC complex then recruits CDC6 and CDT1 to form the PreRC which recruits the heterohexamer minichromosome maintenance complex (MCM).

MCM is composed of 6 subunits MCM2-7 and promotes the recruitment of another MCM2-7 complex forming a double hexamer of MCM2-7s on chromatin during the process of replication licensing (Evrin *et al.*, 2009; Fragkos *et al.*, 2015; Ticaú *et al.*, 2015). Then, cyclin E-bound CDK2 and DDK, promote the recruitment of the CDC45-MCM2-7-GINS complex (CMG) which acts to separate the MCM2-7 hexamers, thereby, activating their helicase activity (Takeda and Dutta, 2005). The activation of CMG cannot occur without the binding of MCM10 which binds with a relatively low efficiency during G1 phase and a much higher efficiency during S phase (Douglas and Diffley, 2016). These structures are called pre-initiation complexes (PreICs), at which the replicative polymerases are now recruited. The replicative polymerase pol α synthesises short strands of RNA that prime DNA replication of the leading strand by the processivity factor PCNA bound pol ϵ and the lagging strand by pol δ (Kelman, 1997). Polymerase ϵ has been shown to be essential for helicase activation and remains associated with the CMG complex (Tanaka and Araki, 2013). Interestingly, there is recent evidence that pol δ is required for the proper balance of the leading and the lagging strand synthesis coupled by the hypothesis that it may have play an important role in DNA synthesis of the leading strand when the cells exhibit replication stress (Yeeles *et al.*, 2016).

Using purified *S.cerevisiae* replication proteins, it was discovered that the basic requirement for DNA replication initiation involves 16 replication factors alongside cyclin A-CDK2 and DDK phosphorylation (Yeeles *et al.*, 2015). It is to be noted that that study involved using replisome protein Mrc1 and Csm3/Tof1, to stabilise the activity of Mrc1 *in vitro*, to be able to achieve replication rates similar to those observed *in vivo* (Yeeles *et al.*, 2016). The average rate of replication observed *in vitro* in those experiments was 4 to 8 times slower than those observed *in vivo* (Yeeles *et al.*, 2016). Interestingly, the same parameters utilised in those studies could be applied to replication stress as it can be quantified or measured by the changes in origin usage and replication fork velocity. The results highlighted the importance of Mrc1 and Csm3/Tof1 as well as the requirement of Polymerase δ in fork progression and lagging-strand DNA synthesis. The assembly of the initiation complex provides an important link between replication machinery and the necessary chromosome functions before the actual DNA synthesis occurs as displayed by Figure 1-1. In fission yeast, another role for CDK is the phosphorylation of Sld3, which is necessary for the recruitment of Cut5, GINS, Drc1 and Cdc45 (Fukuura *et al.*, 2011). CDK is also important in temporally separating the step of replication initiation, origin licensing, from the activation of the helicase activator Cdc45. This separation is important in preventing re-firing of the replication origins which already fired, thus preventing cell death or survival of cells containing abnormal DNA content (Tanaka and Araki, 2010).

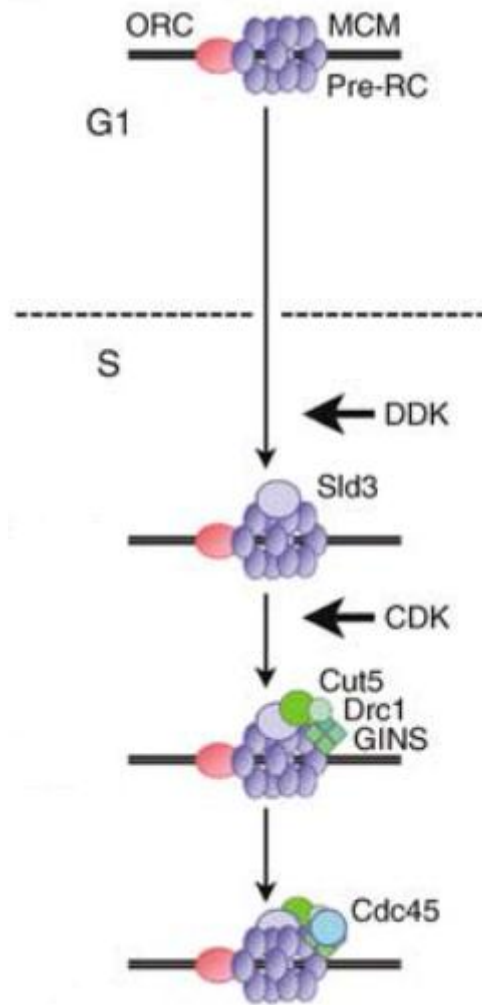


Figure 1-1 The formation of initiation complex in *S.pombe*. At the beginning of the S phase, Sld3 binds to the replication origin in a DDK dependent manner. Depending on Sld3 and CDK, GINS and Rad4/Cut5 then bind to the replication origin. Cdc45 is then recruited depending on all of Sld3, GINS, DDK and CDK. This leads to DNA unwinding and DNA polymerase loading and initiation of DNA replication (Adapted from Yabuuchi *et al.*, 2006).

1.5 DNA Replication Stress

In normal cells, when an event leading to replication stress occurs, the DNA damage response is activated leading to the arrest of the cell cycle until DNA can be effectively repaired or the marking of cells for apoptosis. The marking of cells for apoptosis occurs to provide an effective way to prevent cells from progressing further into tumourigenesis. A classic example of mutations affecting replication stress is the mutation of genes such as p53 which affects the DNA damage response and ultimately inducing genome instability, aiding in tumourigenesis and cancer progression (Gaillard *et al.*, 2015). To protect the information encrypted within the DNA against damage and preserve genomic stability, eukaryotic cells have evolved the DNA structure checkpoint signalling pathways which are often referred to as the DNA-damage response (DDR) (Warmerdam and Kanaar, 2010). During replication stress, long stretches of ssDNA occur due to the uncoupling and dissociation of replicative polymerases and helicases (Byun *et al.*, 2005). This causes ssDNA to become coated with RPA to facilitate the recruitment of ataxia telangiectasia and Rad3 related protein (ATR) which phosphorylates various proteins involved in cell cycle arrest. (Cimprich and Cortez, 2008; Ciccia and Elledge, 2010). The process is summarised in Figure 1-2.

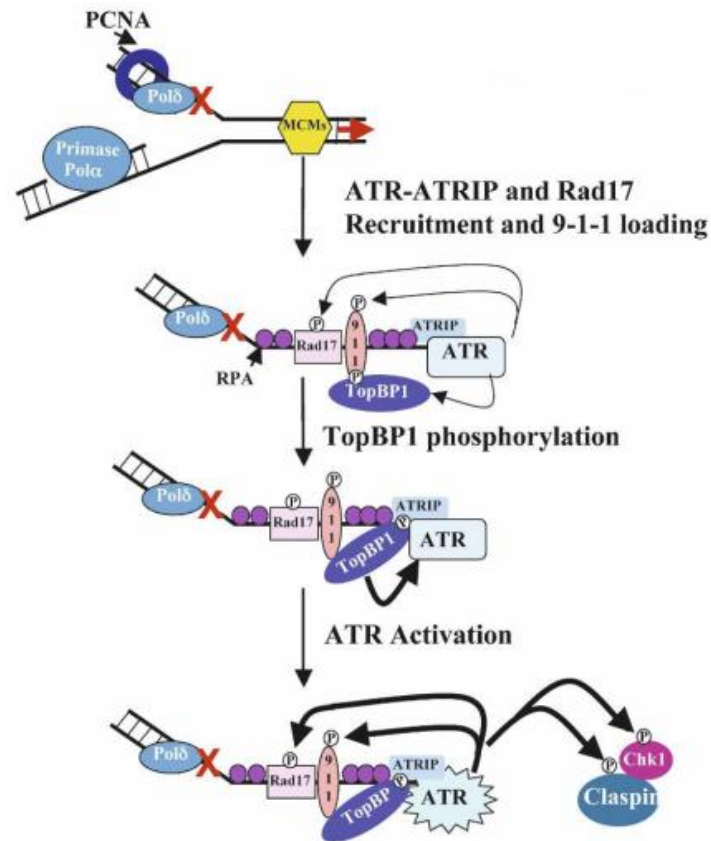


Figure 1-2 A schematic for the TopBP1-ATR activation at the stalled replication fork. When a replication fork is blocked at the red X mark, the coordination between the DNA polymerase and MCM helicase is lost leading to the generation of ssDNA. ssDNA is then coated with RPA as ATR–ATRIP and the RAD17/RFC2–5 complexes are independently recruited onto ssDNA–RPA stretches. The RAD9–HUS1–RAD1 (9–1–1) clamp complex is then loaded as TopBP1 binds to RAD9. TopBP1 phosphorylation leads to the activation of ATR and the activation of downstream effectors including Chk1 and Claspin (Adapted from Burrows and Elledge, 2008).

The DNA damage checkpoint network, originally identified as being involved in preventing cell cycle progression, plays an important in regulating DNA replication in the presence of DNA damage. An important aspect of the checkpoint function is to prevent the irreversible breakdown of replication forks that have stalled or encountered DNA lesions (Tercero *et al.*, 2003). The DNA damage response has

been utilised by tumour cells to survive replicative stress by using the same proteins in ATR and CHK1 . This occurs as the activation of ATR and CHK1 prevents the exposure of longer length ssDNA and thus prevent the collapse of replication forks. It has been confirmed that the activity both of ATR and CHK1 is required to stabilise DNA with RPA, thereby, preventing the collapse of replication fork (Carr *et al.*, 1995; Sanjiv *et al.*, 2016).

During a typical process of chromosome replication, replication forks can pause briefly when faced with sites where non-nucleosomal proteins are bound tightly. Any failure to stabilise these stalled replication forks can result in their collapse and thus, the monitoring of ongoing forks is essential for maintaining the integrity of the genome. Stalled replication forks need to be resolved in a swift manner by the cellular surveillance systems to be able to prevent the forks from collapsing and eventually complete the replication process (Greenfeder and Newlon, 1992 ; Ivessa *et al.*, 2003).

1.6 DNA checkpoint response

Studies in *S. pombe* and *S. cerevisiae* have revealed important information regarding the DNA structure checkpoints and their molecular mode of function (Carr, 2002). In *S. pombe*, the DNA structure checkpoints can be categorised into the DNA replication checkpoint and the DNA damage checkpoint. The major difference is that the DNA replication checkpoint prevents DNA damage in response to replication stress during S-phase, whilst the DNA damage checkpoint detects and resolves DNA damage before entry into mitosis (Caspari and Carr, 1999). An essential checkpoint response involves the arrest of the cell cycle by temporarily reducing CDK levels using CDK inhibitors and Cdc25 activity (Caspari and Carr, 1999; Zeng and Piwnica-Worms, 1999). This prevents daughter cells from inheriting any damaged DNA as the subsequent cell cycle phases progress.

In *S. pombe*, the discovery and characterisation of several radiation-sensitive mutants led to the identification of multiple checkpoint-related genes and have since been identified as the checkpoint *rad* family of genes (Carr, 2002). Whilst the DNA replication checkpoint is generally activated by stalled replication forks, the DNA damage checkpoint comes into play when the DNA is affected by a myriad of DNA lesions. The DNA damage checkpoint can be induced by stalled replication forks, single and double strand breaks, chemical modifications of the DNA or chromatin structure or X-ray radiation among other insults or aberrations (Boddy and Russell, 2001).

Certainly, there are checkpoint proteins that are common to both the DNA replication and the DNA damage checkpoint signalling pathways including the ATR-ATRIP (Rad3- Rad26) complex, the RFC- complex (Rad17, Rfc2, Rfc2, Rfc4, Rfc5),

and the PCNA-like complex (Rad1, Rad9, Hus1) (Furuya and Carr, 2003). The DNA replication checkpoint can be activated by DNA replication stress resulting from stalled replication forks, which can occur due to the depletion of deoxyribonucleotide pools which can be forced by drugs such as hydroxyurea (HU) or DNA replication polymerase inhibition which can be induced by drugs such as aphidicolin (Xu *et al.*, 2006).

In *S.pombe*, the DNA replication checkpoint depends primarily on the Rad3/Cds1 cascade pathway. This occurs as the replisome unwinds DNA downstream of the stalled replication fork to expose ssDNA structures to allow the loading and activation of the phosphatidylinositol 3-kinase-related protein kinase Rad3 in complex with Rad26 to the stalled replication fork areas (Bentley *et al.*, 1996; Chapman *et al.*, 1999; Van *et al.*, 2010). Rad3 null cells exhibit loss in viability, possibly as a result of their inability to arrest their cell cycle following DNA damage or replication stress and that highlights the importance of the role of Rad3 in the DNA replication and DNA damage checkpoints (al-Khodairy and Carr, 1992). Interestingly, Rad3 has the ability to autophosphorylate in a Rad26-dependent manner to be able to enhance its activity during the DNA replication and DNA damage downstream checkpoint responses (Chapman *et al.*, 1999; Wolkow and Enoch, 2002).

Another independent reaction also occurs as the heterotrimeric Rad9-Rad1-Hus1 clamp is loaded using the Rfc2-5-Rad17-like loading complex to be able to fully activate Rad3 and Cds1 (Bermudez *et al.*, 2003). Cds1 is activated by a phosphorylation network composed of one basal and three parallel phosphorylation steps mediated by Rad3, Mrc1 and Rad9 (Xu *et al.*, 2006; Yue *et al.*, 2011). The mediator of replication checkpoint 1, Mrc1, a focus of this study, is a component of

the replisome during the normal progression of replication that travels along the replication fork together with the replication machinery. A study showed that phosphorylation of Mrc1 is necessary for the phosphorylation of Cds1 as Mrc1 binds to inactive Cds1 via its FHA domain to facilitate the subsequent phosphorylation of Cds1 by Rad3. Phospho-Cds1 then, experiences a Rad3- and Mrc1-independent autophosphorylation rendering it fully active (Lindsay *et al.*, 1998; Xu *et al.*, 2006).

As a result of Cds1 activation in *S.pombe*, an increase in Mik1, a CDK inhibitor, levels results in inhibitory phosphorylation of Cdk1 causes the arrest of the cell cycle throughout S phase (Rhind and Russell, 1998; 2001). Another response caused by the activation of Cds1 is the stabilisation of paused replication forks. In *S.pombe*, Ssb3, the RPA ortholog, deletion results in the formation of a high number of Rad52 (Rad22) foci (Cavero *et al.*, 2010). Rad52 is a protein that binds double strand DNA breaks and has a function in both the repair of double strand breaks via homologous recombination and in mating type switching. As in this study, Rad52 is commonly used as a marker of genomic instability with the number of accumulated foci being used to report the extent of genomic instability (Ostermann *et al.*, 1993).

An important pathway for maintaining the stability of stalled replication forks is the Cds1-mediated inactivation of Mus81 which acts as a Holliday junction resolvase that acts to cleave the stalled replication forks (Kai *et al.*, 2005). It is important to consider that the halting of the replication fork is not an event that can be afforded a long period and that once cells resolve the cause of the block causing DNA replication stalling, they readily resume the replication process.

Another response is the DNA replication checkpoint transcriptional response, which includes the maintenance of the MluI Cell Cycle Box (MCB) Binding Factor (MBF) -

dependent G1/S transcriptional network (de Bruin and Wittenberg, 2009).

Continuous expression of MBF-dependent genes has been reported in cells arrested at the S phase with incompletely replicated DNA in an effort to stabilise stalled replication forks and induce DNA repair responses (de Bruin *et al.*, 2008). These responses include the activation of phosphorylated Rad3 to activate Cds1 via phosphorylation which in turn phosphorylates Nrm1, Cdc1 and Ste9 (de Bruin *et al.*, 2008; Dutta *et al.*, 2008; Chu *et al.*, 2009). This causes the activation of MBF-dependent transcription which is essential for the survival of cells in response to replicative stress (Caetano *et al.*, 2011).

Re-replication or over-replication within the same cell cycle causes polyploidy, aneuploidy or double strand breaks which are all hallmarks of tumourigenic development (Legouras *et al.*, 2006; Hook *et al.*, 2007; Truong and Wu, 2011). In *S.pombe* rereplication is prevented by the CDK-directed degradation of the licensing factors Cdc18/Cdc6 and Cdt1, and by CDK-dependent phosphorylation of Mcm2-7 and ORC. Another pathway involved the degradation of Cdt1 by the E3 ubiquitin ligase SCF in a Cdt2- Ddb1-dependent manner (Ralph *et al.*, 2006).

1.7 DNA damage checkpoint

When the DNA damage checkpoint cascade is activated, phosphorylation and activation of the serine/threonine protein kinase Chk1 occurs (Kuntz and O'Connell, 2009). That cascade is conserved across eukaryotic organisms as evident in Tel1/Chk1 and Rad3/Chk1 in *S. pombe* corresponding to Mec1/Chk1 in *S. cerevisiae* and the ATM/Chk1 pathway in mammals (Kuntz and O'Connell, 2009).

Similar to the DNA replication checkpoint, the initial step in the activation of the DNA damage checkpoint cascade involves the transformation of the DNA lesions into ssDNA to be recognised by the 9-1-1 clamp, instead of the Rad3/Rad26 complex. This occurs to allow the loading of the clamp loader Rfc2-5/Rad17 (Parrilla-Castellar *et al.*, 2004). However, with the clamp loader combined with the ATM ortholog, Cut5 and Crb2 recruit and activate Chk1 to the checkpoint complex, allowing it to bind to Rad24 and Rad25. Similar to Mrc1, Crb2 contains TQ/SQ phosphorylation clusters that interact with Chk1 (Saka *et al.*, 1997; Lopez-Girona *et al.*, 2001; Dunaway *et al.*, 2005; Qu *et al.*, 2012 ; 2013). The deactivation of Chk1 is essential for cells to recover and re-enter the cell cycle when the DNA damage is repaired and that deactivation occurs by the action of phosphatases PP1 (den Elzen and O'Connell, 2004).

Chk1 activation can lead to a variety of repair pathways in an exclusive or combinatorial manner, depending on the type of damage being repaired (Helleday *et al.*, 2008). The types are:

1. The homologous recombination (HR) and the non-homologous end joining repair pathways (NHEJ) to repair double strand breaks
2. The base excision repair (BER) to excise and repair any damaged bases
3. The nucleotide excision repair (NER) to repair single stranded DNA
4. The direct reversal DNA repair to repair alkylated and oxidised bases

1.8 TopBP1 Structure

TopBP1 and its homologs are scaffolding proteins capable of phospho-specific protein-protein interactions using BRCT (BRCA1 C-terminus) domains which are formed of tandem repeats allowing the tight regulation over timing of its interactions with its protein partners (Yu *et al.*, 2003). These interactions are essential in DNA replication initiation and checkpoint activation. Even though Rad4 and its homologs act within conserved pathways, the similarity between them as proteins is unexpectedly not strong as the human TopBP1 protein is over twice the size of its *S.pombe* counterpart. The homologs of Rad4 appear to have evolutionarily developed novel functions in multicellular organisms as the *C. elegans*, *D. melanogaster* and human homologs have additional BRCT domains when compared to *S.pombe* and *S.cerevisiae* homologs (Garcia *et al.*, 2005). The main conserved core functions are present in 4 BRCT domains as the first, second on one hand and fourth and fifth domains in *H.sapiens* are conserved in all orthologs (Garcia *et al.*, 2005). All of the orthologs contain ATR Activation Domain (AAD) in their C-terminus but the location and sequence are not conserved (Kumagai *et al.*, 2006; Mordes *et al.*, 2008 a; b). The structure and the conservation of the TopBP1 BRCT domains is shown in Figure 1-3.

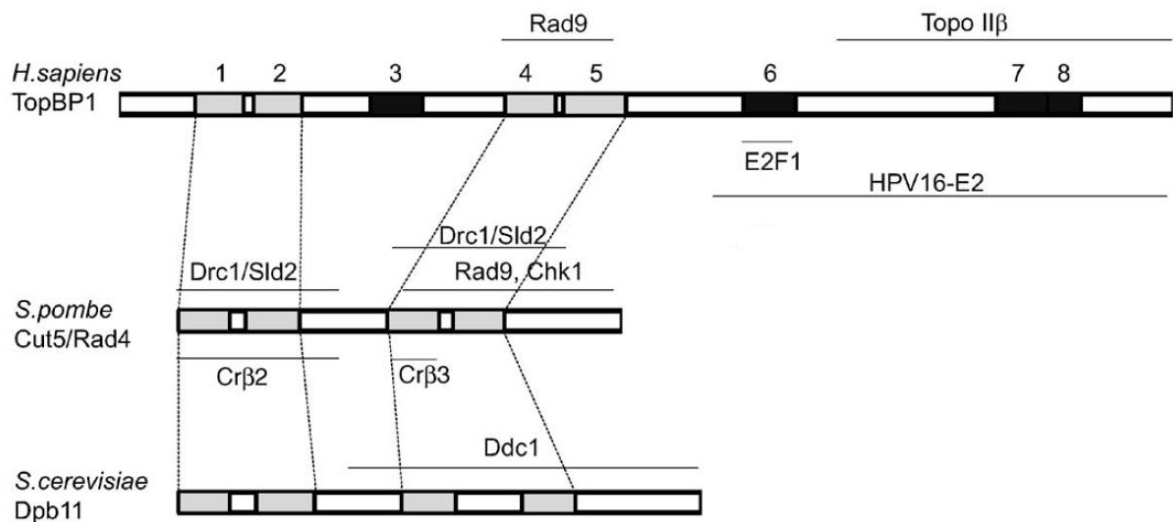


Figure 1-3 showing the structure conservation of TopBP1 and related proteins. *S. pombe* Rad4, *S. cerevisiae* Dpb11, and human TopBP1 are homologous proteins whose structure and function in initiation of DNA replication and DNA replication and DNA damage checkpoints are conserved throughout eukaryotic organisms (Makiniemi *et al.*, 2001; Garcia *et al.*, 2005). (Figure Adapted from Garcia *et al.*, 2005).

1.9 The role of TopBP1 in the DNA replication checkpoint

The third and fourth BRCT domains of Rad4 were shown to interact with phosphorylated Rad9 and this interaction was required for the activation of the Chk1 damage checkpoint as well as the recruitment of Crb2 to the site of damage (Carr *et al.*, 1995; Furuya *et al.*, 2004; Taricani and Wang, 2006). This was mirrored in studies using *S.cerevisiae* (Puddu *et al.*, 2008; Pfander and Diffley, 2011). In higher eukaryotes, that interaction is not dependent on DNA damage as Rad9 is constitutively phosphorylated (Greer *et al.*, 2003).

In human cells the interaction occurs between phosphorylated Rad9 and the first and second BRCT domains of TopBP1 and any mutation in the first domain cause a much more considerable reduction in the binding affinity between Rad9 and TopBP1 compared to the second domain. However, any mutation in the second BRCT domain in the presence of a mutant first BRCT domain causes an even lower synergistic drop of affinity for binding to the phosphorylated Rad9 tail than the first BRCT mutation alone suggesting a role of the both, not just one, domains in the interaction (Rappas *et al.*, 2011).

On the other hand, in human cells, the fifth BRCT domain has also been shown to be important for the recruitment of TopBP1 recruitment on to the sites of DNA damage and replication stress (Yamane *et al.*, 2002). The domain binds to Mdc1, a mediator protein which is involved in the γ H2AX Mdc1 signal cascade, to amplify the checkpoint response signal (Wang *et al.*, 2011, Leung *et al.*, 2013). The fourth and fifth BRCT domains, and their counterparts in other organisms, interact with 53BP1, and its homologs, and this interaction is required for a full G1 checkpoint response (Yamane *et al.*, 2002, Cescutti *et al.*, 2010). In *S. pombe*, Rad4 interacts with Crb2

using the first and second BRCT domains in a CDK dependent manner (Saka *et al.*, 1997, Du *et al.*, 2006).

In higher eukaryotes, the seventh and eighth BRCT domains have been found to be important in the checkpoint activation in response to replication stress and Chk1 activation (Cescutti *et al.*, 2010, Yan and Willis, 2013). This interaction causes the phosphorylation of Bach1 during the S-phase, which is required for the extension of RPA coated single stranded DNA leading to the activation of the checkpoint (Gong *et al.*, 2010; Leung *et al.*, 2011). Furthermore, those two domains appear to bind and activate ATR to facilitate the phosphorylation of ATR's downstream targets leading to the checkpoint response activation (Liu *et al.*, 2011).

The structure and folding of proteins are influenced by the temperature of the cellular microenvironment as a change in temperature could lead to a decrease in enzymatic activity, protein-protein interactions or the stability of protein complexes. Therefore, as a result, temperature sensitive mutants would survive at one permissive temperature but would not be viable at another restrictive temperature when compared to a wild type variant which would be viable at both temperatures. The temperature sensitive mutants carry at least one mutant gene which results in the malfunction of at least one protein or pathway at a defined temperature range. In temperature sensitive mutants, as a result of mutations occurring in genes encoding proteins required for the successful completion of cell cycle, specific stages of the cell cycle are either delayed or blocked leading to cell death in most cases. This concept is the basis of the methodical manipulation of strains to test the presence of these mutations and their lethality by growing the strains on media at different temperatures (Harvey *et al.*, 2003).

Fission yeast *cut* mutations disrupt coordination between M phase and cytokinesis, and cell division takes place in the absence of normal nuclear division (Samejima *et al.*, 1993). There are approximately 20 *cut* genes known, however, DNA synthesis is not inhibited in any *cut* mutants except *cut5* (Samejima *et al.*, 1993, Hirano *et al.*, 1986; Saka and Yanagida, 1993). TopBP1 colocalises with ATR, ATRIP and RPA (replication protein A) at sites of DNA replication stress (Makiniemi *et al.*, 2001; Garcia *et al.*, 2005). In one study, recruitment to these sites was dependent on the fifth BRCT domain, whereas in another study on the first and second BRCT domains (Yamane *et al.*, 2002; Delacroix *et al.*, 2007; Lee *et al.*, 2007). Once recruited to sites of DNA replication stress, TopBP1 interacts with ATR to stimulate its kinase activity (Kumagai *et al.*, 2006; Mordes *et al.*, 2008). In addition to its role as a checkpoint protein, TopBP1 also functions in the initiation of DNA replication; this latter function of TopBP1 is apparently independent of its checkpoint function (Hashimoto and Takisawa, 2003; Tanaka *et al.*, 2007; Zegerman and Diffley, 2007; Kumagai *et al.*, 2010).

1.10 TopBP1 role in ATR Activation

As previously discussed, TopBP1 assembles DNA damage sensors, mediators and effectors together on to the sites of DNA damage. In higher eukaryotes, TopBP1 can also stimulate ATRs kinase activity via its ATR Activation Domain (AAD) between the sixth and seventh BRCT domains (Kumagai *et al.*, 2006). The subsequent downstream Chk1 activation via phosphorylation has been shown to be enhanced when Claspin is added and recruited (Lindsey-Boltz and Sancar, 2011). TopBP1 also needs ATRs binding partner, ATRIP, to activate ATR as any mutation within the interacting domain within ATRIP confers sensitivity to HU and leads to loss of viability (Mordes *et al.*, 2008a).

In summary, TopBP1 activates ATR when replication forks are stalled by recruiting ATR-ATRIP and the 9-1-1 complex. ATR then auto-phosphorylates and phosphorylates ATRIP which then interacts with the N-terminus of TopBP1 to bring it closer to ATR activates it via an interaction between its AAD and the PRD present on the ATR. Finally, ATR phosphorylates TopBP1 leading to further stimulation of ATRs kinase activity and the full activation of the checkpoint response (Kumagai *et al.*, 2006; Yoo *et al.*, 2007; Burrows and Elledge, 2008; Mordes *et al.*, 2008b; Liu *et al.*, 2011; Lin *et al.*, 2012). That interaction is nearly identical in *S. cerevisiae* and *S.pombe*, highlighting the importance of the AAD and its role for the interaction with ATRIP and ATR (Navadgi-Patil *et al.*, 2011; Pfander and Diffley, 2011; Lin *et al.*, 2012).

1.11 The role of TopBP1 in DNA Repair

In *S. cerevisiae*, Dpb11 plays a role in DNA repair that is independent of its role in checkpoint activation. This was observed when the temperature sensitive *dpb11-1* mutant as the cells at the permissive temperature *dpb11-1* showed a repair defect when faced with DNA damage caused by MMS. Yet, the cells were seemingly able to activate their checkpoint response. This repair defect occurs within the homologous recombination pathway a normal reaction was observed using HU (Ogiwara *et al.*, 2006). A mutant of *dpb11-1*, *dpb11-PF*, was used to test the separation of function as the mutant functions competently in checkpoint activation and the initiation of DNA replication but shows increased levels of recombination at heteroallelic repeats and lower levels of direct repeats. This could be due to a shift from sister chromatid to interhomolog repair due to slower DNA repair kinetics. This also carries over to delayed kinetics in switching the mating type due to the delayed extension of the invading strand (Germann *et al.*, 2011; Hicks *et al.*, 2011).

However, other proteins required for the initiation of DNA replication are not required for repair DNA pathways such as GINS, Cdc45, MCM2-7 and Polymerase ϵ (Hicks *et al.*, 2011). In human cells, TopBP1 is required for homologous recombination as its depletion causes an increase to infrared radiation and mitomycin C which cause double strand breaks (Morishima *et al.*, 2007). TopBP1 acts a checkpoint protein that colocalises with ATR at sites of DNA replication stress. The recruitment of TopBP1 to sites of DNA replication stress is highly dependent on BRCT domains 1, 2, 7 and 8 with recruitment to sites of DNA double strand breaks is dependent on BRCT domains 1, 2, 4 and 5. A pathway that is activated by replication stress leads to activation of Chk1, thus, in turn promoting cell survival by preventing entry into

mitosis and then stabilising stalled replication forks to facilitate DNA repair (Chen and Sanchez, 2004).

1.12 The role of TopBP1 in the Initiation of DNA Replication

It has been shown that the essential function of TopBP1 and its homologs of initiating DNA replication (Masumoto *et al.*, 2000, Hashimoto and Takisawa, 2003). An early study showed *dpb11-1* in *S. cerevisiae* genetically interacted with DNA polymerase ϵ to show *dpb11-1*'s role in DNA replication (Araki *et al.*, 1995). It has been shown that the Dpb11 pathway included Sld1 (Polymerase ϵ), Cdc45, Sld3, Sld2 and Sld5 (Kamimura *et al.*, 1998; Wang and Elledge, 1999). More specifically, the interaction between Sld2 and Dpb11 has been shown to be CDK dependent interaction and is required for replication initiation (Masumoto *et al.*, 2002, Tak *et al.*, 2006). Activated Sld2 interacts with the third and fourth BRCT domains of Dpb11 and also binds to Polymerase ϵ and the GINS complex (Moyer *et al.*, 2006; Tak *et al.*, 2006). The GINS complex and the Dpb11-Sld2-Pol ϵ cluster combine to form the Pre-Loading Complex (Pre-LC) (Araki, 2011). Rad4 has been shown to act as a loading factor for Sld2, Sld3 and Mcm10 at the origins of replication and that interaction is not lost at the restrictive temperature for the cells carrying the *rad4-116* allele (Yabuuchi *et al.*, 2006; Taylor *et al.*, 2011).

Importantly, Sld3 is phosphorylated by CDK to be able to bind to the pre-RC complex with Cdc45 in a DDK dependent manner (Yabuuchi *et al.*, 2006; Tanaka *et al.*, 2007; Zegerman and Diffley, 2007; Heller *et al.*, 2011). The Cdc45-Sld3 complex is also essential for the interaction with Dpb11 and replication initiation (Tercero *et al.*, 2000, Kamimura *et al.*, 2001; Tanaka *et al.*, 2007; Zegerman and Diffley, 2007). Subsequently, GINS and Cdc45 interact with the MCM complex to create the active

CMG complex which loads Polymerase α and Polymerase δ for DNA replication can initiate (Moyer *et al.*, 2006, Araki, 2011). The Dpb11-Sld2-Sld3 cluster is then released from the origin when the CMG complex is formed and that also occurs in *S.pombe* (Masumoto *et al.*, 2002; Bruck *et al.*, 2011; Bruck and Kaplan, 2011; Taylor *et al.*, 2011).

In *S.pombe*, Sld2 is phosphorylated at the T111 site by CDK and interacts with the third and fourth BRCT domains of Rad4, whilst the phosphorylated Sld3 binds to the first and second BRCT domains. The Sld2 interaction with Rad4 actually enhances the Sld3 interaction with Rad4 allowing a better binding to Sld3 associated origins (Fukuura *et al.*, 2011). Furthermore, in human cells, the activated Treslin binds to the first and second BRCT domains of TopBP1 in a similar manner to the binding of the third and fourth BRCT domains of Dpb11 to Sld3, which can be interpreted as the switching of the BRCT tandems during evolution (Boos *et al.*, 2011). With regards to the essentiality sixth BRCT domain in higher eukaryotes, there are conflicting reports. Some studies show the requirement of the domain to function in replication while others report no replication alterations when the domain is removed (Makiniemi *et al.*, 2001; Yan *et al.*, 2006; Schmidt *et al.*; 2008).

In several organisms, due to the disruption of the interaction between Rad4 and Sld3, the firing of late or unfired origins is prevented in cells where DNA damage was detected (Santocanale and Diffley, 1998, Shirahige *et al.*, 1998, Larner *et al.*, 1999). For example, Rad53 phosphorylates Dbf4 and Sld3 after the S phase in *S. cerevisiae*, to disrupt the interaction between Cdc45 and Dpb11 (Lopez-Mosqueda *et al.*, 2010, Zegerman and Diffley, 2010). This also occurs in human cells as Chk1 activates Treslin via phosphorylation to prevent the interaction of Treslin with the first

and second TopBP1 BRCT domains (Boos *et al.*, 2011). In *S. cerevisiae*, another mechanism of the prevention of origin firing is by the competition of Ddc1 with Sld2 to bind to Dpb11 (Wang and Elledge, 2002).

1.13 The role of TopBP1 in the Regulation of Transcription.

In addition to its roles in the replication, replication checkpoint response and DNA damage response, TopBP1 also has a role in the regulation of transcription. In human cells, TopBP1 has a transcription activation domain as part of the fourth BRCT domain and two transcription repression domains in the fourth and fifth BRCT domains (Wright *et al.*, 2006).

Moreover, the sixth BRCT domain of TopBP1 has been shown to be involved on the regulation of expression of several genes by the interaction with transcription factors such as E2F-1, which is involved in the regulation of apoptosis (Qin *et al.*, 1994, Field *et al.*, 1996). TopBP1 has been shown to repress the transcriptional activity of E2F-1 by facilitating its interaction with the SWI/SNF chromatin remodelling family (Liu *et al.*, 2004). The interaction between TopBP1 and E2F-1 occurs at the G1-S boundary, to prevent apoptosis during DNA replication. A feedback loop is created at the G1/S phase transition when E2F-1 acts to induce TopBP1 activity (Liu *et al.*, 2004).

On the other hand, the sixth BRCT domain of TopBP1 has also been shown to interact with E2F-1 after DNA damage in a ATR/ATM dependent manner (Lin *et al.*, 2001). This also represses the transcriptional activity of E2F-1 to prevent the entry into S-phase and replication of damaged DNA (Liu *et al.*, 2003b). Interestingly, it has been shown that the seventh and eighth BRCT domains of TopBP1 act in the

prevention of E2F-1 mediated apoptosis in an AKT dependent manner (Liu *et al.*, 2006). Those same domains have been shown to bind to the tumour suppressor p53 to prevent the binding of p53 to promoter sequences of genes involved in the regulation of apoptosis in the cells (Liu *et al.*, 2009).

Several studies have shown the activity of TopBP1 in the inhibition of Miz1 which is a Myc-associated zinc finger protein involved in cell cycle regulation. Miz1 has been shown to activate the transcription of p21 in response to ultraviolet radiation-mediated DNA damage to arrest the cell cycle (Adhikary and Eilers, 2005). When the DNA damage occurs, TopBP1 dissociates from Miz1 leading to the induction of p21 (Herold *et al.*, 2002). Furthermore, the depletion of TopBP1 from cells has been shown to cause the activation of p21 and inhibition of cyclinE /CDK2 in the absence of p53 and activation of checkpoint function (Jeon *et al.*, 2007). A key player in the interaction between Miz1 and TopBP1 is ribosyltransferase PARP1 which interacts with the sixth BRCT domain of TopBP1 to impede the interaction TopBP1's interaction Miz1 after ultraviolet radiation-mediated DNA damage (Wollmann *et al.*, 2007).

Another role of TopBP1 is the regulation of viral transcription as reported with the Human Papilloma virus (HPV)'s transcription/replication factor E2 which controls the transcription and replication of the viral genome (Boner *et al.*, 2002). This is mediated by the sixth, seventh and eighth BRCT domains of TopBP1. On the other hand, using its first and second BRCT domains, has been shown to act to enhance viral replication and transcription (Boner *et al.*, 2002). The exact mechanisms of the interactions of TopBP1 with HPV's E2 remain elusive as the different activity of its

BRCT domains provide a contradictory response (Boner *et al.* 2002; Boner and Morgan 2002).

1.14 The role of TopBP1 in Disease

The links between TopBP1 and several types of cancer have been widely reported, yet, the exact role of its over or underexpression has been disputed. For example, TopBP1 has been linked to breast cancer in histological studies of breast carcinoma that showed that breast cancer samples showed cytoplasmic expression of the typically nuclear TopBP1. There were also samples showing no TopBP1 expression (Going *et al.*, 2007). Another study using RT-QPCR on breast cancer samples showed a similar result in terms of the prevalence of cytoplasmic TopBP1 as well as linking the reduction of TopBP1's expression to the hereditary type of breast cancer (Forma *et al.*, 2012). However, another study showed that higher expression of TopBP1 in breast cancer correlated with a worse prognosis with a higher tumour grade (Liu *et al.*, 2009). Another type of cancer linked to TopBP1, is non-small cell lung cancer, in which elevated levels of expression of TopBP1 correlated with a worse prognosis and an increased possibility of cancer metastasis to the brain (Seol *et al.*, 2011a; b).

The studies of polymorphisms in the region between the second and third BRCT domains and their link to cancer have yielded conflicting results. An increased risk of breast and ovarian cancer was reported to be linked to the heterozygous polymorphism leading to Arg309Cys. The Arg309cys polymorphism was linked to an elevated risk in breast and/or ovarian cancer in a screen of more than 100 Finnish families suffering from cancer (Karppinen *et al.*, 2006). That was later contradicted to show no correlation with the elevated risk of breast cancer in a much larger screen

of more than 1000 German breast cancer patients and 1000 controls (Blaut *et al.*, 2010). The original reported, of the Finnish study, was contradicted again as BRCA1 and BRCA2 mutation carriers with ovarian cancer showed no association with TopBp1 dysregulation (Rebbeck *et al.*, 2009). It can be deduced that this area of research needs to be further investigated in terms of trying to find the correlation between the expression of TopBP1, its localisation within the nucleus and cytoplasm as well as its polymorphisms on one side and cancer progression and patient survival. This also needs to be linked to TopBP1's interactions and functions that have been discussed previously.

1. 15 Rad4

Rad4 was discovered in 2 independent genetic screens in *S. pombe* with the first identification occurring as Rad4 in a screen using UV-sensitive mutants (Schupbach, 1971). Fifteen years later, the second identification was as a mutant with a "CUT" (Cell untimely torn) phenotype. CUT phenotypes occur when cytokinesis occurs with the presence of unsegregated chromatids, being separated by a septum within the nucleus (Hirano *et al.*, 1986). Both *cut5* and *rad4* were then shown to be the same gene and even though the screens showed that *rad4* had a role in the checkpoint response, the exact array of roles of Rad4 and its interactions remained unclear (Saka and Yanagida, 1993).

Afterwards, Rad4 was proven to have a dual role in the initiation of DNA replication and in the G1, S-phase and G2 checkpoints and that was found in both *S.pombe* and *S.cerevisiae* (Araki *et al.*, 1995; Garcia *et al.*, 2005). The name given to the Rad4 homolog in humans, TopBP1, was inspired by a two hybrid screen in human cells that showed that it interacted with Topoisomerase II β and it was named as

Topoisomerase II binding protein 1. It was also identified that the Rad4 is conserved across eukaryotes and that it is an essential gene as multicellular organism cells exhibit lethality when its function is disrupted (Yamamoto *et al.*, 2000, Jeon *et al.*, 2011).

Expression of the *cut* mutant phenotype requires the viable function of Cdc2, Cdc25 and Cdc3 which are all M phase regulators. This occurs due to the role of Rad4 in checkpoint control pathway and that role was characterised and developed over several studies by previous studies (Enoch and Nurse, 1990, 1991; Enoch *et al.*, 1992; Saka and Yanagida, 1993; Saka *et al.*, 1994; Sheldrick and Carr, 1993). Fission yeast *cut* mutations disrupt coordination between M phase and cytokinesis, and cell division takes place in the absence of normal nuclear division (Samejima *et al.*, 1993). There are approximately 20 *cut* genes known, however, DNA synthesis is not inhibited in any *cut* mutants except *cut5* (Samejima *et al.*, 1993, Hirano *et al.*, 1986; Saka and Yanagida, 1993).

1.16 The Temperature Sensitive Mutant

The *rad4-116* mutant is sensitive to ultraviolet light and ionising radiation and is thermo-sensitive at 37 °C. The gene codes for a 579-amino acid neutral protein with a zinc finger and localises in the nucleus (Duck *et al.*, 1976; Fenech *et al.*, 1991). Temperature-sensitive *cut5* mutants at the restrictive temperature (36 °C) block DNA replication but enter mitosis, producing the *cut* phenotype (Saka and Yanagida 1993), which strikingly differs from the arrest phenotype of temperature sensitive *cdc* mutations in DNA polymerase or ligase, or ribonucleotide reductase (Nurse *et al.* 1976; Gordon and Fantes 1986). The *rad4-116* allele mimics conditions of

replication stress in the absence of checkpoint function which makes it an attractive allele to utilise to study the genetic interactions of *rad4* (McFarlane *et al.*, 1997).

1.17 Fission Yeast Morphology

S.pombe is a rod-shaped unicellular eukaryotic organism which divides through medial fission. The dimensions of a normal wildtype *S.pombe* cell is a rod-shaped cell of 7 to 14 μm in length and 2 to 3 μm in diameter with the cell core as a centre point. Cell length and shape are strictly controlled and is directly coupled to the regulation of cell division. As previously mentioned, the time for each cycle of cell division is from 2 to 4 hours. In normal eukaryotic cells, the events of DNA replication and mitosis are ordered; the duplication of chromosomal DNA in S phase then the G2 phase followed by the M phase leading to cell division. One important aspect is that the exponential growth phase, G2, takes about 70% of the division time while each of the other phases take 10% of the division time. With nuclear division occurring in M phase, the new nuclei enter the G1 and S phases prior to cytokinesis. After that, the newly formed progeny are already in the G2 phase when the cell division is complete with a 2C DNA content as a G2 cell or as a binucleate G1 or S phase cell (Sabatinos and Forsburg 2010). The fission yeast cell cycle is summarised in Figure 1-4.

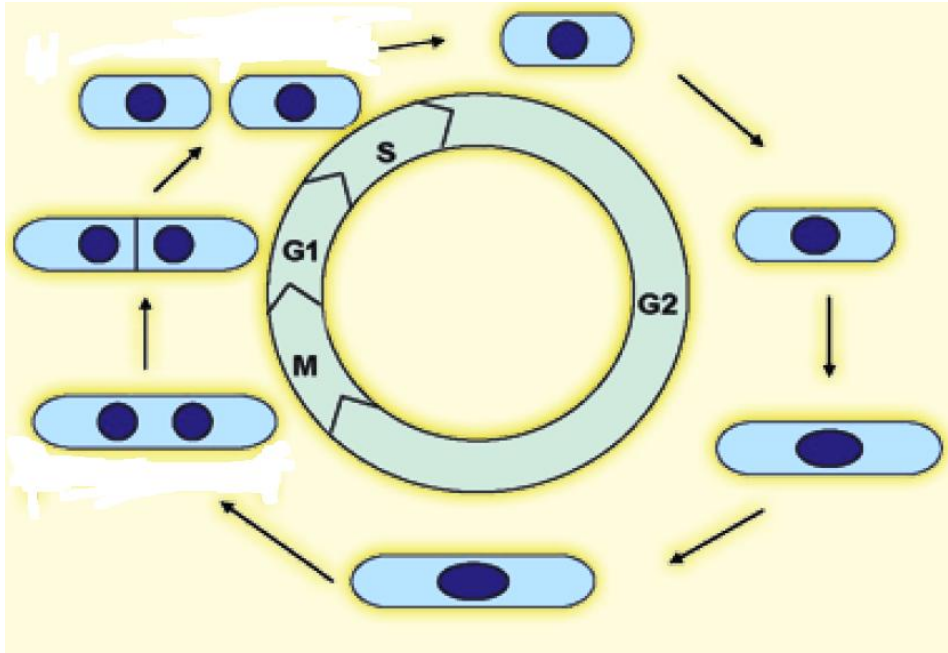


Figure 1-4 The cell cycle in the fission yeast. The fission yeast cell cycle have four sequential phases: G1, S, G2, and M phases. The fission yeast has a typical cell cycle with a long G2 phase which spans 70% of cell cycle and S, G1, and M phase are relatively short in a exponential growing population (Adapted from www.scienceinschool.org/2014/issue28/fungus_cancer).

In contrast to mammals and the budding yeast *S. cerevisiae*, which spend most of their time in G1 phase, wild-type *S. pombe* cells are mostly in the G2 phase and they can take up to 3 hours to complete a full cell cycle (Gómez and Forsburg 2004). Due to the short duration of the G1 period in *S. pombe*, cytokinesis is not completed until near the end of the S phase. This also causes the *S. pombe* haploid cells in the S phase are binucleate cells with 2C-4C DNA content. When the binucleate S phase cell divides through medial fission, each nucleus is directed to a separate cell surrounded by a distinct cell wall. Near the end of S phase, cells contain a 2C DNA content and are now G2 phase cells, ready to grow by polarised tip elongation. Due to their short G1 and S phases, *S.pombe* exhibit a higher degree of control over their cell cycle, cell growth at the G2/M transition compared to the other eukaryotes (Forsburg and Nurse, 1991; Egel, 2004).

As shown in Figure 1.4, the fission yeast life cycle is mostly haploid. Although *S. pombe* can form diploid cells after sporulation in a nitrogen limited environment after mating. The diploids, that exist transiently, go through meiosis and sporulation. Zygotic asci from coupled mating sporulation have a curved form whilst azygotic asci from endoreplicated have a straight linear shape. Under the influence of nitrogen starvation, strains of h+ and h- genotypes are crossed to mate, producing 4-spore tetrads which inherit genes from the parental strains. The tetrads are then examined for their phenotypes and viability via tetrad or random spore analysis; the former used to assess synthetically lethal interactions between distant genes while the latter for interactions between genes close to each other (Sabatinos and Forsburg 2010).

1.18 Fission Yeast as a model

The yeast *Schizosaccharomyces pombe* is a powerful model organism to study DNA replication and cell cycle control due to the conservation of these two mechanisms and the ease of its genetic manipulations (Simanis *et al.*, 1987; Hayles and Nurse, 1992; Nurse *et al.*, 1998). Fission yeast is a unicellular model organism widely used in molecular and cell biology. The *S. pombe* genome has three chromosomes that have been sequenced and showed to contain so far the smallest number of protein coding genes seen in a eukaryote, 4824 (Wood *et al.*, 2002).

The relatively small genome makes it an excellent tool for genetically manipulation. A number of cellular processes in *S. pombe*, such as DNA replication, nuclear signalling, centromeric, telomeric and epigenetic regulation are quite similar to what is observed in other eukaryotes. The first instance of *S. pombe* isolation was from beer from Africa, in turn giving it its namesake as the word "beer" in the Swahili language means "pombe". The link between cancer research and using *S.pombe* as a model is that about twenty *S.pombe* genes share homology and are directly linked with cancer pathology and progression (Wood *et al*, 2002),

Being especially true for cell cycle control and DNA replication and repair, many genes are conserved from *S.pombe* to higher eukaryotes and humans, making it valuable in the study of cellular networks and pathways involved in human pathology. The use of *S.pombe* as a model organism confers the ability to easily deactivate non-essential genes to be able to carry out genome-wide screens. These screens could be used to identify roles for novel genes or interactions between different genes and that is much easier by using the *S. pombe* genome-wide deletion library of over 3000 deletions of non-essential genes from Bioneer.

The life cycle of *S.pombe* as unicellular eukaryote shifts between vegetative asexual division and sexual reproduction stages with the limiting factor being its dependency on the availability of nutrients and growth factors. When carbon and nitrogen are readily available in the media, the cells replicate at a high rate as replicating haploid rod shape cells using asexual division. If there is a shortage of nutrients and growth factors, sexual reproduction of opposite *h* status cells occurs. The cells fuse as pairs by conjugation and exhibit nuclear fusion to form a diploid zygote. Meiosis then occurs as the zygote develops into an elongated tetrad composed of four haploid nuclei called ascospores. These spores remain dormant until the nutrients are available for them to germinate and enter the vegetative cycle again at the G1 phase (Egel, 2004).

Even though it is commonly compared to budding yeast, *S.pombe* possesses more characteristics that can be directly compared to human cells. A relevant example would be that, unlike budding yeast, replication origins in *S.pombe* consist of multiple sequences that are AT-rich sites without a defined sequence and that characteristic is shared with human cells (Clyne and Kelly, 1995; Paixao *et al.*, 2004). Another example would be that previous studies have shown that the loading of Cdc45 requires Rad4 in both *S.pombe* and human cells while the loading of Cdc45 in budding yeast is not dependent on Dpb11, the budding yeast homolog of TopBP1. (Kamimura *et al.*, 2001; Takayama *et al.*, 2003; Dolan *et al.*, 2004; Yabuuchi *et al.*, 2006). It can be deduced that the mechanism of Cdc45 loading appears to be conserved in *S. pombe* and thus, studies involving the interactions of Rad4 in fission yeast will be more relevant when presenting a model for genetic interactions for human cells. Fission yeast, in this study, acted a model for the identification of functional mechanisms involved in the maintenance of genome

stability if the initiation of DNA replication is compromised. The generation time of one cell cycle is short, about 2 to 4 hours, dependant on growth temperature, nutritional input and the relatively cheap laboratory related interference via the employed techniques, equipment and synthetic environment. These advantages combined with the technically easy manipulation of *S.pombe* make it an ideal model organism when utilised in studies of cell growth, division, differentiation, DNA replication, recombination and repair when compared to other eukaryotic organisms (Forsburg, 2003; Forsburg and Rhind 2006).

1.19 Synthetic Genetic Array Analysis

Synthetic Genetic Array Analysis(SGAA) is a rapid and high-throughput technique for the screening of the relationship between two genes within the genome. SGAA explores synthetically lethal and synthetically sick genetic interactions in which double mutants of specific genes lead to cell death. For identifying any synthetically lethal interactions, a query gene deletion mutant is crossed to an entire genomic deletion and yields progeny which carry functional information of the query gene and the genes that it interacts with (Tong *et al.*, 2001). The currently available therapeutic strategies in the form of chemotherapy and radiotherapy present problems with side effects due to their non specific lethal activity affecting both tumour and normal healthy cells. More recently, SGAA-tested synthetic lethality has become a popular potential target for the development of cancer therapeutics. This increase in popularity could be attributed to the fact that SGAA has the promise to provide therapeutic strategies whereby the chosen combination of targets are specific to the tumour cells compared to normal cells, thereby potentially reducing, if not eliminating, any adverse side-effects from off-target toxicity. In preliminary

experiments SGAA was used to analyse the genetic architecture supporting the function of fission yeast TopBP1 (Sung *et al.*, 2007). Using a *rad4-116* bait strain, a preliminary synthetic lethal screen against all viable *S. pombe* deletion mutants at 25°C was carried out as the *rad4-116* mutation was crossed to about 3000 non-essential *S. pombe* deletions. Then, the viability was measured and noted compared to that of the corresponding mutant library grown under the same conditions. A proportion of the double mutants failed to produce viable colonies which could be due to potential synthetic lethal interactions whilst others show a varied level of fitness.

Based on preliminary data of the SGAA, four genes were chosen for their synthetically lethal interactions to be tested. The genes chosen were previously implicated in genetic instability in the form of the resolution of stalled DNA replication fork, such as the *mrc1*, *swi1* and *swi3*, or the modification of chromatin such as *hip1*. The studies of functions of those genes are detailed in the sections below.

1.20 Hip1

During the S phase, nucleosomes are removed before the arrival of the replication machinery on the replication fork and then, nucleosomes are reassembled onto the newly synthesised DNA strand (Ransom *et al.*, 2010). The assembly or reassembly of nucleosomes is a step-wise process where a tetramer of two H3-H4 complexes are deposited followed by the addition of two H2A-H2B dimers flanking the tetramer (Park and Luger, 2008; Burges and Zhang, 2013). The assembly and removal of the nucleosomes also occur during transcription, recombination and repair and this is all mediated by the histone chaperone protein family (Ransom *et al.*, 2010).

Hip1 is one of the members of an evolutionary conserved family of histone chaperones that can act independently from replication (Eitoku *et al.*, 2008). Histone regulatory complex A HIRA is one of the major histone chaperones that are conserved in many eukaryotic organisms, with fission yeast possessing two HIRA related proteins in Slm9 and Hip1. Only one single HIRA protein exists in humans while there two in *S.pombe* as well as *S.cerevisiae* (Lamour *et al.*, 1995; Spector *et al.*, 1997; Kanoh and Russell, 2000; Blackwell *et al.*, 2004) The HIRA proteins in *S.pombe* are Slm9 and Hip1, a focus of this study.

Fission yeast HIRA proteins stably associate with two other proteins, Hip3 and Hip4 to form a tetrameric complex (Chujo *et al.*, 2012). Loss of the fission yeast HIRA complex components results in silencing defects in both mating type and centromeric loci. Hip interacts with Slm9 and becomes involved in centromere silencing and cell cycle delay (Blackwell *et al.*, 2004; Avvakumov *et al.*, 2011). Furthermore, it been reported that the *S.cerevisiae* HIR complex interacts with nucleosomes and prevents the remodelling activity of the SWI/SNF complex (Prochasson *et al.*, 2005). The

HIRA complex also been proven to be able to perform transcriptional silencing at both heterochromatic and euchromatic loci, including subtelomeric regions and LTR retrotranspos (Greenall *et al.*, 2006; Anderson *et al.*, 2009; Mizuki *et al.*, 2011; Yamane *et al.*, 2011). The loss of the HIRA complex function causes an increased susceptibility and sensitivity of cells to genotoxic agents that affect the genome. This indicates that HIRA is crucial in the protection of chromatin and chromatin architecture (Anderson *et al.*, 2009). An interesting observation is that HIRA can affect transcription regulation in a positive or a negative manner, as when fission yeast HIRA was required for the transcriptional activation of stress-responsive genes when faced with stress conditions at a low dose (Chujo *et al.*, 2012). The HIRA complex has been implicated in a wide range of processes including angiogenesis, embryonic development and ageing (Amin *et al.*, 2013).

1.21 Swi1 and Swi3

It has been shown that some factors are essential for DNA replication accuracy, but not DNA synthesis, as they travel with the moving replication fork. Two of those factors are Swi1 and Swi3 which are components of the fork stabilisation complex (FPC) (Lee *et al.*, 2004; Noguchi *et al.*, 2004; McFarlane *et al.*, 2010). Similar to Mrc1, Swi1 is required for the stable association of replisome components with sites of DNA synthesis in the presence of hydroxyurea (Katou *et al.*, 2003). The mechanism of Swi1 action is not known but the role for Tof1 in fork pausing may provide insights into its function at the fork (Calzada *et al.*, 2005; Lambert *et al.*, 2005; 2007). The absence of Swi1 or Swi3 in cells leads to the accumulation of abnormal fork structures as observed with increased Rad52 DNA repair foci formation and recombinations structures during the S phase (Noguchi *et al.*, 2003

a;b) . The Swi1-Swi3 complex directly interacts with the DNA structure and recruits Mrc1 to the replication fork (Shimmoto *et al.*, 2009; Tanaka *et al.*, 2010). The FPC also coordinates leading strand and lagging strand DNA synthesis as well as coordinating the DNA polymerase and helicase activity coupling at the replication forks (Dalgaard *et al.*, 2000; Noguchi *et al.*, 2004;McFarlane *et al.*, 2010). Swi1 contains a DDT domain, which is a domain of about 60 amino acids with three alpha helices typically found in DNA-binding proteins of, which is essential in its interaction with chromatin (Noguchi *et al.*, 2012).

Swi3 is a member of the replication fork protection complex in fission yeast with the Swi1-Swi3 complex being conserved in both budding yeast and mammalian cells (Rapp *et al.*, 2010). Swi3 is also required for stabilisation of replication forks, the activation of the replication checkpoint kinase Cds1 and the establishment of sister chromatid cohesion in fission yeast (Noguchi *et al.*, 2004; Tanaka *et al.*, 2010; Rapp *et al.*, 2010). Activation of the DNA damage response kinases in response to fork stalling agents requires the mediator protein Mrc1 (Alcasabas *et al.*, 2001; Chini and Chen, 2003; Kumagai and Dunphy, 2000; Tanaka and Russell, 2001) as it is present at replication forks even in the absence of DNA damage and is required for normal rates of progression of replication forks (Hodgson *et al.*, 2007; Petermann *et al.*, 2008; Szyjka *et al.*, 2005; Tourrière *et al.*, 2005). Swi3 is able to promote the efficient restart of stalled replication forks in a checkpoint-dependent manner as well as restoring broken replication forks in a checkpoint independent manner (Noguchi *et al.*, 2012).

1.22 Mrc1

Mrc1 is a conserved replication fork factor which is required for the stabilisation of stalled replication forks. In a manner independent of Cdc45 and Hsk1 kinase, it binds to early-firing origins (Hayano *et al.*, 2011). Furthermore, Mrc1 also functions as a replication checkpoint mediator that allows Rad3-Rad26 to activate the effector kinase Cds1 and also interacts with Swi1-Swi3 on stabilisation of stalled replication forks (Zhao and Russell 2004; Tanaka *et al.*, 2007). Activation of the DNA damage response kinases in response to fork stalling agents requires the mediator protein Mrc1 (Alcasabas *et al.*, 2001; Chini and Chen, 2003; Kumagai and Dunphy, 2000; Tanaka and Russell, 2001) as it is present at replication forks even in the absence of DNA damage and is required for normal rates of progression of replication forks (Szyjka *et al.*, 2005; Tourrière *et al.*, 2005; Hodgson *et al.*, 2007; Petermann *et al.*, 2008). In the presence of fork stalling agents, Mrc1 is required to prevent continued replisome progression in the absence of DNA synthesis (Katou *et al.*, 2003). Furthermore, it has been shown that in budding yeast, Mrc1 can bind to the catalytic subunit of the leading strand polymerase, Pol2. This Mrc1–Pol2 interaction is regulated by checkpoint kinase phosphorylation of Mrc1 (Lou *et al.*, 2008). It is interesting to consider that the binding of Mrc1 to the leading strand polymerase of the replication fork, combined with its role in checkpoint activation lends itself to a role in monitoring, signalling and regulating the progression status of the fork itself (Zegerman and Diffley, 2009).

1.23 Aims:

A vast collection of chemotherapeutic drugs act as fork stalling or DNA damaging agents and understanding the cellular response to such agents is crucial to appreciating their use in the clinic. As with a lot of anti-cancer treatments, the long-term efficacy of these drugs is greatly reduced by the methodical development of chemo-resistant mechanisms in cancer cells during treatment. It is interesting to note from research studies, especially, in yeast that several genes can be mutated to increase the survival of checkpoint deficient strains. The aim of the project is to identify the network of genetic interactions of *rad4* that affect its DNA replication and checkpoint functions leading to synthetically lethal phenotypes. These interactions will be explored with both *rad4* and *rad4-116*, the temperature sensitive *rad4* mutation, using molecular techniques. Once the strains are characterised, the *rad4* genetic interactions can be mapped.

These results would greatly enhance the understanding of the early steps of tumorigenesis and would be the basis of designing a parallel and perhaps, more explorative experiments in human normal and cancer cells for comparison. Based on this project as well as future related studies, it will be particularly important to know if mutations or deletions of such genes is a source or even the dynamo behind the emergence of drug-resistant tumours in human patients, which may ultimately provide insight into how to improve the chemotherapeutic strategies.

Chapter 2: Materials and Methods

2.1.1 Yeast Strains

The fission yeast strains used are listed in Table 2.1.

Strain Number	Genotype	Source
SPSC 120	<i>rad4-116 ura4-D18, leu1-32, ade6-M216 h+</i>	Collection
SPSC 573	<i>rad4-GFP::kanMX cdc25-22 ura3-D18 leu1-32 ade6 h-</i>	Collection
SPSC 1003	<i>ade6-M210 leu1-32 ura4-D18 mat1_m-cyhS mt0 rpl42::cyhR(sP56Q) rad4-116::NatMX h-</i>	Collection
SPSC 1005	<i>ura4-D18, leu1-32, ade6-704 h-</i>	Collection
SPSC 1006	<i>ade6-704 ura4-D18 leu1-32 h+</i>	Collection
SPSC 1011	<i>smc6 base :: ura4+ ade6-704 his7-366 leu1:: (leu1+_adh:hENT1) his7+adh1::hsv_TK nda3-KM311 smt0 h-</i>	Collection
SPSC 1017	<i>swi3Δ::KanMX h+ ade6-M216 ura4-D18 leu1-32 h+</i>	D.U. Kim et al (2010)
SPSC 1018	<i>mrc1Δ::KanMX ade6-M216 ura4-D18 leu1-32 h+</i>	D.U. Kim et al (2010)
SPSC 1026	<i>ade6-M216 leu1-32 ura4-D18 hip1Δ::KanMX h+</i>	Collection
SPSC 1029	<i>rad4::NatMX ura4-D18 h-</i>	Collection
SPSC 1047	<i>swi3Δ::KanMX ura4D-18 leu1-32 ade6- h-</i>	This

		project
SPSC 1048	<i>mrc1Δ::KanMX ura4D-18 leu1-32 ade6- h-</i>	This project
SPSC 1049	<i>hip1Δ::KanMX ura4-D18 leu1-32 h-</i>	This project
SPSC 1051	<i>swi1Δ::KanMX h+ ade6-M216 ura4-D18 leu1-32 h+</i>	D.U. Kim et al (2010)
SPSC 1056	<i>ade6-704 ura4-D18 leu1-32 rad52-GFP::KanMX6 h-</i>	Collection
SPSC 1063	<i>ade6-704 ura4-D18 leu1-32 rad52-GFP::KanMX6 mrc1::KanMX</i>	This project
SPSC 1064	<i>ade6-704 ura4-D18 leu1-32 rad52-GFP::KanMX6 swi3::KanMX</i>	This project
SPSC 1065	<i>ade6-704 ura4-D18 leu1-32 rad52-GFP::KanMX6 hip1::KanMX</i>	This project
SPSC 1073	<i>ade6-(704 or 210) ura4-D18 leu1-32 rad52-GFP::KanMX6 mat1_m-cyhS, smt0; rpl42::cyhR (sP56Q) rad4-116::NatMX h-</i>	This project
SPSC 1095	<i>ura4-D18, leu1-32, ade6-704 leu1::hip1::SV5(x3)::ura4+ h-</i>	This project
SPSC 1096	<i>ura4-D18, leu1-32, ade6-704 leu1::swi1::SV5(x3)::ura4+h-</i>	This project
SPSC 1097	<i>ura4-D18, leu1-32, ade6-704 leu1::swi3::SV5(x3)::ura4+h-</i>	This project
SPSC 1098	<i>ura4-D18, leu1-32, leu1::swi1::SV5(x3)::ura4+swi1Δ::KanMX</i>	This

	<i>h-</i>	project
SPSC 1099	<i>ura4-D18, leu1-32, leu1::swi1::SV5(x3)::ura4+swi1Δ::KanMX rad4-116 h+</i>	This project
SPSC 1100	<i>ura4-D18, leu1-32, leu1::hip1::SV5(x3)::ura4+ hip1Δ::KanMX h-</i>	This project
SPSC 1101	<i>ura4-D18, leu1-32, leu1::swi3::SV5(x3)::ura4+swi3Δ::KanMX h-</i>	This project
SPSC 1102	<i>leu1::swi3::SV5(x3)::ura4+ura4-D18, ade6-704 swi3Δ::KanMX rad4-116 h-</i>	This project
SPSC 1103	<i>leu1::hip1::SV5(x3)::ura4+ura4-D18, ade6-704 hip1Δ::KanMX rad4-116 h-</i>	This project
SPSC 1104	<i>leu1::swi3::SV5(x3)::ura4+ura4-D18, ade6-704 swi3Δ::KanMX rad4-116 h+</i>	This project
SPSC 1105	<i>leu1::hip1::SV5(x3)::ura4+ura4-D18, ade6-704 hip1Δ::KanMX rad4-116 h+</i>	This project
SPSC 1106	<i>rad52-GFP::KanMX6 leu1::swi1::SV5(x3)::ura4+ura4-D18, ade6-704 swi1Δ::KanMX rad4-116::NatMX</i>	This project
SPSC 1108	<i>rad52-GFP::KanMX6 leu1::swi3::SV5(x3)::ura4+ura4-D18, ade6-704 swi3Δ::KanMX rad4-116::NatMX</i>	This project
SPSC 1110	<i>rad52-GFP::KanMX6 swi1Δ::KanMX ura4-D18 leu1-32</i>	This project
SPSC 1112	<i>rad52-GFP::KanMX6 leu1::hip1::SV5(x3)::ura4+ ura4-D18, ade6-704 hip1Δ::KanMX rad4-116::NatMX</i>	This project
SPSC 1114	<i>leu1::mrc1::SV5(x3)::ura4+ura4-D18, ade6-704 h-</i>	This project

SPSC 1115	<i>leu1::mrc1::SV5(x3)::ura4+ura4-D18, ade6-704</i> <i>mrc1Δ::KanMX h-</i>	This project
SPSC 1116	<i>leu1::mrc1::SV5(x3)::ura4+ura4-D18, ade6-704</i> <i>mrc1Δ::KanMX rad4-116</i>	This project
SPSC 1117	<i>rad52-GFP::KanMX6 leu1::mrc1::SV5(x3)::ura4+ura4-D18,</i> <i>ade6-704 mrc1Δ::KanMX rad4-116::NatMX</i>	This project

Table 2.1 showing the *S. pombe* strains utilised with the corresponding genotype.

The strains obtained from the Bioneer library are described in this paper (D.U. Kim *et al.*, 2010).

2.1.2 Plasmids

Table 2.2 summarises the plasmids used in this study.

Plasmid Number	Description
240	<i>pACT2</i>
778	<i>pACT-rad4</i>
779	<i>pACT-rad4-116</i>
781	<i>pCRTM-Blunt II-TOPO®-mrc1 (A3)</i>
782	<i>pCRTM-Blunt II-TOPO®-mrc1 (A6)</i>
784	<i>pCRTM-Blunt II-TOPO®-swi3</i>
785	<i>pCRTM-Blunt II-TOPO®-rad4 (1)</i>
786	<i>pCRTM-Blunt II-TOPO®-rad4 (2)</i>
787	<i>pCRTM-Blunt II-TOPO®-rad4 (3)</i>
788	<i>pCRTM-Blunt II-TOPO®-rad4 (4)</i>
789	<i>pCRTM-Blunt II-TOPO®-rad4 (5)</i>
793	<i>pCRTM-Blunt II-TOPO®-rad4-116::NatMX (1)</i>
794	<i>pCRTM-Blunt II-TOPO®-rad4-116::NatMX (2)</i>
807	<i>pINTL rad4-PkC</i>
808	<i>pINTL mrc1-PkC</i>
809	<i>pINTL swi1-PkC</i>
810	<i>pINTL swi3-PkC</i>
811	<i>pINTL hip1-PkC</i>

Table 2.2 showing the plasmids utilised with the corresponding description.

2.2.1 Media

Cultures are usually initiated on rich media and replica plated to test markers on selective media. The recipes for the media and solutions are detailed in the Nurse laboratory manual. A list of the different media used can be found in the Table 2.3. A list of buffers and recipes can be found below in Table 2.4.

YES (yeast extract with supplements)	0.5 g/100 ml yeast extract, 3 g/100 ml glucose, 0.2 mg/l adenine, 0.2 mg/l uracil, 0.2 mg/l leucine, 0.2 mg/l lysine, 0.2 mg/l histidine ddH ₂ O to 1 l (20 g agar for solid media)
2XTY medium	1.6 g/100 ml tryptone, 0.5 g/100 ml sodium chloride, 1 g/100ml yeast extract, ddH ₂ O to 1 l (14 g agar for solid media)
2XTY medium with selective markers	1.6 g/100 ml tryptone, 0.5 g/100 ml sodium chloride, 1 g/100 ml yeast extract, ddH ₂ O to 1 l (14 g agar for solid media) (with 200 µg/ml neursceothricin[NAT] or 200 µg/ml kanamycin or Ampicillin 200 µg/ml added afterwards)

Table 2.3 showing media recipes

2.2.2 Buffers and Solutions

TAE (50x)	242 g Tris base, 57.1 ml glacial acetic acid, 100 ml 0.5 M Na ₂ EDTA (pH 8.0) ddH ₂ O to 1 l
10x SDS-PAGE Running Buffer	30 g Tris base, 144 g glycine, adjust pH to 8.3 and add ddH ₂ O to 1 l with 10%v/v of 10% SDS added to make the 1X buffer
Transfer Buffer	48 mM Tris-Base, 39 mM Glycine, Methanol 20%
Coomassie Stain	450 ml methanol, 100 ml glacial acetic acid, 1 g Coomassie Blue Stain Powder (BioRad) and add ddH ₂ O to 1 l
Coomassie Destain Solution	10% v/v methanol, 10% v/v acetic acid, dd H ₂ O
LiAc/EDTA	1.02 g LiAc, 100 ml distilled H ₂ O, 200 µl of 0.5 M EDTA and the solution filter sterilised
PEG solution	1.02 g LiAc was added to 50ml distilled H ₂ O, 200 µl of 0.5 M EDTA was added and adjusted to pH 4.9 with acetic acid. 40 g PEG 4000 was added and the solution filter sterilised
PEM buffer	100 mM PIPES, 1 mM EGTA, 1 mM

	MgSO ₄ : 1.73 g PIPES was dissolved in 45 ml sterile water and adjusted to pH to 6.9. 19 mg EGTA and 12.3 mg MgSO ₄ were added.
PEMS Buffer	100 mM PIPES, 1 mM EGTA, 1 mM MgCl ₂ , 1.2 M Sorbitol. Solution was adjusted to pH 6.9 with NaOH and filter sterilised.
PEMBAL Buffer	100 mM PIPES, 1 mM EGTA, 1 mM MgCl ₂ , 1 g/100 ml BSA, 0.1 g/100 ml NaN ₃ and 100 mM Lysine. Solution was adjusted to pH 6.9 with NaOH and filter sterilised
30 % Paraformaldehyde	15 g paraformaldehyde was dissolved in 50 ml PEM solution in a 65 °C waterbath for 5 minutes. 300 µl of NaOH was then added to the mixture.

Table 2.4 showing the recipes for buffers and solutions used.

2.3 *Schizosaccharomyces pombe* Methods

Most of the methods for *S. pombe* culturing, experimentation and strain manipulation are described in the Nurse laboratory manual as well as review by Susan Forsburg (Forsburg and Rhind, 2006) and the study by Moreno and colleagues (Moreno *et al.*, 1991). Where modifications were made, these are described below.

2.3.1 *S.pombe* Strain Construction

As part of the preparative work for the experimental procedures and genetic analysis, especially designed *S.pombe* strains were constructed. This was achieved by mating two strains with the desired genes, which have specific markers or reporter genes in the form of antibiotic resistance, supplement deficiency or temperature sensitivity for growth. The resulting colonies were analysed by either tetrad dissection through micromanipulation or random spore analysis. Then, colonies were replicated onto selective media and the colonies with the desired genes selected and grown again on selective media to ensure the presence of the desired genes. The strain was then allowed to grow on non-selective YES, assigned a number and frozen at -80 °C in 20%v/v glycerol for future reference. When strains were taken out of the collection or when strains were obtained from an external source, the strains with gene deletions were checked using colony PCR with the PCR conditions as detailed in Section 2.4.1. A universal 3' primer (CLI 724) was used to check the G418 resistance used to substitute the gene sequence combined with a site specific primer as detailed in Table 2.5. The sequences for the primers used in gene deletions in strain checking are detailed in Table 2.6.

Gene Deletion tested	Primers
<i>swi1</i> Δ	CLI 724, CLI 1117
<i>swi3</i> Δ	CLI 724, CLI 1106
<i>hip1</i> Δ	CLI 724, CLI 1118
<i>mrc1</i> Δ	CLI 724, CLI 1115

Table 2.5. The combinations for primers used in gene deletion testing corresponding to the gene deletion being tested.

Primer Code	Primer Sequence
CLI 724	ATTCCGACTCGTCCAACATCAA
CLI 1106	GCGAGCACTATCACTCAAATACG
CLI1115	GGCTTGAGAGTTATTCTGAGGC
CLI 1117	GTCGGGATTTCAAACCCC
CLI 1118	CTGTTATTACAAGGAAGGACGTGGTTTC

Table 2.6. The sequences for primers used in gene deletion testing.

A V5-tagged version of each experimental gene (*hip1*, *swi1*, *swi3* and *mrc1*) under transcriptional control of the *nmt81* promoter was created. This was achieved by first constructing a plasmid coding for the *nmt81* controlled gene tagged with 3 repeats of V5 tag using the primers detailed in Table 2.7 and restricting the plasmid using *NotI* with the conditions detailed in Section 2.4.4. The digested DNA fragment was used to transform the base strain SPSC 1005, as detailed in Section 2.3.6, for the sequence to be integrated at the *leu1* locus following the methodology described in (Fennessy *et al.*, 2014). The V5- tagged allele was tested in the transformed strains using colony PCR using the conditions detailed in Section 2.4.1 and using the primers detailed in Table 2.8.

Primer Code	Primer Sequence	Gene
CLI 1207	ATAGTCGCTTTGTTAAATCATATGGCATCTTTAGACGAGAACGC	5' <i>mrc1</i>
CLI 1208	GGGTTAGGAATACCCATACCC GTCAAAGTCCGAGTAATTATTC	3' <i>mrc1</i>
CLI 1210	ATAGTCGCTTTGTTAAATCATATGTCTACAGCTGCTTCTGATTTCAGG	5' <i>swi3</i>
CLI 1211	GGGTTAGGAATACCC ATACCC AAGACAACGATACCCAATTAGAA	3' <i>swi3</i>
CLI 1213	ATAGTCGCTTTGTTAAATCATATGAAAATTAATAAAAAATTCCATGGTTA GG	5' <i>hip1</i>
CLI 1214	GGGTTAGGAATACCCATACCCGGTTGATGCGTATTTTTCTATTAA	3' <i>hip1</i>
CLI 1222	ATAGTCGCTTTGTTAAATCATATGGAATTAGATGAGGTGATTC	5' <i>swi1</i>
CLI 1223	GGGTTAGGAATACCCATACCCATCCGATGAAGAATTCTCGC	3' <i>swi1</i>

Table 2.7. The Primers used in the cloning of genes into the *pINTL* plasmid for V5 tagging.

Primer Code	Primer Sequence	Primer Test Position
CLI 1225	ATGGTAGGATACGAGTTCCA	5' <i>leu1</i> sequence
CLI 1226	CCGCTGATGACTTATTCTGTC	3' <i>nmt</i> sequence

Table 2.8. The Primers used in the testing of transformed strains after the integration of V5 tagged alleles.

2.3.2 Spore microdissection

Cells were mated on ME agar by crossing h+ and h- strains and adding sterile water. The plates were incubated at 26 °C for 3-5 days for growth and sporulation to form zygotic asci, which were picked for tetrad dissection. After sporulation, a loop of crossed cells was streak on fresh YES or EMM plates to pick individual asci and place each spore in a grid matrix using the microdissection microscope Singer MSM System Series 400 (Singer Instruments). The four spores of the zygotic ascus were placed each at a unique position in a straight line using the micromanipulator. The plates were then incubated at 26 °C. After colony formation, the plates were replicated onto YES and more importantly, selective plates of YES with an antibiotic or EMM without specific supplements using filter paper (Whatman). When the spores grow after incubation at 26 °C, the plates are photographed using a ChemiDoc (BioRad) for scoring and following genetic patterns. The desired genetic backgrounds for each colony was confirmed using PCR analysis. The viability of colonies on each plate was noted and total viable colonies were counted to calculate percentage viability and to exam the possibility of synthetic lethality by using the Chi-Square Test.

2.3.3 Random Spore Analysis

Random spore analysis was used to assess synthetic lethality between genes which are located near each other at the same chromosome. Strains were mated on ME plates and incubated at 26 °C for 3 days for growth and sporulation to form zygotic asci. The efficiency was checked by microscope and a loop of cells was resuspended in 1 ml of sterile water. 1 µl of Helix Pomatia Juice (Sigma Aldrich) was added and the spores were incubated over night at room temperature. Spores were counted using a Haemocytometer, diluted and a set numbers of spores were plated onto YES plates and in some cases, selective media. After colony formation, the plates were replicated onto YES and more importantly, selective plates of YES with an antibiotic or EMM without specific supplements. The desired genetic backgrounds for each colony was confirmed using PCR analysis. The viability of colonies on each plate was noted and total viable colonies were counted to calculate percentage viability and to exam the possibility of synthetic lethality by using the Chi-Square Test (Sabatinos and Forsburg 2010).

2.3.4 Statistics

The Chi-Square test was used to assess the possibility of synthetic lethality in experimental crosses. The viable cells or spores carried double drug-resistance markers, linked to genes, were counted as true observed value [O] while the expected value [E] was either calculated depending on the genetic segregation of each cross in most cases or in rare cases, as 25% of the total valid cells which include both the viable cells and the dead or unviable cells. Unviable cells are caused by either synthetic lethality or as errors in growth due to media content or micromanipulation errors, in these cases, the Chi-square test eliminates the possibilities of anything but death from synthetic lethality. The general formulae for the calculation of the Chi-square value is as follows:

$$\chi^2 = \sum \frac{(\text{Observed Value} - \text{Expected Value})^2}{(\text{Expected Value})}$$

The probability associated with the value obtained from this test can be compared to a set of values from a χ^2 table for [n-1] degrees of freedom where [n] is the number of categories. For example, in the cases where the degree of freedom value is 1, if the χ^2 value is greater than 3.84, it can be deduced that the difference between the observed and expected value is statistically significant [$p \leq 0.05$] and vice versa.

2.3.5 *S. pombe* Standard Chromosomal DNA preparation

Cells were grown in 10ml YES at 30 °C over night, pelleted (5 minutes, 3000 rpm, room temperature) and resuspended in 1ml buffer SP11.2 M (Sorbitol, 50 mM Sodium Citrate, 50 mM Sodium Phosphate, 40 mM EDTA, adjust pH to pH 5.6, ddH₂O to 1 l) containing 1mg/ml Zymolyase T20 (Seikagaku corporation). Cells were incubated at 37 °C for 15-30 minutes and spheroplasting was monitored by microscope by adding 5% SDS. After 95% digestion was complete, spheroplasts were pelleted (5 minutes, 3000 rpm, room temperature) and resuspended in 450 µl 5xTE, 50 µl of 10% SDS were added and incubated for 5 minutes at room temperature. 150 µl of 5 M potassium acetate (KAc) were added and the samples were incubated for 10 minutes on ice. Samples were pelleted and the supernatant was transferred to a new eppendorf tube. 1 volume of isopropanol was added, incubated on ice for 10 minutes and pelleted again. The pellet was washed with 500 µl 70% ethanol and dried. If the samples were used for PCR analysis, the pellet was resuspended in 250 µl 1xTE and 5 µl of 10mg/ml Ribonuclease A were added. If the DNA was used for restriction fragment length analysis by Southern blotting, the pellet was resuspended in 250 µl 5xTE and 5 µl of 10 mg/ml Ribonuclease A were added. The pellet was incubated at 37 C for 20 minutes to facilitate resuspending. 2 µl of 10% SDS and 20 µl of 5 mg/ml Proteinase K were added and the samples were incubated at 55 °C for 1 hour. The DNA was extracted twice by Phenol chloroform extraction; 500 µl of Phenol:chloroform:isoamyl alcohol were added and the solution was mixed by gentle vortexing. The DNA was pelleted and the upper phase (aqueous phase containing the DNA) was transferred to a new eppendorf tube. After the second extraction, the DNA was precipitated by adding 1/10 volume of Potassium acetate and 1 volume isopropanol and the mixture was incubated on ice

for 10 minutes. The sample was pelleted, washed with 500 μ l 70% ethanol, pelleted again and the pellet was resuspended in 30 μ l 1xTE and incubated at 37 °C for 20 minutes.

2.3.6 Lithium Acetate Yeast Transformation

S. pombe cells were transformed using the lithium acetate transformation method as described by Okazaki and coworkers (Okazaki *et al.*,1990). The technique was modified and the full protocol is detailed in this section. Parental yeast strains were streaked from frozen glycerol stocks onto pre-warmed YES agar plates and allowed to grow at 30 °C for 48 hours before an isolated colony was used to inoculate a 2 ml culture of YES liquid media (unless stated otherwise). This culture was placed at 30 °C with gentle shaking overnight. The overnight culture was then used as the starter culture to seed a 50 ml to 100 ml. Once the OD 600 reached 0.8 , the remainder of the culture was transferred to a 50 ml Falcon tube and centrifuged at 2000 rpm for 2 minutes. The supernatant was decanted and the pellet was resuspended by shaking with 25 ml of sterile water before being centrifuged at 2000 rpm for 2 minutes. The supernatant was removed and the cell pellet was resuspended in 1 ml of sterile 100 mM LiAc (pH 7.4) before being transferred to a sterile 1.5 ml eppendorf tube. The cells were then pelleted at 14000 rpm for 30 seconds and the supernatant was discarded. 1% of the final culture volume of 100 mM LiAc (pH 7.4) was then used to resuspend the pellet. This cell suspension was then equally distributed between the appropriate number of eppendorf tubes depending on the remaining culture volume after having checked the OD periodically, each tube was then centrifuged at 14000 rpm for 1 minute and the supernatant was discarded. Without disturbing the pellet the following were sequentially added; 240 μ l of 50% (w/v) PEG-3350, 36 μ l sterile 1

M LiAc (pH 7.4), The appropriate PCR product mixed with 100 ng of linearised vector in sterile water or 100 ng plasmid DNA suspended in sterile water and 10 μ l boiled and snap-cooled salmon sperm DNA (2 mg/ml) (unless otherwise noted). A sterile toothpick was then used to gently loosen the pellet and the solution was then vortexed at high speed for 1 minute. The cell suspension(s) were then placed at 30 °C for 30 minutes before being heat shocked at 42 °C for 15 minutes in a water bath. After a 1-minute recovery, the cells were centrifuged at 7000 rpm for 1 minute. The supernatant was discarded and the pellet was gently suspended in 100 μ l sterile water. This was then spread onto the appropriate selective media using sterile glass beads. The plates were placed at 30 °C for 2-3 days depending on the strain. Finally, the resulting transformants were streaked for isolated colonies onto the appropriate selective media and allowed to grow at 30 °C until individual colonies could be selected for further use.

2.3.7 Hydroxyurea Block and Release

Cells were grown in YES to mid-log phase to the same OD as measured by a spectrophotometer (typically $\sim 6 \times 10^6$ cells/ml). Fresh 1 M hydroxyurea was made up in YES and then added to the growing cultures to reach 10 mM final hydroxyurea concentration at a dilution factor of 1:100. At the 0 timepoint and after growth in hydroxyurea, the cells were precipitated by spinning down in centrifuge at 4000 rpm. Then the supernatant was discarded and the pellet washed twice with sterile water. The cell pellets were then used for the immunofluorescence protocol.

2.3.8 Fluorescence Microscopy

Cells were prepared for microscopy by fixing in 70% v/v ethanol. Welled microscope slides were used. The wells were filled with 30 g/100 ml agarose solution in sterile water. The agarose solution was boiled for 4 minutes then kept in a 70 °C waterbath. The cells were then placed on the agarose-filled wells of the glass microscope slide. A solution of $\mu\text{g/ml}$ 4',6-diamidino-2-phenylindole (DAPI) and Vectashield (Vector) is then added to each well. DAPI binds strongly to DNA and is excited by ultraviolet light which then emits as a blue/violet colour. The coverslip was sealed with clear nail varnish and the cells visualised. Cells were observed using the Applied Precision Deltavision microscope and the images were deconvolved using the deconvolution software.

2.3.9 Immunofluorescence

The immunofluorescence technique is described in the paper by Hagan and Hyams (Hagan and Hyams, 1988). 5.5 ml 30% paraformaldehyde was added to 10 ml cells with 6 ml of 2.5 M Sorbitol and the sample was incubated at room temperature on a rotating wheel for at least 90 minutes. The cells were harvested at 4000 rpm for 4 minutes and the supernatant discarded. The cells were washed briefly in 1 ml PEM solution and 1 wash in 1 ml PEMS solution with spins between washes at 4000 rpm for 2 minutes. The cell pellet was then re-suspended in 1 ml PEMS containing 1.25 mg/ml Zymolyase T 20 (Seikagaku corporation) and incubated at 37 °C until the cells wall had become digested. The sample was washed by centrifugation at 4000 rpm for 1 minute and the supernatant discarded. The cells were washed 1 x 1 ml PEMS containing 1% triton, 1 ml PEM and 1 ml PEMBAL. The cell pellet was then resuspended in 1 ml PEMBAL and incubated at room temperature for 1 hour on a rotating wheel. The primary antibody was added to the cells and left overnight at room temperature on the rotating wheel. The following day, the cells were washed twice in 1 ml PEMBAL with a spin at 4000 rpm for 1 minute in-between washes. The cells were then centrifuged for 3 minute at 4000 rpm and the cell pellet re-suspended in 100 µl PEMBAL with secondary antibody. The sample was then wrapped in saran wrap and aluminium foil and incubated at room temperature for 3 hours on a rotating wheel. The cells were washed in 3 times in PEM then resuspended in PBS. Welled microscope slides were used for fluorescent microscopy as detailed in section 2.3.8.

2.4.1 Polymerase Chain Reaction (PCR)

Specific genes or DNA fragments were amplified from genomic DNA or plasmid DNA as follows:

Component	50 μ l Reaction	Final Concentration
Nuclease-free water	Up to 50 μ l	
10 μ M Forward Primer	2.5 μ l	0.5 μ M
10 μ M Reverse Primer	2.5 μ l	0.5 μ M
Template DNA	variable	< 250 ng
DMSO	1.5 μ l	3% v/v
2X Phusion Flex Master Mix	25 μ l	1X

Table 2.9 showing the components of the PCR reaction.

A no DNA control was run alongside samples, substituting the DNA template for 1µl of ddH₂O. Thermocycling conditions for a routine PCR:

STEP	TEMPERATURE	TIME
Initial Denaturation	98 °C	30 seconds-3 minutes
25-35 Cycles	98 °C 45-72 °C 72 °C	5-10 seconds 10-30 seconds 15-30 seconds per kb
Final Extension	72 °C	5-10 minutes
Hold	4 °C	

Table 2.10 showing the cycle conditions of the PCR reaction.

2.4.2 Cloning and Transformation of plasmids into *E.coli*

The cloning and transformation kit was obtained from Thermo Fisher and the reactions were performed according to the manufacturer's instructions. The following procedure was used to perform the TOPO® Cloning reaction. The genotype for the TOP10 *E.coli* strain used in the kit was *F- mcrA Δ(mrr-hsdRMS-mcrBC) Φ80lacZΔM15 Δ lacX74 recA1 araD139 Δ(araleu)7697 galU galK rpsL (StrR) endA1 nupG*. The TOPO® Cloning reaction was set using the reagents in the order shown in table 2.11

Reagent	Volume in 6 µl Reaction
Fresh PCR product	0.5–4 µl
Salt Solution	1 µl
pCR™II-Blunt-TOPO	1 µl
Sterile water	Up to a final volume of 6 µl

Table 2.11 showing the components of the TOPO® Cloning reaction.

The reaction was mixed gently and incubated for 5 minutes at room temperature. The reaction was then placed on ice and 2 µl of the TOPO® Cloning reaction was added into a vial of One Shot Chemically Competent *E. coli* and mixed gently. The

cells were incubated on ice for 30 minutes then heat-shocked for 30 seconds at 42 °C without shaking. The tubes were immediately transferred to ice 250 µl of room temperature S.O.C. medium was added to the reaction. The tubes were capped tightly and shaken horizontally at 200 rpm at 37 °C for 1 hour in a shaking incubator. After the incubation, 50 to 300 µl from each transformation was spread on a prewarmed selective plate and incubated overnight at 37 °C.

2.4.3 Purification of plasmid DNA using the QIAprep Spin Miniprep Kit.

The plasmid DNA extraction and purification kit was obtained from Qiagen and the reactions were performed according to the manufacturer's instructions. For each plasmid DNA purification single colonies from overnight transformation plates were used to inoculate 5 ml of LB with appropriate selection and incubated overnight at 37 °C with shaking. Cells were pelleted by centrifugation at 5000 x *g* for 10 minutes at 4 °C. The supernatant was removed and the plasmid DNA was purified according to manufacturer's instructions.

2.4.4 Restriction Digests

All of the restriction enzymes were obtained from New England Biolabs and the reactions were performed according to the manufacturer's instructions in terms of restriction temperature, duration and deactivation protocols. To confirm successful cloning 20 µl digest reactions were performed with the appropriate restriction enzymes and their corresponding buffer(s). Reactions were set up with approximately 1 µg of DNA, 5 units of each desired restriction enzyme, 100 ng of ribonuclease (to degrade RNA, which could hinder DNA migration in an agarose gel), and made to volume with ddH₂O. Reactions were incubated at 37 °C for up to 3 hours. In preparation for extraction of DNA fragments from agarose gels restriction digests were performed as above, but in a reaction volume of 50 µl with approximately 4 µg of DNA and 20 units per restriction enzyme, and omitting the ribonuclease.

2.4.5 DNA ligation with T4 DNA Ligase

The DNA ligation kit was obtained from New England Biolabs and the reactions were performed according to the manufacturer's instructions. The following reaction was set up in a microcentrifuge tube per sample on ice as shown in table 2.12.

COMPONENT	20 μ l REACTION
10X T4 DNA Ligase Buffer	2 μ l
Vector DNA (3 kb)	50 ng (0.025 pmol)
Insert DNA (1 kb)	50 ng (0.076 pmol)
Nuclease-free water	to 20 μ l
T4 DNA Ligase	1 μ l

Table 2.12 showing the components of the ligation reaction.

The reaction was mixed by pipetting up and down and microfuged briefly. For cohesive ends, the mixture was incubated at room temperature for 10 minutes. For blunt ends or single base overhangs, the mixture was incubated at room temperature for 2 hours. The tubes were kept to chill on ice and then 1-5 μ l of the reaction was used to transform into 50 μ l competent cells.

2.4.6 Agarose Gel Electrophoresis

Gel electrophoresis was used to analyse PCR products, plasmid minipreps and restriction digests. 0.8 g/100 ml agarose gels were cast using 1xTAE and Gel Red (at a concentration of 1 μ l per 100ml of 1xTAE) or SYBR Safe™ (at a concentration of 1 μ l per 10 ml of agarose gel). Samples were loaded with 1x DNA loading buffer and 1 μ l 1kb DNA ladder (New England BioSciences) was used as a standard molecular weight marker. Gels were run at 100V for approximately 50 minutes and imaged using the Gel Doc EZ System (Bio-Rad).

2.4.7 Gel Extraction

The DNA bands of interest were cut out of the gel using a scalpel under a UVP Dual-Intensity Transilluminator. DNA was extracted from the agarose gel using the GeneJET™ Gel Extraction Kit (Fermentas) following the QuickProtocol™ GeneJET™ Gel Extraction Kit. The purified DNA was eluted in 50 μ l EB buffer and stored at -20 °C.

2.4.8 RNA Extraction

The RNA extraction and purification protocol was performed according to the manufacturer's manual (Masterpure kit, Epicentre). All of the solutions used were obtained from the kit but Proteinase K was obtained from New England Biolabs. 1 μ l of 50 μ g/ μ l Proteinase K was diluted into 300 μ l of Extraction Reagent for RNA for each sample. mid-log culture cells were pelleted by centrifugation and then resuspended in the Extraction Reagent for RNA containing the Proteinase K by vortexing. The mixture was incubate at 70 °C for 10-15 minutes while vortex mixing every 5 minutes then placed on ice for 3-5 minutes. 175 μ l of MPC Protein

Precipitation Reagent were then added to the 300 μ l of the lysed sample and then vortexed vigorously for 10 seconds. The debris was pelleted by centrifugation for 10 minutes at 4 °C at $\geq 10,000 \times g$ in a microcentrifuge and the supernatant fluid was transferred to a clean microcentrifuge tube. 500 μ l of isopropanol was added to the recovered supernatant fluid and the solutions mixed by inverting 30-40 times. The RNA was pelleted by centrifugation at 4 °C for 10 minutes at $\geq 10,000 \times g$ in a microcentrifuge. The isopropanol was aspirated without dislodging the RNA pellet. 200 μ l of DNase I solution was prepared for each sample. 20 μ l of 10X DNase Buffer was added to 175 μ l of deionised water with 5 μ l of RNase-Free DNase I. The nucleic acid pellet was completely resuspended in 200 μ l of DNase I solution and incubated at 37 °C for 10 minutes. 200 μ l of 2X T and C Lysis Solution and 200 μ l of MPC Protein Precipitation Reagent were added to the solution and vortex mixed for 10 seconds then the tubes were placed on ice for 3-5 minutes. The debris was pelleted by centrifugation at 4 °C for 10 minutes at $\geq 10,000 \times g$ in a microcentrifuge. The supernatant containing the RNA was transferred into a clean microcentrifuge tube and 500 μ l of isopropanol was added to it, followed by inverting the tube 30-40 times. The purified RNA was then pelleted by centrifugation at 4 °C for 10 minutes in a microcentrifuge at $\geq 10,000 \times g$. The isopropanol was aspirated without dislodging the RNA pellet which was then rinsed twice with 70% v/v ethanol. The RNA was finally resuspended in 35 μ l of TE Buffer with 1 μ l of RiboGuard™ RNase Inhibitor added to it.

2.4.9 Reverse transcriptase Real-time PCR:

The Reverse transcriptase SensiFAST SYBR No-ROX kit was obtained from Bioline and the reactions were performed according to the manufacturer's instructions. The kit dictates a 3-step reaction that is described below. The following components were combined in a reaction tube

Component	20 μ l Reaction
2x SensiFAST SYBR® No-ROX Mix	10 μ l
Template RNA	Up to 8.4 μ l
Oligo(dT) primers	0.8 μ l each
RNase-free sterile water	As required

Table 2.13 showing the components of the RT-QPCR reaction.

STEP	TEMPERATURE	TIME	Cycles
Polymerase Activation	95 °C	2 minutes	1
Denaturation	95 °C	5 seconds	40
Annealing	65 °C	10 seconds	
Extension with acquiring at the end of the step	72 °C	20 seconds	

Table 2.14 showing the cycle conditions of the RT-QPCR reaction.

RT-QPCR was utilised to evaluate and quantify the gene expression of genes in the experiments detailed in the results chapters. The combination of primers used are detailed below in Table 2.15 and the primer sequences are shown in Table 2.16. A universal QPCR primer (CLI 1247) coding for the V5 sequence was used for testing all the alleles tagged with V5. Controls using

Gene tested	Primers
<i>act1</i>	CLI 1233, CLI 1234
<i>swi1</i>	CLI 1247, CLI 1251
<i>swi3</i>	CLI 1247, CLI 1252
<i>hip1</i>	CLI 1247, CLI 1248
<i>mrc1</i>	CLI 1247, CLI 1249

Table 2.15. The combinations for primers used in gene expression quantification corresponding to the gene being tested.

Primer Code	Primer Sequence	Primer Test Position
CLI 1233	CTGAAGCTCTTTTCCAACCC	5' <i>act1</i>
CLI 1234	TCCTTTTGCATACGATCGGC	3' <i>act1</i>
CLI 1247	CCAAGCAAAGGGTTAGGAATACCC	5' Universal V5 primer
CLI 1248	CATGGTCTTTGGCAAAAATTGGAGG	3' <i>mrc1</i>
CLI 1249	CCCAACGTCCACAAGGACG	3' <i>hip1</i>
CLI 1251	CGGATGATGACTCAGAAACAG	3' <i>swi1</i>
CLI 1252	GGTTCGACGTCGTGGTTGG	3' <i>swi3</i>

Table 2.16. The sequences for primers used in RT-QPCR.

2.5.1 Protein Extraction

Cells were pelleted by centrifugation at 4000 rpm for 5 minutes. The cells were processed immediately after centrifugation or pellets were frozen at -80 °C. The cells were then resuspended such that 100 µl of Y-PER™ Yeast Protein Extraction Reagent (Thermo Scientific) were used to resuspend 50 mg of dry cell pellet. The cell suspension was homogenised by sonication for 30 seconds at 30 Watts. The mixture was agitated at room temperature for at least 20 minutes by placing on a shaking incubator and inverting every 10 minutes. After the agitation, the mixture was centrifuged at 13000 rpm for 10 minutes to pellet the cell debris. The supernatant was then reserved for analysis and protein concentration determination.

2.5.2 Protein Quantification

The BCA assay was performed according to the user's manual (Thermo Scientific) in a 96 well plate with an albumin dilution range from 1 mg/ml to 0.2 mg/ml. The experimental samples and standard dilution series were performed in duplicates. The absorbance of each well was measured at 600 nm using a spectrophotometer. The average for each sample was calculated and used to draw a standard curve whose gradient and y-intercept were used to calculate the protein concentration for each sample.

2.5.3 SDS-PAGE

SDS PAGE gel electrophoresis was carried out using Biorad Mini Protean II kits. Protein samples were resolved on either a 10% or 12% separating gels. Polymerisation was achieved by the addition of 10% ammonium persulphate (APS) and TEMED to the separating buffer. The recipes for the resolving gels are detailed

below in Table 2.17. The pre-polymerised gel solution was poured between glass plates separated with 1 mm glass spacers and left to set with a layer of isopropanol on top to achieve a level surface. Once set, the isopropanol layer was decanted and the top of the gel between the glass plates dried with Whatman filter paper. The stacking gel (6%) was poured on top of the separating gel and the gel comb positioned. The recipe for the stacking gel is detailed below in Table 2.18. After 30 minutes the comb was removed and the gel kit assembled. Protein samples were mixed with 4 x sample dissociation buffer and denatured at 100 °C for 5 minutes. The 12% SDS-PAGE gels were run using the BioRad mini gel system for 90 minutes at 80 Amps stable current. The All Blue Prestained protein markers (BioRad) were run on the gel to compare sizes with the proteins being run.

Acrylamide Concentration	Water	Acrylamide Solution (30% acrylamide/ bisacrylamide Solution)	1.5 M Tris Buffer (pH8 .8)	100 g/l SDS	100 g/l APS	TEMED
10% Acrylamide Gel	7.9 ml	6.7 ml	5.0 ml	200 µl	200 µl	8 µl
12% Acrylamide Gel	6.6 ml	8.0 ml	5.0 ml	200 µl	200 µl	8 µl

Table 2.17 showing the recipe for 10% and 12% resolving gels used in Polyacrylamide Gel Electrophoresis.

Acrylamide Concentration	Water	Acrylamide Solution (30% acrylamide/ bisacrylamide Solution)	1.0 M Tris Buffer (pH 6.8)	100 g/l SDS	100 g/l APS	TEMED
6% Acrylamide Gel	4.1 ml	1 µl	750 µl	60 µl	60 µl	6 µl

Table 2.18 showing the recipe for 6% stacking gels used in Polyacrylamide Gel Electrophoresis.

2.5.4 Coomassie Staining of Gels

Gels were stained in the Coomassie stain for 30 minutes, then destained using three steps of 10 minute washes of destaining solution until the background was clear and the bands are visible. The gels would then be dried on blotting paper and photographed using a Gel Doc System (BioRad).

2.5.5 Western Blotting

The western blotting technique is based on the technique described by W. N. Burnette (Burnette, 1981). The SDS-PAGE gel, two sheets of Scotch-Brite pads, six layers of blotting paper and Hybond PVDF membrane (Amersham) of the same size (6cmx9cm) were soaked in transfer buffer. Then they were all placed inside a blotting cassette to build up a sandwich. Using a BioRad transfer system and a voltage of 100 V for 70 minutes, the transfer process was carried out. The PVDF membrane was then washed with PBS (Sigma-Aldrich) prior to blocking, antibody incubation and immunodetection. A list of primary and secondary antibodies is present in Table 2.19.

Antibody	Dilution used	Source
Monoclonal Mouse Anti-tubulin	1:1000	Gul Lab (Woods <i>et al.</i> , 1989)
Monoclonal Rabbit Anti-V5	1:1000	Cell Signaling Technology
Monoclonal Mouse Anti-V5	1:5000	Invitrogen
Polyclonal Goat Anti-Rabbit IgG	1:10000	Abcam
Polyclonal Rabbit Anti-Mouse IgG	1:4000	Sigma-Aldrich

Table 2.19 showing the list of antibodies used in the Western Blotting.

2.5.6 Incubation of PVDF membrane with antibodies

Following blocking in 20 ml 4% milk (in PBS), the PVDF membrane was incubated in 10 ml 2% BSA solution containing the primary antibody overnight at 4 °C with gentle shaking. The blot was then washed in a series of 3 10 minute washes in PBS containing 0.1% Tween 20 and 1 x minute wash with PBS. Following washing, 10 ml 2% BSA (in PBS) was added to the membrane and an HRP-conjugated secondary antibody was added. The blot was left to incubate at room temperature for at least 1 hour with gentle shaking. The blot was washed in a series of 3 10 minute washes in PBS and the protein bands detected by ECL.

2.5.7 Enhanced Chemi-Luminescence (ECL)

Western blots were immunodetected using the ThermoFisher enhanced chemiluminescence (ECL) kit at a 1:1 ratio for 5 minutes with agitation. The blot was then wrapped in Saran wrap and exposed to light-sensitive film (Amersham) in the photographic development room and developed manually using a developing agent and a fixer (Sigma Aldrich) to obtain the best signal.

2.5.8 Flow Cytometry

Fission yeast samples were fixed using 70% v/v ethanol overnight. The samples were then sonicated for 20 seconds using a sonication probe (JSP Inc., USA) in a volume of 1.5 ml in a 5 ml polystyrene FACS tube (BD Falcon, USA). The cells were stained for DNA with Propidium Iodide (PI) (Life technologies). The readings were acquired using the CytoFLEX S Flow Cytometer (Beckman Coulter) as a PI histogram. PI was excited using a 561 nm laser line and fluorescence was collected using a 610/20 band pass filter using a PMT voltage of 730. The flow rate was set at "low" in order to provide the best measurement resolution and a minimum of 10,000 events was collected. The data was analysed using Kaluza Software (Beckman Coulter).

Chapter 3: The Genetic Analysis of the interaction between *hip1* and *rad4-116*

3.1 Introduction

Hip1 is one of the members of an evolutionary conserved family of histone chaperones that are conserved in many eukaryotic organisms. Hip1 is involved in centromere silencing and cell cycle delay, which result from spindle damage and an increased rate of chromosomal loss (Blackwell *et al.*, 2004). Thus, the loss of the fission yeast HIRA complex components results in silencing defects in both mating type and centromeric loci. The comparison between the profiles of DNA damage and cellular morphology following depletion of Hip1, in the presence of Rad4-116 to those of the other 3 genes in this thesis could provide more insight to the cellular pathways in which Hip1 is involved with those genes.

3.1.1 Synthetic Lethality on Agar

The aim of the experiment was to investigate the interactions between *rad4* and *hip1* which is implicated in the maintenance of chromatin structure and remodelling. The strains selected had either the *rad4-116* marked with NAT resistance and the *hip1Δ* marked with G418 resistance. This was achieved by mating the strains, after changing the mating type where needed, on EMM-nitrogen agar plates then micromanipulating and dissecting the tetrads, followed by replicating the plates on the appropriate selective media. Tetrad dissection provided clear and separated colonies on the plates, thus, facilitating the assessment of viability and avoiding contaminants forming colony-like growth. The tetrads could segregate as parental di-type, non-parental di-type or as a tetra-type depending on the combination of alleles inherited by each spore. The growth of colonies on YES indicate that the interaction between the genes present in the original spore was not synthetically lethal whereas the spores that were not able to form colonies indicate that a synthetically lethal interaction occurred in the double mutant. The original YES was replicated onto a fresh YES plate as well as YES+NAT, YES+G418 and YES+NAT+G418. The colonies were counted and the growth patterns were observed and noted for each plate and for each cross. The χ^2 was then calculated based on the expected number of viable spores.



Figure 3-1. The growth of individual spores to colonies of the *rad4-116* strain cross with *hip1Δ* strain. The figure shows 4 columns of the YES plates of the crosses of the *rad4-116* strain with a *hip1Δ* strain. The cross shown is a set of spores from tetrads that were inoculated into single spores with a line separating each individual spore set from a single tetrad. The number of spores from each YES plate was counted and recorded.

Cross	<i>hip1Δ</i> x <i>rad4-116</i>
Wild-type	32
G418 ^R	35
NAT ^R	30
G418 ^R /NAT ^R	4
Viability	82
Total valid spores	144
χ^2 value	27.7

Table 3-A showing the crosses between the *rad4-116* strain and *hip1Δ*. The *rad4-116* was tagged with NAT resistance while the *hip1* deletion are marked with G418 (Kanamycin) resistance. The crosses were carried out on EMM-nitrogen agar, then checked after 2 days for sporulation. The tetrads from sporulation were separated using the Singer Micromanipulator onto YES agar plates. After 4 days, the plates were then copied onto fresh YES as shown in Figure 3-1, YES+G418 and YES+NAT plates separately. After another 3 days, the colonies on each plate were counted and recorded as seen in the table. The χ^2 value for each cross was calculated and tabulated at $p \leq 0.05$ with a degree of freedom of 1.

3.1.2 *hip1*Δ causes synthetic lethality when combined with *rad4-116*

After the colonies from the crosses were noted and counted from all the plates, the Chi-Square test was performed and a value of 27.7 was the result as shown in Table 3-A. As this value was calculated using the expected value based on the segregated spores not based on the expected segregation pattern, the values represent a focused measure on whether the double mutants were synthetically lethal or not. These values were all greater than 3.84, which was the threshold value at $p \leq 0.05$ with a degree of freedom of 1. This indicated that the deletion of *hip1* was synthetically lethal when combined with *rad4-116* and that any lethality or observed lack of growth would **not** be due to chance or random occurrence.

3.2 The DNA replication stalled fork profile of *hip1Δ*

The aim of this experiment was to observe and compare the DNA stalled replication fork profiles, in terms of accumulation and resolution of DNA forks, of a *rad4-116* strain to *hip1Δ* and wildtype *rad4* as a control. This ability to assess and monitor such profile would be achieved by utilising Rad52-GFP which is recruited to repair and aid the progress of stalled replication forks. The strains were constructed by direct transformation of PCR-produced deletion *hip1* encoding G418 resistance and PCR-produced *rad4-116* attached to NAT resistance into a *rad52-GFP* base strain. Cells were grown in liquid media then arrested by the addition of hydroxyurea which blocks ribonucleotide reductase leading to the depletion of the ribonucleotides, thus halting DNA replication. Then after 6 hours of arrest with hydroxyurea, the cells were released by the depletion of hydroxyurea from the media, washing the cells then resuspending in rich YES media. Samples were collected every 30 minutes for 210 minutes to be analysed for fluorescence microscopy and testing viability.

The cell nuclei were assessed in two ways; the first being the percentage and number of nuclei that carry GFP fluorescent foci spanning the 210 minutes compared to the starting time point(0) of the release, and the second by assessing the number of foci per nucleus and arranging them in categories. The foci were assessed using the Softworx program by taking a 3D reconstruction of the cells to be able to assess if the foci observed were nuclear foci to be counted. The cells can be seen under 60X magnification using DAPI and after staining with anti-GFP antibody in Figure 3-2. The viability of each strain was tested by spreading 100 colonies per plate on YES plates in triplicate per each strain at each timepoint as shown in Figure 3-4. The viability of cells in all three strains did not change from the arrest up to the 210-minute time point post release. The percentage of nuclei with GFP foci was

tabulated and a graph, as observed in Figure 3-4 for the *hip1Δ* strain, Figure 3-7 for the *rad4⁺* strain and Figure 3-9 for the *rad4-116* strain. As observed in the graph, the *rad4-116* showed a higher level of initial foci at the 0 timepoint compared to the other 2 strains.

The initial levels of Rad-52 GFP nuclear foci were 5% and 6% for the *hip1Δ* and the *rad4⁺* strains respectively contrasting to 26% in the *rad4-116* strain. For the *hip1Δ* strain the number of foci increased at a gradual low rate from 5% at the start of the release up to 13% after 90 minutes which was the peak level of foci recorded for the strain. Then, a gradual decrease occurred from 12% at timepoint 120 minutes to a plateau steady low level of 5% to 3% from 150 minutes after release onwards. The 3% recorded at the endpoint of the experiment, at 210 minutes after release, was lower than the starting level of 5% , showing a complete recovery from DNA stalled forks in a bell-shaped manner.

Similarly, for the *rad4⁺* strain the number of foci increased at a gradual low rate from 6% at the start of the release up to 9% after 60 minutes. A sharp increase occurred from 9% to 24% at 90 minutes followed by the observed value of 27% after 120 minutes which was the peak level of foci recorded for the strain. Then, a sudden decrease occurred from 27% at timepoint 150 minutes to 14% at 180 minutes after release. This was followed by the gradual decrease from 14% at 150 minutes to 9% to 3% at 180 and 210 minutes respectively. The 3% recorded at the endpoint of the experiment, at 210 minutes after release, was lower than the starting level of 6% , showing a complete recovery from DNA stalled forks in a bell-shaped manner.

For the *rad4-116* strain, a different pattern was observed as the initial value of percentage of cells with nuclear Rad52-GFP was 26% then rose sharply to a steady

level at 42% at 30 minutes to fluctuate slightly reaching 28% at 120 minutes then back again up to 49% at 150 minutes. Even at 180 minutes, a 40% level was observed followed by decrease to 21% at 210 minutes. This illustrated that there was no recovery to a level below 10% and that the pattern showed an increase to a flat level near 40% then a decrease to near 20%. These numbers were all higher than their respective timepoints in the other 2 strains.

The values of percentage of cells with nuclear Rad52-GFP at the start and the end of the timecourse were similar when comparing the *rad4⁺* and *hip1Δ* strains but not the *rad4-116* strain. The patterns seen in the *rad4⁺* and *hip1Δ* strains were nearly identical as both show a bell-shaped curve with a peak at 90 to 120 minutes but not with the *rad4-116* strain. The difference between the *rad4⁺* and *hip1Δ* strains was that the peak or highest value recorded was 27% with the *rad4⁺* strain and 13% with the *hip1Δ*. However, both strains showed a decrease back to below initial levels of recorded GFP foci.

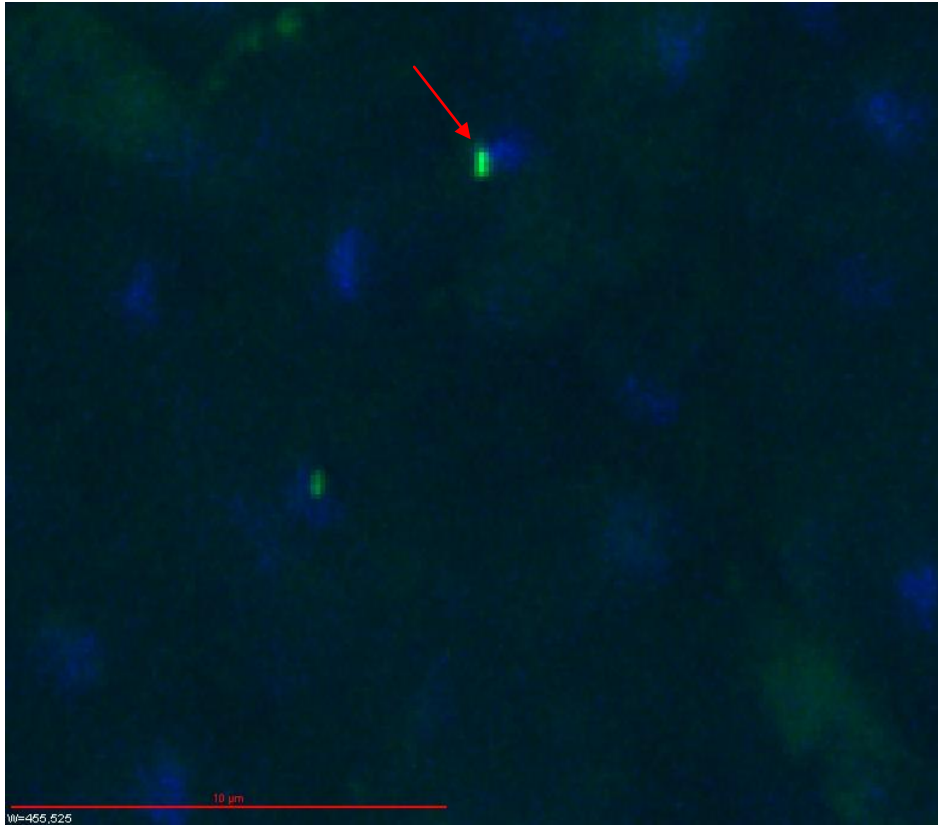
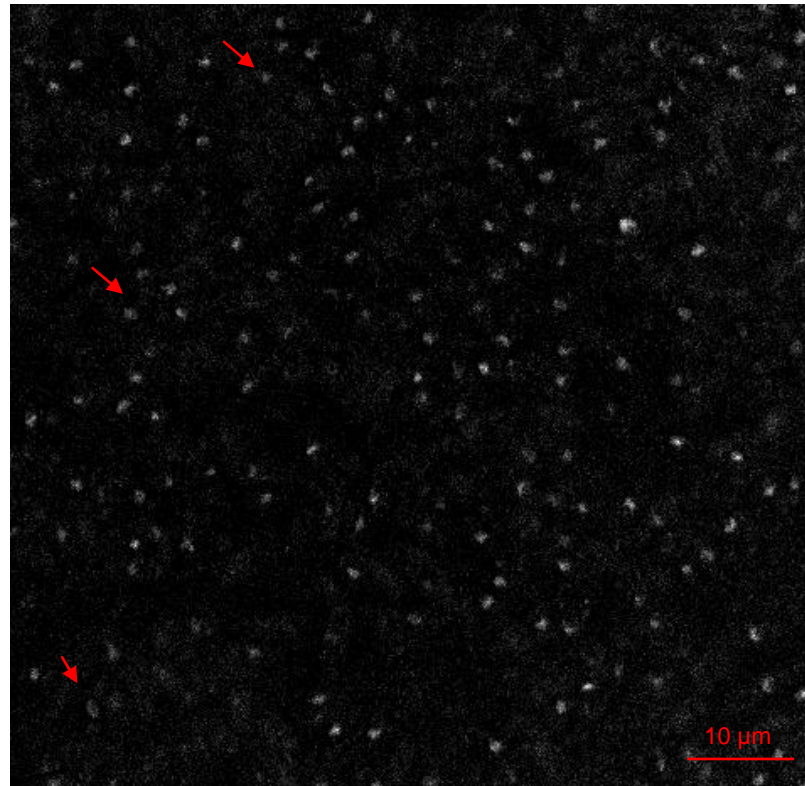
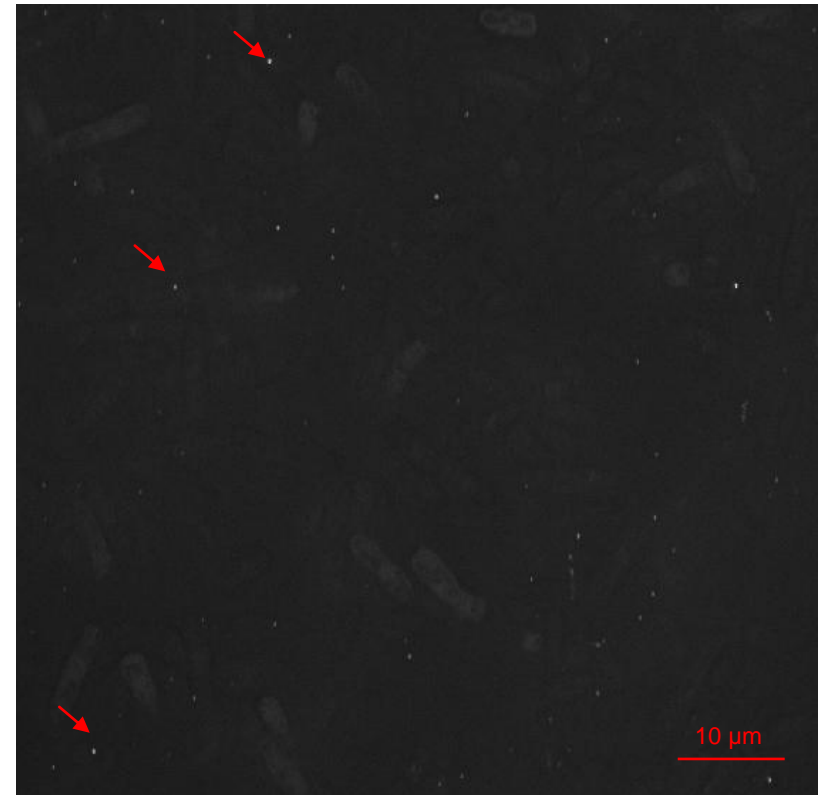


Figure 3-2. A merged image of *hip1Δ* cells after 90 minutes of incubation with Hydroxyurea. The nucleus (blue) highlighted by the arrow contains a single GFP signal (bright green). The cells were reconstructed into 3D using the Softworx program to reinsure that the foci seen are indeed nuclear foci.



A (*hip1Δ* DAPI)



B (*hip1Δ* GFP)

Figure 3-3 . Rad52-GFP foci of the *hip1Δ* strain at its peak. The figure shows the cells of the *hip1Δ* strain at 60X magnification stained with (A) DAPI to show the nuclei and (B) anti-GFP to show the Rad52-GFP foci. The cells were reconstructed into 3D using the Softworx program to identify nuclear foci. The peak value for nuclear foci was 27% of total number of nuclei. The red arrows point to examples of nuclei with Rad52-GFP foci.

Viability Comparison of *rad4-116*, *rad4*⁺ and *hip1*Δ

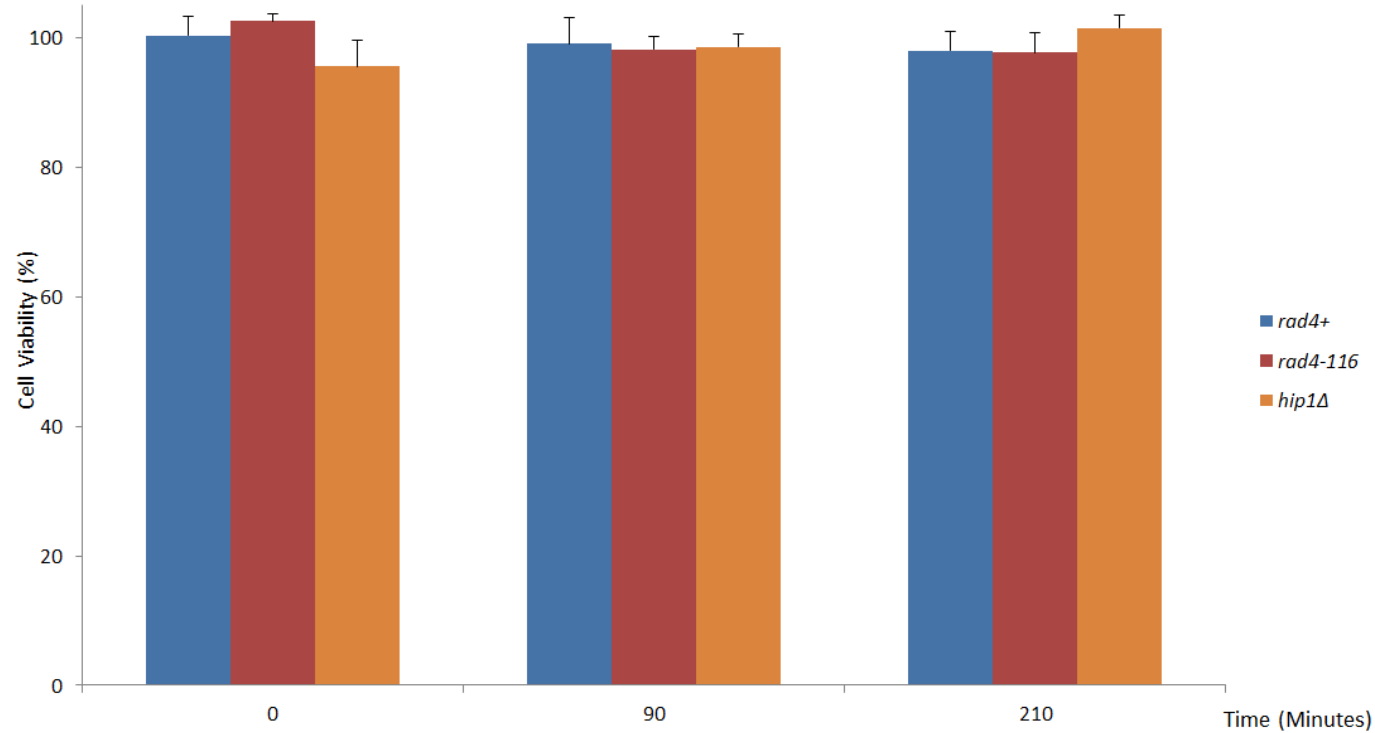


Figure 3-4. Viability counts for the *rad4*⁺, *rad4-116* and *hip1*Δ strains carrying the *rad52-GFP* gene. The figure shows the bar chart graph representing the comparison between cell viability across the three strains of *rad4-116*, *rad4*⁺ and *hip1*Δ at the start of the experiment, at 90 minutes after the start and at the end of the experiment at 210 minutes. As observed, there was no significant change in viability across all three strains at these three timepoints.

Rad52-GFP Foci Profile of *hip1Δ*

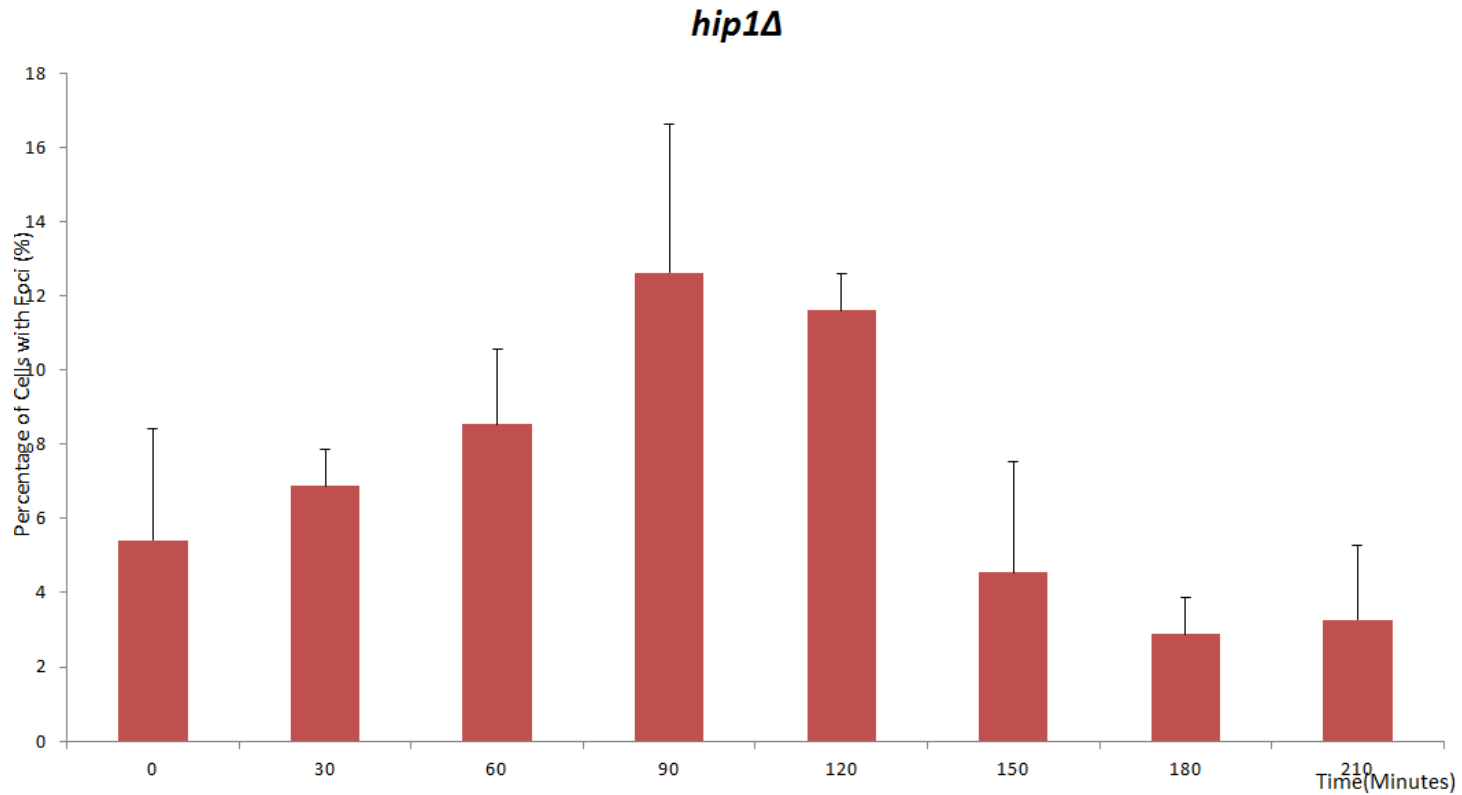


Figure 3-5. The Rad52-GFP profile of the *hip1Δ* strain. The figure shows the bar chart graph representing the percentage of cells with Rad52-GFP foci in the *hip1Δ* strain across timepoints from 0 to 210. The peak occurred at 90 minutes after the start of the experiment with a value of 13% of cells carrying nuclei with Rad52-GFP foci.

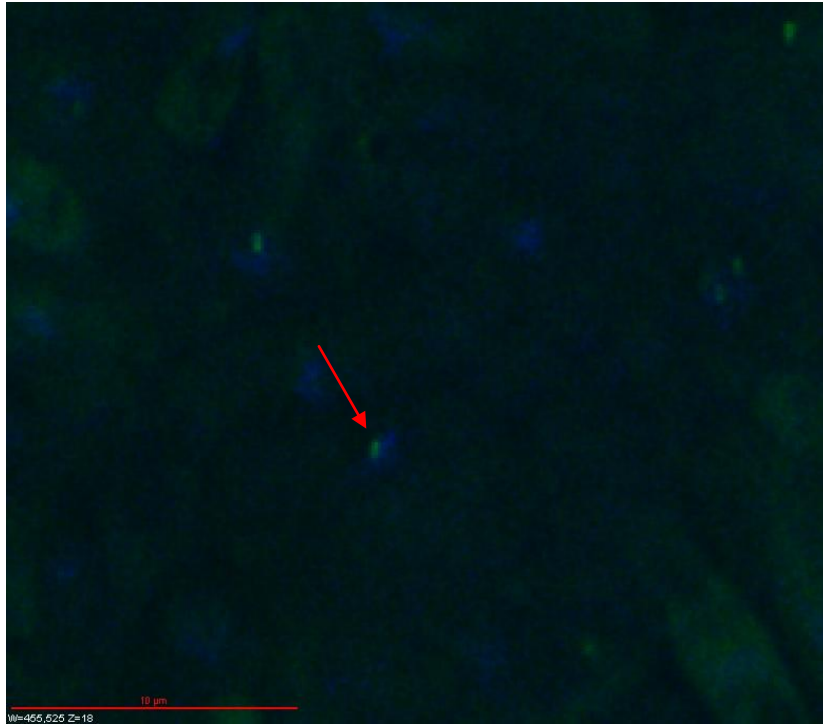


Figure 3-6. A merged image of *rad4*⁺ cells after 120 minutes of incubation with Hydroxyurea. The nucleus (blue) highlighted by the arrow contains a single GFP signal (bright green). The cells were reconstructed into 3D using the Softworx program to reensure that the foci seen are indeed nuclear foci.

Rad52-GFP Foci Profile of *rad4*⁺

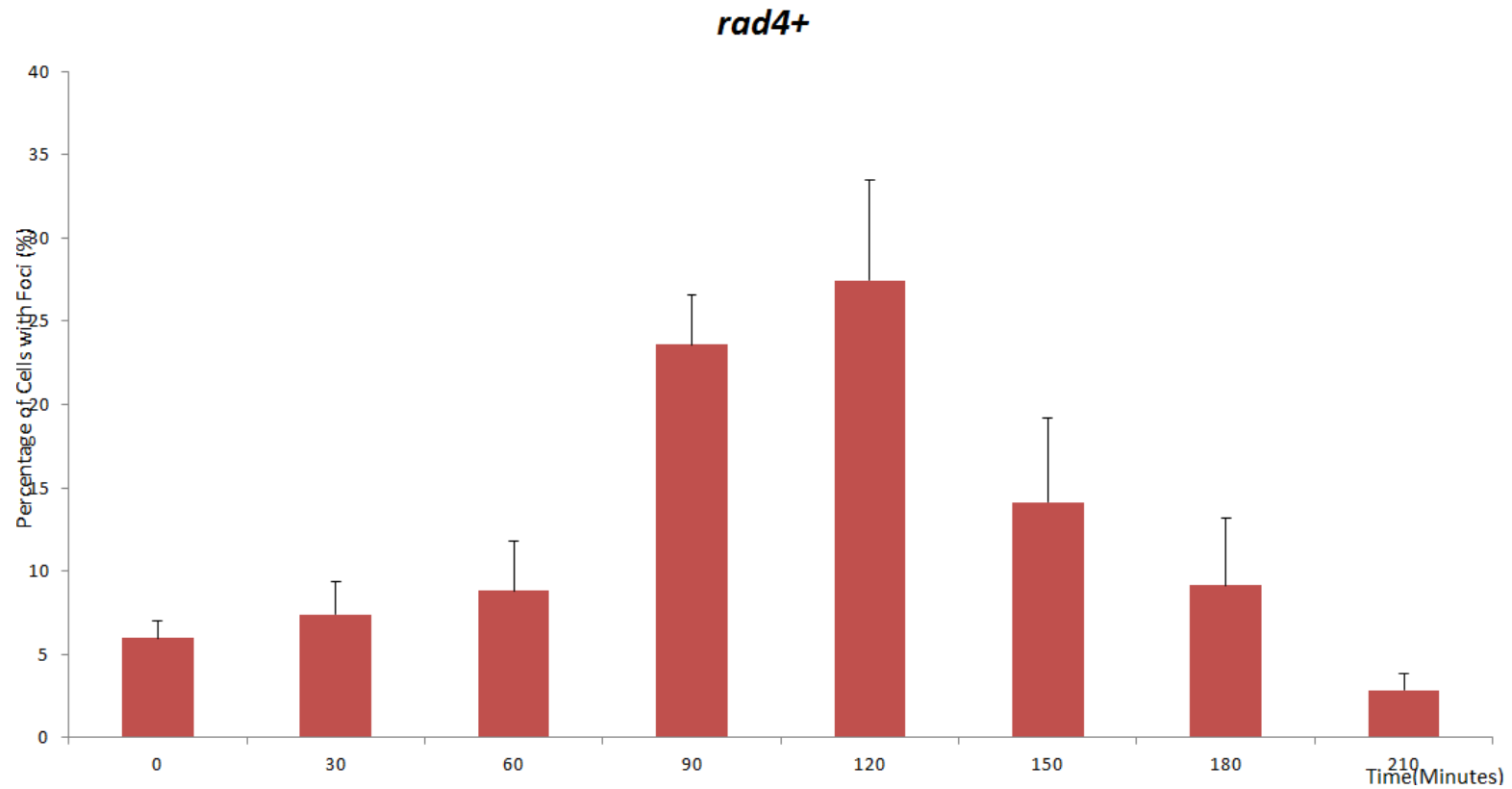


Figure 3-7 . The Rad52-GFP profile of the *rad4*⁺ strain. The figure shows the bar chart graph representing the percentage of cells with Rad52-GFP foci in the *rad4*⁺ strain across timepoints from 0 to 210. The peak occurred at 120 minutes after the start of the experiment with a value of 28% of cells carrying nuclei with Rad52-GFP foci.

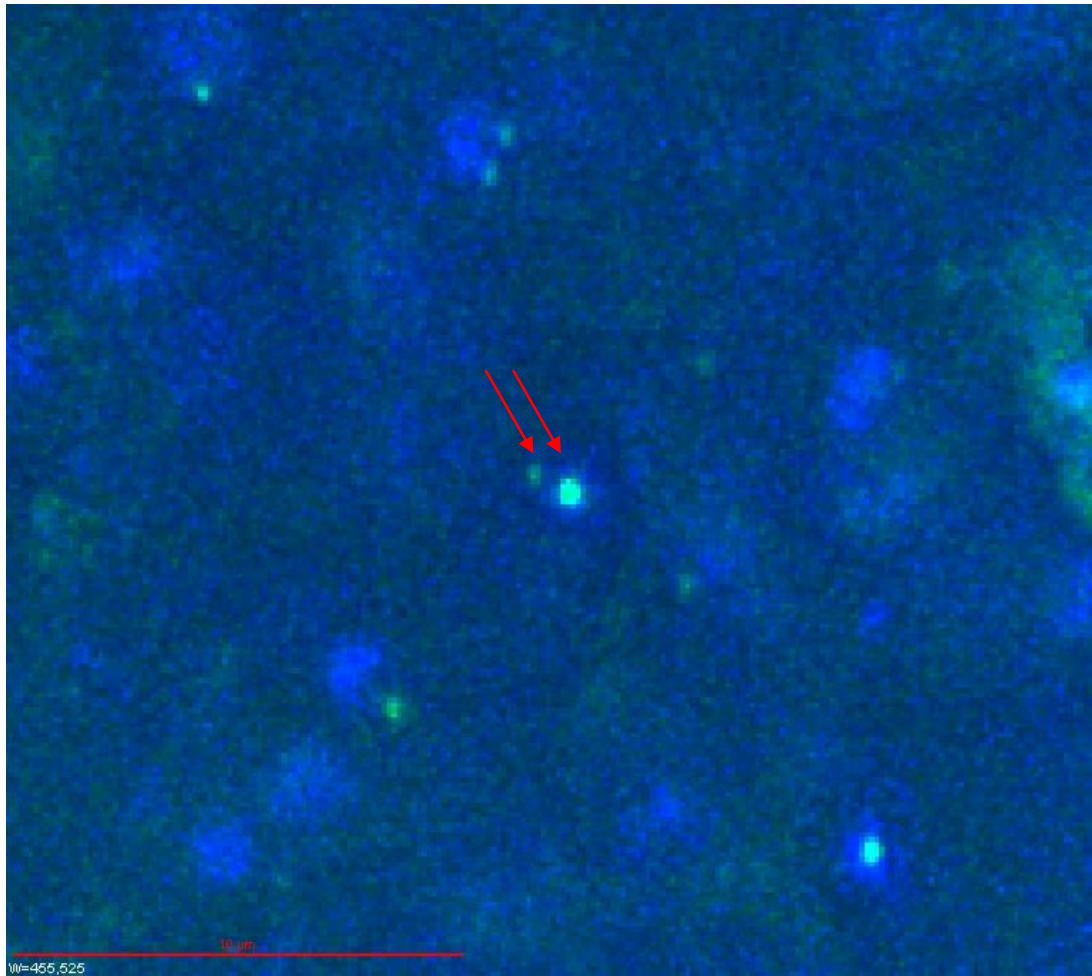


Figure 3-8. A merged image of *rad4-116* cells after 150 minutes of incubation with Hydroxyurea. The nucleus (blue) highlighted by the arrow contains multiple GFP signals (bright green). The cells were reconstructed into 3D using the Softworx program to reensure that the foci seen are indeed nuclear foci. The presence of multiple foci per nucleus is common in *rad4-116* cells.

Rad52-GFP Foci Profile of *rad4-116*

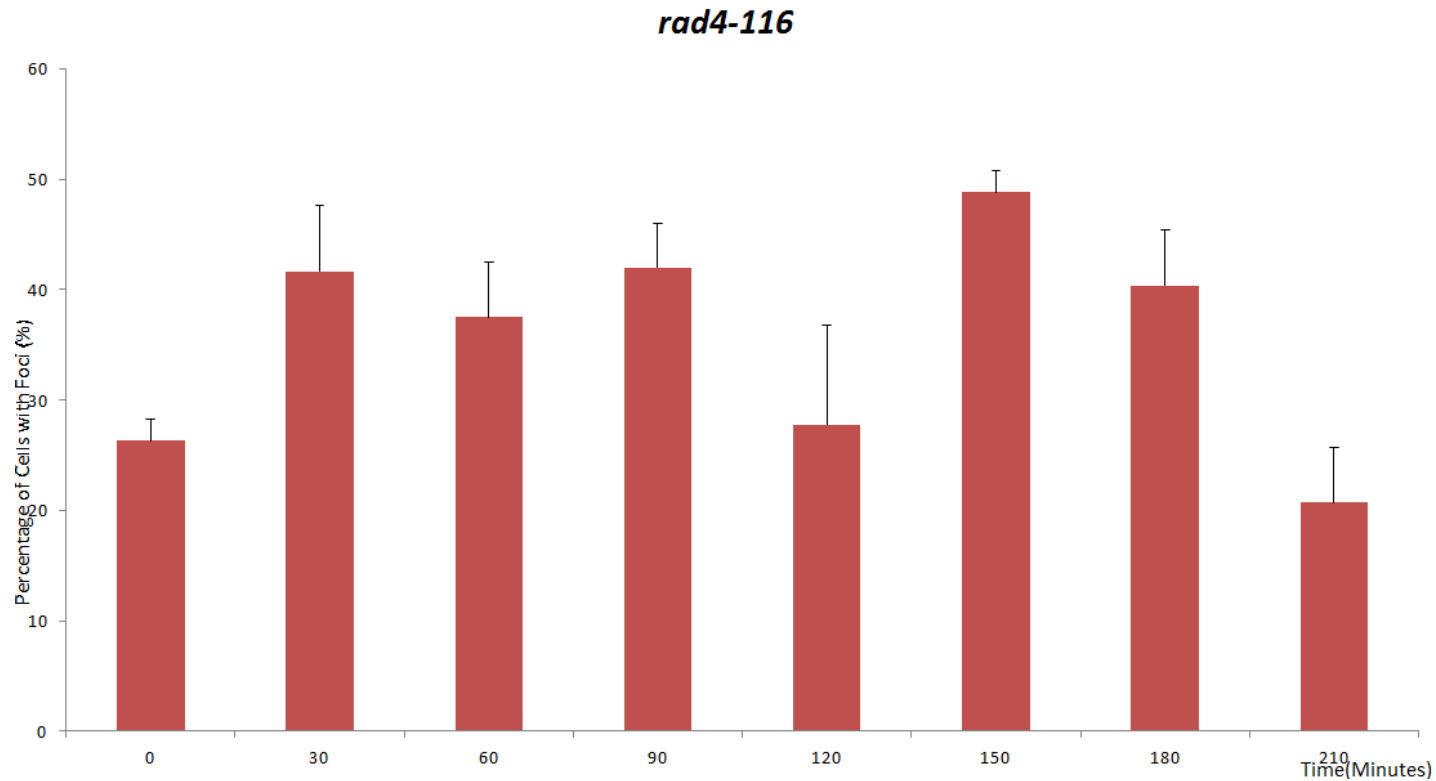


Figure 3-9. The Rad52-GFP profile of the *rad4-116* strain. The figure shows the bar chart graph representing the percentage of cells with Rad52-GFP foci in the *rad4-116* strain across timepoints from 0 to 210. The peak occurred at 150 minutes after the start of the experiment with a value of 49% of cells carrying nuclei with Rad52-GFP foci.

Rad52-GFP Foci Profile Comparison of *rad4-116*, *rad4*⁺ and *hip1*Δ

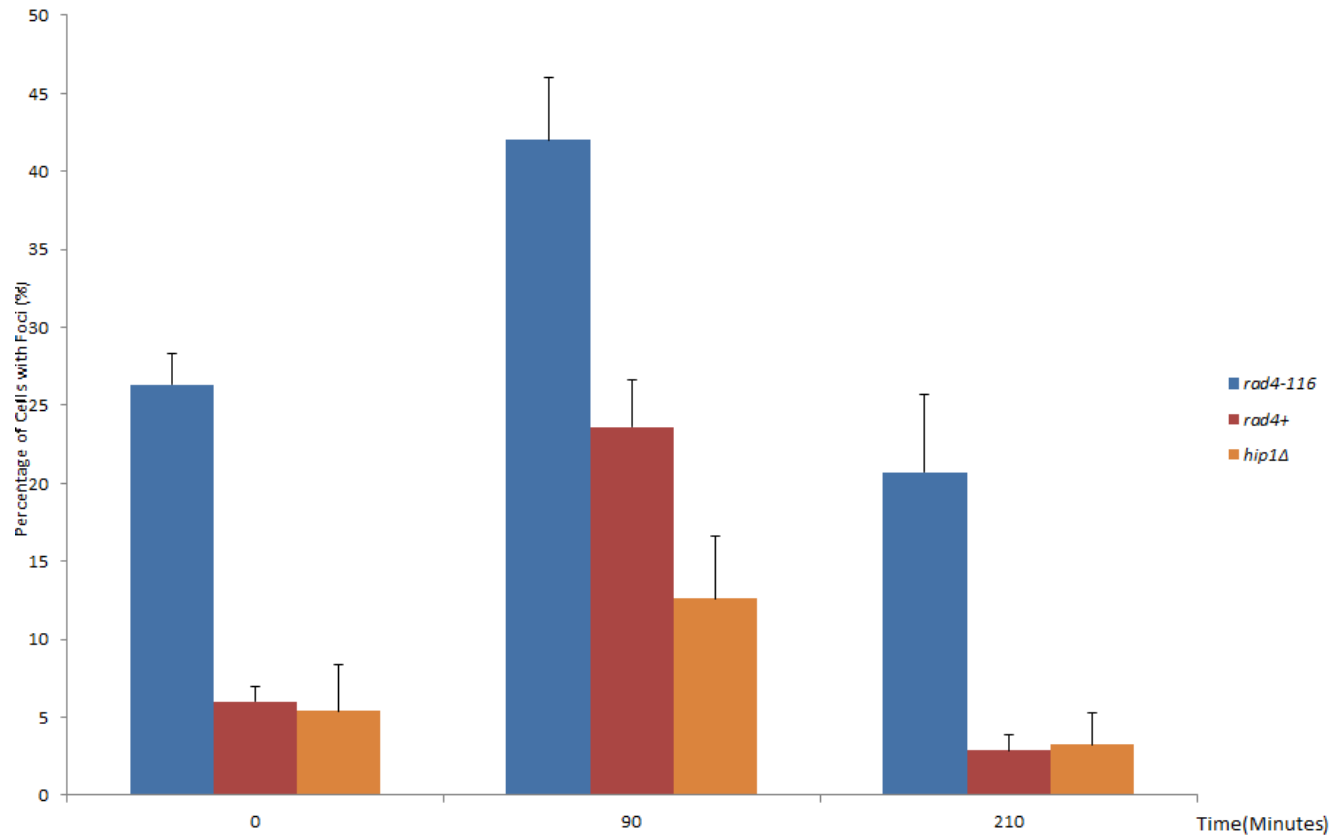


Figure 3-10. A comparison of the Rad52-GFP profiles of the *rad4-116*, *rad4*⁺ and *hip1*Δ strains. The figure shows the bar chart graph representing the comparison between the percentage of cells with Rad52-GFP foci across the three strains of *rad4-116*, *rad4*⁺ and *hip1*Δ at the start of the experiment, at 90 minutes after the start and at the end of the experiment at 210 minutes.

3.2.1 The Rad52-GFP foci profile of *hip1Δ* was similar to that of *rad4⁺* and not to *rad4-116*

After the Rad52-GFP foci from the *hip1Δ* strain from each timepoint were counted, the unpaired Student T-test was performed to compare to the *rad4⁺* strain at timepoints 0, 90 and 210 minutes after the depletion of hydroxyurea from the media. Each value of foci was determined using an average of triplicate experiments, where 100 nuclei were scored from the *hip1Δ* strain and compared to the *rad4⁺* strain at its corresponding timepoint. The variance for both samples were similar allowing the use of the 2-tailed Student T-test. The degree of freedom for each sample used at each timepoint was 4 and the critical value over which the difference was significant was 4.604 at $p \leq 0.01$. $p \leq 0.01$ was chosen over the standard $p \leq 0.05$ as the critical values, calculated and determined to be significant at $p \leq 0.05$, were also significant at $p \leq 0.01$ and some, not all, at $p \leq 0.001$. It should be noted that some significant differences between values recorded for the *hip1Δ* reflect a **significantly** lower value than the wildtype such as the 90 minute foci value at 13% compared to 24% in the wildtype at $p < 0.001$. The values at 0 minutes and 210 minutes were not significantly different between the wildtype and *hip1Δ*. This indicated that the deletion of *hip1* was not significantly different when compared to the wildtype *rad4⁺* strain in terms of Rad52-GFP recruitment onto stalled replication forks induced by hydroxyurea at the 0 and 210 timepoints but failed to reach the peak level recorded by *rad4⁺* strain at 90 minutes. As the Rad52-GFP foci profiles of the *rad4⁺* strain and *rad4-116* were statistically significantly different from each other at all 3 chosen timepoints and the *hip1Δ* strain was similar to the *rad4⁺* strain, it can be deduced that the *hip1Δ* strain was statistically significantly different from *rad4-116* strain.

3.3 The Phenotypic characterisation of the *hip1-V5* strains

A V5-tagged version of *hip1* under transcriptional control of the *nmt81* promoter was created using plasmid p811 and integrated at the *leu1* locus following the methodology described in (Fennessy *et al.*, 2014). The *hip1-V5* base strain was constructed by transformation using SPSC 1005 as the transformed strain to create SPSC 1095. The V5- tagged allele was tested using PCR and by performing a western blot of protein samples of an overnight culture of SPSC 1095 growing in EMM+uracil+leucine broth. By crossing SPSC 1095 with SPSC 1026, and selecting *ura*⁺ G418 resistant colonies, the *hip1-V5 hip1Δ h-* strain SPSC 1100 was constructed. The SPSC 1100 was used in a cross with SPSC 120 to create *hip1-V5 hip1Δ rad4-116* SPSC 1103 by selecting *ura*⁺ G418 resistant temperature sensitive colonies. The *hip1-V5 hip1Δ rad4-116 rad52-GFP* strain SPSC 1112 was created by crossing SPSC 1105, a result of the cross of SPSC 1100 and SPSC120, and SPSC 1073 and selecting *ura*⁺ G418 resistant NAT resistant colonies growing in a 2:2 tetrad pattern. All the strains carrying the *hip1-V5* allele were tested using PCR before using them in the experimental procedures and adding them to the collection.

The aim of this experiment was to be able to analyse the phenotypic profile of Hip1-V5 depletion in the presence of *rad4-116* with control strains carrying *hip1-V5* as well as a control strain carrying *rad4*⁺ and a control strain carrying *rad4-116*. To be able to characterise the *hip1-V5* strains, all the strains were grown into cultures up to 0.8OD overnight at 26 °C in EMM+uracil+leucine (no thiamine) then inoculated into a total volume of 200ml EMM+uracil+leucine+ 50 µg/ml thiamine. The cultures were then incubated at 26 °C in a shaking incubator. Samples for RNA and protein extraction were collected at 0,4, 8, 12 and 24 hours till the cultures for both experimental

strains reached 1.00 OD from 0.2 OD. At each timepoint, samples for immunofluorescence and FACS were taken by fixing in formaldehyde and ethanol respectively. The viability of each strain was tested at each timepoint by plating 100 cells on EMM+uracil+leucine+50 µg/ml thiamine agar plates in triplicates. The pellets for protein and RNA extraction were snap-frozen in liquid nitrogen and stored at -80 °C. SPSC 120 (*rad4-116*) and SPSC 1005 (*rad4⁺*) were used as controls, with SPSC 120 being sampled every time the experiment was repeated. The experiment was repeated 4 times under identical conditions and the results show the averages of the repeats.

A series of concentrations of thiamine of 5 µg/ml, 10 µg/ml, 25 µg/ml, 50 µg/ml, 100 µg/ml were tested using the *hip1-V5* strain (SPSC1095) to be able to assess the best concentration for the depletion of the Hip-V5 in the cells. Overnight cultures of SPSC 1095 were treated with the different concentrations as well as a no-thiamine culture. Protein samples and RNA samples were collected and the viability of each culture was tested. No change in viability occurred across all the tested thiamine concentrations. However, using 5 µg/ml, 10 µg/ml and 25 µg/ml showed partial depletion of the V5 product at RNA and protein levels. Using 50 µg/ml and 100 µg/ml thiamine showed identical results in depletion at the RNA and protein levels including the times of signal abolishment at 12 hours and 24 hours and strength of signals at the 4 hour and 8 hour timepoints. The same preliminary experiment was used for all the other genes tagged with V5 to ensure signal abolishment profiles and the results were identical to those seen in the *hip1-V5* strain. Thus, the concentration of thiamine that was used at 50 µg/ml.

3.3.1 The depletion of *hip1-V5* expression by RT-QPCR

RT-QPCR was used to be able to assess the depletion of the transcript of *hip1-V5* in the strains carrying *hip1-V5*. RNA was extracted from each strain at each timepoint and then purified from DNA and proteins. 50 ng of RNA of each sample was loaded per well in triplicates to be able to obtain a signal for the V5 sequence. A control triplicate was loaded for the same sample to be able to assess the transcription level of actin (*act1*). For each sample, a negative control using no reverse transcriptase, a negative control using no RNA sample and a negative control using no primers were loaded onto the same plate as the experimental wells. Each experiment was carried out in triplicate using separate samplings. Using the average readings for the V5 signal and the actin, the adjusted relative quantity of V5 transcript in each sample was calculated. The formula for the adjusted relative quantity value:

Adjusted relative quantity

$$\begin{aligned} &= (\text{Relative Quantity Value for Sample}) \\ &- (\text{Relative Quantity Value for Sample without Reverse Transcriptase}) \\ &\times \left(\frac{\text{The Highest Relative Quantity Value for act1 of the same set(strain)}}{\text{Relative Quantity Value for act1 of the same sample}} \right) \end{aligned}$$

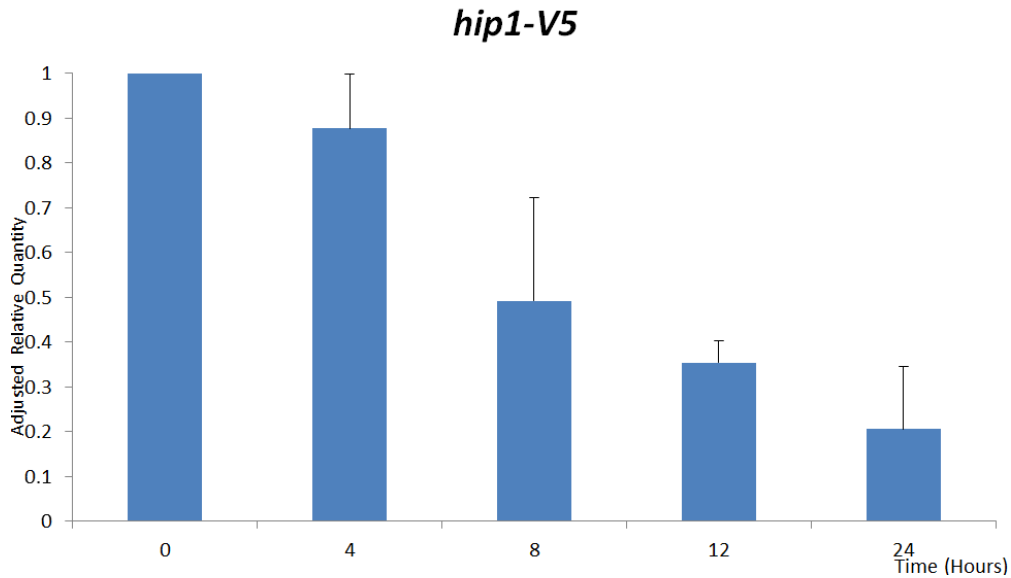


Figure 3-11. The adjusted relative quantity of RNA measured by RT-QPCR for the *hip1-V5* strain SPSC 1095. The figure shows the adjusted relative quantity of the RT-QPCR SPSC 1095 culture across 24 hours of incubation with thiamine added.

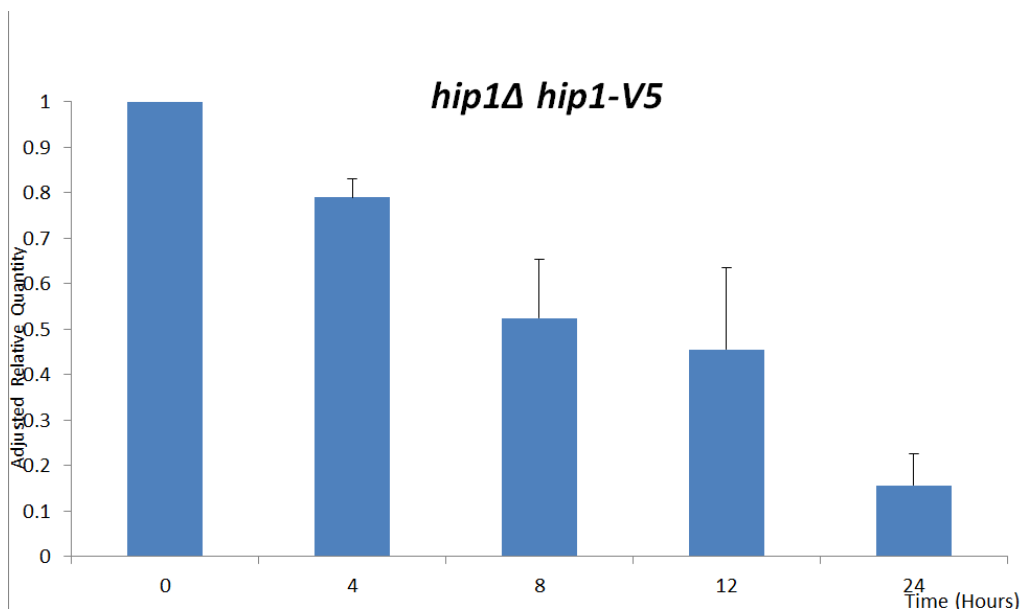


Figure 3-12. The adjusted relative quantity of RNA measured by RT-QPCR for the *hip1Δ hip1-V5* strain SPSC 1100. The figure shows the adjusted relative quantity of the RT-QPCR SPSC 1100 culture across 24 hours of incubation with thiamine added.

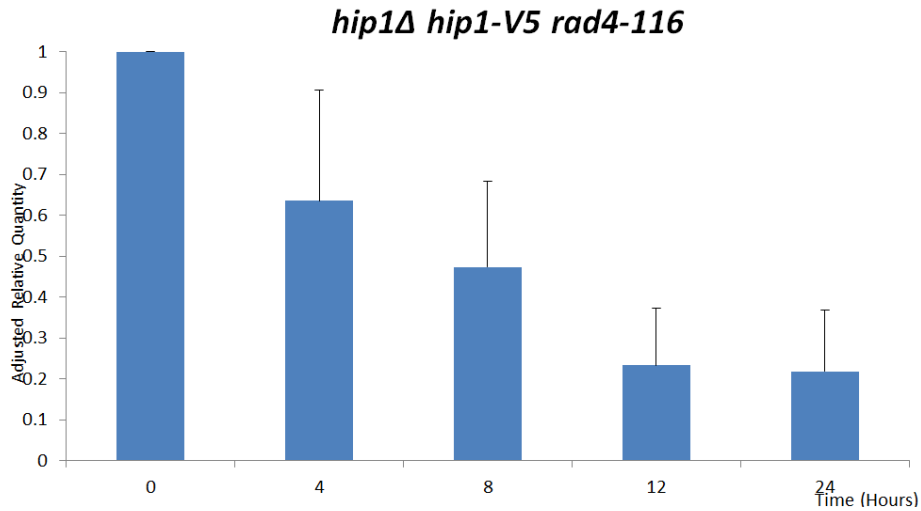


Figure 3-13 . The adjusted relative quantity of RNA measured by RT-QPCR for the *hip1Δ hip1-V5 rad4-116* strain SPSC 1103. The figure shows the adjusted relative quantity of the RT-QPCR SPSC 1103 culture across 24 hours of incubation with thiamine added.

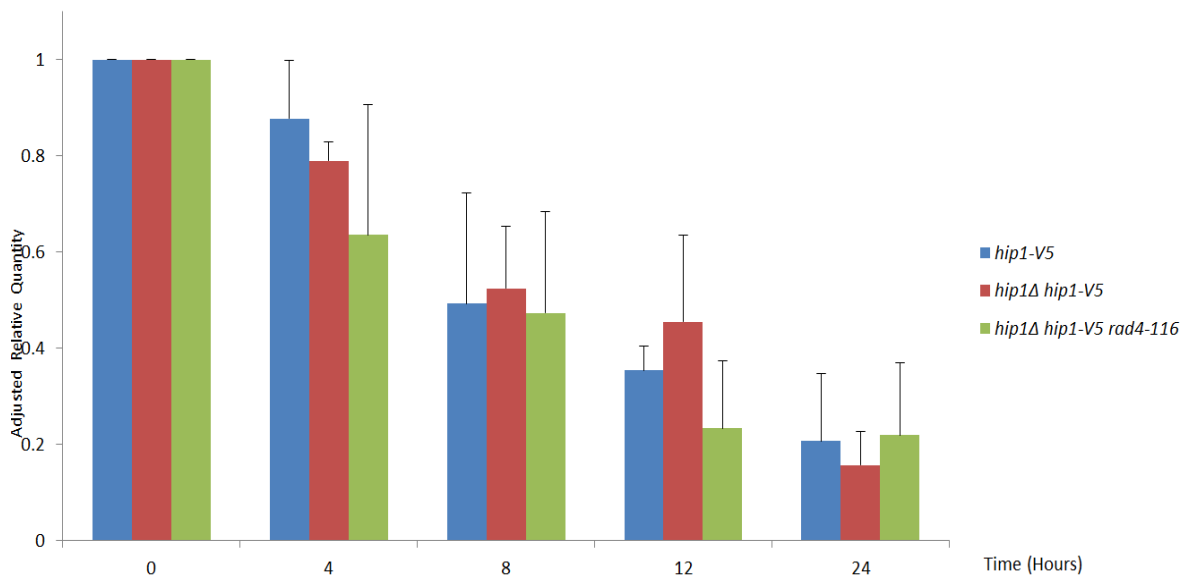


Figure 3-14. The comparison the adjusted relative quantity of RNA of strains carrying the *hip1-V5* allele. The figure shows the gradual decrease through graphical representation of the adjusted relative quantity between all the *Hip1-V5* strains across the 24 hour timecourse after the addition of thiamine to the media.

3.3.2 The depletion of Hip1-V5 expression by Western Blotting

Western blotting was used to be able to assess the depletion of the Hip1-V5 protein in the strains carrying *hip1-V5* (Figure 3-15, 3-16, 3-17 and 3-18). The protein was extracted from each strain at each timepoint and then purified using the Y-PER™ Yeast Protein Extraction Reagent. Proteins separated by SDS PAGE were then transferred onto Amersham Hybond™-PVDF membranes using a transfer cell (Bio Rad) and then probed using the primary antibodies. Each PVDF membrane was separated based on the expected signal size and each separate section was probed with its corresponding antibody. After secondary antibody probing, each PVDF membrane was wrapped in saran wrap and the chemiluminescent signal was detected and imaged using the BioRad Chemidoc XRS+ Imaging System or using an X-ray film. For each strain the western blotting was repeated at least three times using separate samplings. A preliminary blot was carried out to test the V5 signal depletion after 16 hours(overnight) of thiamine addition using the Hip1-V5 base strain (Figure 3-15).

The effect of thiamine addition on the *hip1-V5* strain

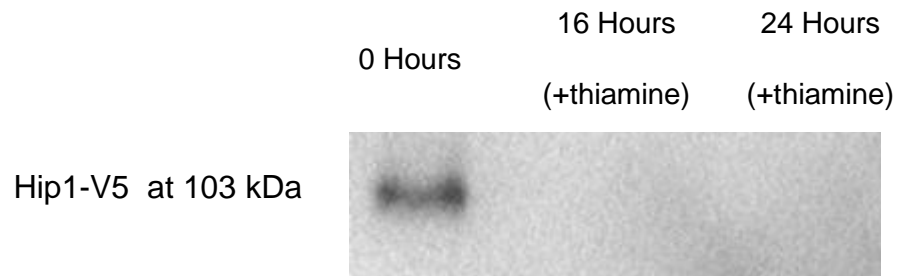


Figure 3-15. Expression of V5 tag in the base *hip1-V5* strain SPSC 1095 after the addition of thiamine. Protein samples were taken from SPSC 1095 incubated for 16 hours and 24 hours in EMM+uracil+leucine with and without the addition of thiamine to the media. The western blot shown represents the samples after being probed with anti-V5. The sample without the addition of thiamine expresses the V5 tag whilst the sample with the addition of thiamine does not express the V5 tag.

The effect of thiamine addition on the *hip1-V5* strain across 24 hours

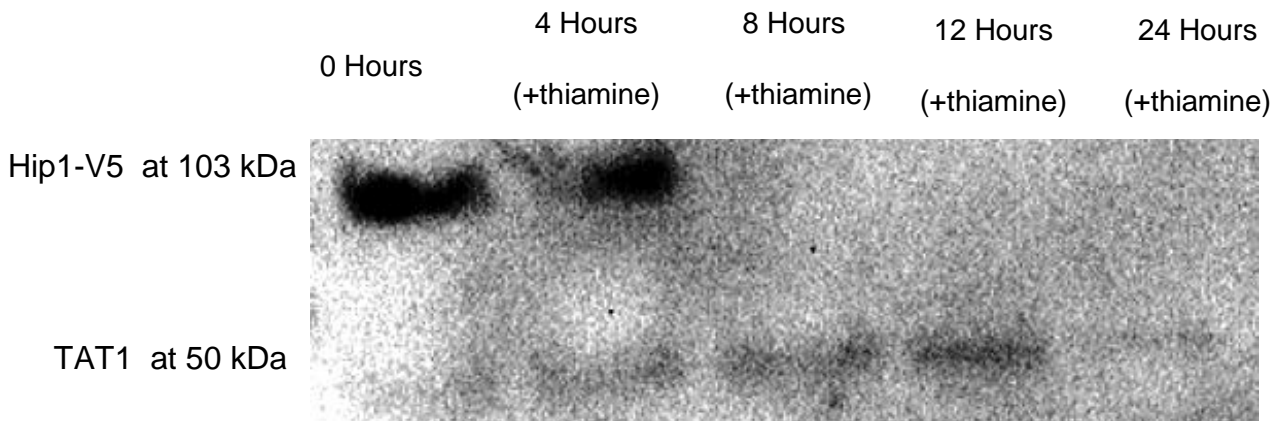


Figure 3-16 .Depletion of V5 tag in the base *hip1-V5* strain SPSC 1095 after the addition of thiamine. Protein samples were taken from SPSC 1095 incubated for 24 hours in EMM+uracil+leucine with the addition of thiamine to the media. The protein samples were taken from 0, the time of addition of thiamine to the 0.5 OD culture, to 12 hours at 4 hour-intervals then an additional sample at 24 hours. The western blot shown represents the samples after being probed with anti-V5 (top signal) and anti-TAT1 (bottom signal) as control. The 0 hour and 4 hour samples express the V5 tag while there was no visible signal for the 8 hour, 12 hour or 24 hours samples. The TAT1 signal shows no signs of depletion across all 5 samples.

The effect of thiamine addition on the *hip1Δ hip1-V5* strain across 24 hours

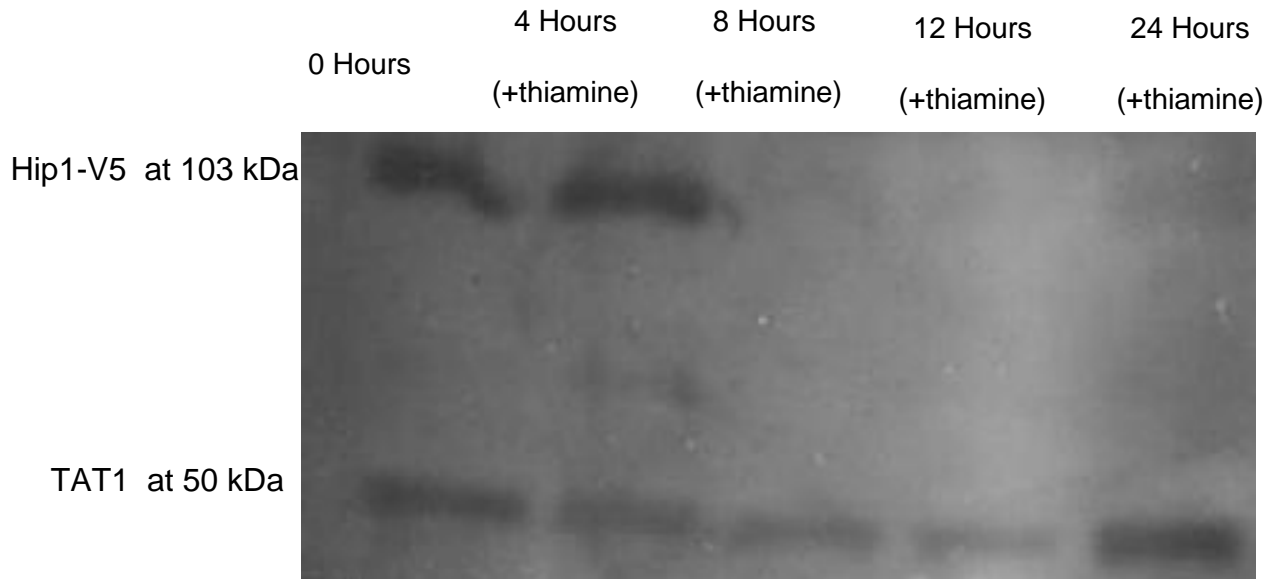


Figure 3-17. Depletion of V5 tag in the *hip1-V5 hip1Δ* strain SPSC 1100 after the addition of thiamine. Protein samples were taken from SPSC 1100 incubated for 24 hours in EMM+uracil+leucine with the addition of thiamine to the media. The protein samples were taken from 0, the time of addition of thiamine to the 0.5 OD culture, to 12 hours at 4 hour-intervals then an additional sample at 24 hours. The western blot shown represents the samples after being probed with anti-V5 (top signal) and anti-TAT1 (bottom signal) as control. The 0 hour and 4 hour samples express the V5 tag while there was no visible signal for the 8 hour, 12 hour or 24 hours samples. The TAT1 signal shows no signs of depletion across all 5 samples.

The effect of thiamine addition on the *rad4-116 hip1Δ hip1-V5* strain across 24 hours

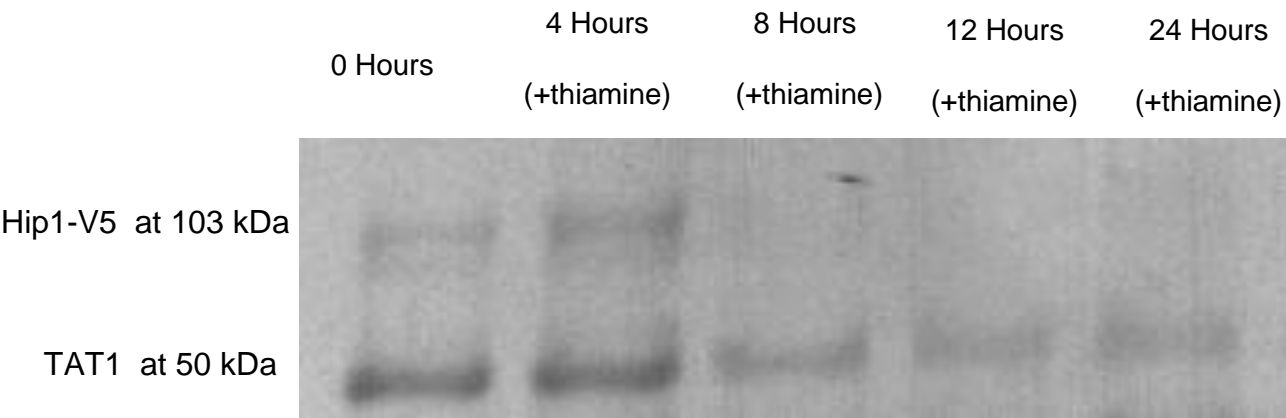
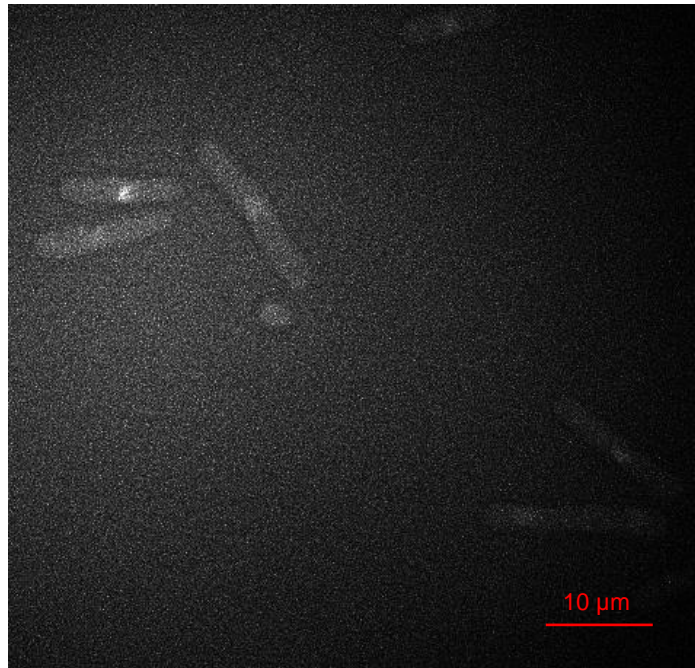


Figure 3-18. Depletion of V5 tag in the *hip1-V5 hip1Δ rad4-116* strain SPSC 1103 after the addition of thiamine. Protein samples were taken from SPSC 1103 incubated for 24 hours in EMM+uracil+leucine with the addition of thiamine to the media. The protein samples were taken from 0, the time of addition of thiamine to the 0.5 OD culture, to 12 hours at 4 hour-intervals then an additional sample at 24 hours. The western blot shown represents the samples after being probed with anti-V5 (top signal) and anti-TAT1 (bottom signal) as control. The 0 hour and 4 hour samples express the V5 tag while there was no visible signal for the 8 hour, 12 hour or 24 hours samples. The TAT1 signal shows no signs of depletion across all 5 samples.

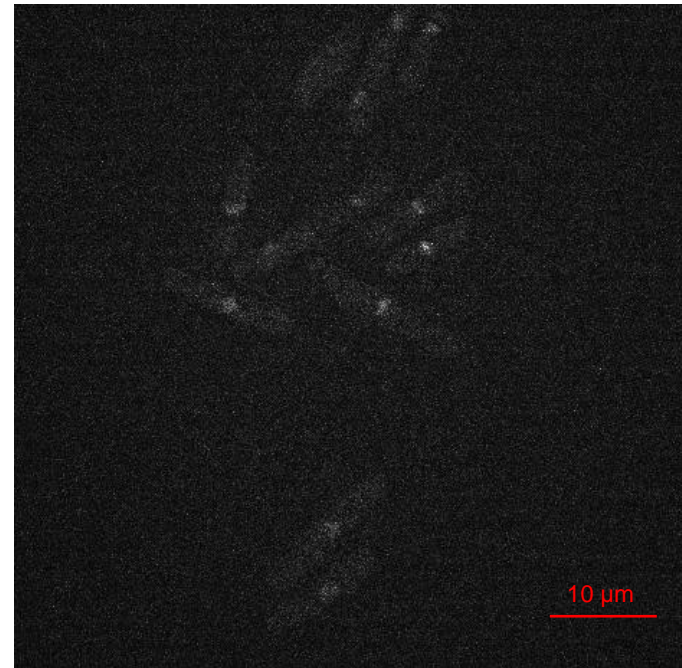
3.3.3 Phenotypic Characterisation of *hip1-V5* strains by microscopy

To be able to phenotypically characterise each strain carrying *hip1-V5*, cell pellets from each strain at each timepoint was taken. The cell pellets were fixed using paraformaldehyde and probed for the V5 tag using anti-V5 antibody. After primary and secondary antibody incubation, the cells were mounted onto well glass slides using mounting media with DAPI. The cellular length, size and nuclear shape were observed and noted for at least 100 cells in triplicates of different samplings.

The effect of thiamine addition on the *hip1-V5* strain SPSC 1095 across 24 hours



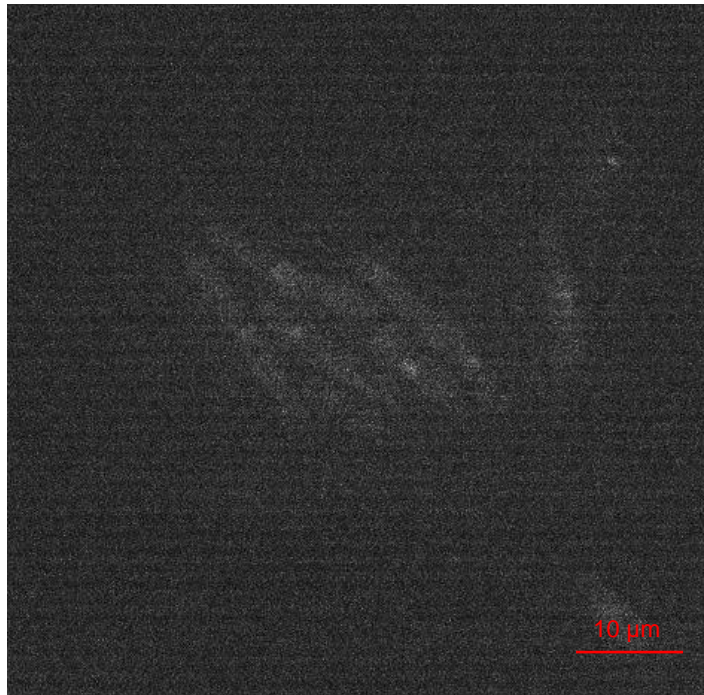
(A)



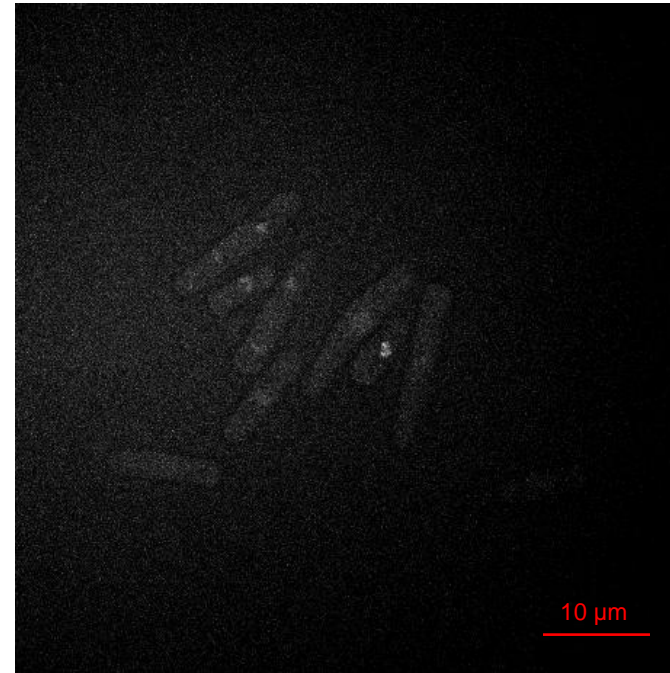
(B)

Figure 3-19. The cell morphology of the *hip1-V5* strain SPSC 1095 at 60X magnification across 24 hours after thiamine induction. The figure shows the cells of the *hip1-V5* strain stained with DAPI to show the nuclei at (A) the 0 hour timepoint and the (B) 24 hour timepoint. There is no significant difference between the cells across those 2 timepoints in terms of cell length, cell shape and nuclear shape.

The effect of thiamine addition on the *hip1Δ hip1-V5* strain SPSC 1100 across 24 hours



(A)



(B)

Figure 3-20. The cell morphology of the *hip1Δ hip1-V5* strain SPSC 1100 at 60X magnification across 24 hours after thiamine induction. The figure shows the cells of the SPSC 1100 strain stained with DAPI to show the nuclei at (A) the 0 hour timepoint and the (B) 24 hour timepoint. There is no significant difference between the cells across those 2 timepoints in terms of cell length, cell shape and nuclear shape.

The effect of thiamine addition on the *rad4-116 hip1Δ hip1-V5* strain SPSC 1103 across 24 hours

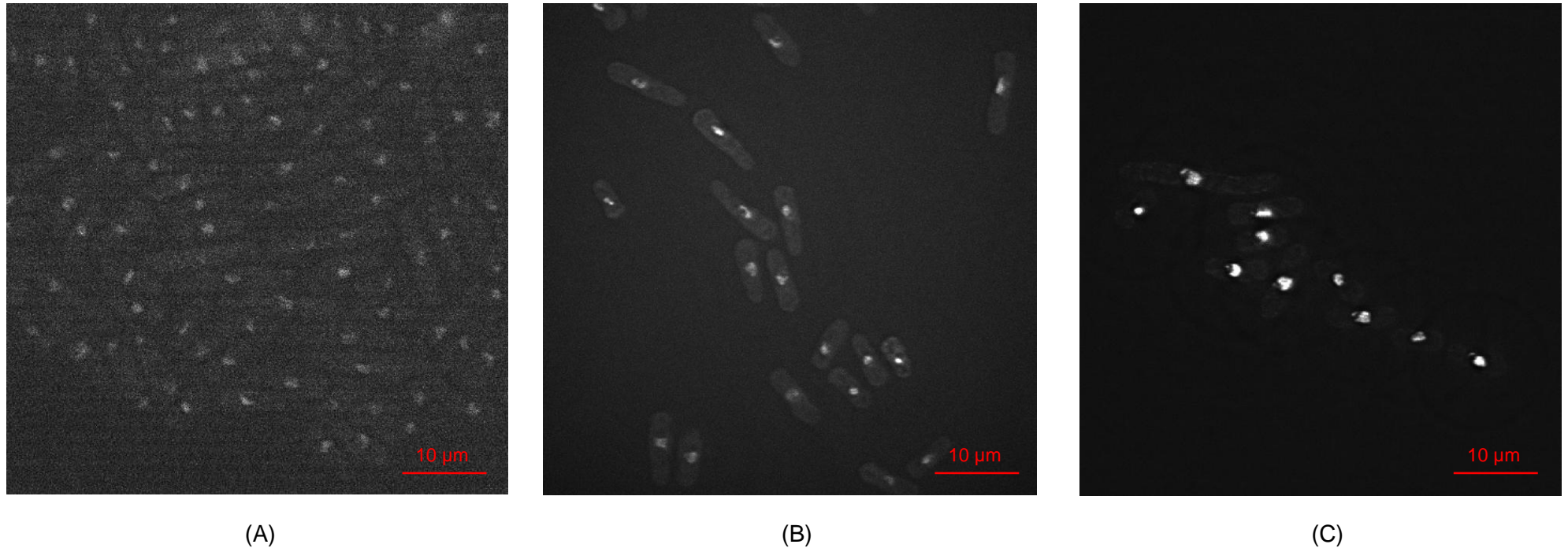


Figure 3-21. The cell morphology of the *hip1Δ hip1-V5 rad4-116* strain SPSC 1103 at 60X magnification across 24 hours after thiamine induction. The figure shows the cells of the SPSC 1103 strain stained with DAPI to show the nuclei at (A) the 0 hour timepoint, (B) the 12 hour timepoint and (C) the 24 hour timepoint. The cells show two distinct phenotypes, that develop from timepoint 0 to 12 to 24 hours, for cells to increase or decrease in length. The nuclei of most these cells show a fragmentation that becomes more pronounced at the 24 hour timepoint and some cells show a compacted nucleus.

3.3.4 The effect of thiamine addition on the *rad4-116 hip1Δ hip1-V5* strain SPSC 1103 across 24 hours on cell length

Figure 3-22 to Figure 3-26. The population of SPSC 1103 divided by cell length across the 24 hour period after thiamine addition. The figures shows the graphical representation of the percentage of cells by cell length at each timepoint.

SPSC 1103 at Timepoint 0 Hours

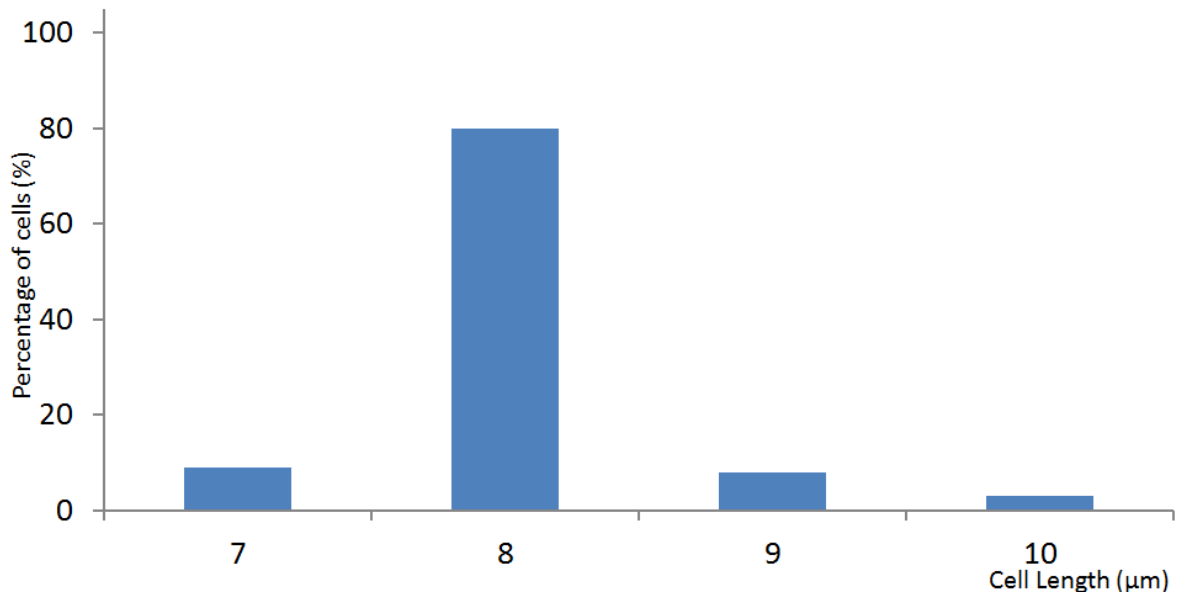


Figure 3-22. The population of SPSC 1103 divided by cell length at the 0 hour timepoint after thiamine addition.

SPSC 1103 at Timepoint 4 Hours

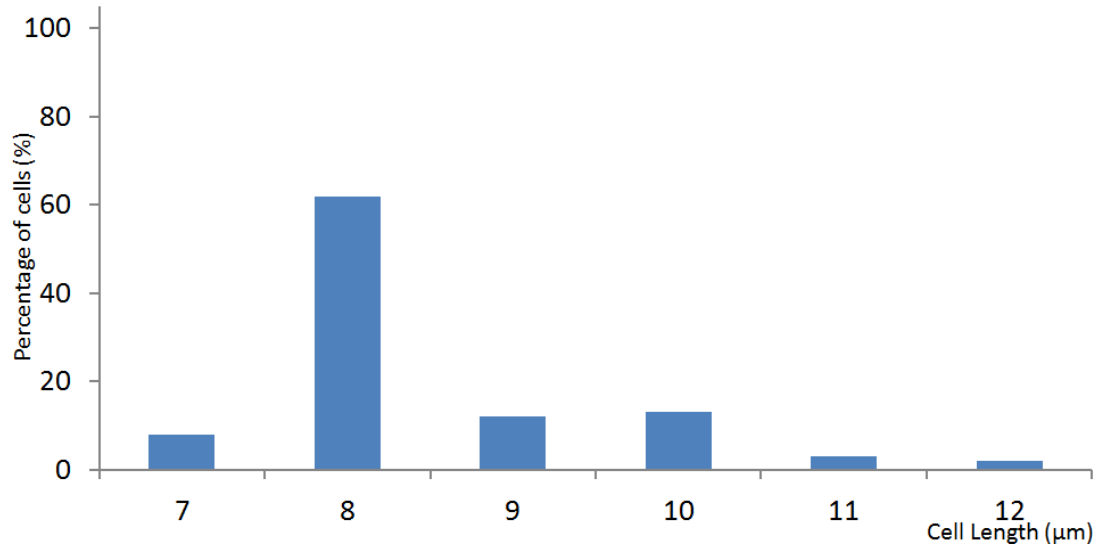


Figure 3-23. The population of SPSC 1103 divided by cell length at the 4 hour timepoint after thiamine addition.

SPSC 1103 at Timepoint 8 Hours

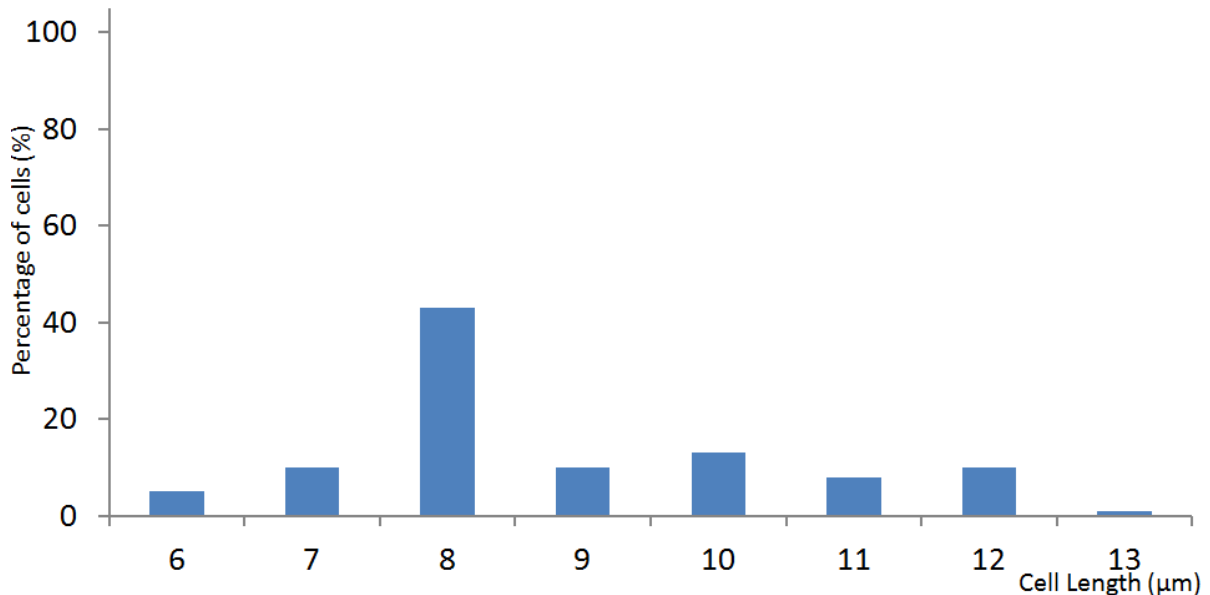


Figure 3-24. The population of SPSC 1103 divided by cell length at the 8 hour timepoint after thiamine addition.

SPSC 1103 at Timepoint 12 Hours

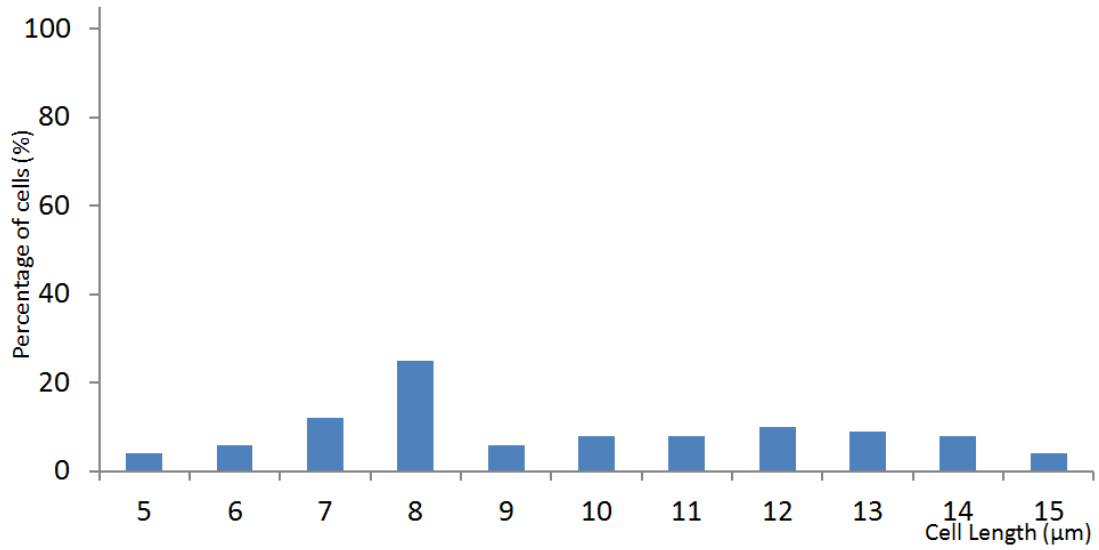


Figure 3-25. The population of SPSC 1103 divided by cell length at the 12 hour timepoint after thiamine addition.

SPSC 1103 at Timepoint 24 Hours

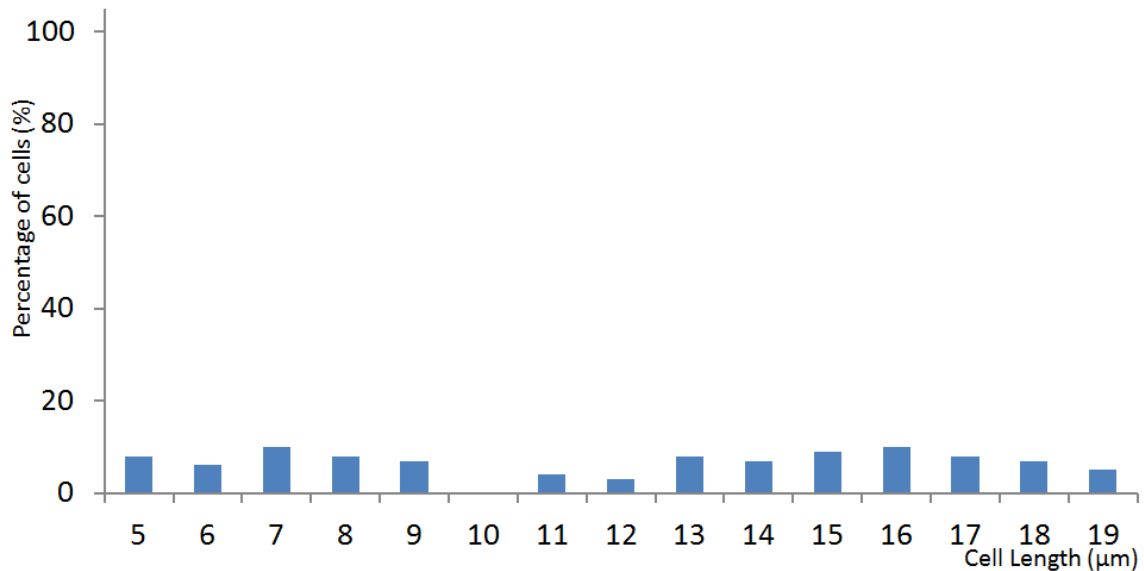


Figure 3-26. The population of SPSC 1103 divided by cell length at the 24 hour timepoint after thiamine addition.

The effect of thiamine addition on the average cell length of *hip1-V5* strains across 24 hours

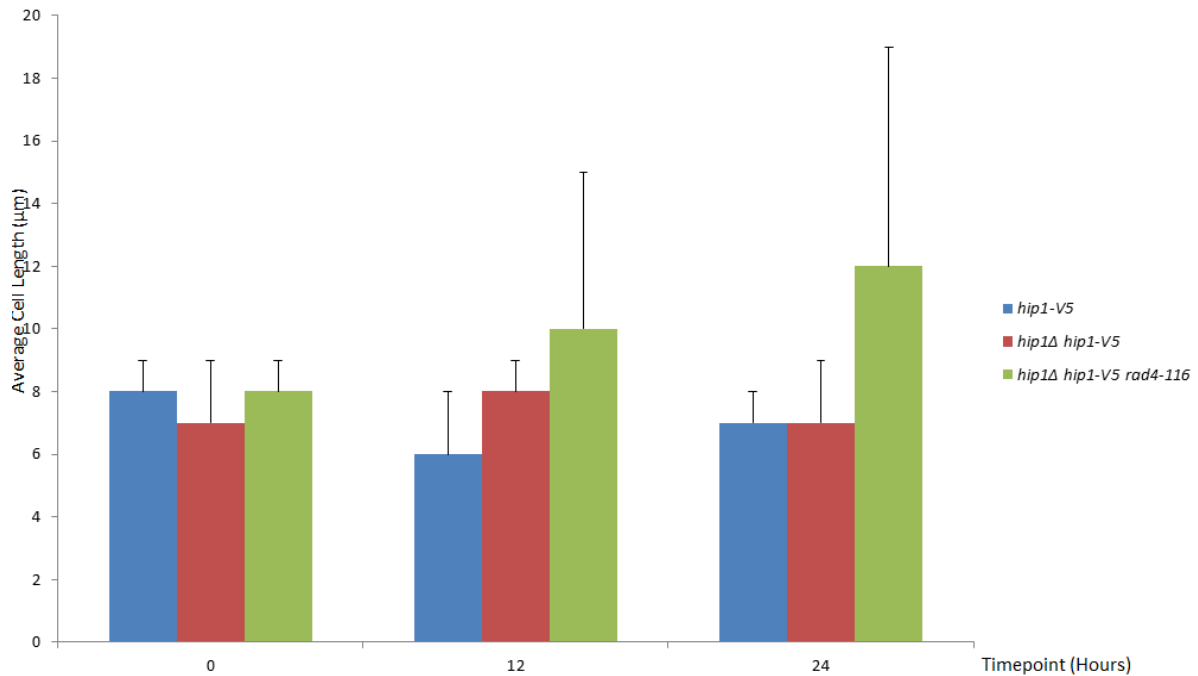


Figure 3-27. The average cell length of the strains carrying the *hip1-V5* allele. The figure shows the graphical representation of the comparison of average cell length between the base *hip1-V5* strain, the *hip1-V5 hip1Δ* strain and the *hip1-V5 hip1Δ rad4-116* strain. No significant change in average cell length occurred in both the base *hip1-V5* strain and the *hip1-V5 hip1Δ* strain as the value is between 6 and 8µm between the 0 hour to 24 hours to finally reach 7µm for both strains at 24 hours after thiamine addition. As for the *hip1-V5 hip1Δ rad4-116* strain, the initial average cell length at 0 is similar to the other two strains at 8 µm. However, a gradual increase is then observed from 8 µm to 10 µm at 12 hours then 12 µm at 24 hours after the addition of thiamine. The cells of the *hip1-V5 hip1Δ rad4-116* strain contain 2 phenotypic cell sizes with the predominant one being an elongated cell of more than 13 µm in length and the other, less common, much shorter phenotype, being of 3 to 5 µm in length.

As observed in Figure 3-14 for QPCR and Figures 3-16, 3-17, 3-18 for western blotting, the expression of the RNA product and protein for Hip1-V5 were successfully depleted after 24 hours of incubation in media with thiamine. The adjusted relative quantity for the *hip1-V5* RNA expression reached 0.2065 for the *hip1-V5* strain in Figure 3-11, 0.1565 for the *hip1Δ hip1-V5* strain in Figure 3-12 and 0.219 for the *hip1Δ hip1-V5 rad4-116* strain in Figure 3-13. The adjusted relative quantity for all the *hip1-V5* strains across the 24 hour timecourse is summarised in Figure 3-14. The preliminary experiment in Figure 3-15 using the *hip1-V5* strain (SPSC1095), showed that the signal present using the anti-V5 antibody, was abolished completely following a 16 hour incubation with thiamine. The Hip1-V5 protein signal was present at timepoints 0 and 4 hours in all the three strains SPSC 1095, SPSC 1100 and SPSC 1103 as observed in Figure 3-16, Figure 3-17 and Figure 3-18 respectively. In all 3 figures, the signal was abolished below the detectable level from 8 hours after thiamine addition onwards. The level of expression of the control α -Tubulin for all three strains across all the timepoints did not show any change.

Indeed, the levels of RNA expression did not reach 0 as seen in Figure 3-14, yet, those levels were sufficient to lead to an abolishment of Hip-V5 protein expression below detectable levels as observed in the western blots. The depletion of RNA expression and protein signals also caused a decrease in viability, as seen in Figure 3-28, consistent with the time and level of abolishment of the V5-tagged protein in the *hip1Δ hip1-V5 rad4-116* strain but not in any of the other strains. The *hip1Δ hip1-V5 rad4-116* strain showed a gradual loss of viability dropping from 99% viability at 0 timepoint to 51% after 12 hours, then to 39% viability at 24 hours. The decrease in

viability at timepoints 8, 12 and 24 was statistically significant at $p \leq 0.01$ with values of 62%, 51% and 39% respectively compared to the 0 hour timepoint which is consistent with the depletion of V5 protein signal. However, the presence of viable cells indicated that the level of depletion per cell in the culture population is not equal. This is also reflected in the presence of 0.219 adjusted relative quantity value of V5 RNA for the *hip1 Δ hip1-V5 rad4-116* strain as represented in Figure 3-13.

In terms of cell morphology, as observed in Figure 3-21 and Figure 3-20, the cell size and length and nuclear integrity of SPSC 1095 (*hip1-V5*) and SPSC 1100 (*hip1 Δ hip1-V5*) respectively did not show any change across the 24 hour timecourse. However, as seen in Figure 3-21 and Figure 3-27, the *hip1 Δ hip1-V5 rad4-116* strain SPSC 1103, showed two distinct phenotypes in terms of cell size. The more common phenotype being longer of more than 10 μm in length and the less common phenotype being a shorter cell of less than 7 μm in length as observed in Figure 3-20. Both phenotypes show irregular nuclear size and shape with some nuclei being elongated and others fragmented or compacted. Those changes were detectable after 12 hours of thiamine incubation and more pronounced at the 24 hour timepoint. The changes in average cell length for SPSC 1103 was compared at the 0, 12 and 24 hours timepoints to the SPSC 1095 (*hip1-V5*) and SPSC 1100 (*hip1 Δ hip1-V5*) strains and summarised in Figure 3-27.

3.3.5 The viability profile of *hip1Δ hip1-V5 rad4-116*

The paired Student T-test was performed to compare the viability of each *hip1-V5* strain at each timepoints 4, 8, 12 and 24 hours after the addition of thiamine to the media to the starting 0 hour viability value. Each value of viable cells was obtained from an average of a triplicate separate cultures of strain at each timepoint at which a triplicate of EMM+ uracil+ leucine+ thiamine plates were used to grow 100 colonies. After 3 days of incubation at 26 °C, the number of viable colonies on each plate was counted and recorded and the average calculated for the *hip1Δ* strain and compared to the *rad4⁺* strain at its corresponding timepoint. The variance for both samples were similar allowing the use of the 2-tailed Student T-test. The degree of freedom for each sample used at each timepoint was 2 and the critical value over which the difference is significant is 9.925 at $p \leq 0.01$. $p \leq 0.01$ was chosen over the standard $p \leq 0.05$ as the critical values, calculated and determined to be significant at $p \leq 0.05$, were also significant at $p \leq 0.01$. For the *hip1-V5* and *hip1Δ hip1-V5*, there was no significant difference the viability counts observed across all the timepoints recorded from 0 to 24 hours. However, for *hip1Δ hip1-V5 rad4-116* strain, timepoints 8, 12 and 24 showed a significant decrease in viability at $p \leq 0.01$ with values of 62%, 51% and 39% respectively compared to the 0 hour timepoint.

Viability Comparison of *hip1-V5* strains

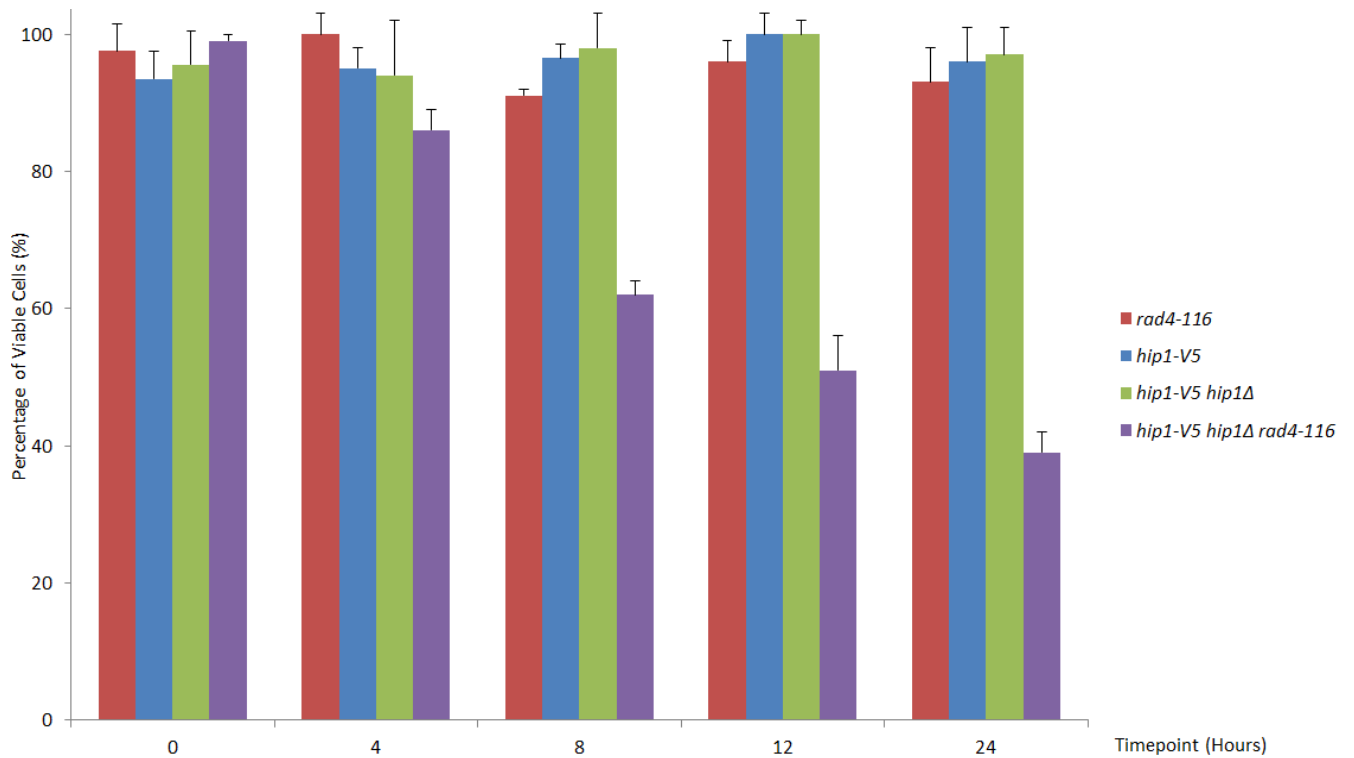


Figure 3-28. The viability comparison of strains carrying the *hip1-V5* allele against the control *rad4-116* strain. The figure shows the graphical representation of the comparison of viability between the *Hip1-V5* strains and the *Rad4-116* strain across the 24 hour timecourse after the addition of thiamine to the media. Only SPSC 1103 showed a gradual loss of viability dropping from 99% viability at 0 timepoint to 51% after 12 hours, then to 39% viability at 24 hours. All the other strains represented showed no significant loss of viability across the 24 hour timecourse ranging from 100% to 91% viability.

3.3.6 Phenotypic Characterisation of *hip1-V5* strains by FACS

To be able to assess the DNA content and analyse the cell cycle profile of each strain, Fluorescence-activated cell sorting (FACS) using Propidium Iodide (PI) was carried out. The synchronised cultures used in the previous sections of this chapter were utilised to sample cell pellets for use in FACS. As previously stated, the timepoints were chosen based on the recommendations provided in the study by Fennessey and coworkers (Fennessey *et al.*, 2014) and the preliminary results of RT-QPCR and western blotting. Cell pellets were collected from each strain at each timepoint and were fixed in 70% ethanol. Then fixed cells were stained with PI and analysed using the CytoFlex FACS platform. Control samples of 1C and 4C DNA content were collected during each sampling and used to observe a minimum and maximum staining threshold using PI.

Phenotypic Characterisation of *hip1-V5* (SPSC 1095) and *hip1Δ hip1-V5* (SPSC 1100) strains by FACS

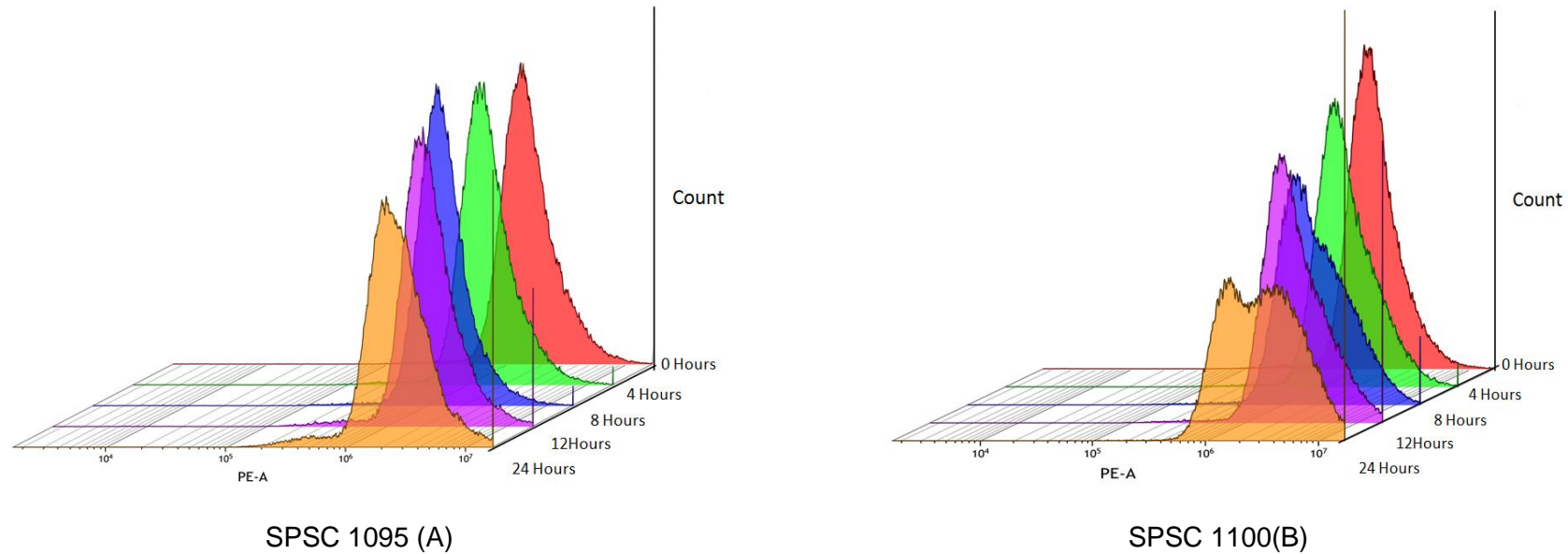


Figure 3-29. Cell population as investigated through FACS. The figure shows the analysis of the populations of SPSC 1095 (A) and SPSC 1100 (B) as representation of count (y-axis) against the phycoerythrin channel PE-A (x-axis) across 24 hours with 0 hour being the furthest along the z-axis followed by 4, 8, 12 and finally, 24 hours being the nearest along the z-axis. For (A) SPSC 1095, no change in staining occurred or shift in peaks across the 24 hours with only the 24 hour sample showing a decreased peak level. For (B) SPSC 1100, a general decrease in peak occurred from 0 to 24 hours. No shift occurs from 0 to 12 hours but the 24 hour sample showed a double peak.

Phenotypic Characterisation of *rad4-116 hip1Δ hip1-V5* strain SPSC 1103 by FACS

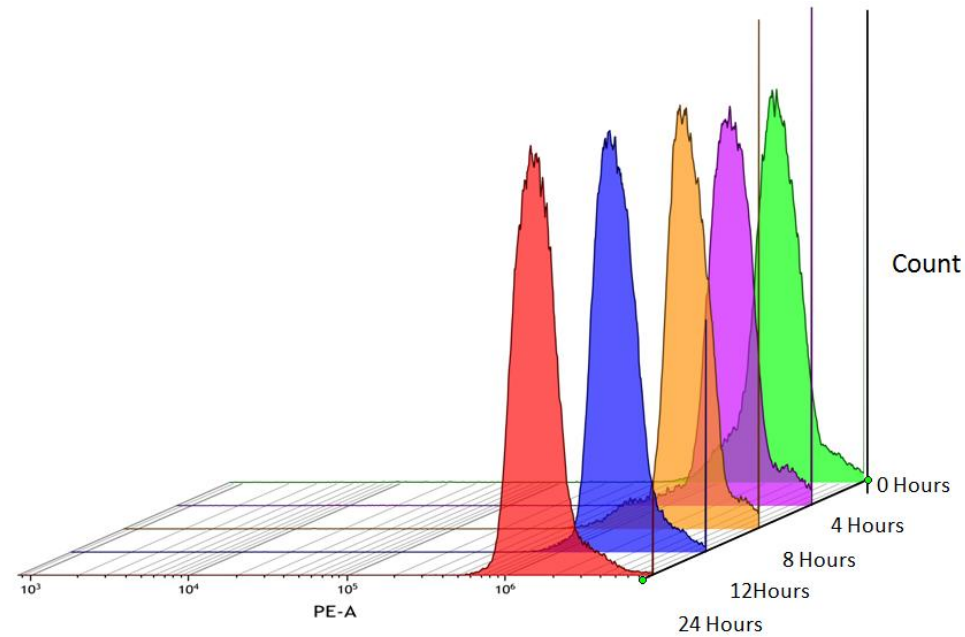


Figure 3-30. Cell population as investigated through FACS. The figure shows the analysis of the population of SPSC 1103 as representation of count (y-axis) against the phycoerythrin channel PE-A (x-axis) across 24 hours with 0 hour being the furthest along the z-axis followed by 4, 8, 12 and finally, 24 hours being the nearest along the z-axis. There was no change in staining or shift in peaks across the 24 hours.

3.4 Hip1 Chapter Discussion

By mapping the spores from crossing the *rad4-116* strain with the *hip1Δ* strain in Figure 3-1 and tabulating 144 valid spores in total in Table 3-A, the χ^2 value was calculated at 27.7. The χ^2 value was consistent with values calculated previously in preliminary studies carried out (results not shown). The χ^2 value was significant to prove that the results obtained in terms of synthetic lethality of combining *rad4-116* and *hip1Δ* was not due to chance but due to the interference occurring in one or more biological pathways. In this case, the hypomorphic function of *rad4-116* and possibly at least one of the functions of *hip1*.

The comparison of DNA damage profiles of *rad4-116* and *hip1Δ* strains after incubation with HU using Rad52-GFP foci was carried out. There are several categories or aspects in which the profiles were compared. The Deltavision microscope and the Softworx program were used to analyse the slides after fixation. The cells were stained for DAPI to show nuclei and anti-GFP to show foci as presented in Figure 3-3 for the *hip1Δ* strain. It should be noted that the *rad4-116*, *rad4⁺* and *hip1Δ* strains did not show a significant change in viability across the timecourse of the experiment as presented in the graph of Figure 3-4.

Firstly, the number of foci per nucleus present were different as *hip1Δ* cells showed at most a single focus per nucleus whilst *rad4-116* cells, not uncommonly, showed multiple foci per nucleus as well as a single focus per nucleus. This can be easily observed in Figure 3-2 for *hip1Δ* cells and Figure 3-8 for *rad4-116* cells with the green foci present in dark blue stained nuclei. In this aspect, *hip1Δ* cells were more similar to *rad4⁺* cells as both present single foci-containing nuclei as demonstrated in Figure 3-2 for *hip1Δ* cells and Figure 3-6 for *rad4⁺* cells.

The second aspect was the percentage of nuclei containing foci as a section of all the population of nuclei counted at the starting point, timepoint 0, of the experiment. The starting percentage was similar in *hip1Δ* cells and *rad4⁺* cells at 5% , as presented in Figure 3-5, and 6%, as presented in Figure 3-7, respectively. This was in contrast to the much higher value of 26% for *rad4-116* cells at timepoint 0 as shown in Figure 3-9. This highlights the difference in the accumulation of DNA damage, as shown by Rad52-GFP recruitment onto DNA damage sites, after fork stalling before the activity of HU in cells. This also underscores the key difference in the roles of *rad4* and *rad4-116* in terms of maintenance of the replication fork and stalled fork resolution.

Another aspect was the peak of the percentage of nuclei with GFP foci as a section of the total population of nuclei across the duration of the experiment, 210 minutes. The peak values of each of the strains did not match each other in terms of time reached or the level of accumulation of foci. For the *hip1Δ* strain, the peak was reached at 90 minutes for a value of 13% as seen in Figure 3-5. For the *rad4⁺* strain, the peak was reached at 120 minutes for a value of 27% as observed in Figure 3-7. For the *rad4-116* strain, the peak was reached at 150 minutes for a value of 49% as seen in Figure 3-9. For both the *hip1Δ* strain and the *rad4⁺* strain, the shape of the graph was similar with a gradual increase up to a peak point occurring after 90 minutes or 120 minutes which are consecutive timepoints. The percentage of nuclei with foci began to decrease, also in a gradual manner, after the 120 minute timepoint in both cases to present a bell-shaped figure. This lied in stark contrast to the *rad4-116* strain which showed a sharp increase from 0 to 30 minutes and levelled off at 38% or above, with the exception of the 120 minute timepoint, till the 210 minute timepoint at the end of the experiment.

The final and, perhaps, most interesting aspect was the final reading of nuclei with foci and the comparison between the starting and final timepoints for each strain. For both the *hip1Δ* strain and the *rad4⁺* strain, the final reading of 3% was nearly half the initial reading of 5% and 6% as observed in Figure 3-5 and Figure 3-7 respectively. This differed from the *rad4-116* strain, which reached a final reading of 21% which is only a 5% decrease in value from the initial reading of 26% as observed in Figure 3-9. It could be argued that all three strains recovered to below the initial value of percentage of nuclei with foci, but that does not take into account the raw values of the readings as a percentage. By dividing the final values over the initial values, it could be highlighted that both the *hip1Δ* strain and the *rad4⁺* strain recovered well to a value nearly half the initial reading. However, the *rad4-116* strain would have needed a value below 13% for the final reading to show a comparable recovery or decrease. The initial values, peak values and final readings for all three strains are summarised in Figure 3-10 to further highlight the recovery patterns of all three strains. In contrast to the other two strains, the *rad4-116* strain failed to recover from the incubation with HU as cells accumulated stalled, and possibly collapsed, DNA replication forks without resolution. This is also supported by the fact that the *rad4-116* strain kept accumulating nuclei with multiple foci as time increased fluctuating between 9% and 5% of all nuclei counted.

By constructing strains carrying the repressible *hip1-V5* allele in the presence of *rad4-116*, it was possible to observe the behaviour of cells during cell death as the V5-tagged Hip1 activity was abolished. Strains carrying the *hip1-V5* and *hip1-V5 hip1Δ* genes were constructed before introducing *rad4-116* to a final strain. Those strains were useful in validating the activity of the *hip1-V5* allele in terms of mRNA transcription and the presence of the final protein Hip1-V5 product in cells.

The use of the adjusted relative quantity formula was to be able to justly assess the increase or decrease in RNA product of the desired gene in relation to a house-keeping gene after thiamine addition. This acts to mirror and confirm the use of western blotting and protein analysis of the protein product of the desired gene barring any post transcriptional modification or aberrant changes in the half-life of the protein. By using RT-QPCR, it was confirmed that a gradual decrease in the relative quantity of RNA encoding *hip1-V5* in all the strains tested as observed in Figure 3-14. Evidence of Hip1-V5 depletion was confirmed using western blotting using the V5 antibody, alongside TAT1 as a control, for the strains carrying *hip1-V5*. By observing Figures 3-16, 3-17 and 3-18, all three *hip1-V5* strains showed total abolishment of the Hip1-V5 signal, at the 103 kDa mark, after 8 hours of the addition of thiamine to the media.

The depletion of the RNA signal and tagged protein product did not cause a visible change in cell morphology in both the *hip1-V5* and *hip1Δ hip1-V5* strains across the 24 hour time course as observed in Figure 3-19 and Figure 3-20 respectively. However, the cell morphology began to change significantly in the *hip1Δ hip1-V5 rad4-116* in response to the depletion of the RNA signal and Hip1-V5 as observed in Figure 3-21. The correlation in the time of decrease of RNA product leading to the decrease in protein product appeared as change in cell morphology and length as soon as 8 hours after thiamine addition. The difference from 4 to 8 hours, a lag period of 4 hours, could be due to the degradation of protein product before repression of the *hip1-V5* gene. Nonetheless, a visible and significant change was observed after 12 hours, as seen in Figure 3-21(B), as well as a more pronounced change after 24 hours, as seen in Figure 3-21(C).

There are several changes that occur in the cell morphology of the *hip1Δ hip1-V5 rad4-116* strain in terms of nuclear integrity, cellular shape and cell length and. Interestingly, two distinct phenotypes could be followed through the 24 hour time course. In Figure 3-21(B), most of the cells develop compact nuclei observed as soon as 12 hours after thiamine addition. This escalates into further decrease in nuclear area stained with DAPI as well as the appearance of nuclear fragmentation in most cells, as seen in Figure 3-21(C), 24 hours after thiamine addition. This could be related to the combined roles of *rad4-116* and, more importantly, *hip1* in the maintenance of nuclear integrity as histone modifiers.

The more important aspect of change in cellular morphology of the *hip1Δ hip1-V5 rad4-116* strain, was the changes in cell length which was mapped in detail in Figure 3-22 for timepoint 0 till Figure 3-26 for timepoint 24 hours to include all the timepoints at 4-hour intervals. The starting timepoint 0 showed a similar cell length distribution to the *hip1-V5* and *hip1Δ hip1-V5* strains. The *hip1-V5* and *hip1Δ hip1-V5* strains did not show a significant change in cell length across the 24 hour time course, with a slight decrease that was not statistically significant possibly due to the initiation of starvation in a sub-section of the cell cultures after 24 hours. In contrast, the *hip1Δ hip1-V5 rad4-116* strain began to deviate in cell length in two directions being a gradual increase in length on one hand and a gradual decrease on the other hand to develop the two distinct phenotypes. It should be noted that the shorter phenotype of less than 7 μ m did not significantly appear till after 8 hours of thiamine addition as observed in the difference between Figure 3-23 to Figure 3-24 to Figure 3-25. By the end of the experiment, the fully developed phenotypes were far apart in length such that the subset of lengths between 8 to 12 μ m comprised a distinctly small subset of the population as observed in Figure 3-26. The long-length phenotype was the more

predominant phenotype, as cells grew to a range between 13 to 19 μm compared to the 8 μm at the starting point. The subpopulation of cells whose lengths range between 5 to 7 μm were present to a lesser degree as seen in Figure 3-26. The analysis of the subpopulations based on length was crucial, as the average length of cells did not fully provide the best understanding of the changes occurring in the cells following the abolishment of Hip1-V5 across 24 hours as represented in Figure 3-27. The development of two distinct phenotypes showed that the interaction between *rad4-116* and *hip1* occurred at not one but possibly, at least two pathways in DNA modification. Both phenotypes ultimately led to the death of cells in a gradual manner as observed in Figure 3-28. The same figure, Figure 3-28, showed that no cell death occurred in other strains carrying *hip1-V5* or the control strain carrying *rad4-116* with a wildtype *hip1* allele. This could be due to the presence of an undiscovered function of *hip1* or another interaction, leading to synthetic lethality in the case of *hip1* Δ , between *rad4-116* and *hip1*. Similar results in terms of the recorded increase in cell length were observed in *hip1* Δ cells in previous studies (Blackwell *et al.*, 2004). It should be noted that given the novelty of observing the morphological effects of the combination of *hip1* Δ and *rad4-116* during a synthetically lethal interaction, the shorter phenotype has not been recorded previously in the studies published with *hip1* Δ cells.

Finally, in terms of using PI to investigate the nuclear content of the cells across the 24 hour timecourse after thiamine addition, no conclusion could be reached. All three figures, Figure 3-29 (A), Figure 3-29 (B) and Figure 3-30, should no significant change across the 24 hours. This could be similar to the changes developed in average cell length in that the subpopulations could not be separated, given the available equipment, into the distinct phenotypes which could show different

fluorescence readings. Naturally, this is a route that needs to be pursued with these strains, especially SPSC 1103, to be able to analyse any change through FACS.

It should be noted that a strain carrying the genotype *hip1Δ hip1-V5* and *rad4-116 rad52-GFP* was constructed and tested using RT-QPCR, western blotting and microscopy. The strain showed nearly identical results in terms of RNA depletion, V5 signal abolishment and loss of viability. However, the main reason this strain was constructed was to be able to observe the accumulation of Rad52-GFP foci during the 24-hour timecourse, after the addition of thiamine to the media. The *hip1Δ hip1-V5* and *rad4-116 rad52-GFP* strain did not show detectable foci from the starting point and did not accumulate any foci even after 24 hours. The experiment was repeated twice, to achieve a triplicate set, and the results were confirmed. The strain was reconstructed once again from a different cross and the experiment was then again, repeated in triplicate and the results were reaffirmed.

**Chapter 4: The Genetic Analysis of the
interaction between the Swi complex
members and *rad4-116***

4.1 Introduction

It has been shown that some factors are essential for DNA replication accuracy. Two of those factors are Swi1 and Swi3 which are components of the fork stabilisation complex (FPC) (Lee *et al.*, 2004; Noguchi *et al.*, 2004; McFarlane *et al.*, 2010). The members of the replication fork protection complex in fission yeast are conserved in both budding yeast and mammalian cells (Rapp *et al.*, 2010). The absence of Swi1 or Swi3 in cells leads to the accumulation of abnormal fork structures as observed with increased Rad52 DNA repair foci formation and recombination structures during the S phase (Noguchi *et al.*, 2003 a;b) . The Swi1-Swi3 complex directly interacts with the DNA structure and recruits Mrc1 to the replication fork (Shimmoto *et al.*, 2009; Tanaka *et al.*, 2010).

The mechanism of Swi1 action is not known but the role for Tof1 in fork pausing may provide insights into its function at the fork (Calzada *et al.*, 2005; Lambert *et al.*, 2005; 2007). On the other hand, Swi3 is able to promote the efficient restart of stalled replication forks in a checkpoint-dependent manner as well as restoring broken replication forks in a checkpoint independent manner (Noguchi *et al.*, 2012). The comparison between the profiles of DNA damage and cellular morphology of the members of the FPC is important to contrast the roles executed by Swi1 and Swi3. Then, the profiles would be compared to that of Mrc1 to be able to explore the mechanism of interaction between Mrc1 and the Swi1-Swi3 complex.

4.1.1 Synthetic Lethality on Agar

The aim of the investigation was to investigate the interactions between *rad4* and *swi1*, which is implicated in the maintenance of chromatin structure and remodelling.

The strains selected had either the *rad4-116* marked with NAT resistance and the *swi1* Δ marked with G418 resistance. The synthetic lethality method and analysis were carried out as detailed in Section 3.1.1.



Figure 4-1. The growth of individual spores to colonies of the *rad4-116* strain cross with *swi1Δ* strain. The figure shows 4 columns of the YES plates of the crosses of the *rad4-116* strain with a *swi1Δ* strain. The cross shown was a set of spores from tetrads that were inoculated into single spores with a line separating each individual spore set from a single tetrad. The number of spores from each YES plate was counted and recorded.

Cross	<i>swi1</i> Δ x <i>rad4-116</i>
Wild-type	32
G418 ^R	42
NAT ^R	32
G418 ^R /NAT ^R	14
Viability	125
Total valid spores	192
χ^2 value	23.4

Table 4-A showing the crosses between the *rad4-116* strain and *swi1*Δ. The *rad4-116* was tagged with NAT resistance while the *swi1* deletion were marked with G418 (Kanamycin) resistance. The crosses were carried out on EMM-nitrogen agar , then checked after 2 days for sporulation. The tetrads from sporulation were separated using the Singer Micromanipulator onto YES agar plates. After 4 days, the plates were then copied onto fresh YES, as shown in Figure 4-1, YES+G418 and YES+NAT plates separately. After another 3 days, the colonies on each plate were counted and recorded as seen in the table. The χ^2 value for each cross was calculated and tabulated at $p \leq 0.05$ with a degree of freedom of 1.

4.1.2 *swi1* Δ cause synthetic lethality when combined with *rad4-116*

After the colonies from the crosses were noted and counted from all the plates, the Chi-Square test was performed and a value of 23.4 was the result as shown in Table 4-A. As this value was calculated using the expected value based on the segregated spores not based on the expected segregation pattern, the values represent a focused measure on whether the double mutants were synthetically lethal or not. These values were all greater than 3.84, which was the threshold value at $p \leq 0.05$ with a degree of freedom of 1. This indicated that the deletion of *swi1* was synthetically lethal when combined with *rad4-116* and that any lethality or observed lack of growth would **not** be due to chance or random occurrence.

4.2 The DNA replication stalled fork profile of *swi1Δ*

The aim of this experiment was to be able to observe and compare the DNA stalled replication profiles, in terms of accumulation and resolution of DNA forks, of a *rad4-116* strain to *swi1Δ* and wildtype *rad4* as a control. This ability to assess and monitor such profile would be achieved by utilising Rad52-GFP which is recruited to repair and aid the progress of stalled replication forks. The strains were constructed by direct transformation of PCR-produced deletion *hip1* encoding G418 resistance and PCR-produced *rad4-116* attached to NAT resistance into a *rad52-GFP* base strain. Cells were grown in liquid media then arrested by the addition of hydroxyurea which blocks ribonucleotide reductase leading to the depletion of the ribonucleotides, thus halting DNA replication. Then after 6 hours of arrest with hydroxyurea, the cells were released by the depletion of hydroxyurea from the media, washing the cells then resuspending in rich YES media. Samples were collected every 30 minutes for 210 minutes to be analysed for fluorescence microscopy and testing viability.

The cell nuclei were assessed in two ways; the first being the percentage and number of nuclei that carry GFP fluorescent foci spanning the 210 minutes compared to the starting time point(0) of the release, and the second by assessing the number of foci per nucleus and arranging them in categories. The foci were assessed using the Softworx program by taking a 3D reconstruction of the cells to be able to assess if the foci observed were nuclear foci to be counted. The viability of each strain was tested by spreading 100 colonies per plate on YES plates in triplicate per each strain at each timepoint. The viability of cells in all three strains did not change from the arrest up to the 210-minute time point post release. The

percentage of nuclei with GFP foci was tabulated and a graph was drawn for each strain. As observed in the graph, the *rad4-116* showed a higher level of initial foci at the 0 timepoint compared to the other 2 strains.

The initial levels of Rad-52 GFP nuclear foci were 6% for both the *swi1Δ* and the *rad4⁺* strains contrasting to 26% in the *rad4-116* strain. For the *swi1Δ* strain the number of foci increased at a gradual low rate from 6% at the start of the release up to 11% after 60 minutes which was the peak level of foci recorded for the strain. Then, a gradual decrease occurred from 14% at timepoint 90 minutes to a plateau steady low level of 8% to 4% from 180 minutes after release onwards. The 2% recorded at the endpoint of the experiment, at 210 minutes after release, was lower than the starting level of 6% , showing a complete recovery from DNA stalled forks in a bell-shaped manner.

The values of percentage of cells with nuclear Rad52-GFP at the start and the end of the timecourse were similar when comparing the *rad4⁺* and *swi1Δ* strains but not the *rad4-116* strain. The patterns seen in the *rad4⁺* and *swi1Δ* strains were nearly identical as both show a bell-shaped curve with a peak at 90 to 120 minutes but not with the *rad4-116* strain. The difference between the *rad4⁺* and *swi1Δ* strains was that the peak or highest value recorded was 27% with the *rad4⁺* strain and 14% with the *swi1Δ*. However, both strains showed a decrease back to below initial levels of recorded GFP foci.

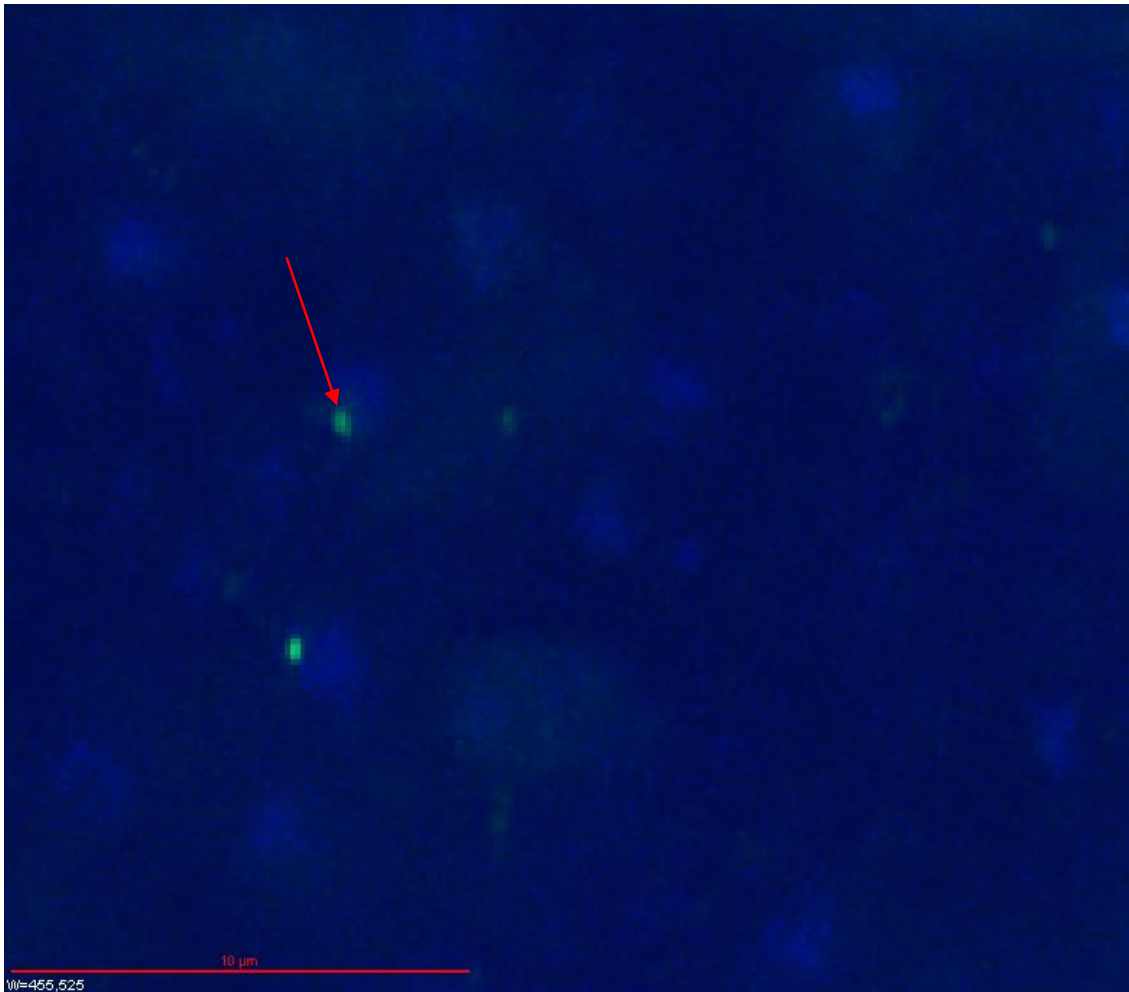
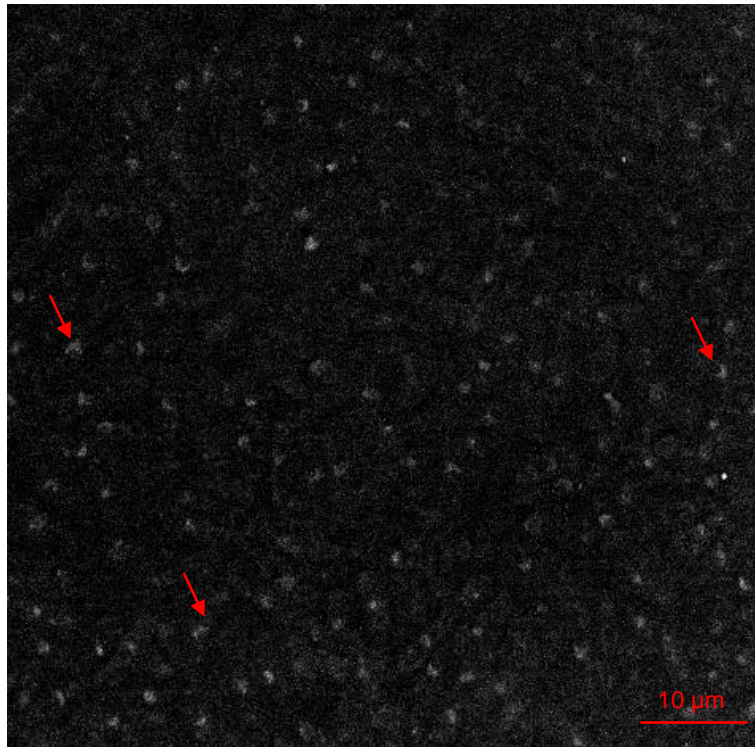
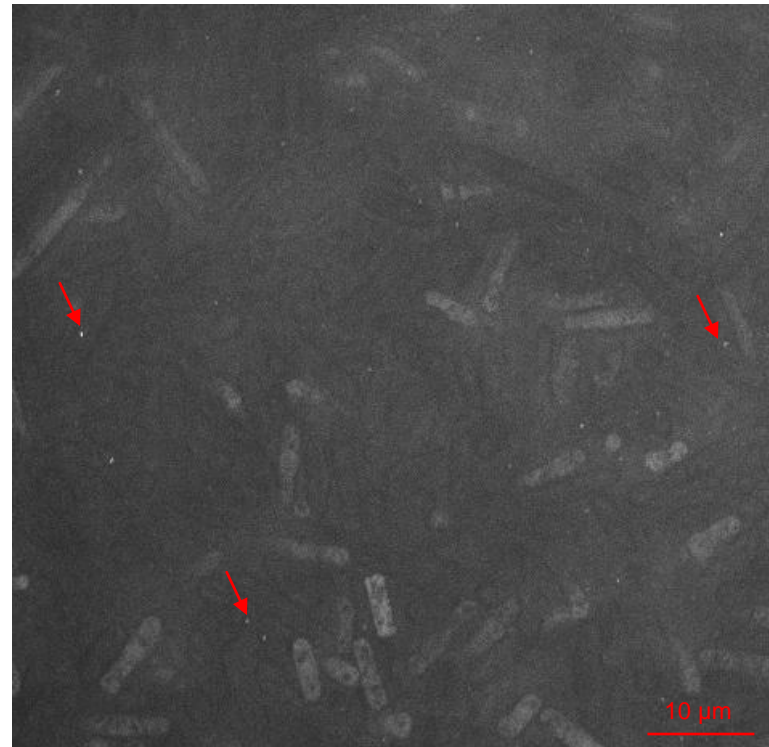


Figure 4-2. A merged image of *swi1Δ* cells after 90 minutes of incubation with Hydroxyurea. The nucleus (blue) highlighted by the arrow contains a single GFP signal (bright green). The cells were reconstructed into 3D using the Softworx program to reensure that the foci seen are indeed nuclear foci.



(A) (*swi1Δ* DAPI)



(B) (*swi1Δ* GFP)

Figure 4-3. Rad52-GFP foci of the *swi1Δ* strain at its peak. The figure shows the cells of the *swi1Δ* strain at 60X magnification stained with (A) DAPI to show the nuclei and (B) anti-GFP to show the Rad52-GFP foci. The cells were reconstructed into 3D using the Softworx program to identify nuclear foci. The peak value for nuclear foci was 14% of total number of nuclei. The red arrows point to some nuclei with Rad52-GFP foci.

Viability Comparison of *rad4-116*, *rad4*⁺ and *swi1*Δ

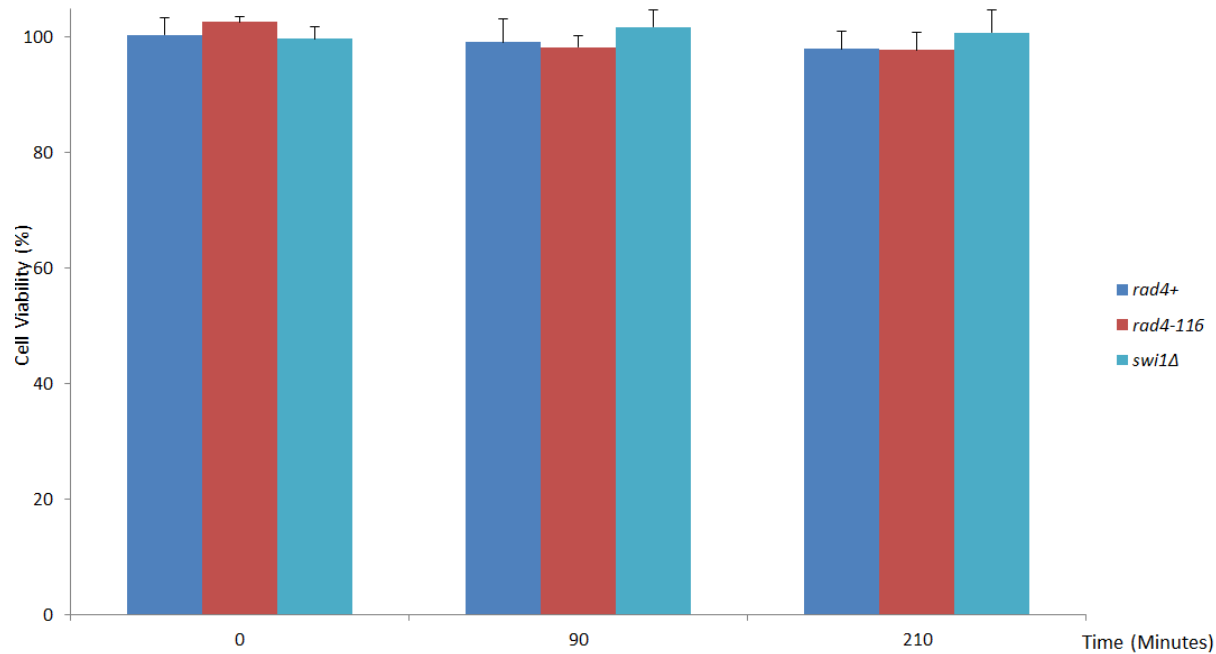


Figure 4-4. Viability counts for the *rad4*⁺, *rad4-116* and *swi1*Δ strains carrying the *rad52-GFP* gene. The figure shows bar chart graph representing the comparison between cell viability across the three strains of *rad4-116*, *rad4*⁺ and *swi1*Δ at the start of the experiment, at 90 minutes after the start and at the end of the experiment at 210 minutes. As observed, there was no significant change in viability across all three strains at these three timepoints.

Rad52-GFP Foci Profile of *swi1Δ*

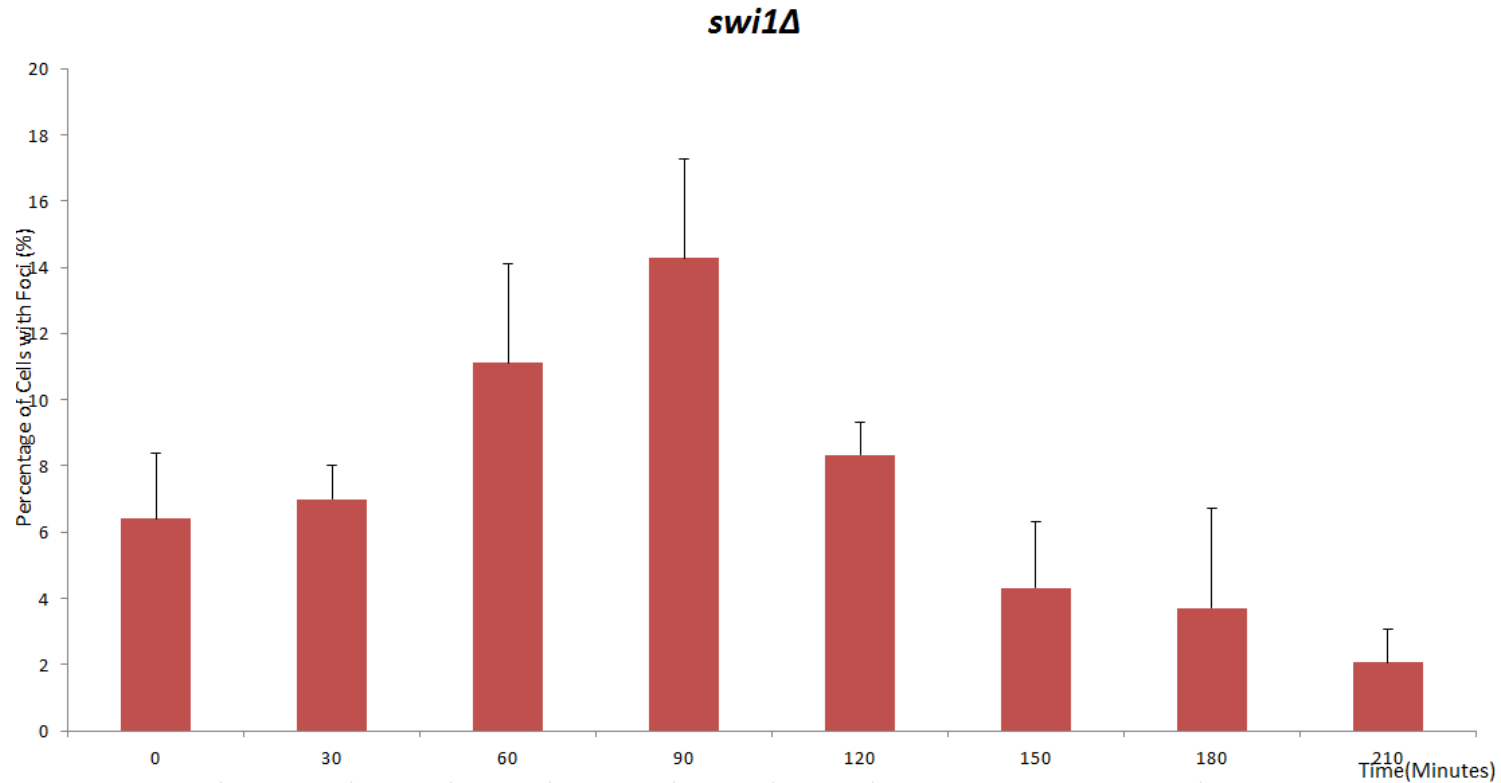


Figure 4-5. The Rad52-GFP profile of the *swi1Δ* strain. The figure shows the bar chart graph representing the percentage of cells with Rad52-GFP foci in the *swi1Δ* strain across timepoints from 0 to 210. The peak occurred at 90 minutes after the start of the experiment with a value of 14% of cells carrying nuclei with Rad52-GFP foci.

Rad52-GFP Foci Profile Comparison of *rad4-116*, *rad4*⁺ and *swi1*Δ

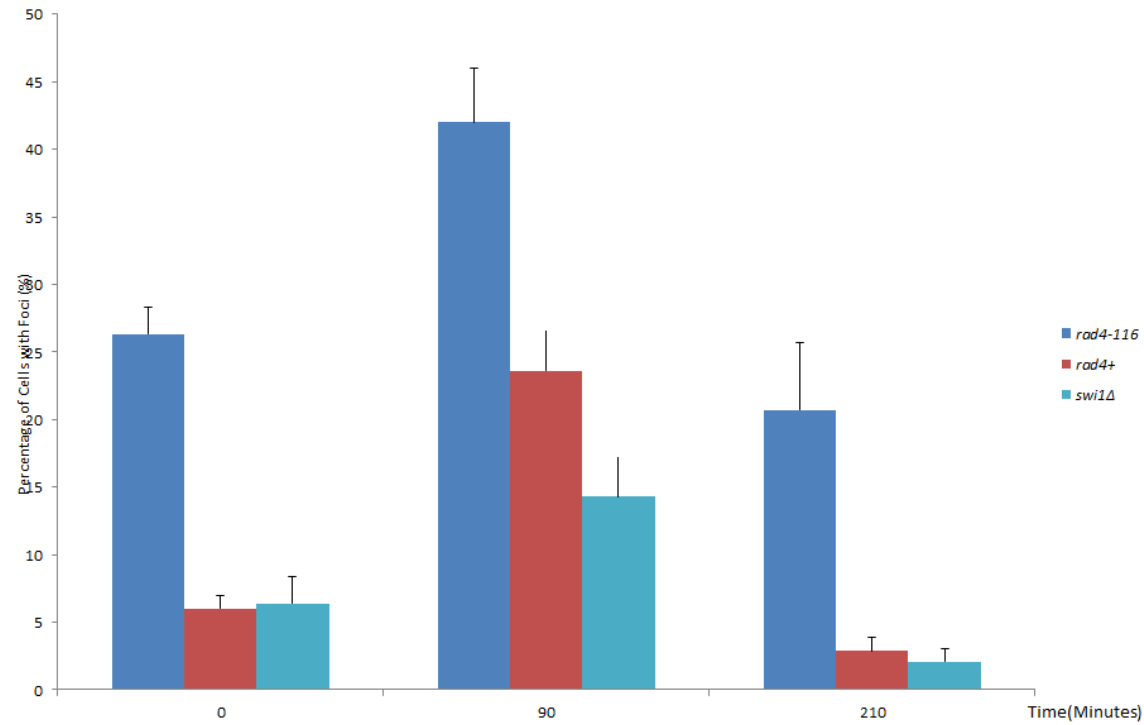


Figure 4-6. A comparison of the Rad52-GFP profiles of the *rad4-116*, *rad4*⁺ and *swi1*Δ strains. The figure shows the bar chart graph representing the comparison between the percentage of cells with Rad52-GFP foci across the three strains of *rad4-116*, *rad4*⁺ and *swi1*Δ at the start of the experiment, at 90 minutes after the start and at the end of the experiment at 210 minutes.

4.2.1 The Rad52-GFP foci profile of *swi1Δ* was similar to that of *rad4⁺* and not to *rad4-116*

After the Rad52-GFP foci from the *swi1Δ* strain from each timepoint were counted, the unpaired Student T-test was performed to compare to the *rad4⁺* strain at timepoints 0, 90 and 210 minutes after the depletion of hydroxyurea from the media. Each value of foci was determined using an average of triplicate experiments, where 100 nuclei were scored from the *swi1Δ* strain and compared to the *rad4⁺* strain at its corresponding timepoint. The variance for both samples were similar allowing the use of the 2-tailed Student T-test. The degree of freedom for each sample used at each timepoint was 4 and the critical value over which the difference was significant was 4.604 at $p \leq 0.01$. $p \leq 0.01$ was chosen over the standard $p \leq 0.05$ as the critical values, calculated and determined to be significant at $p \leq 0.05$, were also significant at $p \leq 0.01$ and some, not all, at $p \leq 0.001$. It should be noted that some significant differences between values recorded for the *swi1Δ* reflect a **significantly** lower value than the wildtype such as the 90 minute foci value at 14% compared to 24% in the wildtype at $p < 0.001$. The values at 0 minutes and 210 minutes were not significantly different between the wildtype and *swi1Δ*. This indicated that the deletion of *swi1* was not significantly different when compared to the wildtype *rad4⁺* strain in terms of Rad52-GFP recruitment onto stalled replication forks induced by hydroxyurea at the 0 and 210 timepoints but failed to reach the peak level recorded by *rad4⁺* strain at 90 minutes. As the Rad52-GFP foci profiles of the *rad4⁺* strain and *rad4-116* were statistically significantly different from each other at all 3 chosen timepoints and the *swi1Δ* strain was similar to the *rad4⁺* strain, it can be deduced that the *swi1Δ* strain was statistically significantly different from *rad4-116* strain.

4.3 The Phenotypic characterisation of the *swi1-V5* strains

A V5-tagged version of *swi1* under transcriptional control of the *nmt81* promoter was created using plasmid p809 and integrated at the *leu1* locus following the methodology described in (Fennessy *et al.*, 2014). The *swi1-V5* base strain was constructed by transformation using SPSC 1005 as the transformed strain to create SPSC 1096. The V5- tagged allele was tested using PCR and by performing a western blot of protein samples of an overnight culture of SPSC 1096 growing in EMM+uracil+leucine broth. By crossing SPSC 1096 with SPSC 1051, and selecting *ura*⁺ G418 resistant colonies, the *swi1-V5 swi1Δ h-* strain SPSC 1098 was constructed. The SPSC 1098 was used in a cross with SPSC 120 to create *swi1-V5 swi1Δ rad4-116* SPSC 1099 by selecting *ura*⁺ G418 resistant temperature sensitive colonies. The *swi1-V5 swi1Δ rad4-116 rad52-GFP* strain SPSC 1106 was created by crossing SPSC 1098 and SPSC 1073 and selecting *ura*⁺ G418 resistant NAT resistant colonies growing in a 2:2 tetrad pattern. All the strains carrying the *swi1-V5* allele were tested using PCR before using them in the experimental procedures and adding them to the collection.

The aim of this experiment was to be able to analyse the phenotypic profile of Swi1-V5 depletion in the presence of *rad4-116* with control strains carrying *swi1-V5* as well as a control strain carrying *rad4*⁺ and a control strain carrying *rad4-116*. To be able to characterise the *swi1-V5* strains, all the strains were grown into cultures up to 0.8OD overnight at 26 °C in EMM+uracil+leucine (no thiamine) then inoculated into a total volume of 200ml EMM+uracil+leucine+ 50 µg/ml thiamine. The cultures were then incubated at 26 °C in a shaking incubator. Samples for RNA and protein extraction were collected at 0,4, 8, 12 and 24 hours till the cultures for both

experimental strains reached 1.00 OD from 0.2 OD. At each timepoint, samples for immunofluorescence and FACS were taken by fixing in formaldehyde and ethanol respectively. The viability of each strain was tested at each timepoint by plating 100 cells on EMM+uracil+leucine+50 µg/ml thiamine agar plates in triplicates. The pellets for protein and RNA extraction were snap-frozen in liquid nitrogen and stored at -80 °C. SPSC 120 (*rad4-116*) and SPSC 1005 (*rad4⁺*) were used as controls, with SPSC 120 being sampled every time the experiment was repeated. The experiment was repeated 4 times under identical conditions and the results show the averages of the repeats.

4.3.1 The depletion of *swi1-V5* expression by RT-QPCR

RT-QPCR was used to be able to assess the depletion of the transcript of *swi1-V5* in the strains carrying *swi1-V5*. The RT-QPCR method and analysis were carried out as detailed in Section 3.3.1.

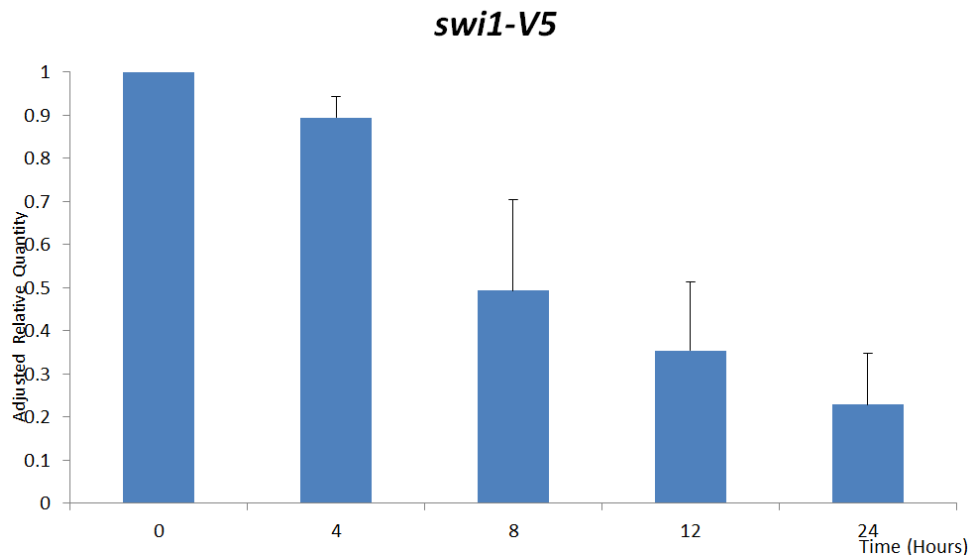


Figure 4-7. The adjusted relative quantity of RNA measured by RT-QPCR for the *swi1-V5* strain SPSC 1096. The figure shows the adjusted relative quantity of the RT-QPCR SPSC 1096 culture across 24 hours of incubation with thiamine added.

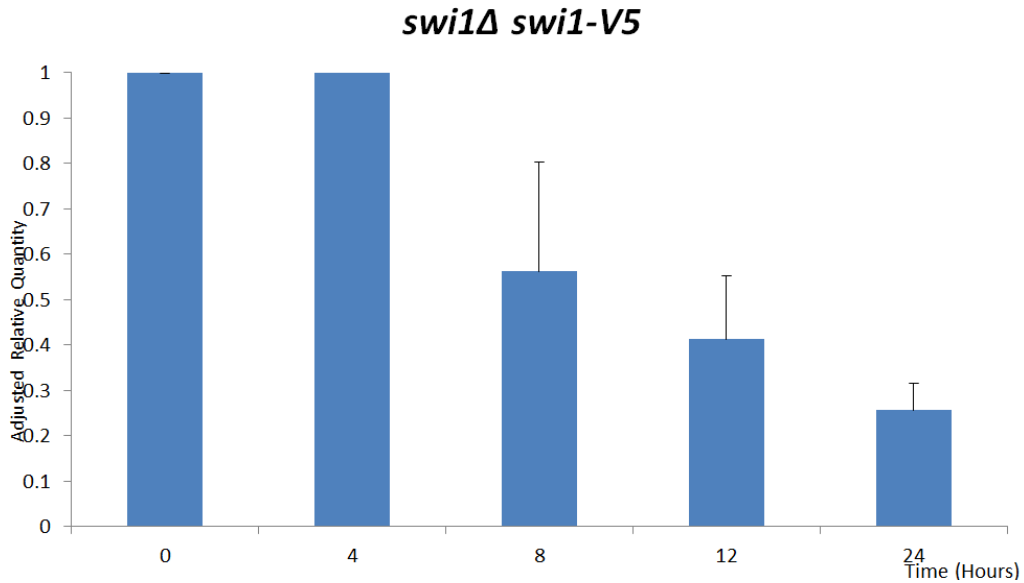


Figure 4-8. The adjusted relative quantity of RNA measured by RT-QPCR for the *swi1Δ swi1-V5* strain SPSC 1098. The figure shows the adjusted relative quantity of the RT-QPCR SPSC 1098 culture across 24 hours of incubation with thiamine added.

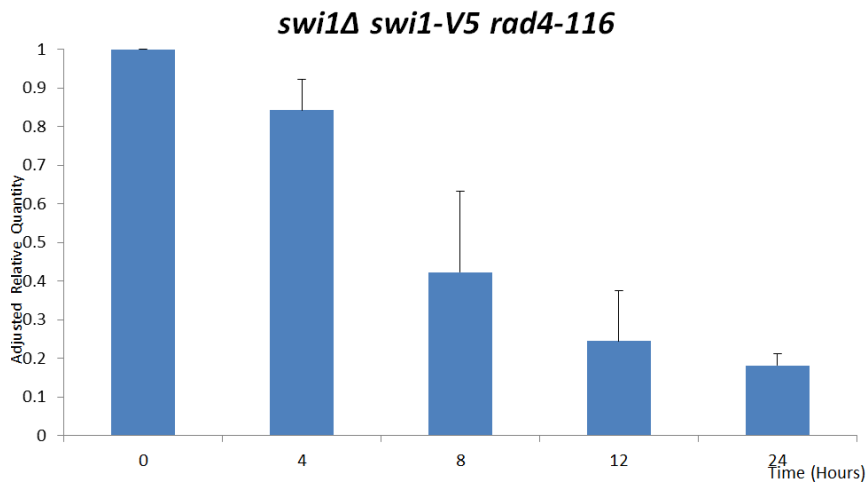


Figure 4-9. The adjusted relative quantity of RNA measured by RT-QPCR for the *swi1Δ swi1-V5 rad4-116* strain SPSC 1099. The figure shows the adjusted relative quantity of the RT-QPCR SPSC 1099 culture across 24 hours of incubation with thiamine added.

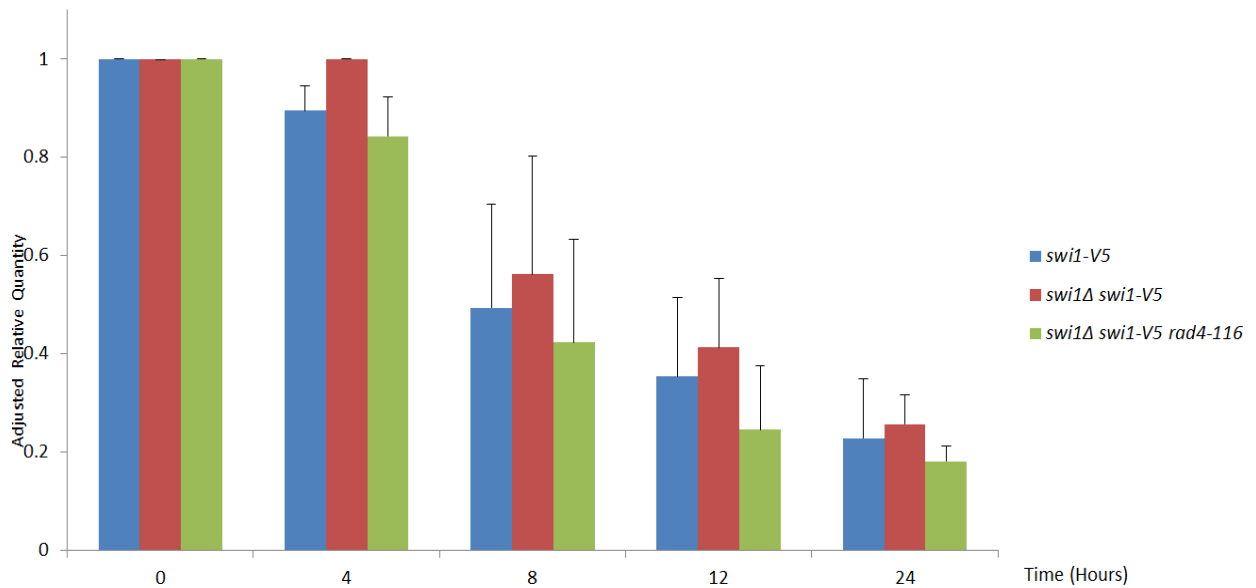


Figure 4-10. The comparison the adjusted relative quantity of RNA of strains carrying the *swi1-V5* allele. The figure shows the gradual decrease through graphical representation of the adjusted relative quantity between all the *Swi1-V5* strains across the 24 hour timecourse after the addition of thiamine to the media.

4.3.2 The depletion of Swi1-V5 expression by Western Blotting

Western blotting was used to be able to assess the depletion of the Swi1-V5 protein in the strains carrying *swi1-V5* (Figure 4-11, 4-12, 4-13 and 4-14). The western blotting method and analysis were carried out as detailed in Section 3.3.2. A preliminary blot was carried out to test the V5 signal depletion after 16 hours (overnight) of thiamine addition using the Swi1-V5 base strain (Figure 4-11).

The effect of thiamine addition on the *swi1-V5* strain

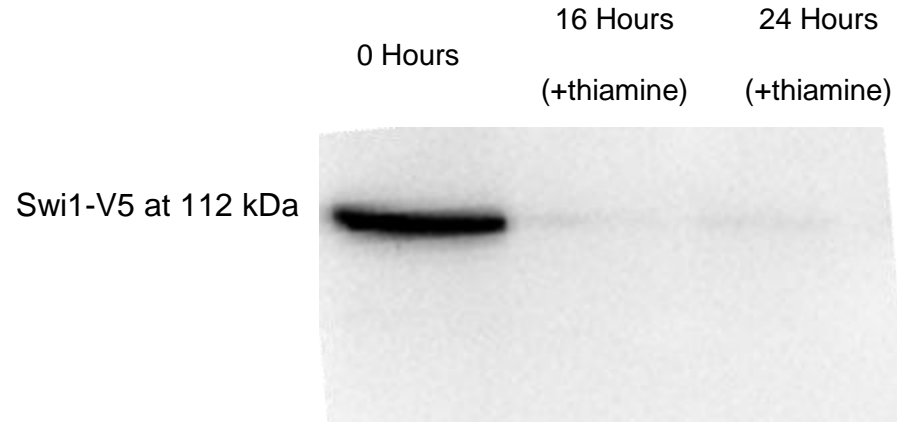


Figure 4-11. Expression of V5 tag in the base *swi1-V5* strain SPSC 1096 after the addition of thiamine. Protein samples were taken from SPSC 1095 incubated for 16 and 24 hours in EMM+uracil+leucine with and without the addition of thiamine to the media. The western blot shown represents the samples after being probed with anti-V5. The sample without the addition of thiamine expresses the V5 tag whilst the samples with the addition of thiamine do not express the V5 tag.

The effect of thiamine addition on the *swi1-V5* strain across 24 hours

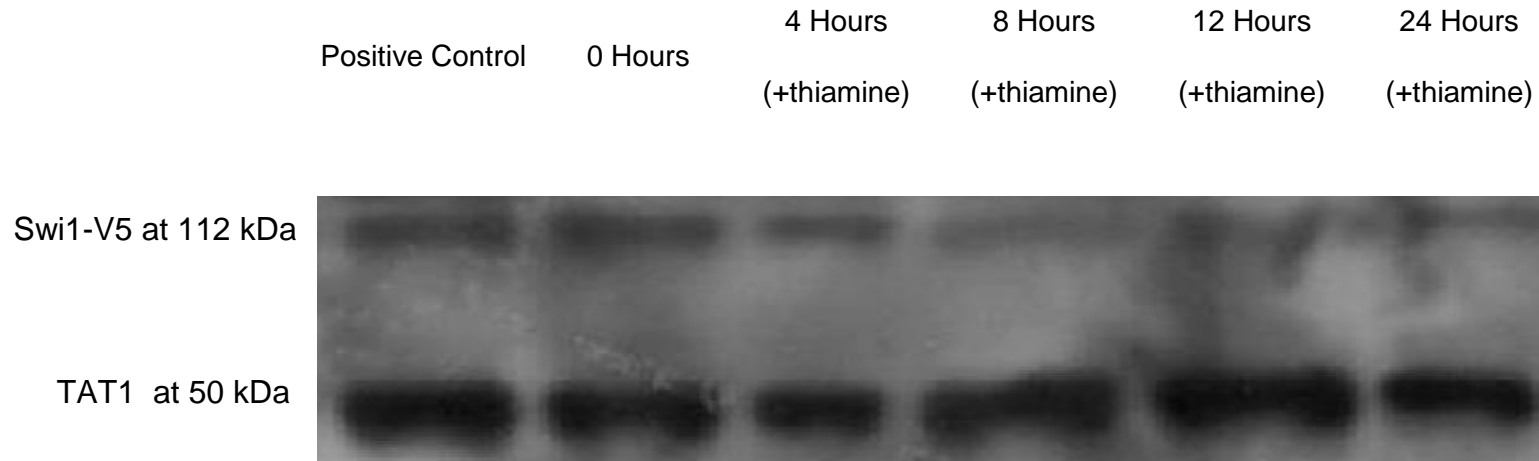


Figure 4-12. Depletion of V5 tag in the base *swi1-V5* strain SPSC 1096 after the addition of thiamine. Protein samples were taken from SPSC 1096 incubated for 24 hours in EMM+uracil+leucine with the addition of thiamine to the media. The protein samples were taken from 0, the time of addition of thiamine to the 0.5 OD culture, to 12 hours at 4 hour-intervals then an additional sample at 24 hours. The western blot shown represents the samples after being probed with anti-V5 (top signal) and anti-TAT1 (bottom signal) as control. The 0 hour and 4 hour samples express the V5 tag while there was no visible signal for the 8 hour, 12 hour or 24 hours samples. The TAT1 signal shows no signs of depletion across all 5 samples. An additional control of SPSC 1095 without thiamine was added as a positive control and expresses the V5 protein similar to that of the 0-hour SPSC 1096 sample.

The effect of thiamine addition on the *swi1Δ swi1-V5* strain across 24 hours

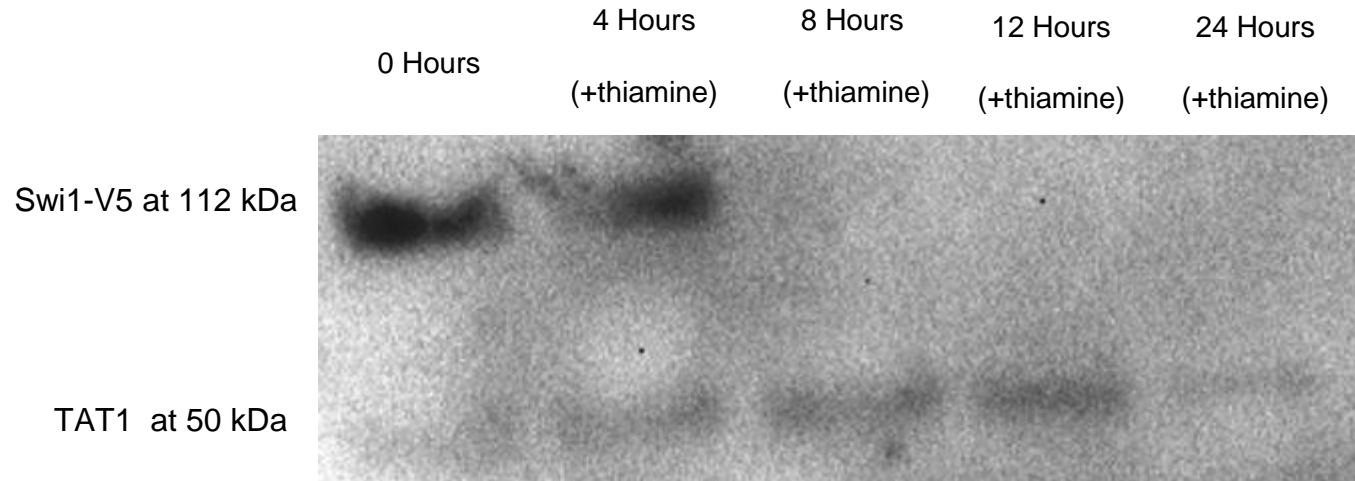


Figure 4-13. Depletion of V5 tag in the *swi1-V5 swi1Δ* strain SPSC 1098 after the addition of thiamine. Protein samples were taken from SPSC 1098 incubated for 24 hours in EMM+uracil+leucine with the addition of thiamine to the media. The protein samples were taken from 0, the time of addition of thiamine to the 0.5 OD culture, to 12 hours at 4 hour-intervals then an additional sample at 24 hours. The western blot shown represents the samples after being probed with anti-V5 (top signal) and anti-TAT1 (bottom signal) as control. The 0 hour and 4 hour samples express the V5 tag while there was no visible signal for the 8 hour, 12 hour or 24 hours samples. The TAT1 signal shows no signs of depletion across all 5 samples.

The effect of thiamine addition on the *rad4-116 swi1Δ swi1-V5* strain across 24 hours

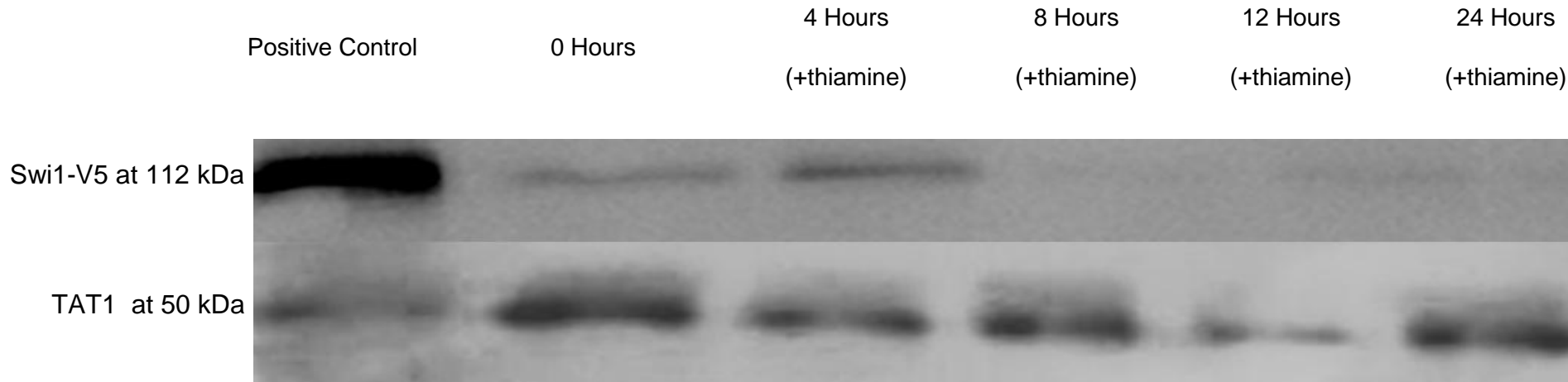


Figure 4-14. Depletion of V5 tag in the *swi1-V5 swi1Δ rad4-116* strain SPSC 1099 after the addition of thiamine. Protein samples were taken from SPSC 1099 incubated for 24 hours in EMM+uracil+leucine with the addition of thiamine to the media. The protein samples were taken from 0, the time of addition of thiamine to the 0.5 OD culture, to 12 hours at 4 hour-intervals then an additional sample at 24 hours. The western blot shown represents the samples after being probed with anti-V5 (top signal) and anti-TAT1 (bottom signal) as control. The 0 hour, 4 hour and 8 hour samples express the V5 tag while there was no visible signal for the 12 hour or 24 hours samples. An additional positive control SPSC 1099 sample is shown on the right where no thiamine added.

4.3.3 Phenotypic Characterisation of *hip1-V5* strains by microscopy

To be able to phenotypically characterise each strain carrying *swi1-V5*, cell pellets from each strain at each timepoint was taken. The microscopy method and analysis were carried out as detailed in Section 3.3.3.

The effect of thiamine addition on the *swi1-V5* strain SPSC 1096 across 24 hours

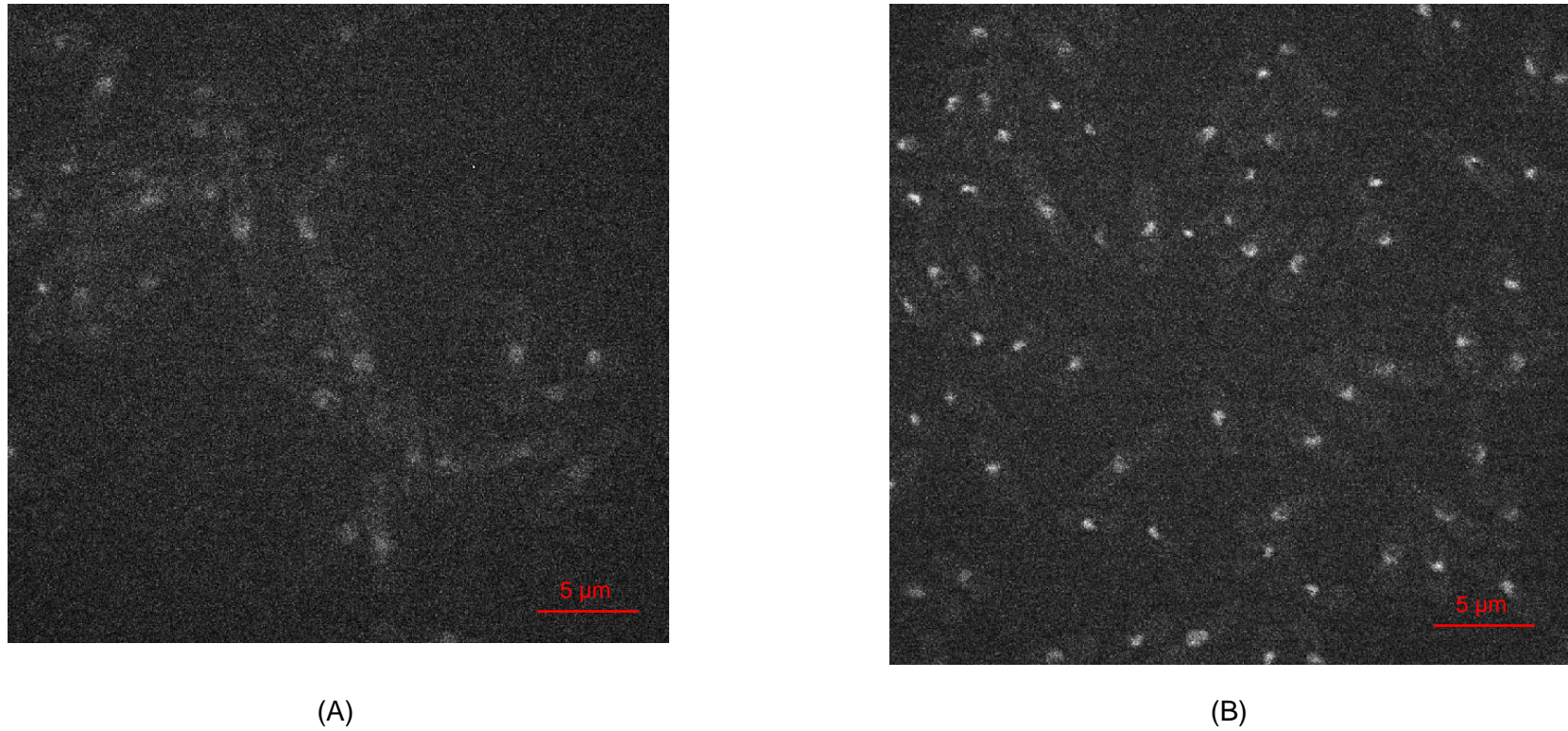


Figure 4-15. The cell morphology of the *swi1-V5* strain SPSC 1096 at 100X magnification across 24 hours after thiamine induction. The figure shows the cells of the SPSC 1096 strain stained with DAPI to show the nuclei at (A) the 0 hour timepoint and (B) the 24 hour timepoint. There is no significant difference between the cells across those 2 timepoints in terms of cell length, cell shape and nuclear shape.

The effect of thiamine addition on the *swi1Δ swi1-V5* strain SPSC 1098 across 24 hours

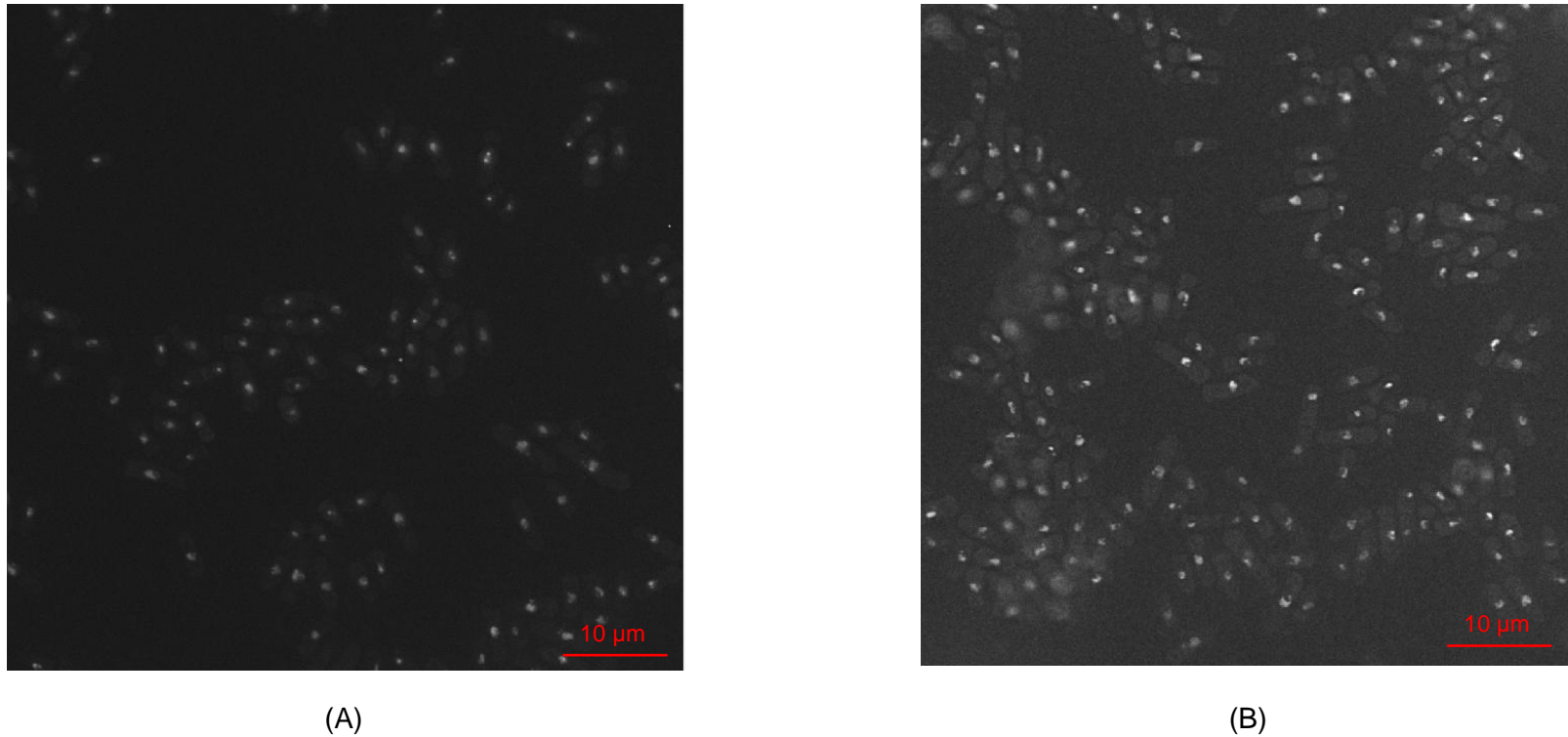


Figure 4-16. The cell morphology of the *swi1Δ swi1-V5* strain SPSC 1098 at 60X magnification across 24 hours after thiamine induction. The figure shows the cells of the SPSC 1098 strain stained with DAPI to show the nuclei at (A) the 0 hour timepoint and the (B) 24 hour timepoint. There is no significant difference between the cells across those 2 timepoints in terms of cell length, cell shape and nuclear shape.

The effect of thiamine addition on the *rad4-116 swi1Δ swi1-V5* strain SPSC 1099 across 24 hours

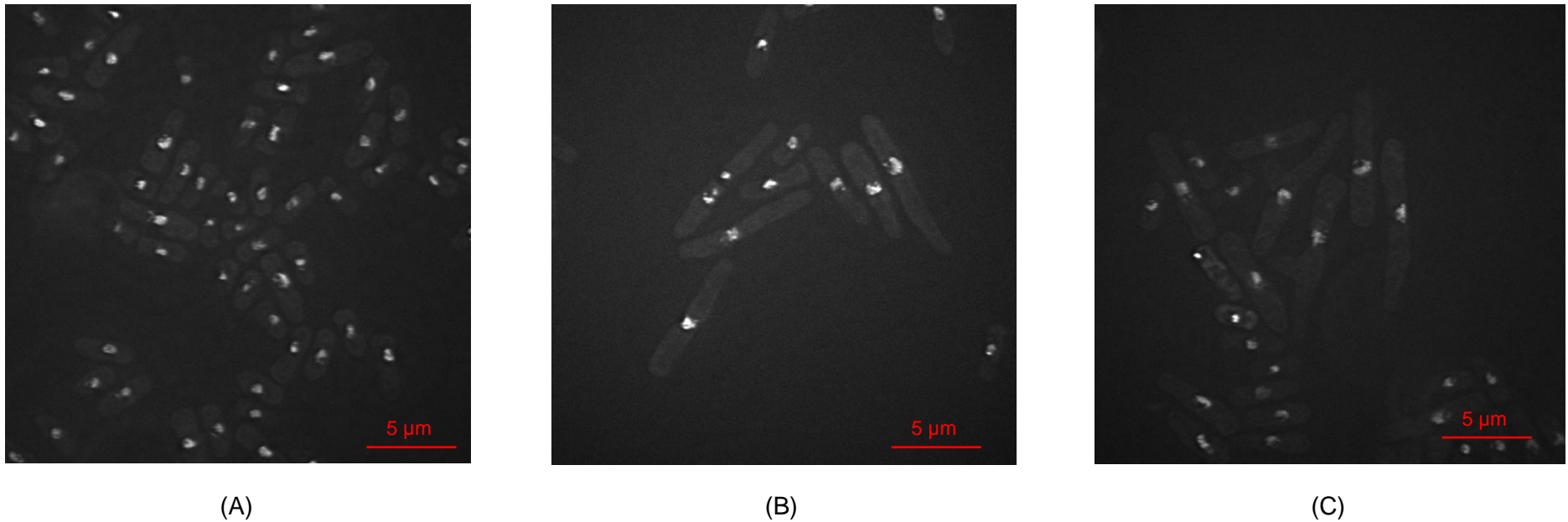


Figure 4-17. The cell morphology of the *swi1Δ swi1-V5 rad4-116* strain SPSC 1099 at 100X magnification across 24 hours after thiamine induction. The figure shows the cells of the SPSC 1099 strain stained with DAPI to show the nuclei at (A) the 0 hour timepoint, (B) the 12 hour timepoint and (C) the 24 hour timepoint. The cells show a distinct phenotype, that develops from timepoint 0 to 12 to 24 hours, for cells to increase in length. The nuclei of most these cells show a fragmentation that becomes more pronounced at the 24 hour timepoint and some cells show a compacted nucleus. Some mutant cells show an abnormal cell shape with one nucleus and three ends to the cytoplasm.

4.3.4 The effect of thiamine addition on the average cell length of *swi1-V5* strains across 24 hours

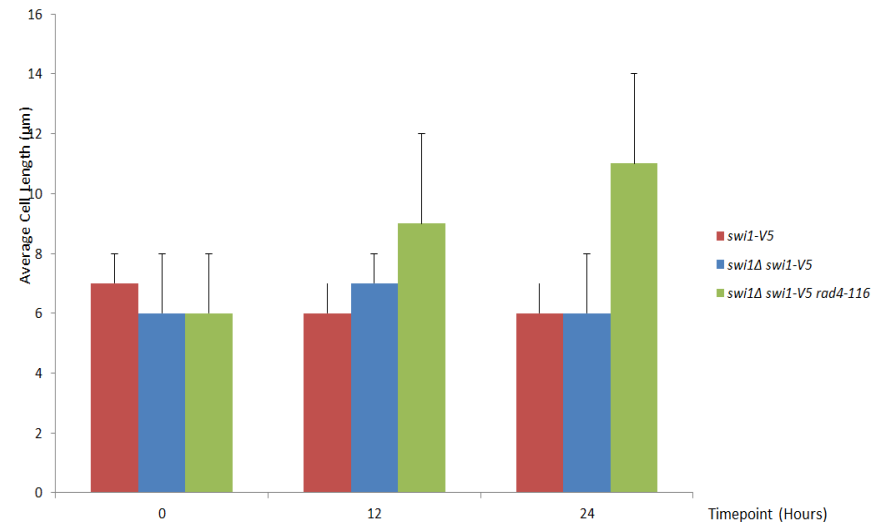


Figure 4-18. The average cell length of strains carrying the *swi1-V5* allele. The figure shows showing the graphical representation of the comparison of average cell length between the base *swi1-V5* strain, the *swi1-V5 swi1Δ* strain and the *swi1-V5 swi1Δ rad4-116* strain. No significant change in average cell length occurred in both the base *swi1-V5* strain and the *swi1-V5 swi1Δ* strain as the value is between 7 and 6 µm between the 0 hour to 24 hours, eventually reaching 6µm at 24 hours after thiamine addition. As for the *swi1-V5 swi1Δ rad4-116* strain, the initial average cell length at 0 is similar to the other two strains at 6 µm, but then a significant increase occurs from 6 µm to 9 µm at 12 hours before reaching 11 µm at 24 hours after the addition of thiamine.

As observed in Figure 4-10 for QPCR and Figures 4-12, 4-13, 4-14 for western blotting, the expression of the RNA product and protein for Swi1-V5 were successfully depleted after 24 hours of incubation in media with thiamine. The adjusted relative quantity for the *swi1-V5* RNA expression reached 0.22854 for the *swi1-V5* strain in Figure 4-7, 0.25663 for the *swi1Δ swi1-V5* strain in Figure 4-8 and 0.18146 for the *swi1Δ swi1-V5 rad4-116* strain in Figure 4-9. The adjusted relative quantity for all the *swi1-V5* strains across the 24 hour timecourse is summarised in Figure 4-10. The preliminary experiment in Figure 4-11 using the *swi1-V5* strain (SPSC1096), showed that the signal present using the anti-V5 antibody, was abolished completely following 16 hour and 24 hour incubation with thiamine. The Swi1-V5 protein signal was present at timepoints 0 and 4 hours in all the three strains SPSC 1096, SPSC 1098 and SPSC 1099 as observed in Figure 4-12, Figure 4-13 and Figure 4-14 respectively. In all 3 figures, the signal was abolished below the detectable level from 8 hours after thiamine addition onwards. The level of expression of the control α -Tubulin for all three strains across all the timepoints did not show any change.

Indeed, the levels of RNA expression did not reach 0 as seen in Figure 4-10, yet, those levels were sufficient to lead to an abolishment of Swi1-V5 protein expression below detectable levels as observed in the western blots. The depletion of RNA expression and protein signals also caused a decrease in viability, as seen in Figure 4-19, consistent with the time and level of abolishment of the V5-tagged protein in the *swi1Δ swi1-V5 rad4-116* strain but not in any of the other strains. The *swi1Δ swi1-V5 rad4-116* strain showed a gradual loss of viability dropping from 99% viability at 0 timepoint to 61% after 12 hours, then to 32% viability at 24 hours. The

decrease in viability at timepoints 12 and 24 was statistically significant at $p \leq 0.01$ with values of 61% and 32% respectively compared to the 0 hour timepoint which is consistent with the depletion of V5 protein signal. However, the presence of viable cells indicated that the level of depletion per cell in the culture population is not equal. This is also reflected in the presence of 0.18146 adjusted relative quantity value of V5 RNA for the *swi1* Δ *swi1-V5* *rad4-116* strain as represented in Figure 4-9.

In terms of cell morphology, as observed in Figure 4-15 and Figure 4-16, the cell size and length and nuclear integrity of SPSC 1096(*swi1-V5*) and SPSC 1098 (*swi1* Δ *swi1-V5*) respectively did not show any change across the 24 hour timecourse. However, as seen in Figure 4-17, the *swi1* Δ *swi1-V5* *rad4-116* strain SPSC 1099, showed a distinct phenotype in terms of cell size. The phenotype shown was longer than 10 μm with irregular nuclear size and shape with some nuclei being elongated and others fragmented or compacted. The cells also show multiple cellular polarisation with a common phenotype being 3 cytoplasmic ends. Decrease cell size was observed in rare cases, but still with abnormal compact nuclei. Those changes were detectable after 12 hours of thiamine incubation and more pronounced at the 24 hour timepoint. The changes in average cell length for SPSC 1099 was compared at the 0, 12 and 24 hours timepoints to the SPSC 1096(*swi1-V5*) and SPSC 1098 (*swi1* Δ *swi1-V5*) strains and summarised in Figure 4-18. A general increase of average cell length was detected from 6 μm at timepoint 0 to 9 μm at 12 hours before reaching 11 μm at 24 hours after the addition of thiamine.

4.3.5 The viability profile of *swi1Δ swi1-V5 rad4-116*

The paired Student T-test was performed to compare the viability of each *swi1-V5* strain at each timepoints 4, 8, 12 and 24 hours after the addition of thiamine to the media to the starting 0 hour viability value. Each value of viable cells was obtained from an average of a triplicate separate cultures of strain at each timepoint at which a triplicate of EMM+ uracil+ leucine+ thiamine plates were used to grow 100 colonies. After 3 days of incubation at 26 °C, the number of viable colonies on each plate was counted and recorded and the average calculated for the *swi1Δ* strain and compared to the *rad4⁺* strain at its corresponding timepoint. The variance for both samples were similar allowing the use of the 2-tailed Student T-test. The degree of freedom for each sample used at each timepoint was 2 and the critical value over which the difference is significant is 9.925 at $p \leq 0.01$. $p \leq 0.01$ was chosen over the standard $p \leq 0.05$ as the critical values, calculated and determined to be significant at $p \leq 0.05$, were also significant at $p \leq 0.01$. For the *swi1-V5* and *swi1Δ swi1-V5*, there was no significant difference the viability counts observed across all the timepoints recorded from 0 to 24 hours. However, for *swi1Δ swi1-V5 rad4-116* strain, timepoints 12 and 24 showed a significant decrease in viability at $p \leq 0.01$ with values of 61% and 32% respectively compared to the 0 hour timepoint.

Viability Comparison of *swi1-V5* strains

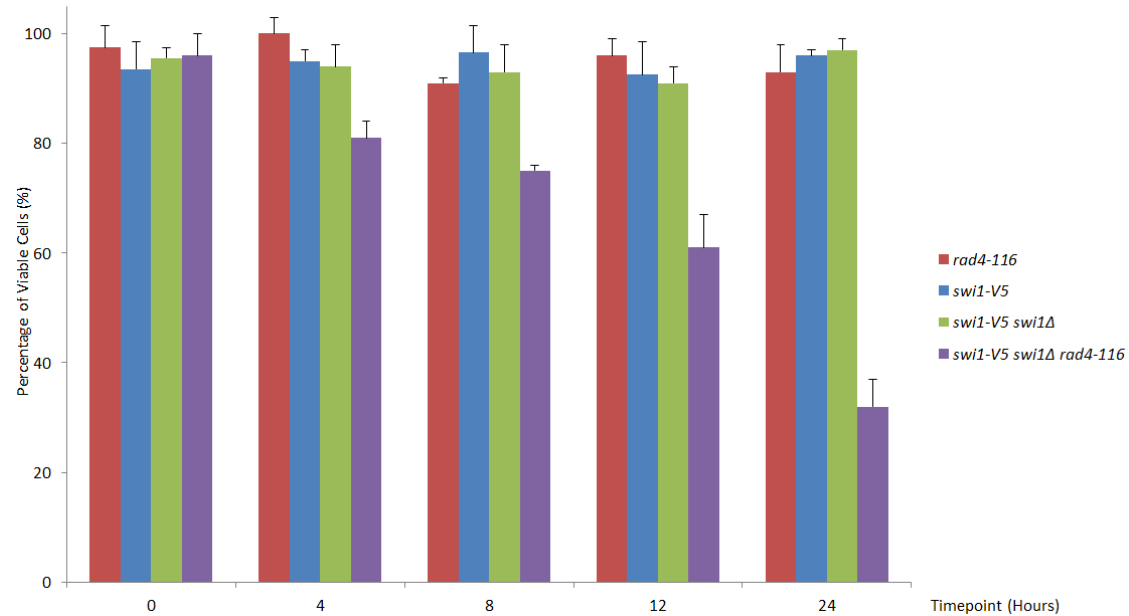


Figure 4-19. The viability comparison of strains carrying the *swi1-V5* allele against the control *rad4-116* strain. The figure shows the graphical representation of the comparison of viability between the *Swi1-V5* strains and the *Rad4-116* strain. Only SPSC 1099 showed a gradual loss of viability dropping from 96% viability at 0 timepoint to 61% after 12 hours, then to 32% viability at 24 hours. All the other strains represented showed no significant loss of viability across the 24 hour timecourse ranging from 100% to 91% viability.

4.3.6 Phenotypic Characterisation of *swi1-V5* strains by FACS

The characterisation of the *swi1-V5* strains by FACS as detailed in Section 3.3.6.

Phenotypic Characterisation of *swi1-V5* (SPSC 1096) and *swi1Δ swi1-V5* (SPSC 1098) strains by FACS

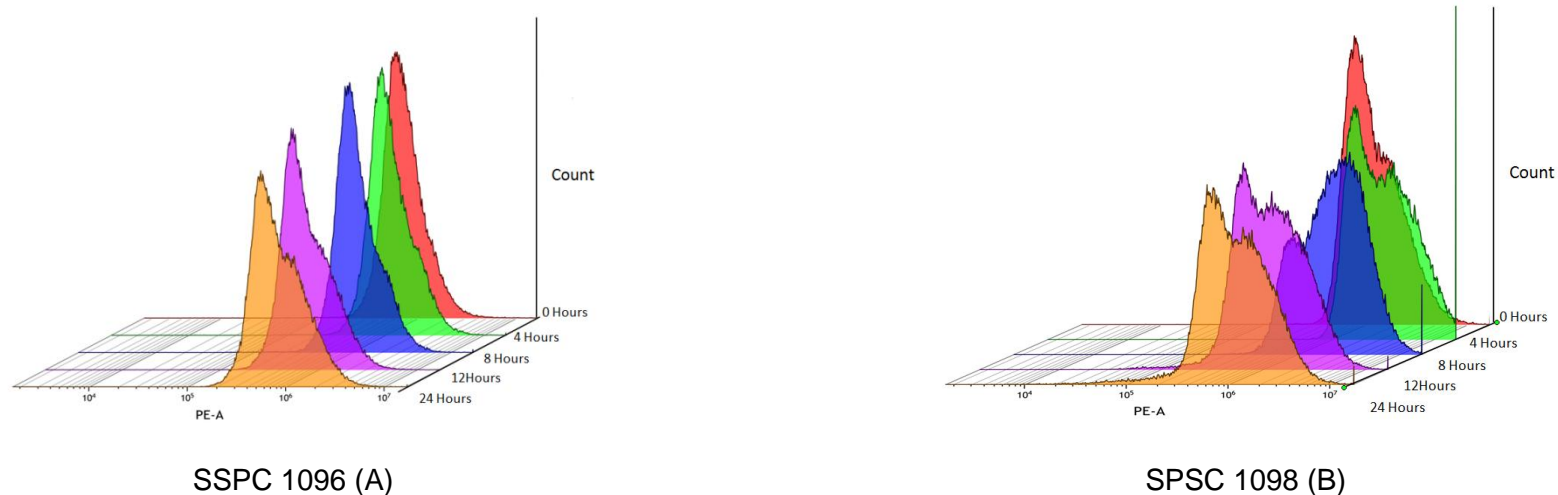


Figure 4-20. Cell population as investigated through FACS. The figure shows the analysis of the populations of SPSC 1096 (A) and SPSC 1098 (B) as representation of count (y-axis) against the phycoerythrin channel PE-A (x-axis) across 24 hours with 0 hour being the furthest along the z-axis followed by 4, 8, 12 and finally, 24 hours being the nearest along the z-axis. For (A) SPSC 1096, a general gradual slight decrease in peak occurred from 0 to 24 hours with the development of a minor second peak visible at the 12 and 24 hour samples. For (B) SPSC 1098, a general decrease in peak occurred from 0 to 24 hours. A shift in peak occurred from 0 to 12 hours with the stronger signal shifting from 0 to 4 hours. The 12 and 24 hour samples showed the same double peak pattern and are nearly identical in shape.

Phenotypic Characterisation of *rad4-116 swi1Δ swi1-V5* strain SPSC 1099 by FACS

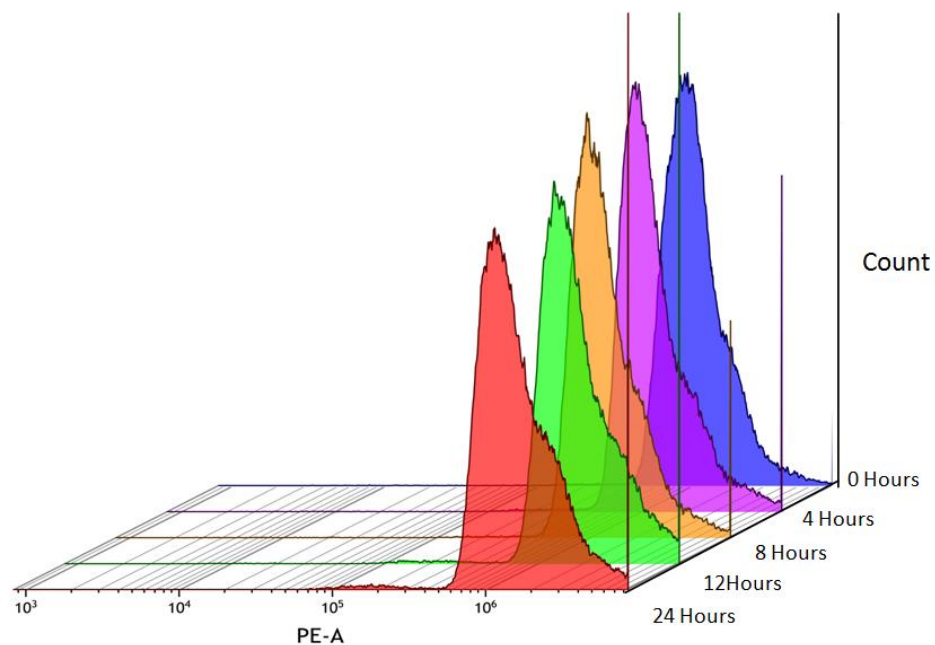


Figure 4-21. Cell population as investigated through FACS. The figure shows the analysis of the population of SPSC 1099 as representation of count (y-axis) against the phycoerythrin channel PE-A (x-axis) across 24 hours with 0 hour being the furthest along the z-axis followed by 4, 8, 12 and finally, 24 hours being the nearest along the z-axis. There was no change in staining or shift in peaks across the 24 hours but a weak gradual decrease in peak was observed from 0 to 24 hours.

4.4.1 Synthetic Lethality on Agar

The aim of the investigation was to investigate the interactions between *rad4* and *swi3* which is implicated in the maintenance of chromatin structure and remodelling.

The strains selected had either the *rad4-116* marked with NAT resistance and the *swi3Δ* marked with G418 resistance. The synthetic lethality method and analysis were carried out as detailed in Section 3.1.1.

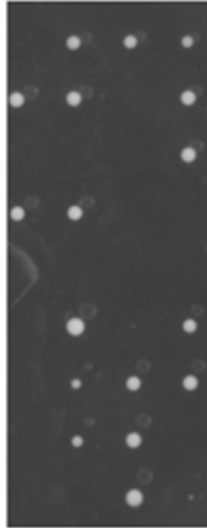


Figure 4-22. The growth of individual spores to colonies of the *rad4-116* strain cross with *swi3Δ* strain. The figure shows 4 columns of the YES plates of the crosses of the *rad4-116* strain with a *swi3Δ* strain. The cross shown was a set of spores from tetrads that were inoculated into single spores with a line separating each individual spore set from a single tetrad. The number of spores from each YES plate was counted and recorded.

Cross	<i>swi3Δ</i> x <i>rad4-116</i>
Wild-type	45
G418 ^R	51
NAT ^R	46
G418 ^R /NAT ^R	1
Viability	143
Total valid spores	212
χ^2 value	22.5

Table 4-B showing the crosses between the *rad4-116* strain and *swi3Δ*. The *rad4-116* was tagged with NAT resistance while the *swi3* deletion are marked with G418 (Kanamycin) resistance. The crosses were carried out on EMM-nitrogen agar , then checked after 2 days for sporulation. The tetrads from sporulation were separated using the Singer Micromanipulator onto YES agar plates. After 4 days, the plates were then copied onto fresh YES, as shown in Figure 4-22, YES+G418 and YES+NAT plates separately. After another 3 days, the colonies on each plate were counted and recorded as seen in the table. The χ^2 value for each cross was calculated and tabulated at $p \leq 0.05$ with a degree of freedom of 1.

4.4.2 *swi3Δ* cause synthetic lethality when combined with *rad4-116*

After the colonies from the crosses were noted and counted from all the plates, the Chi-Square test was performed and a value of 22.5 was the result as shown in Table 4-B. As this value was calculated using the expected value based on the segregated spores not based on the expected segregation pattern, the values represent a focused measure on whether the double mutants were synthetically lethal or not. These values were all greater than 3.84, which was the threshold value at $p \leq 0.05$ with a degree of freedom of 1. This indicated that the deletion of *swi3* was synthetically lethal when combined with *rad4-116* and that any lethality or observed lack of growth would **not** be due to chance or random occurrence.

4.5 The DNA replication stalled fork profile of *swi3Δ*

The aim of this experiment was to observe and compare the DNA stalled replication profiles, in terms of accumulation and resolution of DNA forks, profiles of a *rad4-116* strain to *swi3Δ* and wildtype *rad4* as a control. This ability to assess and monitor such profile would be achieved by utilising Rad52-GFP which is recruited to repair and aid the progress of stalled replication forks. The strains were constructed by direct transformation of PCR-produced deletion *hip1* encoding G418 resistance and PCR-produced *rad4-116* attached to NAT resistance into a *rad52-GFP* base strain. Cells were grown in liquid media then arrested by the addition of hydroxyurea which blocks ribonucleotide reductase leading to the depletion of the ribonucleotides, halting DNA replication. Then after 6 hours of arrest with hydroxyurea, the cells were released by the depletion of hydroxyurea from the media, washing the cells then resuspending in rich YES media. Samples were collected every 30 minutes for 210 minutes to be analysed for fluorescence microscopy and testing viability.

The cell nuclei were assessed in two ways; the first being the percentage and number of nuclei that carry GFP fluorescent foci spanning the 210 minutes compared to the starting time point(0) of the release, and the second by assessing the number of foci per nucleus and arranging them in categories. The foci were assessed using the Softworx program by taking a 3D reconstruction of the cells to be able to assess if the foci observed were nuclear foci to be counted. The viability of each strain was tested by spreading 100 colonies per plate on YES plates in triplicate per each strain at each timepoint. The viability of cells in all three strains did not change from the arrest up to the 210-minute time point post release. The percentage of nuclei with GFP foci was tabulated and a graph was drawn for each

strain. As observed in the graph, the *rad4-116* showed a higher level of initial foci at the 0 timepoint compared to the other 2 strains.

The initial levels of Rad-52 GFP nuclear foci were 6% for both the *swi3Δ* and the *rad4⁺* strains contrasting to 26% in the *rad4-116* strain. For the *swi1Δ* strain the number of foci increased at a gradual low rate from 6% at the start of the release up to 7% after 30 minutes which was the peak level of foci recorded for the strain. Then, a gradual decrease occurred from 7% at timepoint 30 minutes to 5% at 60 minutes then to a plateau steady low level of 2% to 0% from 180 minutes after release onwards. The 0% recorded at the endpoint of the experiment, at 210 minutes after release, was lower than the starting level of 6% , showing a complete recovery from DNA stalled forks in a bell-shaped manner.

The values of percentage of cells with nuclear Rad52-GFP at the start and the end of the timecourse were similar when comparing the *rad4⁺* and *swi3Δ* strains but not the *rad4-116* strain. The patterns seen in the *rad4⁺* and *swi1Δ* strains were nearly identical as both show a bell-shaped curve with a peak at 30 to 120 minutes but not with the *rad4-116* strain. The difference between the *rad4⁺* and *swi3Δ* strains was that the peak or highest value recorded was 27% with the *rad4⁺* strain and 7% with the *swi1Δ*. However, both strains showed a decrease back to below initial levels of recorded GFP foci.

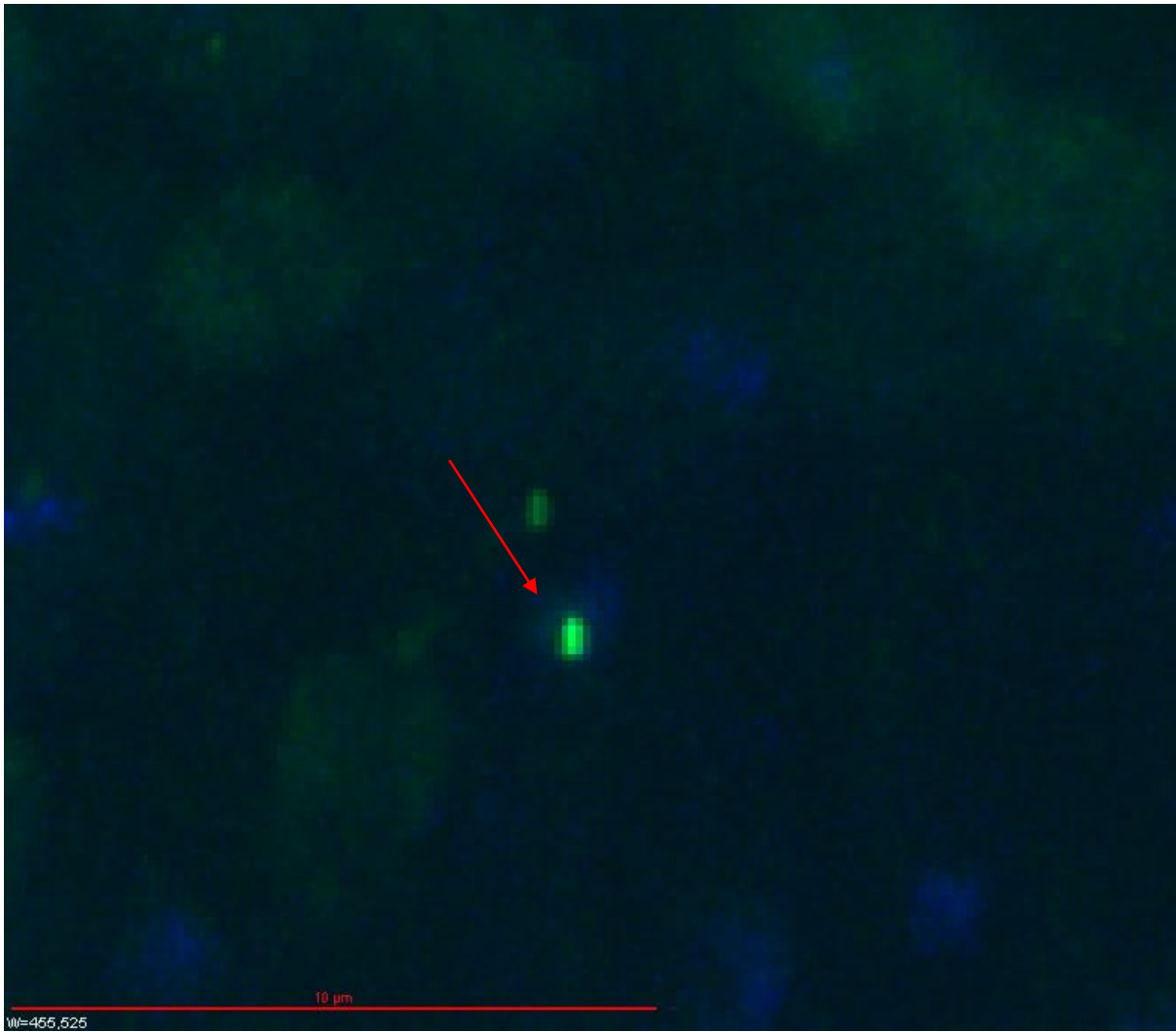
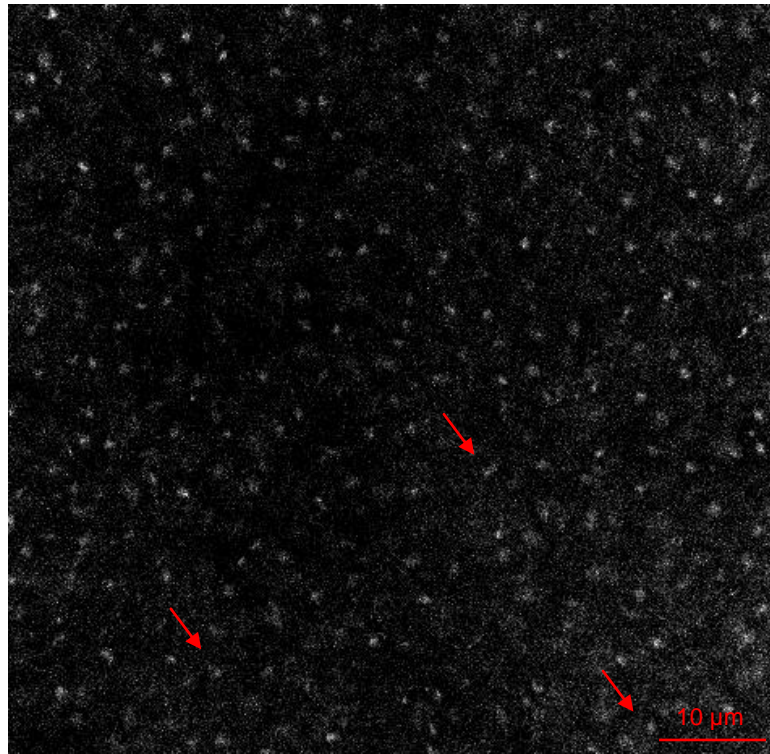
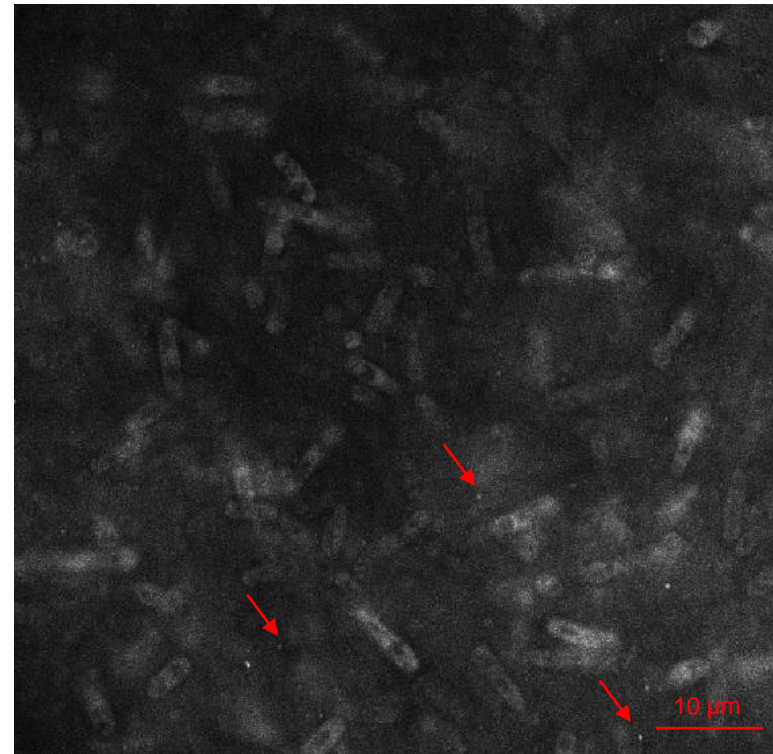


Figure 4-23. A merged image of *swi3Δ* cells after 30 minutes of incubation with Hydroxyurea. The nucleus (blue) highlighted by the arrow contains a single GFP signal (bright green). The cells were reconstructed into 3D using the Softworx program to reensure that the foci seen are indeed nuclear foci.



(A) (*swi3Δ* DAPI)



(B) (*swi3Δ* GFP)

Figure 4-24. Rad52-GFP foci of the *swi3Δ* strain at its peak. The figure shows the cells of the *swi3Δ* strain at 60X magnification stained with (A) DAPI to show the nuclei and (B) anti-GFP to show the Rad52-GFP foci. The cells were reconstructed into 3D using the Softworx program to identify nuclear foci. The peak value for nuclear foci was 7% of total number of nuclei. The red arrows point to some nuclei with Rad52-GFP foci.

Viability Comparison of *rad4-116*, *rad4*⁺ and *swi3Δ*

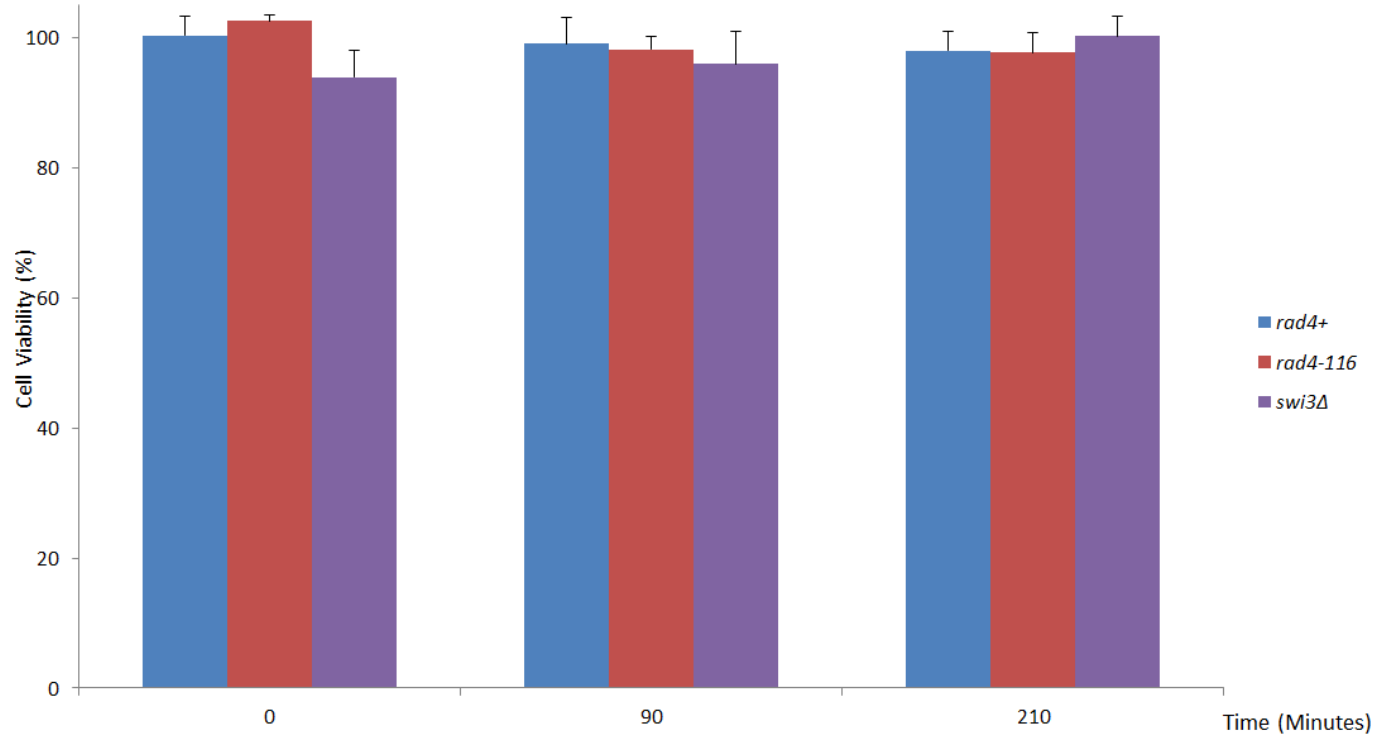


Figure 4-25. Viability counts for the *rad4*⁺, *rad4-116* and *swi3Δ* strains carrying the *rad52-GFP* gene. The figure shows the bar chart graph representing the comparison between cell viability across the three strains of *rad4-116*, *rad4*⁺ and *swi3Δ* at the start of the experiment, at 90 minutes after the start and at the end of the experiment at 210 minutes. As observed, there was no significant change in viability across all three strains at these three timepoints.

Rad52-GFP Foci Profile of *swi3Δ*

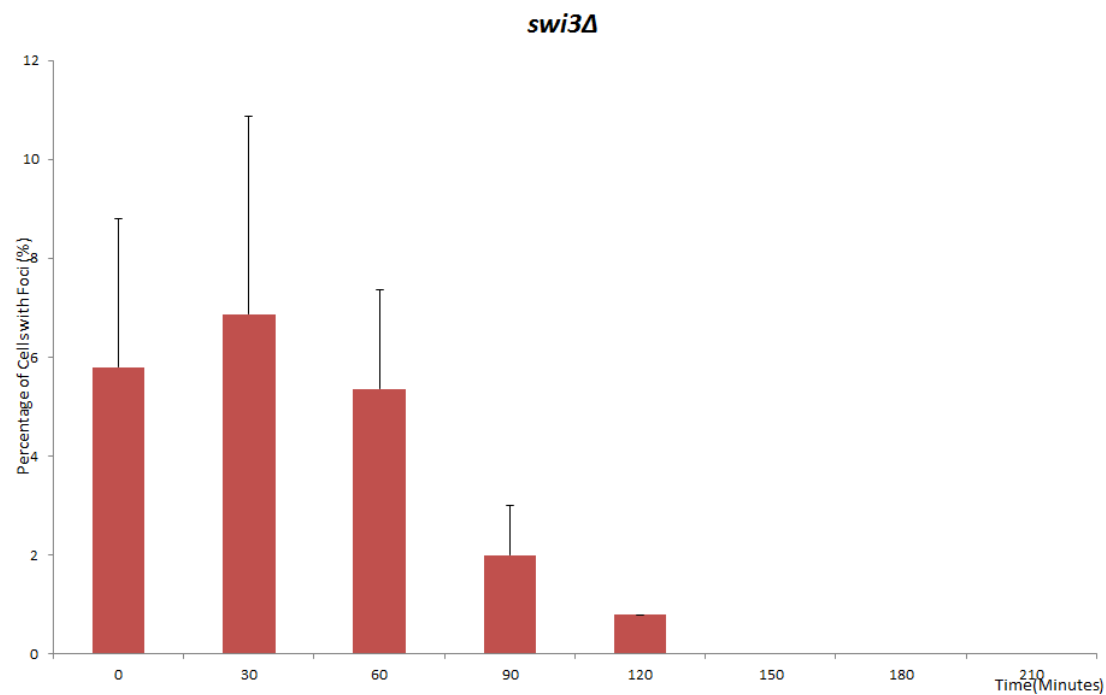


Figure 4-26. The Rad52-GFP profile of the *swi3Δ* strain. The figure shows the bar chart graph representing the percentage of cells with Rad52-GFP foci in the *swi3Δ* strain across timepoints from 0 to 210. The peak occurred at 30 minutes after the start of the experiment with a value of 7% of cells carrying nuclei with Rad52-GFP foci.

Rad52-GFP Foci Profile Comparison of *rad4-116*, *rad4*⁺ and *swi3Δ*

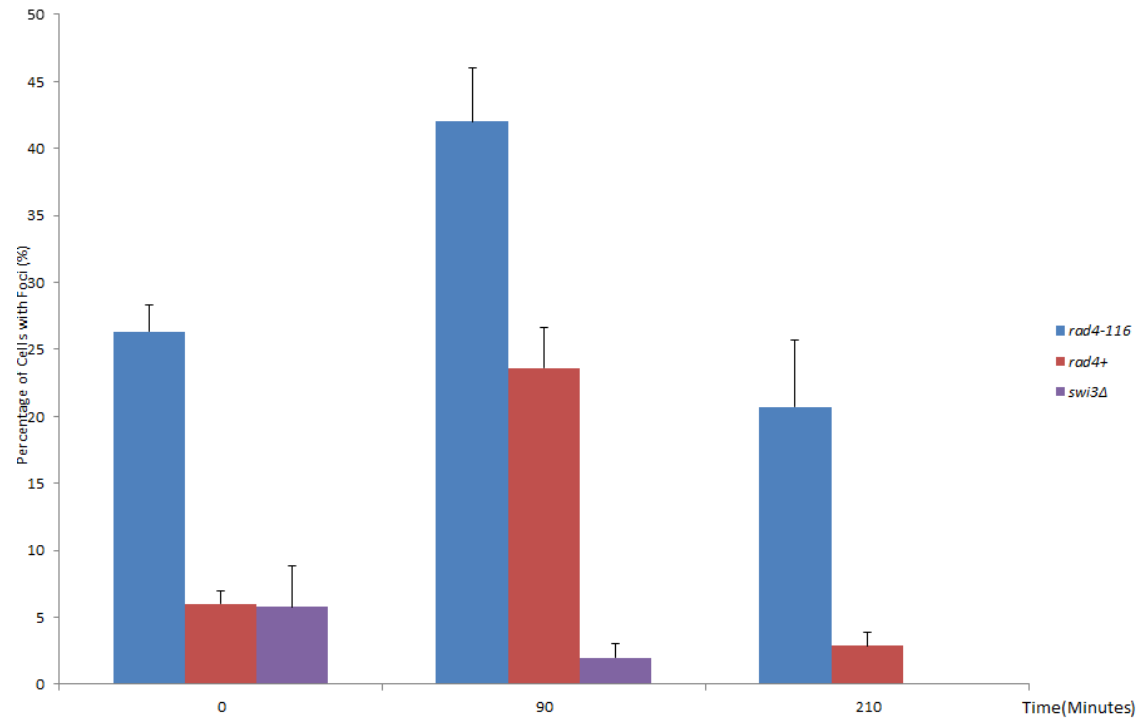


Figure 4-27. A comparison of the Rad52-GFP profiles of the *rad4-116*, *rad4*⁺ and *swi3Δ* strains. The figure shows the bar chart graph representing the comparison between the percentage of cells with Rad52-GFP foci across the three strains of *rad4-116*, *rad4*⁺ and *swi3Δ* at the start of the experiment, at 90 minutes after the start and at the end of the experiment at 210 minutes.

4.5.1 The Rad52-GFP foci profile of *swi3Δ* was similar to that of *rad4⁺* and not to *rad4-116*

After the Rad52-GFP foci from the *swi3Δ* strain from each timepoint were counted, the unpaired Student T-test was performed to compare to the *rad4⁺* strain at timepoints 0, 90 and 210 minutes after the depletion of hydroxyurea from the media. Each value of foci was determined using an average of triplicate experiments, where 100 nuclei were scored from the *swi3Δ* strain and compared to the *rad4⁺* strain at its corresponding timepoint. The variance for both samples were similar allowing the use of the 2-tailed Student T-test. The degree of freedom for each sample used at each timepoint was 4 and the critical value over which the difference was significant was 4.604 at $p \leq 0.01$. $p \leq 0.01$ was chosen over the standard $p \leq 0.05$ as the critical values, calculated and determined to be significant at $p \leq 0.05$, were also significant at $p \leq 0.01$ and some, not all, at $p \leq 0.001$. It should be noted that some significant differences between values recorded for the *swi3Δ* reflect a **significantly** lower value than the wildtype such as the 90 minute foci value at 2% compared to 24% in the wildtype at $p < 0.001$. The values at 0 minutes and 210 minutes were not significantly different between the wildtype and *swi3Δ*. This indicated that the deletion of *swi3* was not significantly different when compared to the wildtype *rad4⁺* strain in terms of Rad52-GFP recruitment onto stalled replication forks induced by hydroxyurea at the 0 and 210 timepoints but failed to reach the peak level recorded by *rad4⁺* strain at 90 minutes. As the Rad52-GFP foci profiles of the *rad4⁺* strain and *rad4-116* were statistically significantly different from each other at all 3 chosen timepoints and the *swi3Δ* strain was similar to the *rad4⁺* strain, it can be deduced that the *swi3Δ* strain was statistically significantly different from *rad4-116* strain.

4.6 The Phenotypic characterisation of the *swi3-V5* strains

A V5-tagged version of *swi3* under transcriptional control of the *nmt81* promoter was created using plasmid p810 and integrated at the *leu1* locus following the methodology described in (Fennessy *et al.*, 2014). The *swi3-V5* base strain was constructed by transformation using SPSC 1005 as the transformed strain to create SPSC 1097. The V5- tagged allele was tested using PCR and by performing a western blot of protein samples of an overnight culture of SPSC 1097 growing in EMM+uracil+leucine broth. By crossing SPSC 1097 with SPSC 1017, and selecting *ura*⁺ G418 resistant colonies, the *swi3-V5 swi3Δ h-* strain SPSC 1101 was constructed. The SPSC 1101 was used in a cross with SPSC 120 to create *swi3-V5 swi3Δ rad4-116* SPSC 1102 by selecting *ura*⁺ G418 resistant temperature sensitive colonies. The *swi3-V5 swi3Δ rad4-116 rad52-GFP* strain SPSC 1108 was created by crossing SPSC 1104, a result of the cross of SPSC 1101 and SPSC120, and SPSC 1073 and selecting *ura*⁺ G418 resistant NAT resistant colonies growing in a 2:2 tetrad pattern. All the strains carrying the *swi3-V5* allele were tested using PCR before using them in the experimental procedures and adding them to the collection.

The aim of this experiment was to be able to analyse the phenotypic profile of Swi3-V5 depletion in the presence of *rad4-116* with control strains carrying *swi3-V5* as well as a control strain carrying *rad4*⁺ and a control strain carrying *rad4-116*. To be able to characterise the *swi3-V5* strains, All the strains were grown into cultures up to 0.8OD overnight at 26 °C in EMM+uracil+leucine (no thiamine) then inoculated into a total volume of 200ml EMM+uracil+leucine+ 50 µg/ml thiamine. The cultures were then incubated at 26 °C in a shaking incubator. Samples for RNA and protein extraction were collected at 0,4, 8, 12 and 24 hours till the cultures for both

experimental strains reached 1.00 OD from 0.2 OD. At each timepoint, samples for immunofluorescence and FACS were taken by fixing in formaldehyde and ethanol respectively. The viability of each strain was tested at each timepoint by plating 100 cells on EMM+uracil+leucine+50 µg/ml thiamine agar plates in triplicates. The pellets for protein and RNA extraction were snap-frozen in liquid nitrogen and stored at -80 °C. SPSC 120 (*rad4-116*) and SPSC 1005 (*rad4⁺*) were used as controls, with SPSC 120 being sampled every time the experiment was repeated. The experiment was repeated 4 times under identical conditions and the results show the averages of the repeats.

4.6.1 The depletion of *swi3-V5* expression by RT-QPCR

RT-QPCR was used to be able to assess the depletion of the transcript of *swi3-V5* in the strains carrying *swi3-V5*. The RT-QPCR method and analysis were carried out as detailed in Section 3.3.1.

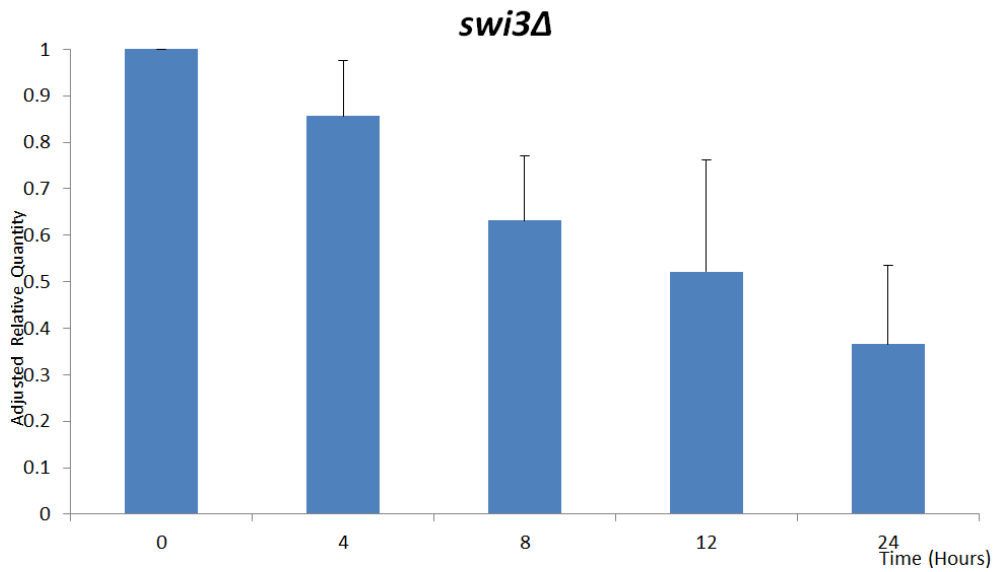


Figure 4-28. The adjusted relative quantity of RNA measured by RT-QPCR for the *hip1-V5* strain SPSC 1097. The figure shows the adjusted relative quantity of the RT-QPCR SPSC 1097 culture across 24 hours of incubation with thiamine added.

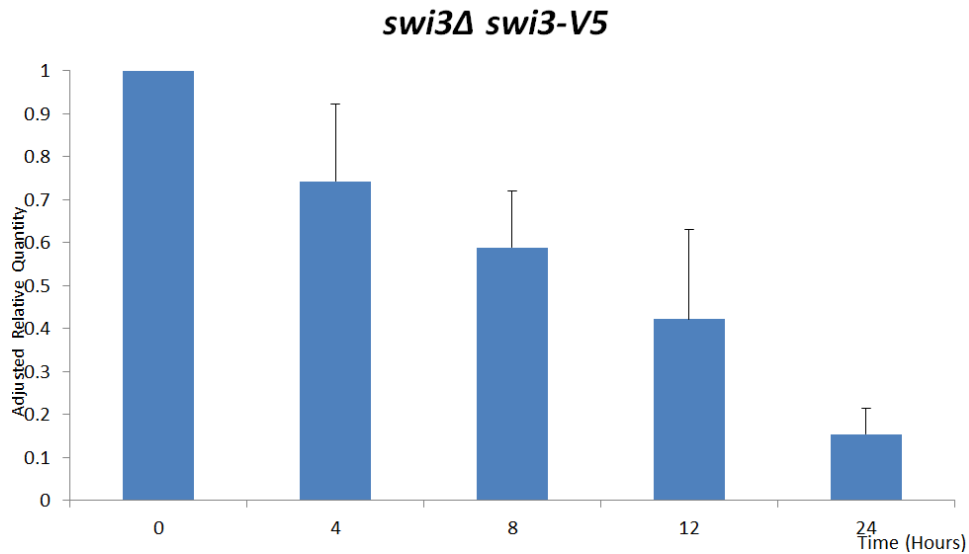


Figure 4-29. The adjusted relative quantity of RNA measured by RT-QPCR for the *swi3Δ swi3-V5* strain SPSC 1101. The figure shows the adjusted relative quantity of the RT-QPCR SPSC 1101 culture across 24 hours of incubation with thiamine added.

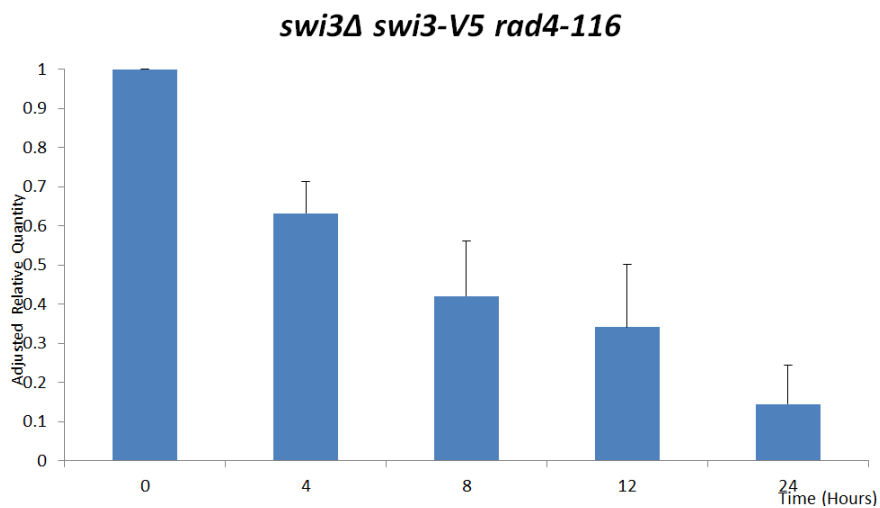


Figure 4-30. The adjusted relative quantity of RNA measured by RT-QPCR for the *swi3Δ swi3-V5 rad4-116* strain SPSC 1102. The figure shows the adjusted relative quantity of the RT-QPCR SPSC 1102 culture across 24 hours of incubation with thiamine added.

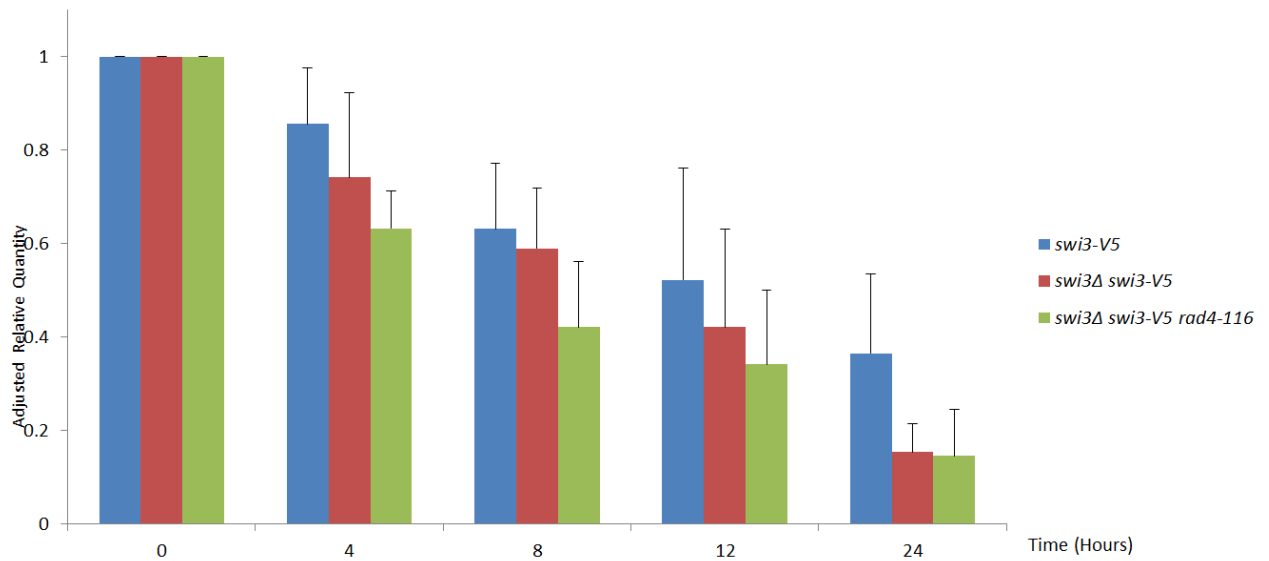


Figure 4-31. The comparison the adjusted relative quantity of RNA of strains carrying the *swi3-V5* allele. The figure shows the gradual decrease through graphical representation of the adjusted relative quantity between all the *Swi3-V5* strains across the 24 hour timecourse after the addition of thiamine to the media.

4.6.2 The depletion of Swi1-V5 expression by Western Blotting

Western blotting was used to be able to assess the depletion of the Swi3-V5 protein in the strains carrying *swi3-V5* (Figure 4-32, 4-33, 4-34 and 4-35). The synthetic lethality method and analysis were carried out as detailed in Section 3.3.2. A preliminary blot was carried out to test the V5 signal depletion after 16 hours (overnight) of thiamine addition using the Swi3-V5 base strain (Figure 4-32).

The effect of thiamine addition on the *swi3-V5* strain

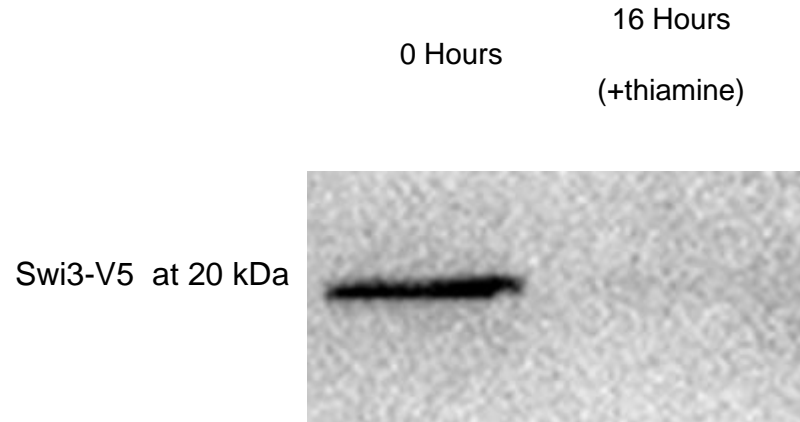


Figure 4-32. Expression of V5 tag in the base *swi3-V5* strain SPSC 1097 after the addition of thiamine. Protein samples were taken from SPSC 1097 incubated for 16 hours in EMM+uracil+leucine with and without the addition of thiamine to the media. The western blot shown represents the samples after being probed with anti-V5. The sample without the addition of thiamine expresses the V5 tag whilst the sample with the addition of thiamine does not express the V5 tag.

The effect of thiamine addition on the *swi3-V5* strain across 24 hours

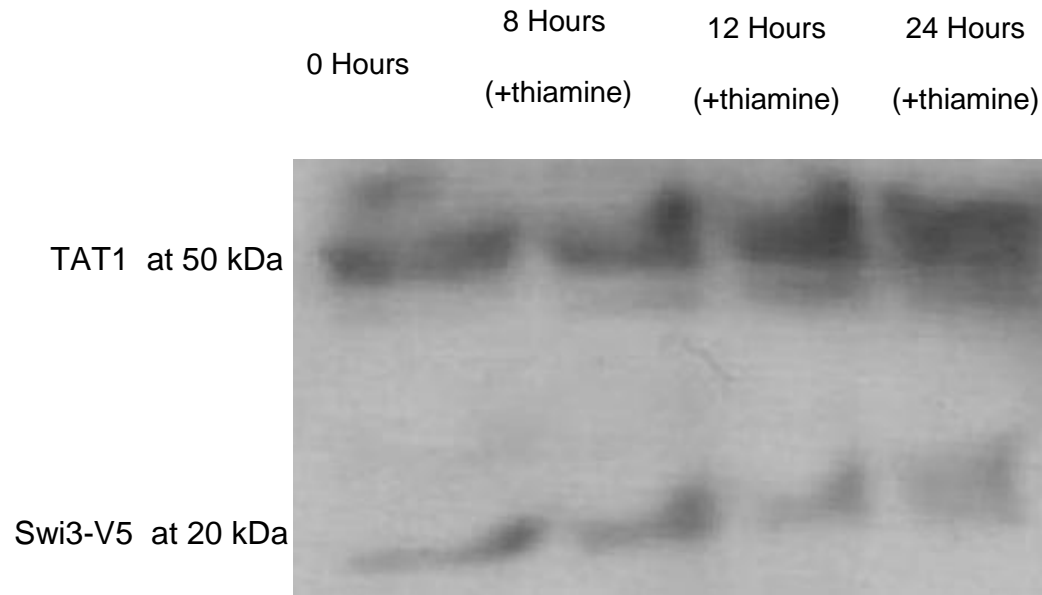


Figure 4-33. Depletion of V5 tag in the *swi3-V5* strain SPSC 1097 after the addition of thiamine. Protein samples were taken from SPSC 1097 incubated for 24 hours in EMM+uracil+leucine with the addition of thiamine to the media. The protein samples were taken from 0, the time of addition of thiamine to the 0.5 OD culture, to 12 hours at 4 hour-intervals then an additional sample at 24 hours. The western blot shown represents the samples after being probed with anti-TAT1 (top signal) and anti-V5 (bottom signal) as control. The 0 hour, 4 hour and 8 hour samples express the V5 tag while there were much weaker visible signals for the 12 hour or 24 hours samples.

The effect of thiamine addition on the *swi3Δ swi3-V5* strain across 24 hours

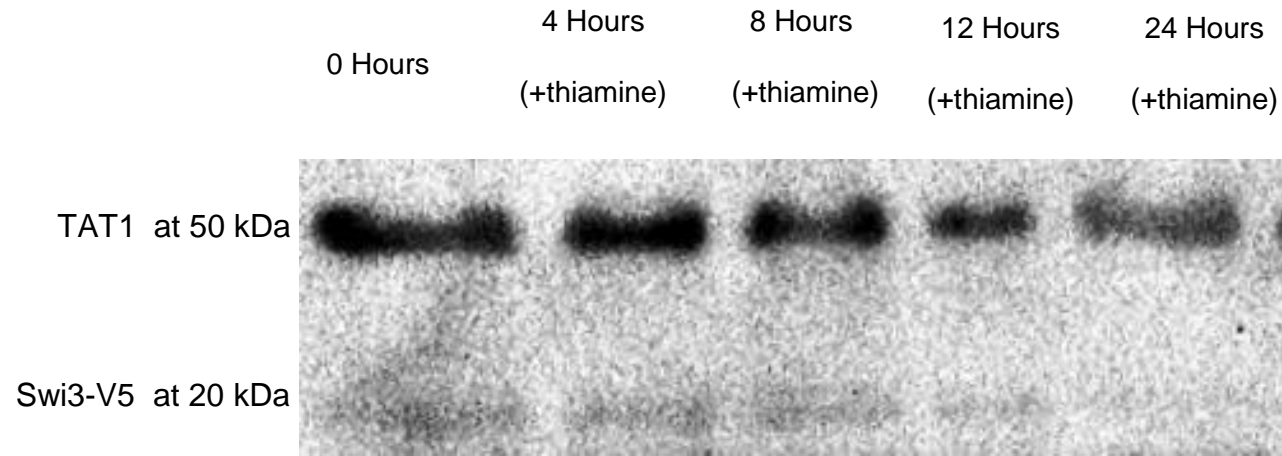


Figure 4-34. Depletion of V5 tag in the *swi3-V5 swi3Δ* strain SPSC 1101 after the addition of thiamine. Protein samples were taken from SPSC 1101 incubated for 24 hours in EMM+uracil+leucine with the addition of thiamine to the media. The protein samples were taken from 0, the time of addition of thiamine to the 0.5 OD culture, to 12 hours at 4 hour-intervals then an additional sample at 24 hours. The western blot shown represents the samples after being probed with anti-TAT1 (top signal) and anti-V5 (bottom signal) as control. The 0 hour, 4 hour and 8 hour samples express the V5 tag while there was no visible signal for the 12 hour or 24 hours samples.

The effect of thiamine addition on the *rad4-116 swi3Δ swi3-V5* strain across 24 hours

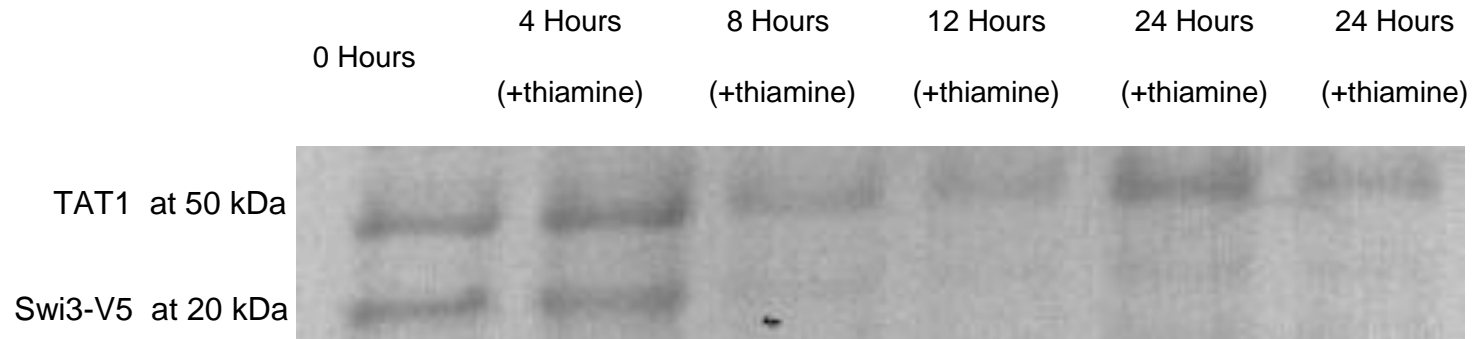


Figure 4-35. Depletion of V5 tag in the *swi3-V5 swi3Δ rad4-116* strain SPSC 1102 after the addition of thiamine. Protein samples were taken from SPSC 1102 incubated for 24 hours in EMM+uracil+leucine with the addition of thiamine to the media. The protein samples were taken from 0, the time of addition of thiamine to the 0.5 OD culture, to 12 hours at 4 hour-intervals then an additional sample at 24 hours. The western blot shown represents the samples after being probed with anti-TAT1 (top signal) and anti-V5 (bottom signal) as control. The 0 hour and 4 hour samples express the V5 tag while there was no visible signal for the 8 hour, 12 hour or 24 hours samples. An additional sample at 24 hour was taken to underline complete depletion of the V5 tag.

4.6.3 Phenotypic Characterisation of *swi3-V5* strains by microscopy

To be able to phenotypically characterise each strain carrying *swi3-V5*, cell pellets from each strain at each timepoint was taken. The microscopy method and analysis were carried out as detailed in Section 3.3.3.

The effect of thiamine addition on the *swi3-V5* strain SPSC 1097 across 24 hours

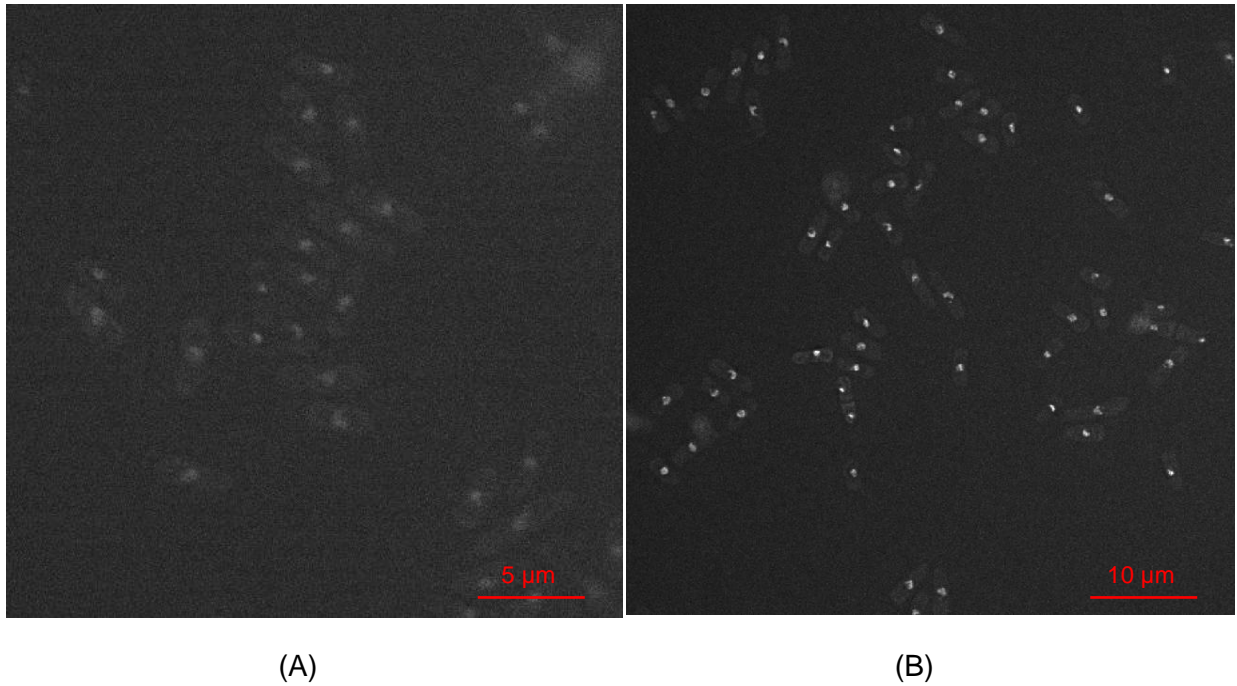


Figure 4-36. The cell morphology of the *swi3-V5* strain SPSC 1097 across 24 hours after thiamine induction. The figure shows the cells of the SPSC 1097 strain stained with DAPI to show the nuclei at (A) the 0 hour timepoint at 100X magnification and the (B) 24 hour timepoint at 60X magnification . There is no significant difference between the cells across those 2 timepoints in terms of cell length, cell shape and nuclear shape.

The effect of thiamine addition on the *swi3Δ swi3-V5* strain SPSC 1101 across 24 hours

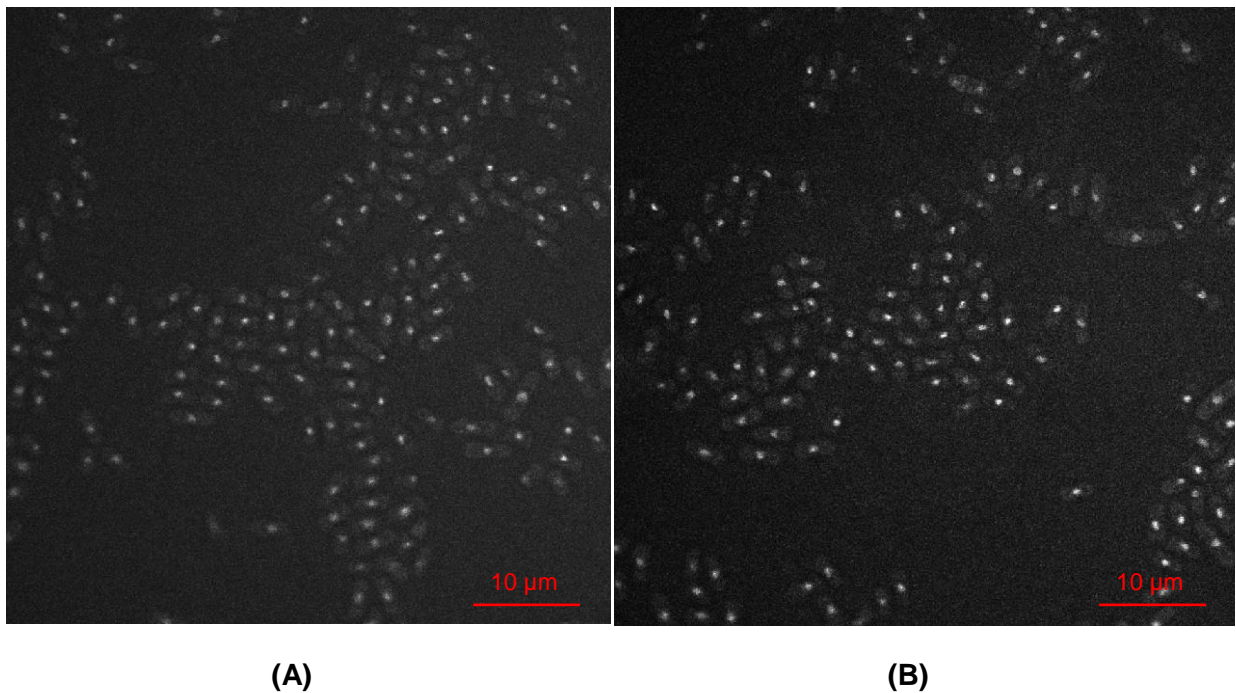


Figure 4-37. The cell morphology of the *swi3Δ swi3-V5* strain SPSC 1101 at 60X magnification across 24 hours after thiamine induction. The figure shows the cells of the SPSC 1101 strain stained with DAPI to show the nuclei at (A) the 0 hour timepoint and the (B) 24 hour timepoint. There is no significant difference between the cells across those 2 timepoints in terms of cell length, cell shape and nuclear shape.

The effect of thiamine addition on the *rad4-116 swi3Δ swi3-V5* strain SPSC 1102 across 24 hours

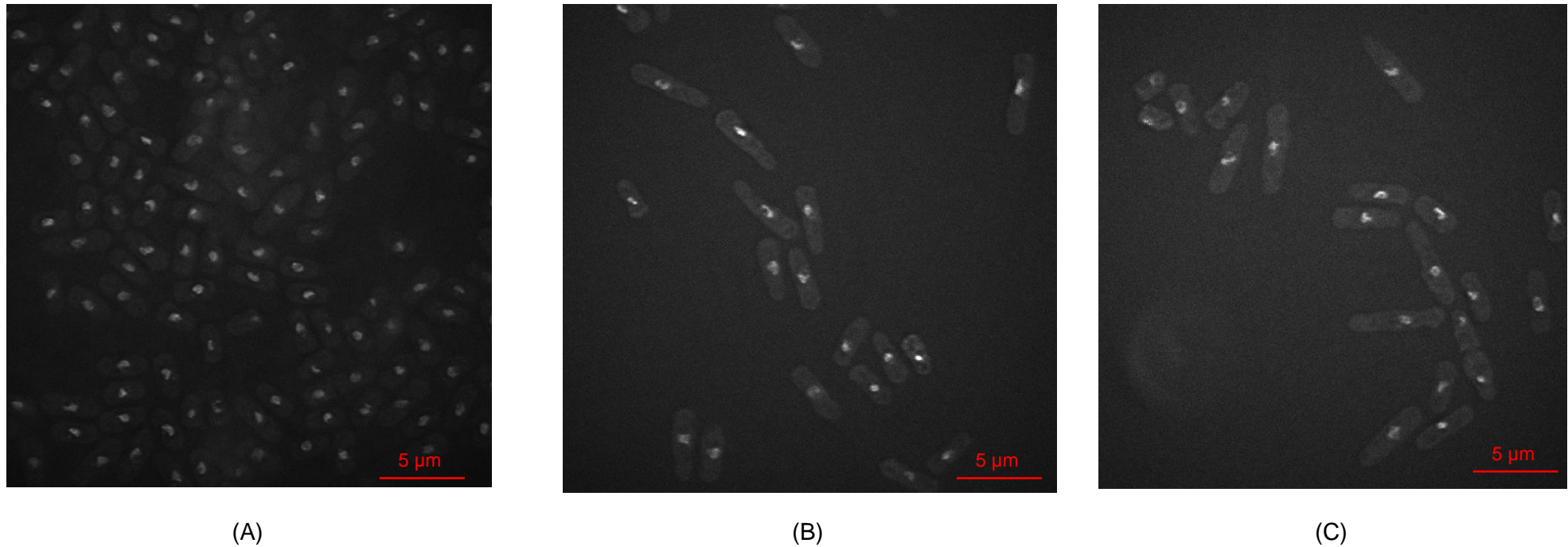


Figure 4-38. The cell morphology of the *swi3Δ swi3-V5 rad4-116* strain SPSC 1102 at 100X magnification across 24 hours after thiamine induction. The figure shows the cells of the SPSC 1102 strain stained with DAPI to show the nuclei at (A) the 0 hour timepoint, (B) the 12 hour timepoint and (C) the 24 hour timepoint. The cells show two distinct phenotypes, that develop from timepoint 0 to 12 to 24 hours, for cells to increase or decrease in length. The nuclei of most these cells show a irregular nuclear shapes that becomes more pronounced at the 24 hour timepoint and some cells show a compacted nucleus.

4.6.4 The effect of thiamine addition on the *rad4-116 swi3Δ swi3-V5* strain SPSC 1102 across 24 hours on cell length

Figure 4-39 to Figure 4-43. The population of SPSC 1102 divided by cell length across the 24 hour period after thiamine addition. The figures shows the graphical representation of the percentage of cells by cell length at each timepoint.

SPSC 1102 at Timepoint 0 Hours

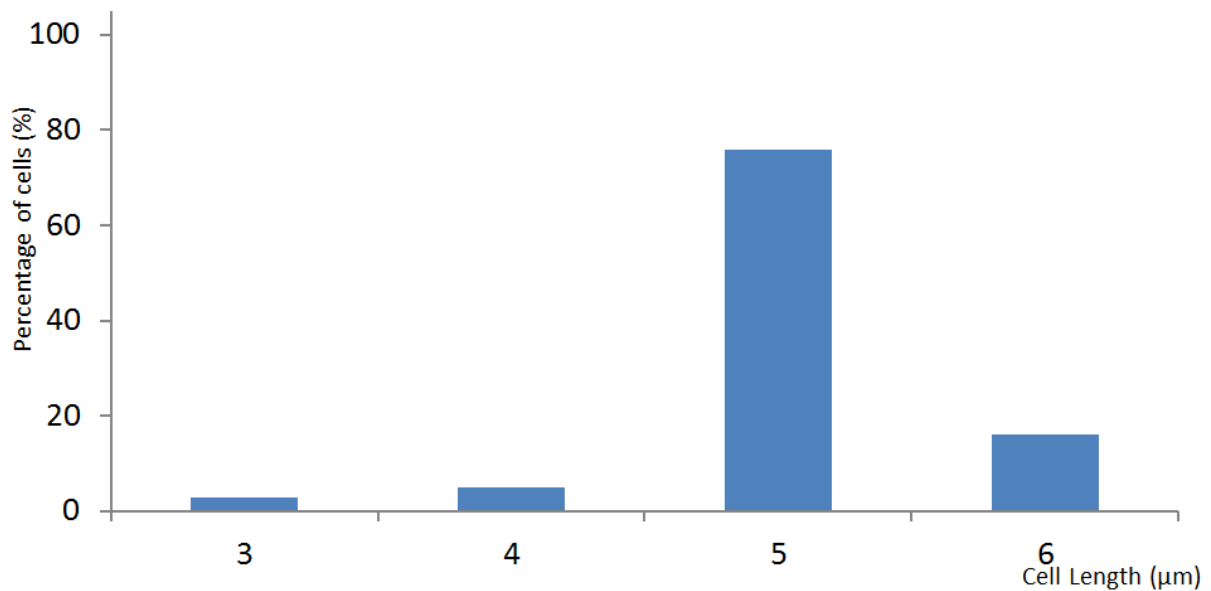


Figure 4-39. The population of SPSC 1102 divided by cell length at the 0 hour timepoint after thiamine addition.

SPSC 1102 at Timepoint 4 Hours

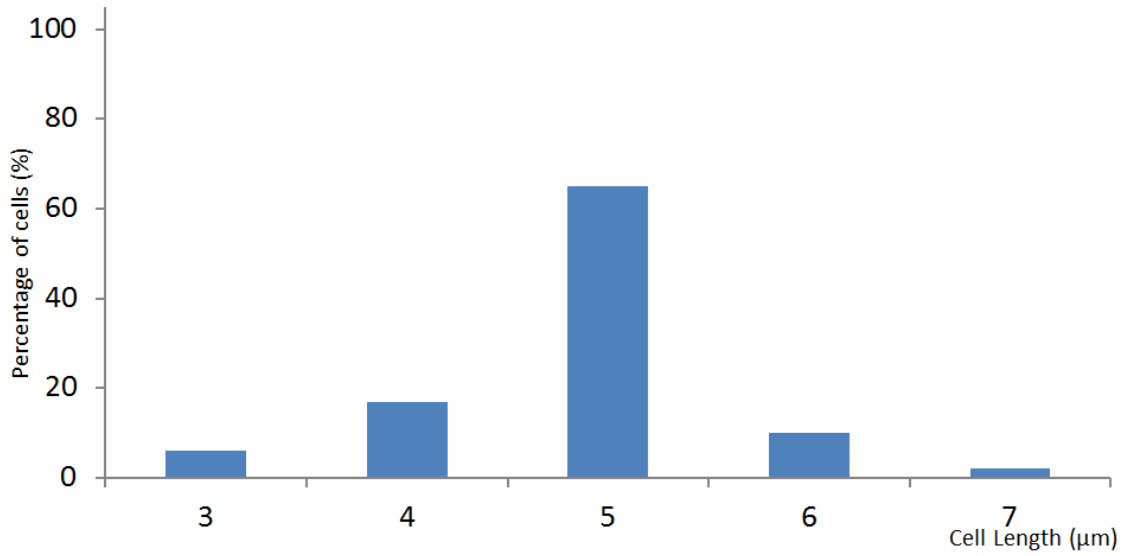


Figure 4-40. The population of SPSC 1102 divided by cell length at the 4 hour timepoint after thiamine addition.

SPSC 1102 at Timepoint 8 Hours

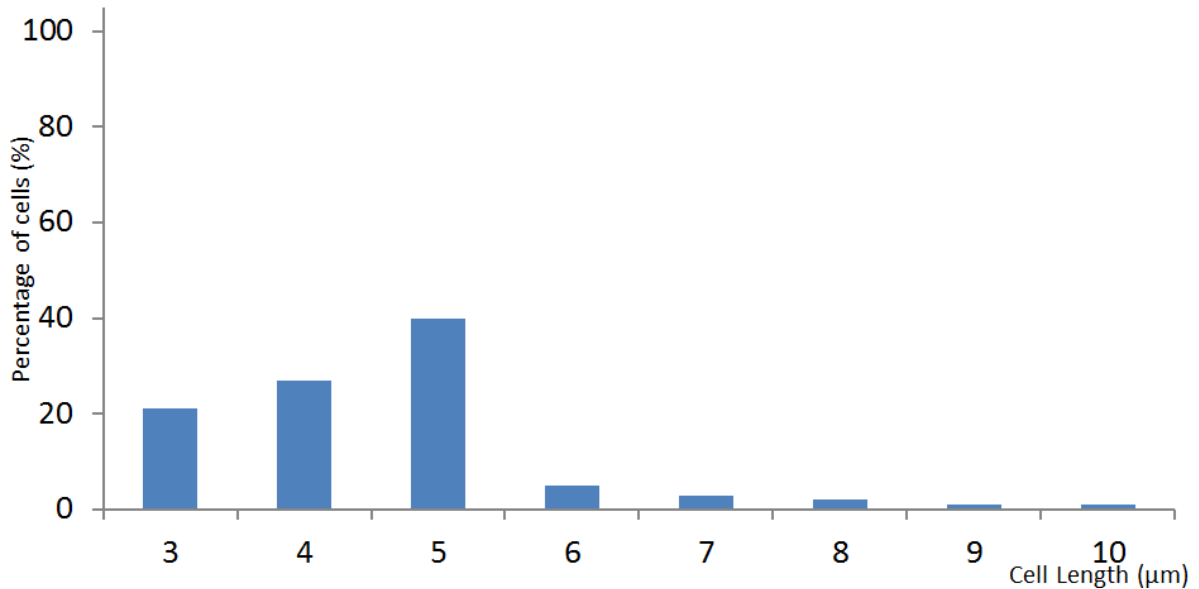


Figure 4-41. The population of SPSC 1102 divided by cell length at the 8 hour timepoint after thiamine addition.

SPSC 1102 at Timepoint 12 Hours

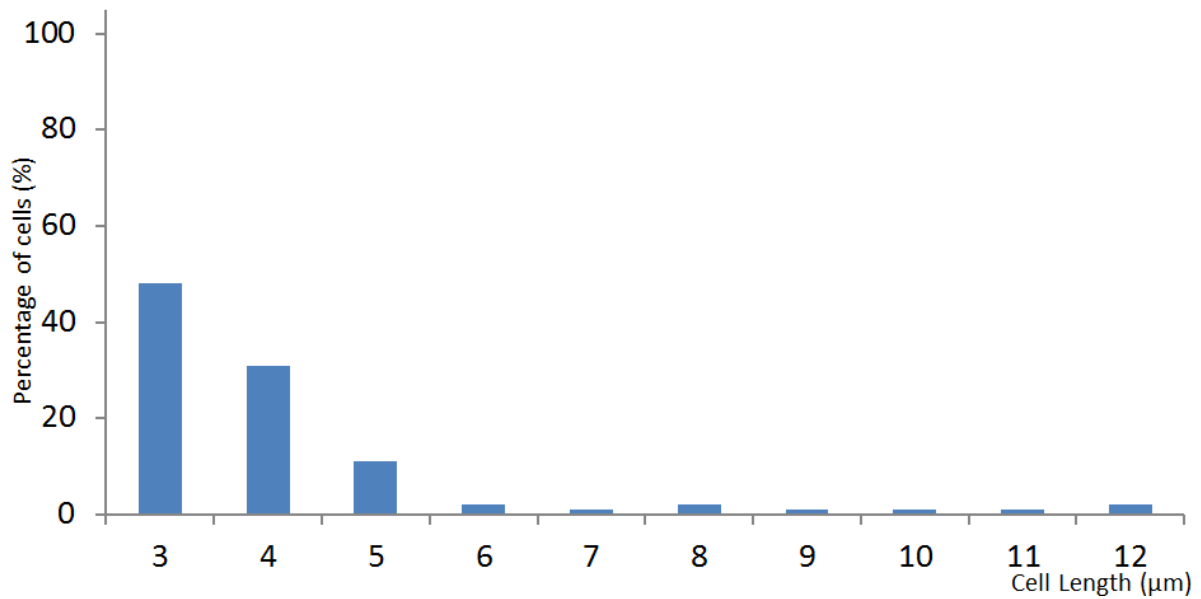


Figure 4-42. The population of SPSC 1102 divided by cell length at the 12 hour timepoint after thiamine addition.

SPSC 1102 at Timepoint 24 Hours

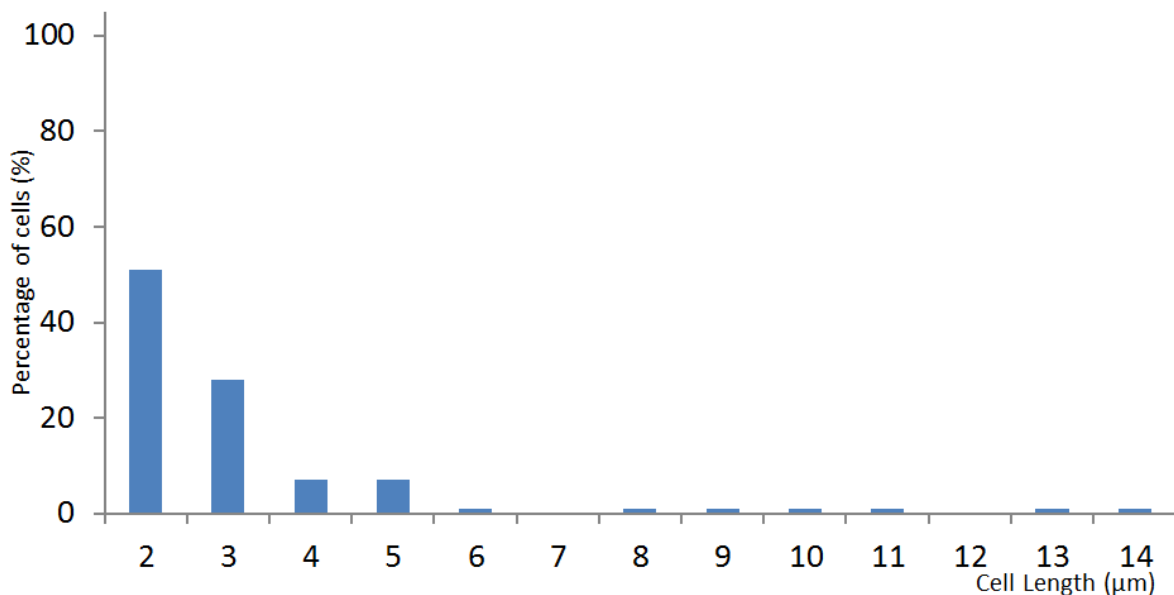


Figure 4-43. The population of SPSC 1102 divided by cell length at the 24 hour timepoint after thiamine addition.

The effect of thiamine addition on the average cell length of *swi3-V5* strains across 24 hours

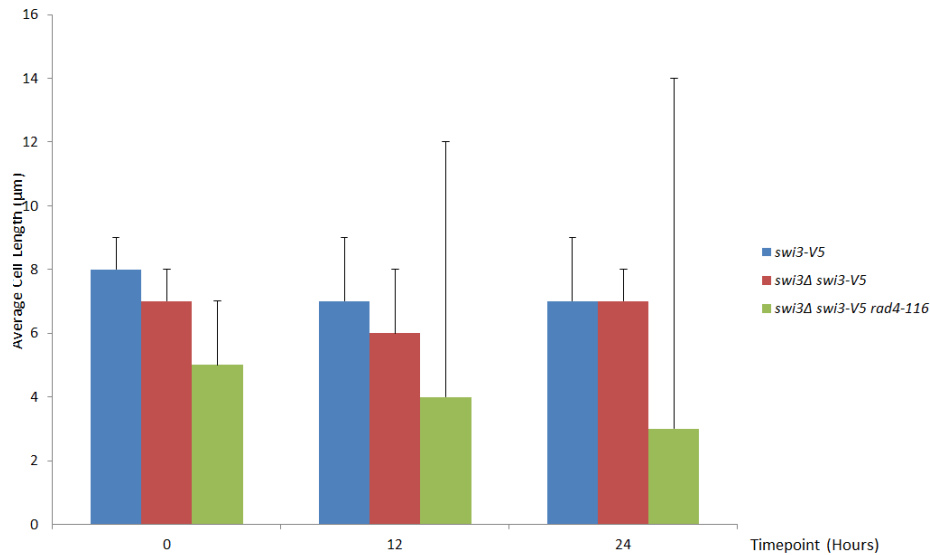


Figure 4-44. The average cell length of the strains carrying the *swi3-V5* allele. The figure shows the graphical representation of the comparison of average cell length between the base *swi3-V5* strain, the *swi3-V5 swi3Δ* strain and the *swi3-V5 swi3Δ rad4-116* strain. No significant change in average cell length occurred in both the base *swi3-V5* strain and the *swi3-V5 swi3Δ* strain as the value is between 6 and 8µm between the 0 hour to 24 hours to finally reach 7µm for both strains at 24 hours after thiamine addition. As for the *swi3-V5 swi3Δ rad4-116* strain, the initial average cell length at 0 is lower than the other two strains at 5 µm. A gradual decrease is then observed from 5 µm to 4 µm at 12 hours then 3 µm at 24 hours after the addition of thiamine. The cells of the *swi3-V5 swi3Δ rad4-116* strain contain 2 phenotypic cell sizes with the predominant one being a short, almost spherical, cell of 2 to 3 µm in length and the other, less common phenotype, being of 9 to 12 µm in length.

As observed in Figure 4-31 for QPCR and Figures 4-33, 4-34, 4-35 for western blotting, the expression of the RNA product and protein for Swi3-V5 were successfully depleted after 24 hours of incubation in media with thiamine. The adjusted relative quantity for the *swi3-V5* RNA expression reached 0.3651 for the *swi3-V5* strain in Figure 4-28, 0.1542 for the *swi3Δ swi3-V5* strain in Figure 4-29 and 0.14536 for the *swi3Δ swi3-V5 rad4-116* strain in Figure 4-30. The adjusted relative quantity for all the *swi3-V5* strains across the 24 hour timecourse is summarised in Figure 4-31. The preliminary experiment in Figure 4-32 using the *swi3-V5* strain (SPSC1097), showed that the signal present using the anti-V5 antibody, was abolished completely following 16 hour incubation with thiamine. The Swi3-V5 protein signal was present at timepoints 0 and 4 hours in all the three strains SPSC 1097, SPSC 1101 and SPSC 1102 as observed in Figures 4-33, 4-34, 4-35 respectively. In all 3 figures, the signal was abolished below the detectable level from 8 hours after thiamine addition onwards. The level of expression of the control α -Tubulin for all three strains across all the timepoints did not show any change.

Indeed, the levels of RNA expression did not reach 0 as seen in Figure 4-31, yet, those levels were sufficient to lead to an abolishment of Swi3-V5 protein expression below detectable levels as observed in the western blots. The depletion of RNA expression and protein signals also caused a decrease in viability, as seen in Figure 4-45, consistent with the time and level of abolishment of the V5-tagged protein in the *swi3Δ swi3-V5 rad4-116* strain but not in any of the other strains. The *swi3Δ swi3-V5 rad4-116* strain showed a gradual loss of viability dropping from 99% viability at 0 timepoint to 56% after 12 hours, then to 29% viability at 24 hours. The decrease in viability at timepoints 12 and 24 was statistically significant at $p \leq 0.01$

with values of 56% and 29% respectively compared to the 0 hour timepoint which is consistent with the depletion of V5 protein signal. However, the presence of viable cells indicated that the level of depletion per cell in the culture population is not equal. This is also reflected in the presence of 0.14536 adjusted relative quantity value of V5 RNA for the *swi3Δ swi3-V5 rad4-116* strain as represented in Figure 4-30.

In terms of cell morphology, as observed in Figure 4-36 and Figure 4-37, the cell size and length and nuclear integrity of SPSC 1097(*swi3-V5*) and SPSC 1101 (*swi3Δ swi3-V5*) respectively did not show any change across the 24 hour timecourse. However, as seen in Figure 4-38, the *swi3Δ swi3-V5 rad4-116* strain SPSC 1102, showed two distinct phenotypes in terms of cell size. The more common phenotype being shorter of less than 5 μm in length and the less common phenotype being a longer cell of more than 5 μm in length as observed in Figure 4-38. Both phenotypes show irregular nuclear size and shape with some nuclei being elongated or compacted. Those changes were detectable after 12 hours of thiamine incubation and more pronounced at the 24 hour timepoint. The changes in average cell length for SPSC 1102 was compared at the 0, 12 and 24 hours timepoints to the SPSC 1096(*swi3-V5*) and SPSC 1098 (*swi3Δ swi3-V5*) strains and summarised in Figure 4-44.

4.6.5 The viability profile of *swi3Δ swi3-V5 rad4-116*

The paired Student T-test was performed to compare the viability of each *swi3-V5* strain at each timepoints 4, 8, 12 and 24 hours after the addition of thiamine to the media to the starting 0 hour viability value. Each value of viable cells was obtained from an average of a triplicate separate cultures of strain at each timepoint at which a triplicate of EMM+ uracil+ leucine+ thiamine plates were used to grow 100 colonies. After 3 days of incubation at 26 °C, the number of viable colonies on each plate was counted and recorded and the average calculated for *swi3Δ* strain and compared to the *rad4⁺* strain at its corresponding timepoint. The variance for both samples were similar allowing the use of the 2-tailed Student T-test. The degree of freedom for each sample used at each timepoint was 2 and the critical value over which the difference is significant is 9.925 at $p \leq 0.01$. $p \leq 0.01$ was chosen over the standard $p \leq 0.05$ as the critical values, calculated and determined to be significant at $p \leq 0.05$, were also significant at $p \leq 0.01$. For the *swi3-V5* and *swi3Δ swi3-V5*, there was no significant difference the viability counts observed across all the timepoints recorded from 0 to 24 hours. However, for *swi3Δ swi3-V5 rad4-116* strain, timepoints 12 and 24 showed a significant decrease in viability at $p \leq 0.01$ with values of 56% and 29% respectively compared to the 0 hour timepoint.

Viability Comparison of *swi3-V5* strains

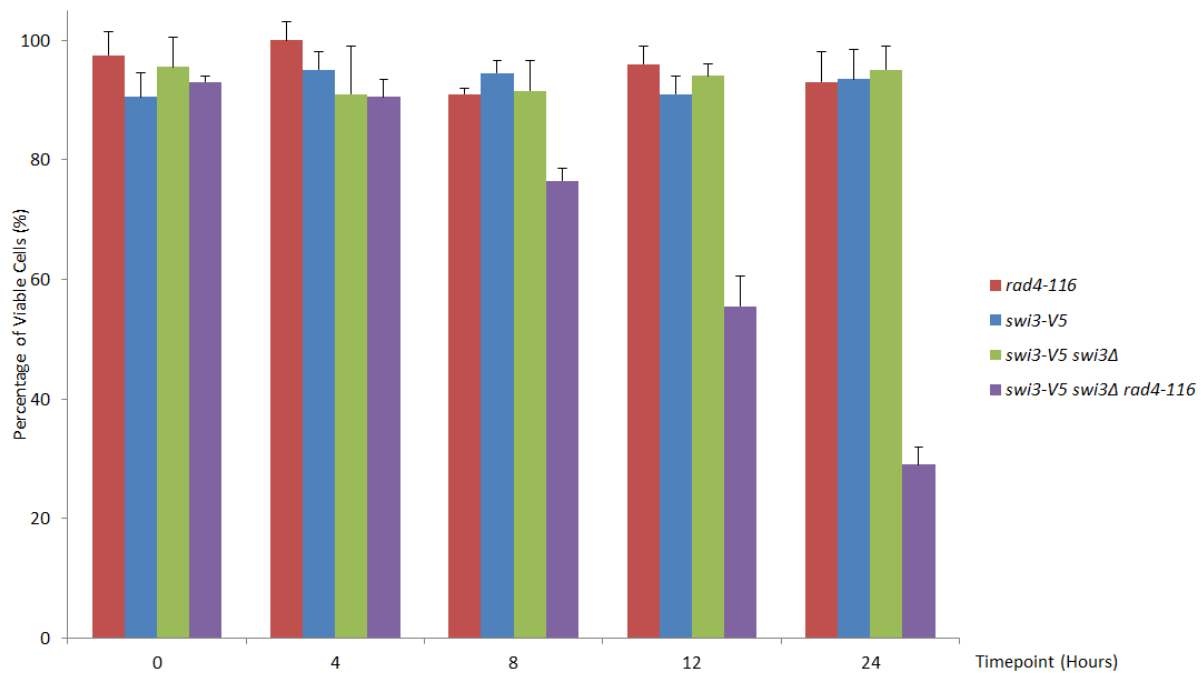


Figure 4-45. The viability comparison of strains carrying the *swi3-V5* allele against the control *rad4-116* strain. The figure shows the graphical representation of the comparison of viability between the *Swi3-V5* strains and the *Rad4-116* strain. Only SPSC 1102 showed a gradual loss of viability dropping from 93% viability at 0 timepoint to 56% after 12 hours, then to 29% viability at 24 hours. All the other strains represented showed no significant loss of viability across the 24 hour timecourse ranging from 100% to 91% viability.

4.6.6 Phenotypic Characterisation of *swi3-V5* strains by FACS

The FACS method and analysis were carried out as detailed in Section 3.3.6.

Phenotypic Characterisation of *swi3-V5* (SPSC 1097) and *swi3Δ swi3-V5* (SPSC 1101) strains by FACS

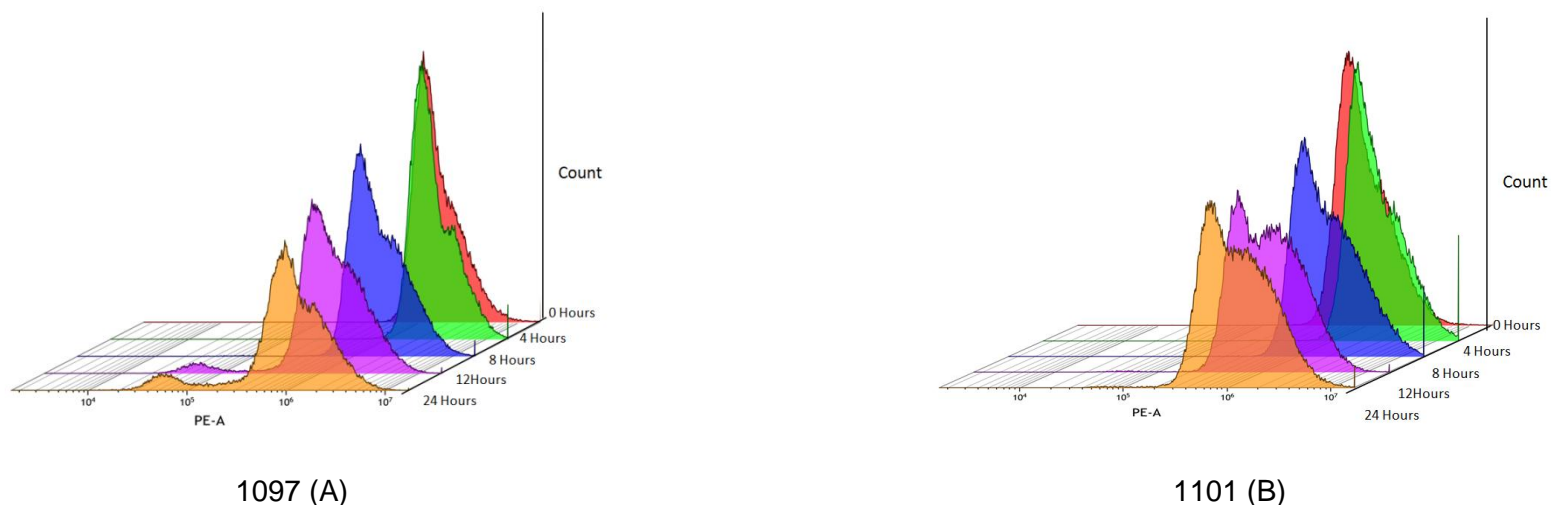


Figure 4-46. Cell population as investigated through FACS. The figure shows the analysis of the populations of SPSC 1097 (A) and SPSC 1101(B) as representation of count (y-axis) against the phycoerythrin channel PE-A (x-axis) across 24 hours with 0 hour being the furthest along the z-axis followed by 4, 8, 12 and finally, 24 hours being the nearest along the z-axis. For (A) SPSC 1097, a general decrease in peak occurred from 0 to 24 hours. A shift in peak occurred from 0 to 12 hours with the no change from 0 to 4 hours. Across 4 to 24 hours, a second peak rises towards the 10^7 mark and a minor third peak towards the 10^4 mark. The 12 and 24 hour samples showed the same peak pattern with the third peak (10^5) higher. For (B) SPSC 1101, a general decrease in peak occurred from 0 to 24 hours. A shift in peak occurred from 0 to 12 hours with the no change from 0 to 4 hours. The 12 and 24 hour samples showed the same double peak pattern and are nearly identical in shape.

Phenotypic Characterisation of *rad4-116 swi3Δ swi3-V5* strain SPSC 1102 by FACS

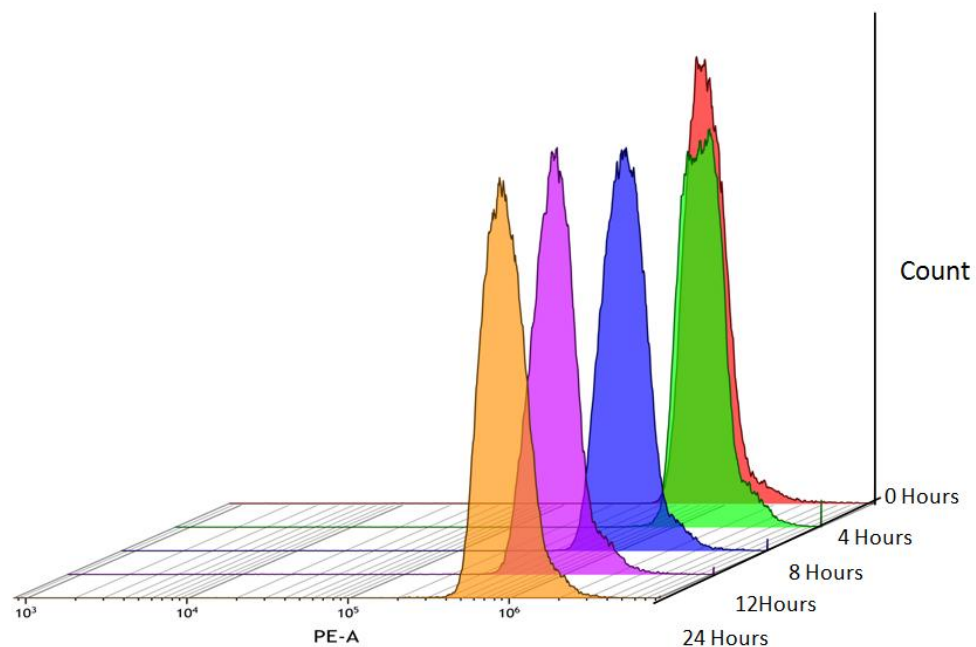


Figure 4-47. Cell population as investigated through FACS. The figure shows the analysis of the population of SPSC 1102 as representation of count (y-axis) against the phycoerythrin channel PE-A (x-axis) across 24 hours with 0 hour being the furthest along the z-axis followed by 4, 8, 12 and finally, 24 hours being the nearest along the z-axis. There was no change in staining or shift in peaks across the 24 hours but a slight decrease occurs between 0 to 4 hours.

4.7 The Swi complex members chapter discussion

By mapping the spores from crossing the *rad4-116* strain with the *swi1Δ* strain in Figure 4-1 and tabulating 192 valid spores in total in Table 4-A, the χ^2 value was calculated at 23.4. Similarly, crossing the *rad4-116* strain with the *swi3Δ* strain in Figure 4-22 and tabulating 212 valid spores in total in Table 4-B, the χ^2 value was calculated at 22.5. In both cases, the χ^2 value was significant to prove that the results obtained in terms of synthetic lethality of combining *rad4-116* and *swi1Δ* or *swi3Δ* was not due to chance but due to the interference occurring in one or more biological pathways. In this case, the interaction of *rad4-116* and members of the Swi complex in the stabilisation of stalled replication forks.

The comparison of DNA damage profiles of *rad4-116* against the *swi1Δ* and *swi3Δ* strains after incubation with HU using Rad52-GFP foci was carried out using the aspects detailed in the previous chapter. The cells were stained for DAPI to show nuclei and anti-GFP to show foci as presented in Figure 4-3 for the *swi1Δ* strain and Figure 4-24 for the *swi3Δ* strain. The merged image of both DAPI and GFP staining, concentrating on a single nucleus with a single bright green GFP focus in each case highlighted by a red arrow, can be seen in Figure 4-2 for the *swi1Δ* strain and Figure 4-23 for the *swi3Δ* strain. None of the *rad4-116*, *rad4⁺*, *swi1Δ* or *swi3Δ* strains showed any significant change in viability across the timecourse of the experiment as presented in the graph of Figure 4-4 and Figure 4-25.

In terms of the number of foci per nucleus present, *swi1Δ* and *swi3Δ* cells both showed singular foci per nucleus, similar to *rad4⁺* cells and in contrast to *rad4-116* cells. This can be easily observed in Figure 4-2 for *swi1Δ* cells, Figure 4-23 for *swi3Δ* cells, Figure 3-8 for *rad4-116* cells and Figure 3-6 for *rad4⁺* cells.

The second aspect was the percentage of nuclei containing foci as a section of all the population of nuclei counted at the starting point, timepoint 0, of the experiment. The starting percentage was identical in *rad4⁺* cells, *swi1Δ* cells and *swi3Δ* cells at 6% , as presented in Figure 3-7, Figure 4-5 and Figure 4-26, respectively. This was in contrast to the much higher value of 26% for *rad4-116* cells at timepoint 0 as shown in Figure 3-9.

The next aspect was the peak of the percentage of nuclei with GFP foci as a section of the total population of nuclei across the duration of the experiment, 210 minutes. The peak values of each of the strains did not match each other in terms of time reached or the level of accumulation of foci. For the *swi1Δ* strain, the peak was reached at 90 minutes for a value of 14% as seen in Figure 4-5. For the *swi3Δ* strain, the peak was reached at 30 minutes for a value of 7% as seen in Figure 4-26. For the *rad4⁺* strain, the peak was reached at 120 minutes for a value of 27% as observed in Figure 3-7. For the *rad4-116* strain, the peak was reached at 150 minutes for a value of 49% as seen in Figure 3-9.

For both the *swi1Δ* strain and the *rad4⁺* strain, the shape of the graph was similar with a gradual increase up to a peak point occurring after 90 minutes or 120 minutes which are consecutive timepoints. The percentage of nuclei with foci began to decrease, also in a gradual manner, after the 120 minute timepoint in both cases to present a bell-shaped figure. This lied in stark contrast to the *rad4-116* strain which showed a sharp increase from 0 to 30 minutes and levelled off at 38% or above, with the exception of the 120 minute timepoint, till the 210 minute timepoint at the end of the experiment. More interestingly, in the case of the *swi3Δ* strain, given that the peak value of foci was reached at the 30 minute-mark, the decrease and recovery

began as soon as the 60 minute timepoint in a gradual manner reaching 0% at the 150 minute-mark. This presents a unique pattern from all the other strains tested showing that not only is the level of Rad52-GFP foci accumulation is much lower than the wildtype and other strains carrying deletions, but that the apparent complete recovery and resolution of stalled forks occurred much faster in the *swi3Δ* strain.

The final aspect was the final reading of nuclei with foci and the comparison between the starting and final timepoints for each strain. For both the *swi1Δ* strain and the *rad4⁺* strain, the final readings were similar at 2% and 3% respectively and are quite near to the starting values of 6% as observed in Figure 4-5 and Figure 3-7 respectively. As previously mentioned, in the case of the *swi3Δ* strain, no visible foci were detected for the final three timepoints of the experiment and thus, the final reading was 0% at 210 minutes as seen in Figure 4-26. All three strains differed from *rad4-116* strain, which reached a final reading of 21% which is only a 5% decrease in value from the initial reading of 26% as observed in Figure 3-9. In the case of the *swi1Δ* strain, the final reading was 4% lower than the initial reading and in the case of the *swi3Δ* strain, 6% less. Both strains showed similar recovery in terms of initial and final points to the *rad4⁺* strain. The initial values, peak values and final readings for all the strains are summarised in Figure 4-6 for *swi1* and Figure 4-26 for *swi3* to further highlight the recovery patterns of all three strains. The results presented here were consistent with previous studies that utilised *swi1Δ* strains to test the effect of HU arrest (Katou *et al.*, 2003). Results concerning the accumulation of Rad52 foci are comparable to the studies by Noguchi and colleagues, albeit the experiments carried out did not investigate the accumulation patterns as closely as the results presented in this study (Noguchi *et al.*, 2003 a;b).

By constructing strains carrying the repressible the *swi1-V5* allele or the *swi3-V5* allele in the presence of *rad4-116*, it was possible to observe the behaviour of cells during cell death as the V5-tagged protein activity was abolished in both cases. By using RT-QPCR, it was confirmed that a gradual decrease in the relative quantity of RNA encoding *swi1-V5* and *swi3-V5* in all the strains tested as observed in Figure 4-10 and Figure 4-31. Evidence of Swi1-V5 and Swi3-V5 depletion was confirmed using western blotting using the V5 antibody, alongside TAT1 as a control. By observing Figures 4-12, 4-13 and 4-14, all three *swi1-V5* strains showed total abolishment of the Swi1-V5 signal, at the 112 kDa mark, after 8 to 12 hours of the addition of thiamine to the media. In a parallel manner, Figures 4-33, 4-34 and 4-35 showed that all three *swi3-V5* strains exhibited total abolishment of the Swi1-V5 signal, at the 20 kDa mark, after 4 to 12 hours of the addition of thiamine to the media.

The depletion of the RNA signal and tagged protein product did not cause a visible change in cell morphology in the *swi1-V5* and *swi1Δ swi1-V5* strains or the *swi3-V5* and *swi3Δ swi3-V5* strains across the 24 hour time course as observed in Figure 4-15, Figure 4-16, Figure 4-36 and Figure 4-37 respectively. However, the cell morphology began to change significantly in the *swi1Δ swi1-V5 rad4-116* and *swi3Δ swi3-V5 rad4-116* in response to the depletion of the RNA signal and V5-tagged protein as observed in Figures 4-17 and Figure 4-38 respectively. In both cases, the correlation in the time of decrease of RNA product leading to the decrease in protein product appeared as change in cell morphology and length as soon as 8 hours after thiamine addition. In the case of the *swi1Δ* strain, a significant change was observed after 12 hours, as seen in Figure 4-17(B), as well as a more pronounced change after 24 hours, as seen in Figure 4-17(C). In the case of the *swi3Δ* strain, a

significant change was observed after 12 hours, as seen in Figure 4-38(B), and the cells appeared similar to the 12 hour timepoint after 24 hours, as seen in Figure 4-38(C).

There are several changes that occur in the cell morphology of the *swi1Δ swi1-V5 rad4-116* strain in terms of nuclear integrity, cellular shape and cell length and. In Figure 4-17(B), most of the cells develop nuclei with a high degree of nuclear fragmentation, which then develops into compact nuclei with the fragmentation becoming less as seen in Figure 4-17(C), 24 hours after thiamine addition. As for *swi3Δ swi3-V5 rad4-116* strain, in Figure 4-38(B), most of the cells develop abnormally shaped nuclei and compact nuclei with no visible fragmentation and that continued in Figure 4-38(C), 24 hours after thiamine addition. The difference in the appearance of the nuclei of both strains show that there are distinct roles that separate *swi1* and *swi3*, which may include the maintenance or control of histone remodelling.

The more important aspect of change in cellular morphology of the *swi1Δ swi1-V5 rad4-116* strain, was the gradual in cell length in Figure 4-18 compared to the *swi1-V5* and *swi1Δ swi1-V5* strains did not show a significant change in cell length across the 24 hour time course. The starting timepoint 0 showed a similar cell length distribution to the *swi1-V5* and *swi1Δ swi1-V5* strains. In contrast, the *swi1Δ swi1-V5 rad4-116* strain began to increase in cell length in a gradual manner. By the 24 hour timepoint, cells could be seen as long as 14µm with elongated cytoplasm that sometimes develop in three directions with the nucleus at its centre.

That was different from the changes occurring with the *swi3Δ swi3-V5 rad4-116* strain. The most important aspect of change in cellular morphology of the *swi3Δ*

swi3-V5 rad4-116 strain, was the changes in cell length which was mapped in detail in Figure 4-39 for timepoint 0 till Figure 4-43 for timepoint 24 hours to include all the timepoints at 4-hour intervals. The starting timepoint 0 showed a similar cell length distribution to the *swi3-V5* and *swi3Δ swi3-V5* strains which did not show a significant change in cell length across the 24 hour time course. In contrast, the *swi3Δ swi3-V5 rad4-116* strain began to deviate in cell length in two directions being a gradual increase in length on one hand and a gradual decrease on the other hand to develop the two distinct phenotypes.

It should be noted that the shorter phenotype of 2 to 3 μm in length did not significantly appear till after 8 hours of thiamine addition as observed in the difference between Figure 4-41 to Figure 4-42 to Figure 4-43, by which it becomes the predominant phenotype. By the end of the experiment, Figure 4-43, the fully developed phenotypes were far apart in length such that the subset of lengths between 6 to 8 μm comprised a distinctly small subset of the population as observed in Figure 4-43. The short-length phenotype was the more predominant phenotype, as cells grew to a range between 2 to 3 μm compared to the 5 μm at the starting point and even after 4 hours of thiamine addition, as in Figure 4-40. The subpopulation of cells whose lengths range between 11 to 14 μm were present to a lesser degree as seen in Figure 4-43. The analysis of the subpopulations based on length was essential, as the average length of cells metric masked the presence of the long cell phenotype due to the overwhelming difference in number between the short cells and the long cells as represented in Figure 4-44. The development of two distinct phenotypes showed that the interaction between *rad4-116* and *swi3* occurred at multiple pathways in DNA modification, elucidating additional roles to *swi3* that are not shared by *swi1*.

Both *swi3* phenotypes ultimately led to the death of cells in a gradual manner as observed in Figure 4-45. The same figure, Figure 4-45, showed that no cell death occurred in other strains carrying *swi3-V5* or the control strain carrying *rad4-116* with a wildtype *swi3* allele. The loss of viability corresponded to the depletion of RNA and protein product of *swi3-V5*. Similarly, as seen in Figure 4-19, only the *swi1Δ swi1-V5 rad4-116* strain showed a gradual cell death whilst no cell death occurred in other two strains carrying *swi1-V5* or the control strain carrying *rad4-116* with a wildtype *swi1* allele. The loss of viability corresponded to the depletion of RNA and protein product of *swi1-V5*.

Finally, in terms of using PI to investigate the nuclear content of the cells across the 24 hour timecourse after thiamine addition, no conclusion could be reached. For the *swi1-V5*, *swi1Δ swi1-V5 rad4-116* and *swi3Δ swi3-V5 rad4-116* strains, Figure 4-20 (A), 4-21 and 4-47 respectively, show that no significant change occurred across the 24 hours. However, as seen in Figure 4-20 (B) and Figure 4-46 (A and B), the *swi1Δ swi1-V5* strain as well as *swi3-V5*, *swi3Δ swi3-V5* showed a general gradual decrease in the sharpness of each peak and development of multiple peaks. With regards to the lack of change exhibited by the *swi1Δ swi1-V5 rad4-116* and *swi3Δ swi3-V5 rad4-116* strains, subpopulations need to be separated to be able to show different fluorescence readings. This experiment could be also be carried out such that samples would be taken in an hourly manner instead of each 4 hours and that could possibly provide a clearer pattern to the change occurring.

Chapter 5: The Genetic Analysis of the interaction between *mrc1* and *rad4-116*

5.1 Introduction

Mrc1 is a conserved replication fork factor which is required for the stabilisation of stalled replication forks and selectively binds to the early-firing origins (Hayano *et al.*, 2011). Furthermore, Mrc1 also functions as a replication checkpoint mediator that allows Rad3-Rad26 to activate the effector kinase Cds1 (Zhao and Russell 2004). Activation of the DNA damage response kinases in response to fork stalling agents requires the mediator protein Mrc1 (Alcasabas *et al.*, 2001; Chini and Chen, 2003).

Mrc1 is required for normal rates of progression of replication forks and is present in replication forks even in the absence of DNA damage (Hodgson *et al.*, 2007; Petermann *et al.*, 2008). Mrc1 interacts with Swi1-Swi3 on stabilisation of stalled replication forks (Tanaka *et al.*, 2007). The comparison between the profiles of DNA damage and cellular morphology of Mrc1 and members of the FPC following depletion of Mrc1, in the presence of Rad4-116, could provide new insight into the mechanism of interaction between Mrc1 and the Swi1-Swi3 complex.

5.1.1 Synthetic Lethality on Agar

The aim of the experiment was to investigate the interactions between *rad4* and *mrc1* which is implicated in the maintenance of chromatin structure and remodelling.

The strains selected had either the *rad4-116* marked with NAT resistance and the *hip1Δ* marked with G418 resistance. The synthetic lethality method and analysis were carried out as detailed in Section 3.1.1.

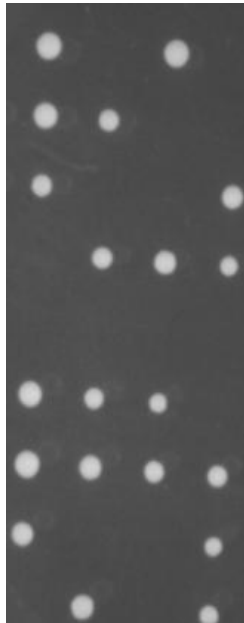


Figure 5-1. The growth of individual spores to colonies of the *rad4-116* strain cross with *mrc1Δ* strain. The figure shows 4 columns of the YES plates of the crosses of the *rad4-116* strain with a *mrc1Δ* strain. The cross shown was a set of spores from tetrads that were inoculated into single spores with a line separating each individual spore set from a single tetrad. The number of spores from each YES plate was counted and recorded.

Cross	<i>mrc1Δ</i> x <i>rad4-116</i>
Wild-type	35
G418 ^R	46
NAT ^R	41
G418 ^R /NAT ^R	12
Viability	132
Total valid spores	180
χ^2 value	12.8

Table 5-A showing the crosses between the *rad4-116* strain and *mrc1Δ*. The *rad4-116* was tagged with NAT resistance while the *mrc1* deletion were marked with G418 (Kanamycin) resistance. The crosses were carried out on EMM-nitrogen agar , then checked after 2 days for sporulation. The tetrads from sporulation were separated using the Singer Micromanipulator onto YES agar plates. After 4 days, the plates were then copied onto fresh YES, as shown in Figure 5-1, YES+G418 and YES+NAT plates separately. After another 3 days, the colonies on each plate were counted and recorded as seen in the table. The χ^2 value for each cross was calculated and tabulated at $p \leq 0.05$ with a degree of freedom of 1.

5.1.2 *mrc1* Δ cause synthetic lethality when combined with *rad4-116*

After the colonies from the crosses were noted and counted from all the plates, the Chi-Square test was performed and a value of 12.8 was the result as shown in Table 5-A. As this value was calculated using the expected value based on the segregated spores not based on the expected segregation pattern, the values represent a focused measure on whether the double mutants were synthetically lethal or not. These values were all greater than 3.84, which was the threshold value at $p \leq 0.05$ with a degree of freedom of 1. This indicated that the deletion of *mrc1* was synthetically lethal when combined with *rad4-116* and that any lethality or observed lack of growth would **not** be due to chance or random occurrence.

5.2 The DNA replication stalled fork profile of *mrc1Δ*

The aim of this experiment was to be able to observe and compare the DNA stalled replication profiles, in terms of accumulation and resolution of DNA forks, profiles of a *rad4-116* strain to *mrc1Δ* and wildtype *rad4* as a control. This ability to assess and monitor such profile would be achieved by utilising *rad52-GFP*. *rad52* encodes the Rad52 protein which is recruited to repair and aid the progress of stalled replication forks. The strains were constructed by direct transformation of PCR-produced deletion *mrc1* encoding G418 resistance and PCR-produced *rad4-116* attached to NAT resistance into a *rad52-GFP* base strain. Cells were grown in liquid media then arrested by the addition of hydroxyurea which blocks ribonucleotide reductase leading to the depletion of the ribonucleotides, halting DNA replication. Then after 6 hours of arrest with hydroxyurea, the cells were released by the depletion of hydroxyurea from the media, washing the cells then resuspending in rich YES media. Samples were collected every 30 minutes for 210 minutes to be analysed for fluorescence microscopy and testing viability. The cell nuclei were assessed in two ways; the first being the percentage and number of nuclei that carry GFP fluorescent foci spanning the 210 minutes compared to the starting time point(0) of the release, and the second by assessing the number of foci per nucleus and arranging them in categories. The foci were assessed using the Softworx program by taking a 3D reconstruction of the cells to be able to assess if the foci observed were nuclear foci to be counted, otherwise they were not counted. The viability of each strain was tested by spreading 100 colonies per plate on YES plates in triplicate per each strain at each timepoint. The viability of cells in all three strains did not change from the arrest up to the 210-minute time point post release. The percentage of nuclei with GFP foci was tabulated and a graph was drawn for each

strain. As observed in the graph, the *rad4-116* showed a higher level of initial foci at the 0 timepoint compared to the other 2 strains.

The initial levels of Rad-52 GFP nuclear foci were 27% and 6% for the *mrc1Δ* and the *rad4⁺* strains respectively contrasting to 26% in the *rad4-116* strain. For the *mrc1Δ* strain the number of foci increased from 26% at the start of the release up to 40% after 30 minutes, which was the peak level of foci for this strain. The foci level then reached a relatively steady level from 31% to 38% after 90 minutes to 26% after 120 minutes. Then, a decrease occurred from 30% at timepoint 150 minutes to 20% at 180 minutes to reach a plateau steady low level of 24% at 210 minutes after release. The 24% recorded at the endpoint of the experiment, at 210 minutes after release, was slightly lower than the starting level of 27% , showing a weak recovery from DNA stalled forks in a bell-shaped manner.

The values of percentage of cells with nuclear Rad52-GFP at the start and the end of the timecourse were similar when comparing the *rad4-116* and *mrc1Δ* strains but not the *rad4⁺* strain. The patterns seen in the *rad4-116* and *mrc1Δ* strains were nearly identical as both show a high initial value of foci then a relative plateau at that high level, albeit with occasional drops, but never seem to recover fully to a significant level below the starting point.

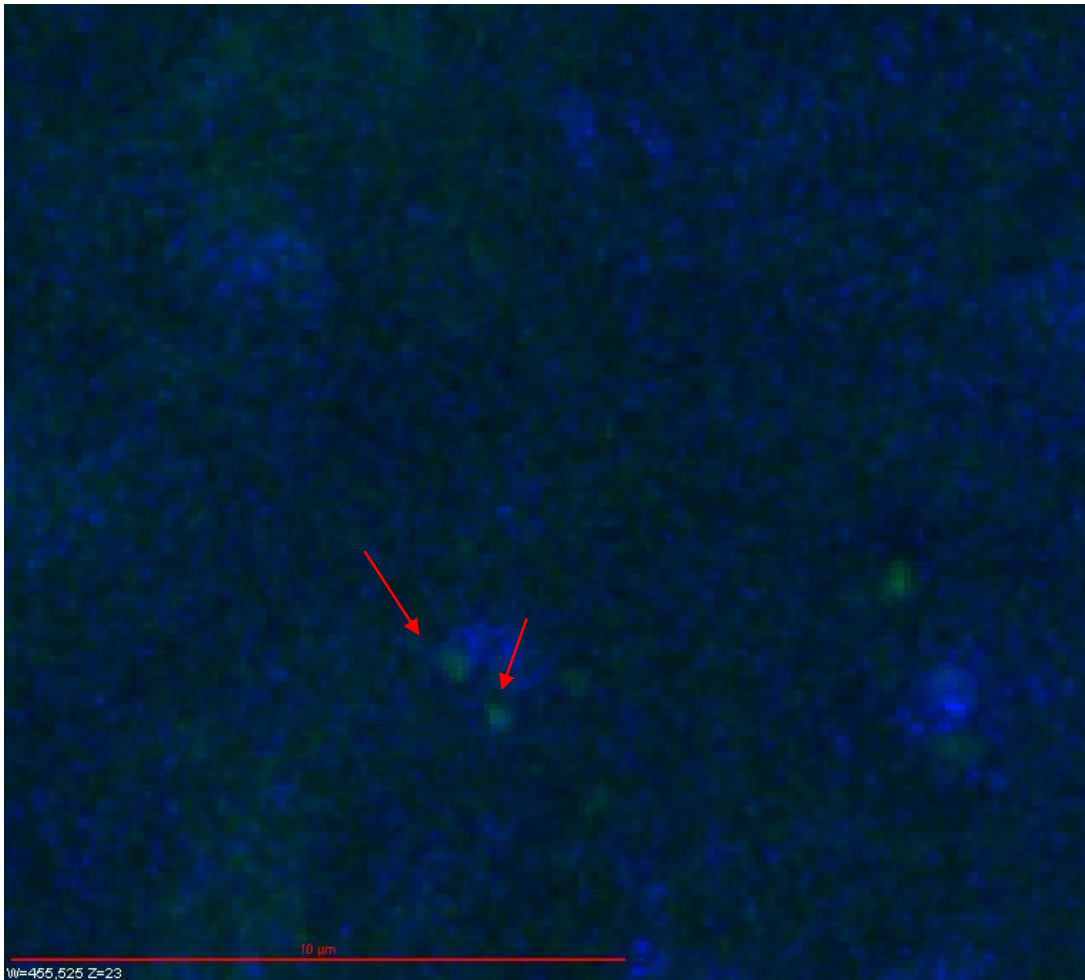
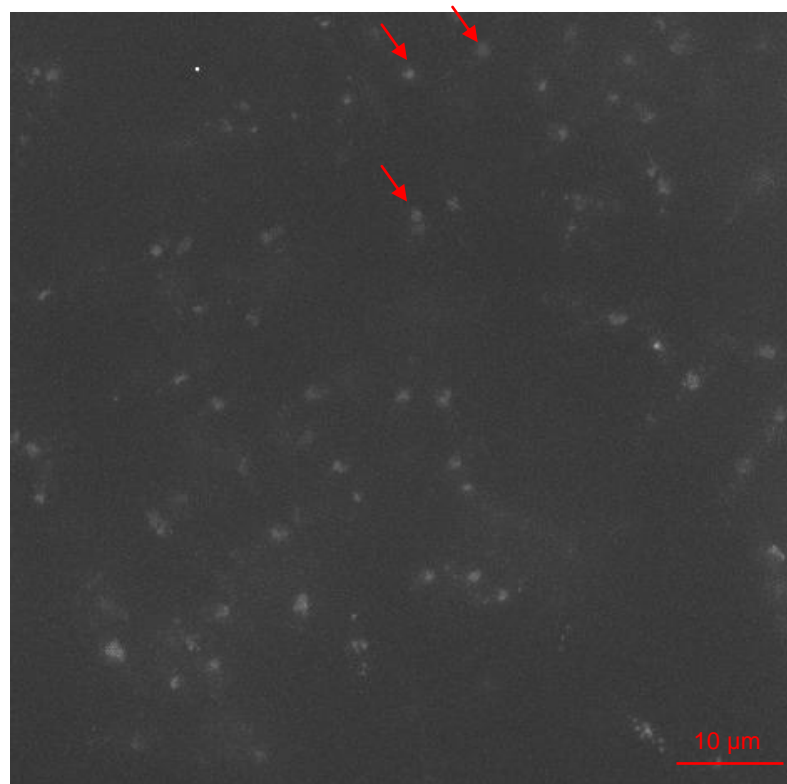
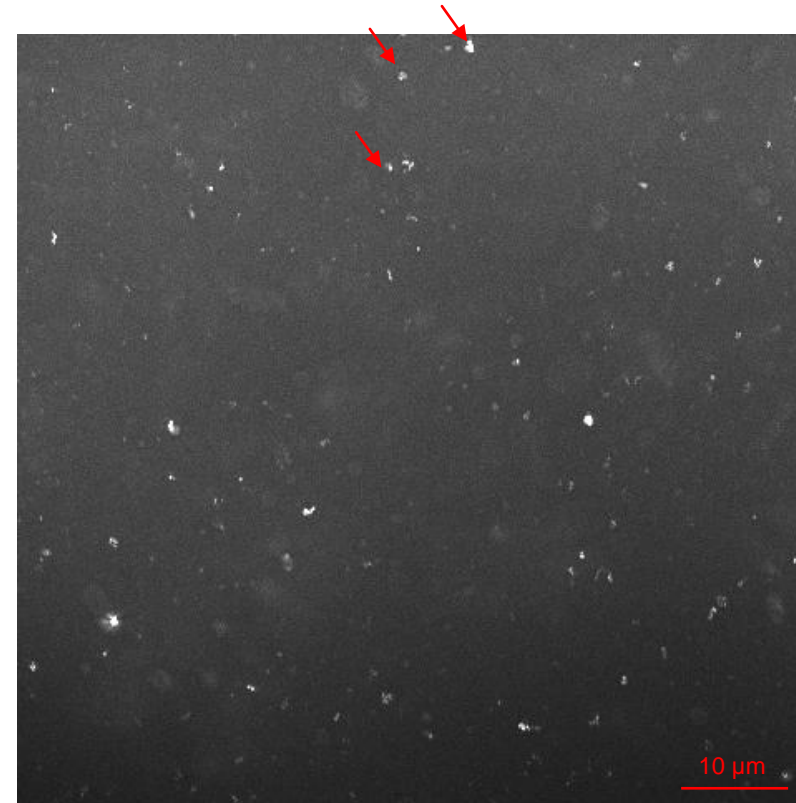


Figure 5-2. A merged image of *mrc1Δ* cells after 150 minutes of incubation with Hydroxyurea. The nucleus (blue) highlighted by the arrow contains multiple GFP signals (bright green). The cells were reconstructed into 3D using the Softworx program to reensure that the foci seen are indeed nuclear foci. The presence of multiple foci per nucleus is common in *mrc1Δ* cells.



(A) (*mrc1Δ* DAPI)



(B) (*mrc1Δ* GFP)

Figure 5-3. Rad52-GFP foci of the *mrc1Δ* strain at its peak. The figure shows the cells of the *mrc1Δ* strain at 60X magnification stained with (A) DAPI to show the nuclei and (B) anti-GFP to show the Rad52-GFP foci. The cells were reconstructed into 3D using the Softworx program to identify nuclear foci. The peak value for nuclear foci was 40% of total number of nuclei. The red arrows point to some nuclei with Rad52-GFP foci.

Viability Comparison of *rad4-116*, *rad4⁺* and *mrc1Δ*

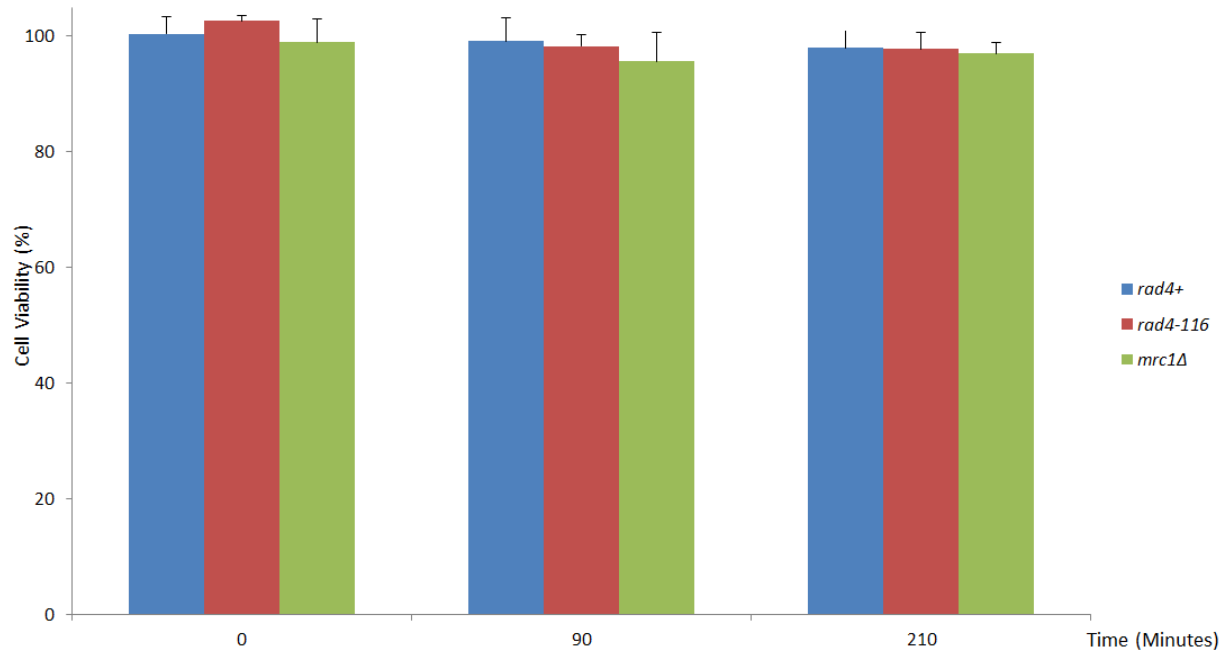


Figure 5-4. Viability counts for the *rad4⁺*, *rad4-116* and *mrc1Δ* strains carrying the *rad52-GFP* gene. The figure shows the bar chart graph representing the comparison between cell viability across the three strains of *rad4-116*, *rad4⁺* and *mrc1Δ* at the start of the experiment, at 90 minutes after the start and at the end of the experiment at 210 minutes. As observed, there was no significant change in viability across all three strains at these three timepoints.

Rad52-GFP Foci Profile of *mrc1Δ*

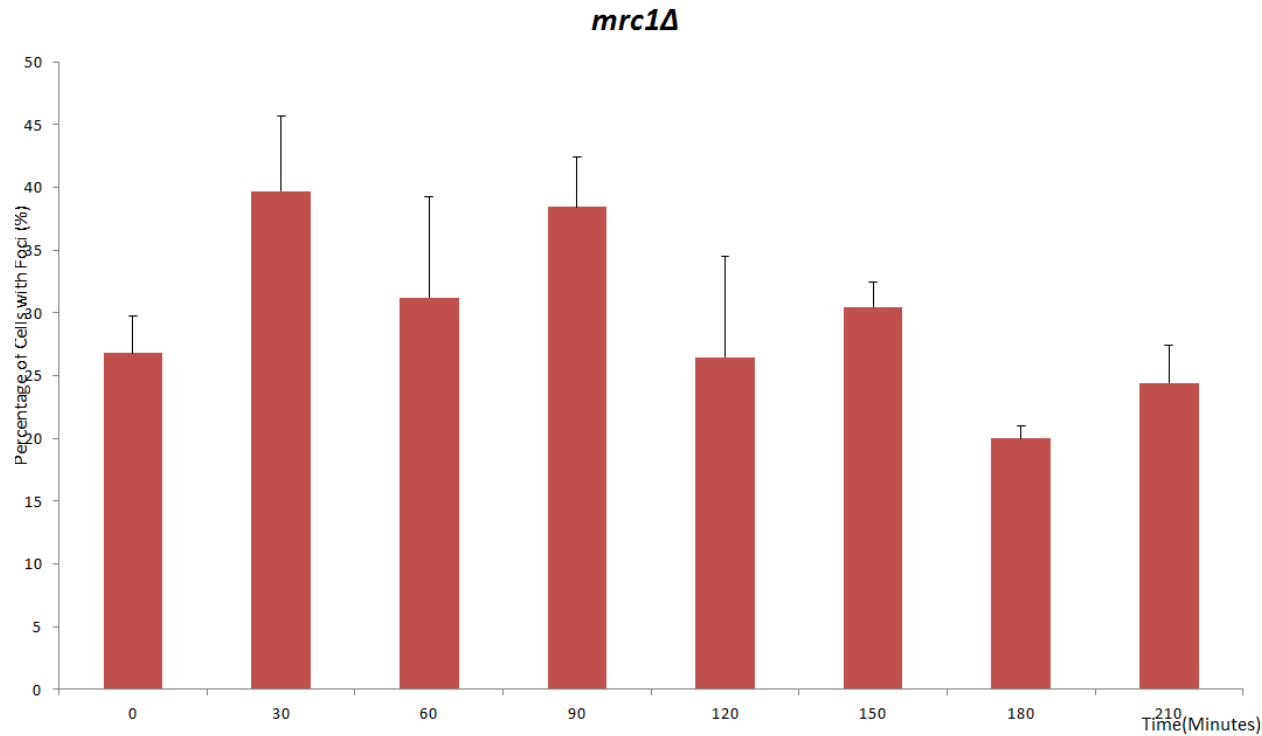


Figure 5-5. The Rad52-GFP profile of the *mrc1Δ* strain. The figure shows the bar chart graph representing the percentage of cells with Rad52-GFP foci in the *mrc1Δ* strain across timepoints from 0 to 210. The peak occurred at 30 minutes after the start of the experiment with a value of 40% of cells carrying nuclei with Rad52-GFP foci.

Rad52-GFP Foci Profile Comparison of *rad4-116*, *rad4*⁺ and *mrc1*Δ

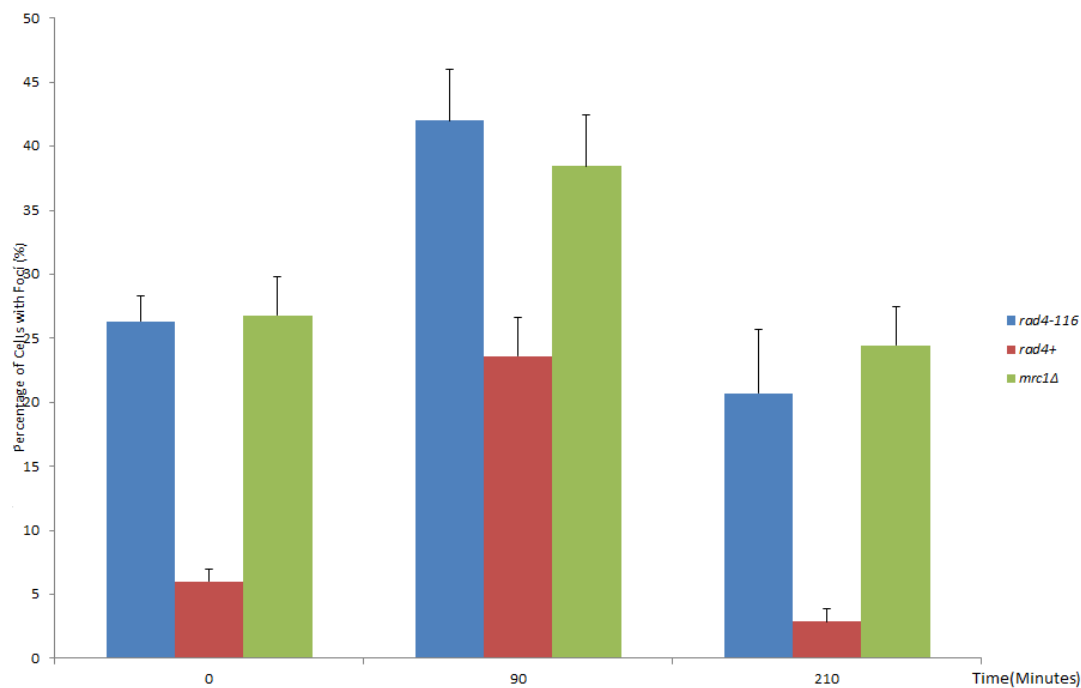


Figure 5-6. A comparison of the Rad52-GFP profiles of the *rad4-116*, *rad4*⁺ and *mrc1*Δ strains. The figure shows the bar chart graph representing the comparison between the percentage of cells with Rad52-GFP foci across the three strains of *rad4-116*, *rad4*⁺ and *mrc1*Δ at the start of the experiment, at 90 minutes after the start and at the end of the experiment at 210 minutes.

5.2.1 The Rad52-GFP foci profile of *mrc1Δ* was similar to that of *rad4-116* and not to *rad4⁺*

After the Rad52-GFP foci from the *swi1Δ* strain from each timepoint were counted, the unpaired Student T-test was performed to compare to the *rad4⁺* strain at timepoints 0, 90 and 210 minutes after the depletion of hydroxyurea from the media. Each value of foci was determined using an average of triplicate experiments, where 100 nuclei were scored from the *mrc1Δ* strain and compared to the *rad4⁺* strain at its corresponding timepoint. The variance for both samples were similar allowing the use of the 2-tailed Student T-test. The degree of freedom for each sample used at each timepoint was 4 and the critical value over which the difference was significant was 4.604 at $p \leq 0.01$. $p \leq 0.01$ was chosen over the standard $p \leq 0.05$ as the critical values, calculated and determined to be significant at $p \leq 0.05$, were also significant at $p \leq 0.01$ and some, not all, at $p \leq 0.001$. The values at all 3 timepoints were significantly different between the wildtype and *mrc1Δ*. This indicated that the deletion of *mrc1* was significantly different when compared to the wildtype *rad4⁺* strain in terms of Rad52-GFP recruitment onto stalled replication forks induced by hydroxyurea at the 0, 90 and 210 timepoints. When the 2-tailed Student T-test was applied to compare the Rad52-GFP foci profiles of *mrc1Δ* and *rad4-116* strains, all 3 timepoints compared were not statistically significant in terms of difference, underlining the similarity between both profiles and their shared difference compared to the wildtype *rad4⁺* strain.

5.3 The Phenotypic characterisation of the *mrc1-V5* strains

A V5-tagged version of *mrc1* under transcriptional control of the *nmt81* promoter was created using plasmid p808 and integrated at the *leu1* locus following the methodology described in (Fennessy *et al.*, 2014). The *mrc1-V5* base strain was constructed by transformation using SPSC 1005 as the transformed strain to create SPSC 1114. The V5- tagged allele was tested using PCR and by performing a western blot of protein samples of an overnight culture of SPSC 1114 growing in EMM+uracil+leucine broth. By crossing SPSC 1114 with SPSC 1018, and selecting *ura*⁺ G418 resistant colonies, the *mrc1-V5 mrc1Δ h-* strain SPSC 1115 was constructed. The SPSC 1115 was used in a cross with SPSC 120 to create *mrc1-V5 mrc1Δ rad4-116* SPSC 1116 by selecting *ura*⁺ G418 resistant temperature sensitive colonies. The *mrc1-V5 mrc1Δ rad4-116 rad52-GFP* strain SPSC 1117 was created by crossing SPSC 1115 and SPSC 1073 and selecting *ura*⁺ G418 resistant NAT resistant colonies growing in a 2:2 tetrad pattern. All the strains carrying the *mrc1-V5* allele were tested using PCR before using them in the experimental procedures and adding them to the collection.

The aim of this experiment was to be able to analyse the phenotypic profile of Mrc1-V5 depletion in the presence of *rad4-116* with control strains carrying *mrc1-V5* as well as a control strain carrying *rad4*⁺ and a control strain carrying *rad4-116*. To be able to characterise the *mrc1-V5* strains, all the strains were grown into cultures up to 0.8OD overnight at 26 °C in EMM+uracil+leucine (no thiamine) then inoculated into a total volume of 200ml EMM+uracil+leucine+ 50 µg/ml thiamine. The cultures were then incubated at 26 °C in a shaking incubator. Samples for RNA and protein extraction were collected at 0,4, 8, 12 and 24 hours till the cultures for both

experimental strains reached 1.00 OD from 0.2 OD. At each timepoint, samples for immunofluorescence and FACS were taken by fixing in formaldehyde and ethanol respectively. The viability of each strain was tested at each timepoint by plating 100 cells on EMM+uracil+leucine+50 µg/ml thiamine agar plates in triplicates. The pellets for protein and RNA extraction were snap-frozen in liquid nitrogen and stored at -80 °C. SPSC 120 (*rad4-116*) and SPSC 1005 (*rad4*⁺) were used as controls, with SPSC 120 being sampled every time the experiment was repeated. The experiment was repeated 4 times under identical conditions and the results show the averages of the repeats.

5.3.1 The depletion of *mrc1-V5* expression by RT-QPCR

RT-QPCR was used to be able to assess the depletion of the transcript of *mrc1-V5* in the strains carrying *mrc1-V5*. The RT-QPCR method and analysis were carried out as detailed in Section 3.3.1.

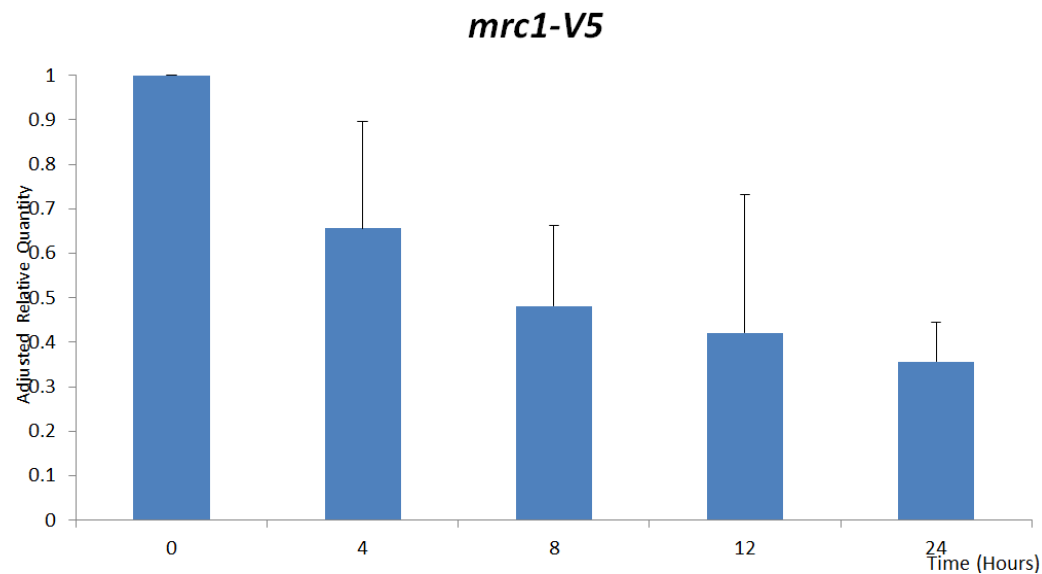


Figure 5-7. The adjusted relative quantity of RNA measured by RT-QPCR for the *mrc1-V5* strain SPSC 1114. The figure shows the adjusted relative quantity of the RT-QPCR SPSC 1114 culture across 24 hours of incubation with thiamine added.

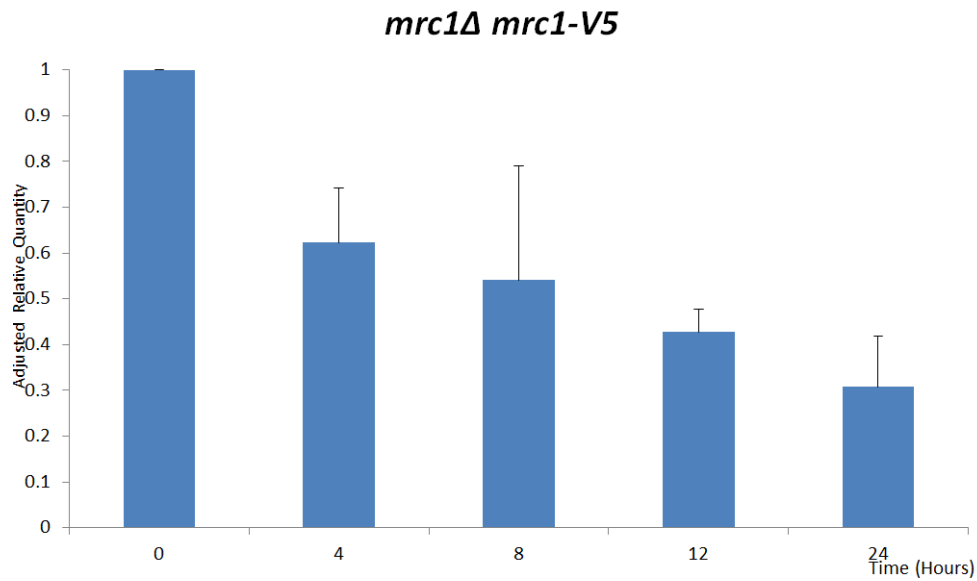


Figure 5-8. The adjusted relative quantity of RNA measured by RT-QPCR for the *mrc1Δ mrc1-V5* strain SPSC 1115. The figure shows the adjusted relative quantity of the RT-QPCR SPSC 1115 culture across 24 hours of incubation with thiamine added.

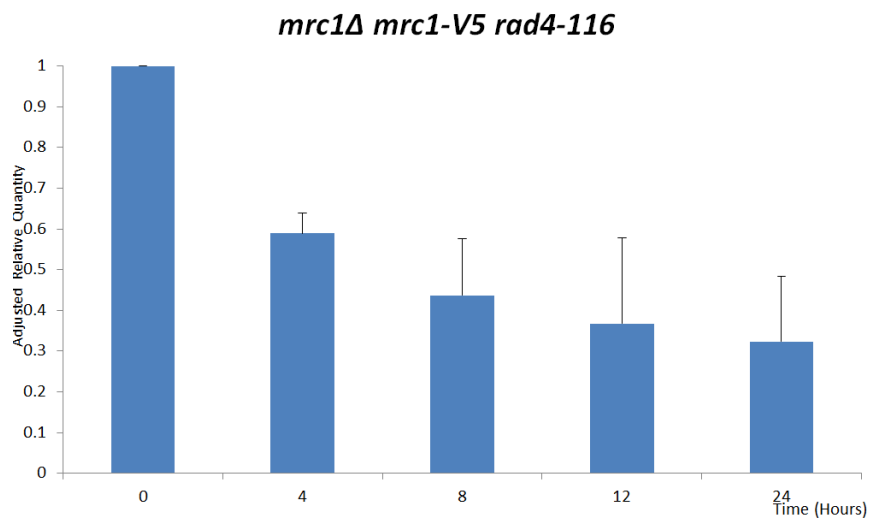


Figure 5-9. The adjusted relative quantity of RNA measured by RT-QPCR for the *mrc1Δ mrc1-V5 rad4-116* strain SPSC 1116. The figure shows the adjusted relative quantity of the RT-QPCR SPSC 1116 culture across 24 hours of incubation with thiamine added.

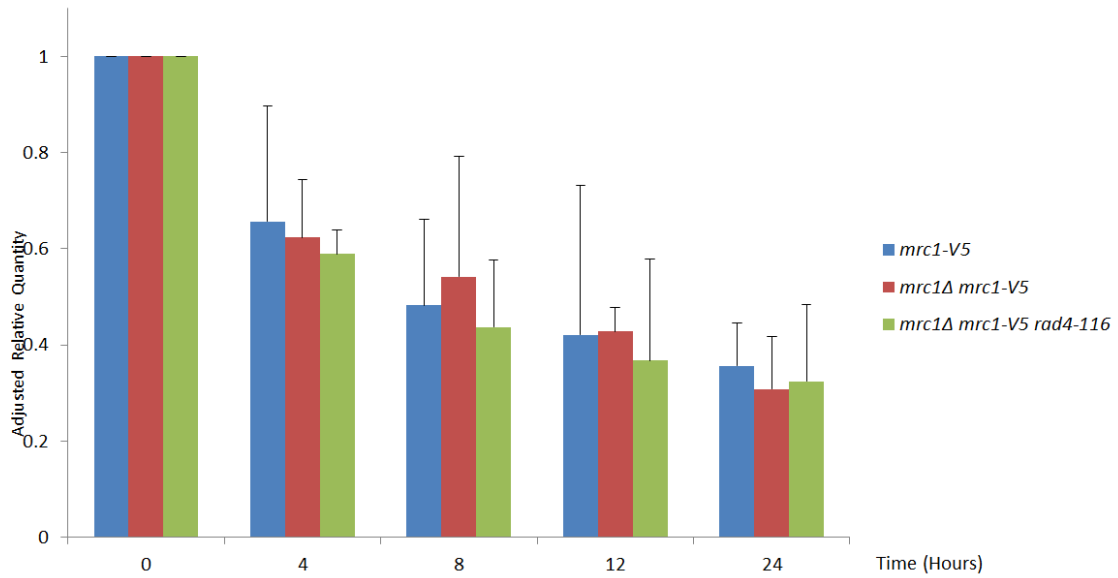


Figure 5-10. The comparison the adjusted relative quantity of RNA of strains carrying the *mrc1-V5* allele. The figure shows the gradual decrease through graphical representation of the adjusted relative quantity between all the *Mrc1-V5* strains across the 24 hour timecourse after the addition of thiamine to the media.

5.3.2 The depletion of Mrc1-V5 expression by Western Blotting

Western blotting was used to be able to assess the depletion of the Mrc1-V5 protein in the strains carrying *mrc1-V5* (Figure 5-11, 5-12, 5-13 and 5-14). The synthetic lethality method and analysis were carried out as detailed in Section 3.3.2. A preliminary blot was carried out to test the V5 signal depletion after 16 hours (overnight) of thiamine addition using the Mrc1-V5 base strain (Figure 5-11).

The effect of thiamine addition on the *mrc1-V5* strain

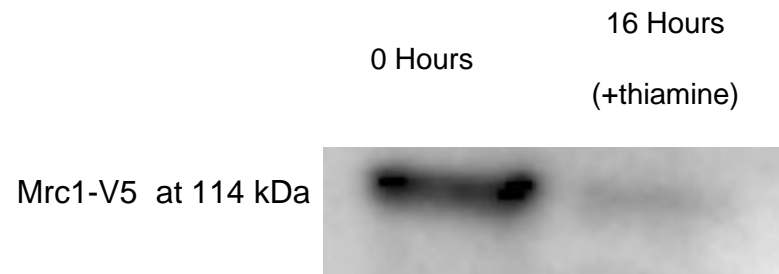


Figure 5-11. Expression of V5 tag in the base *mrc1-V5* strain SPSC 1114 after the addition of thiamine. Protein samples were taken from SPSC 1114 incubated for 16 hours in EMM+uracil+leucine with and without the addition of thiamine to the media. The western blot shown represents the samples after being probed with anti-V5. The sample without the addition of thiamine expresses the V5 tag whilst the sample with the addition of thiamine does not express the V5 tag.

The effect of thiamine addition on the *mrc1-V5* strain across 24 hours

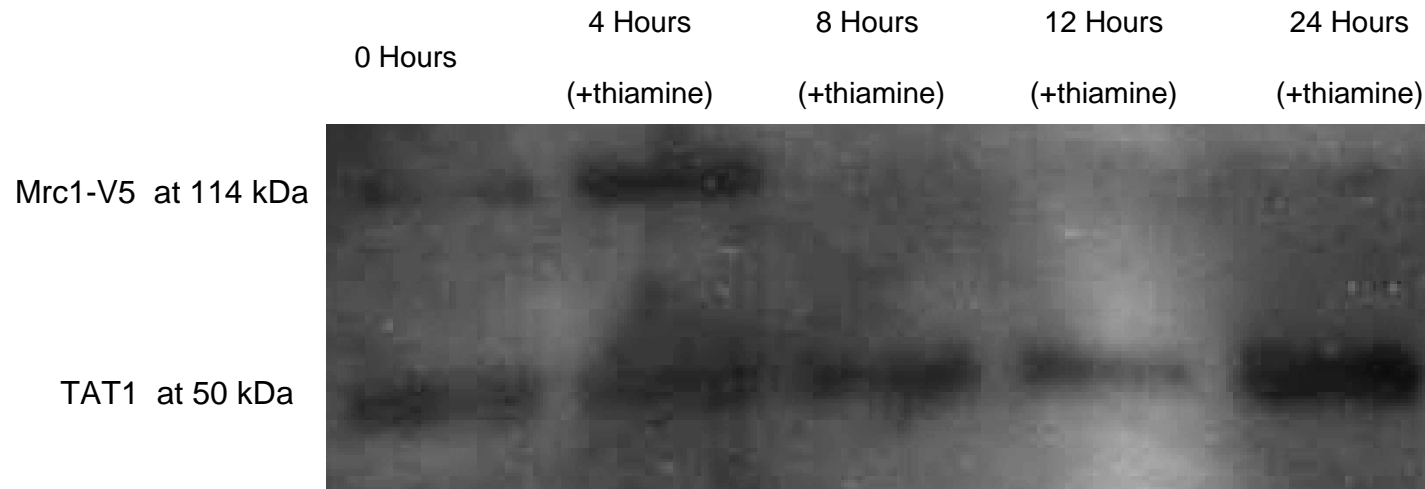


Figure 5-12. Depletion of V5 tag in the *mrc1-V5* base strain SPSC 1114 after the addition of thiamine. Protein samples were taken from SPSC 1114 incubated for 24 hours in EMM+uracil+leucine with the addition of thiamine to the media. The protein samples were taken from 0, the time of addition of thiamine to the 0.5 OD culture, to 12 hours at 4 hour-intervals then an additional sample at 24 hours. The western blot shown represents the samples after being probed with anti-V5 (top signal) and anti-TAT1 (bottom signal) as control. The 0 hour and 4 hour samples express the V5 tag while there was no visible signal for the 8 hour, 12 hour or 24 hours samples.

The effect of thiamine addition on the *mrc1Δ mrc1-V5* strain across 24 hours

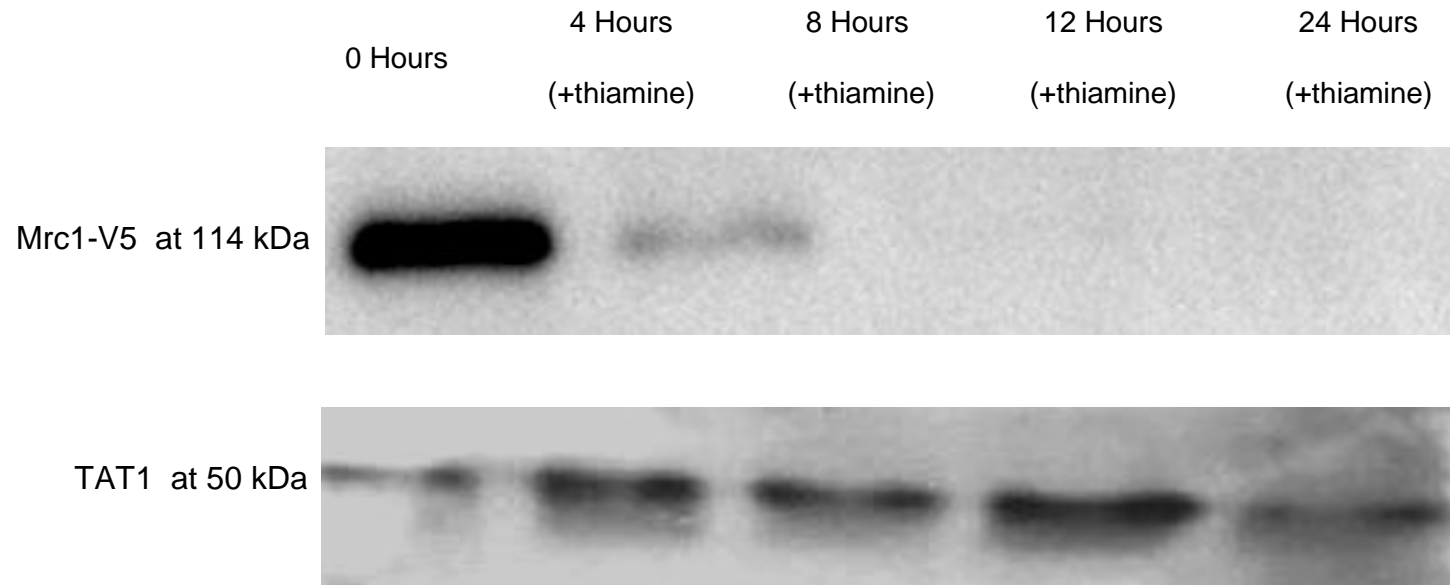


Figure 5-13. Depletion of V5 tag in the *mrc1-V5 mrc1Δ* strain SPSC 1115 after the addition of thiamine. Protein samples were taken from SPSC 1115 incubated for 24 hours in EMM+uracil+leucine with the addition of thiamine to the media. The protein samples were taken from 0, the time of addition of thiamine to the 0.5 OD culture, to 12 hours at 4 hour-intervals then an additional sample at 24 hours. The western blot shown represents the samples after being probed with anti-V5 (top signal) and anti-TAT1 (bottom signal) as control. The 0 hour and 4 hour samples express the V5 tag while there was no visible signal for the 8 hour, 12 hour or 24 hours samples.

The effect of thiamine addition on the *rad4-116 mrc1Δ mrc1-V5* strain across 24 hours

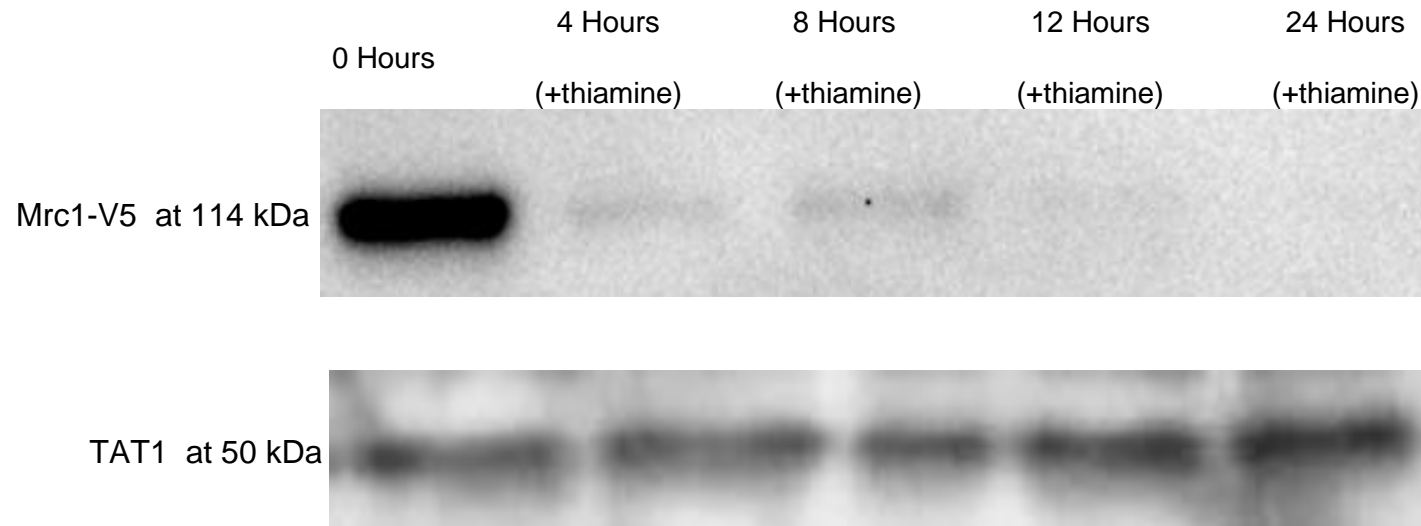


Figure 5-14. Depletion of V5 tag in the *mrc1-V5 mrc1Δ rad4-116* strain SPSC 1116 after the addition of thiamine. Protein samples were taken from SPSC 1116 incubated for 24 hours in EMM+uracil+leucine with the addition of thiamine to the media. The protein samples were taken from 0, the time of addition of thiamine to the 0.5 OD culture, to 12 hours at 4 hour-intervals then an additional sample at 24 hours. The western blot shown represents the samples after being probed with anti-V5 (top signal) and anti-TAT1 (bottom signal) as control. The 0 hour sample strongly expresses the V5 tag while the 4 hour and 8 hour samples express very weak V5 signals but there was no visible signal for the 12 hour or 24 hour samples.

5.3.3 Phenotypic Characterisation of *mrc1-V5* strains by microscopy

To be able to phenotypically characterise each strain carrying *mrc1-V5*, cell pellets from each strain at each timepoint was taken. The microscopy method and analysis were carried out as detailed in Section 3.3.3.

The effect of thiamine addition on the *mrc1-V5* strain SPSC 1114 across 24 hours

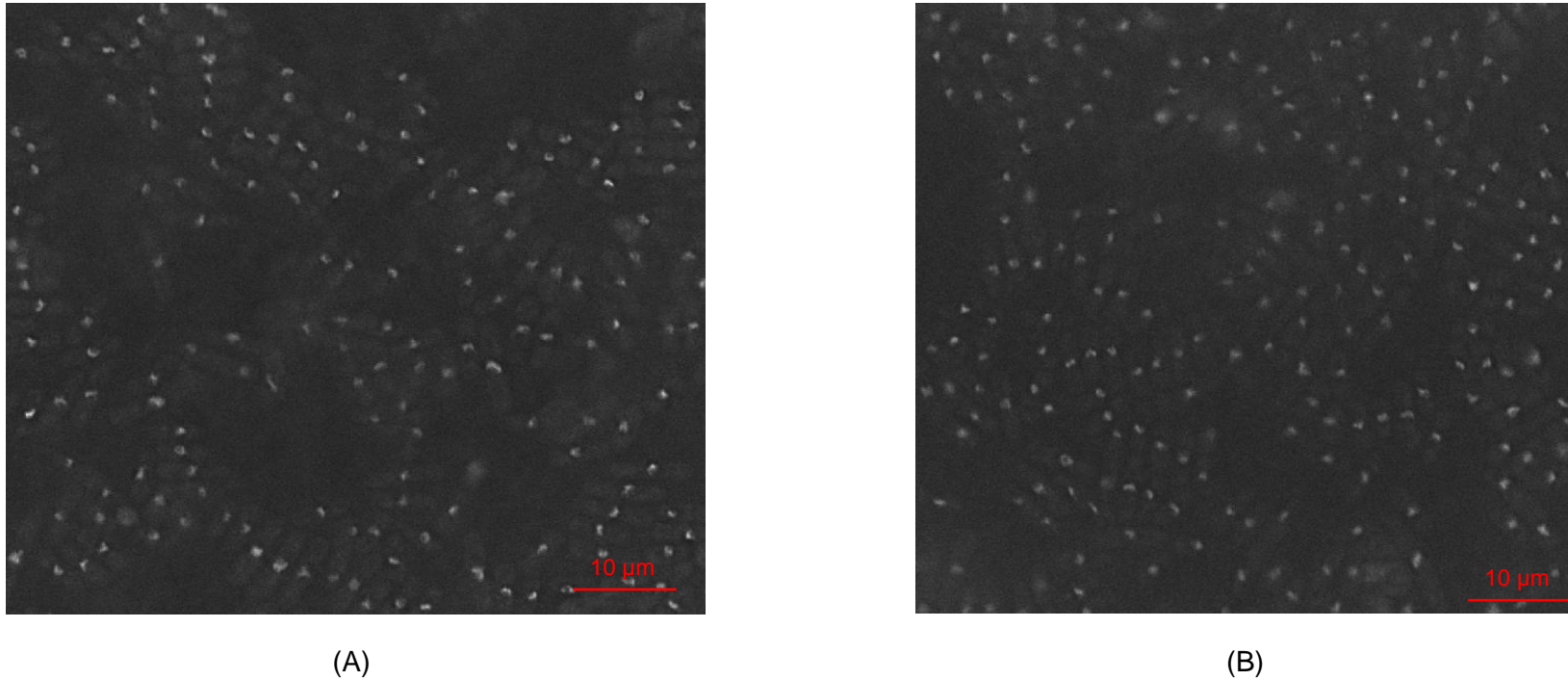


Figure 5-15. The cell morphology of the *mrc1-V5* strain SPSC 1114 at 60X magnification across 24 hours after thiamine induction. The figure shows the cells of the SPSC 1114 strain stained with DAPI to show the nuclei at (A) the 0 hour timepoint and the (B) 24 hour timepoint. There is no significant difference between the cells across those 2 timepoints in terms of cell length, cell shape and nuclear shape.

The effect of thiamine addition on the *mrc1Δ mrc1-V5* strain SPSC 1115 across 24 hours

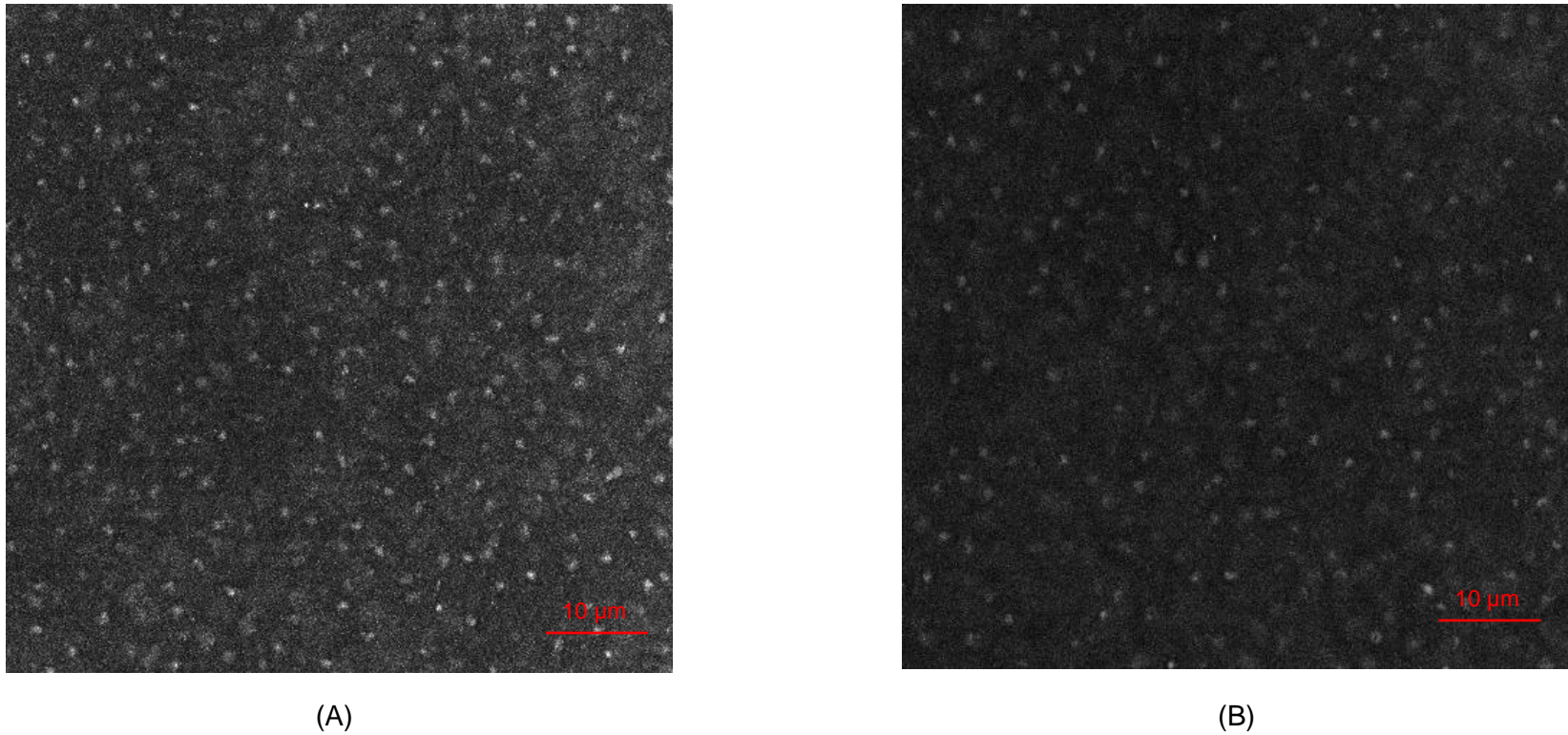


Figure 5-16. The cell morphology of the *mrc1Δ mrc1-V5* strain SPSC 1115 at 60X magnification across 24 hours after thiamine induction. The figure shows the cells of the SPSC 1115 strain stained with DAPI to show the nuclei at (A) the 0 hour timepoint and the (B) 24 hour timepoint. There is no significant difference between the cells across those 2 timepoints in terms of cell length, cell shape and nuclear shape.

The effect of thiamine addition on the *rad4-116 mrc1Δ mrc1-V5* strain SPSC 1116 across 24 hours

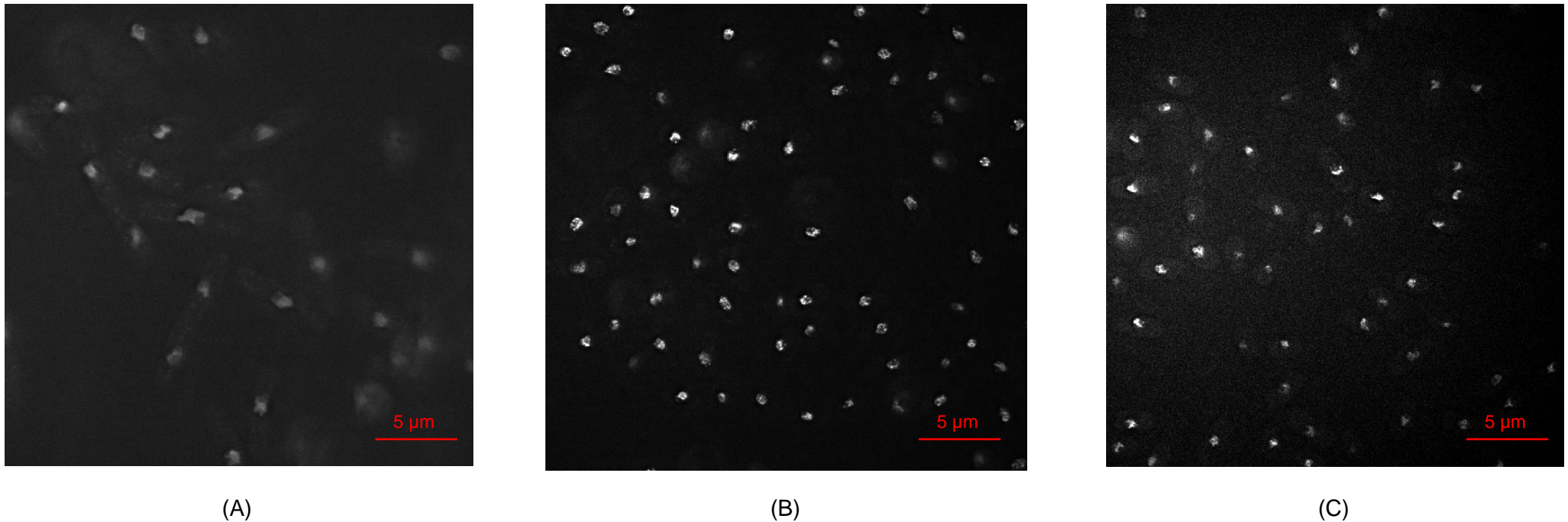


Figure 5-17. The cell morphology of the *mrc1Δ mrc1-V5 rad4-116* strain SPSC 1116 at 100X magnification across 24 hours after thiamine induction. The figure shows the cells of the SPSC 1116 strain stained with DAPI to show the nuclei at (A) the 0 hour timepoint, (B) the 12 hour timepoint and (C) the 24 hour timepoint. The cells show a distinct phenotype, that develop from timepoint 0 to 12 to 24 hours, for cells to decrease in length. The nuclei of most these cells show a fragmentation that becomes more pronounced at the 24 hour timepoint and some cells show a compacted nucleus.

5.3.4 The effect of thiamine addition on the average cell length of *mrc1-V5* strains across 24 hours

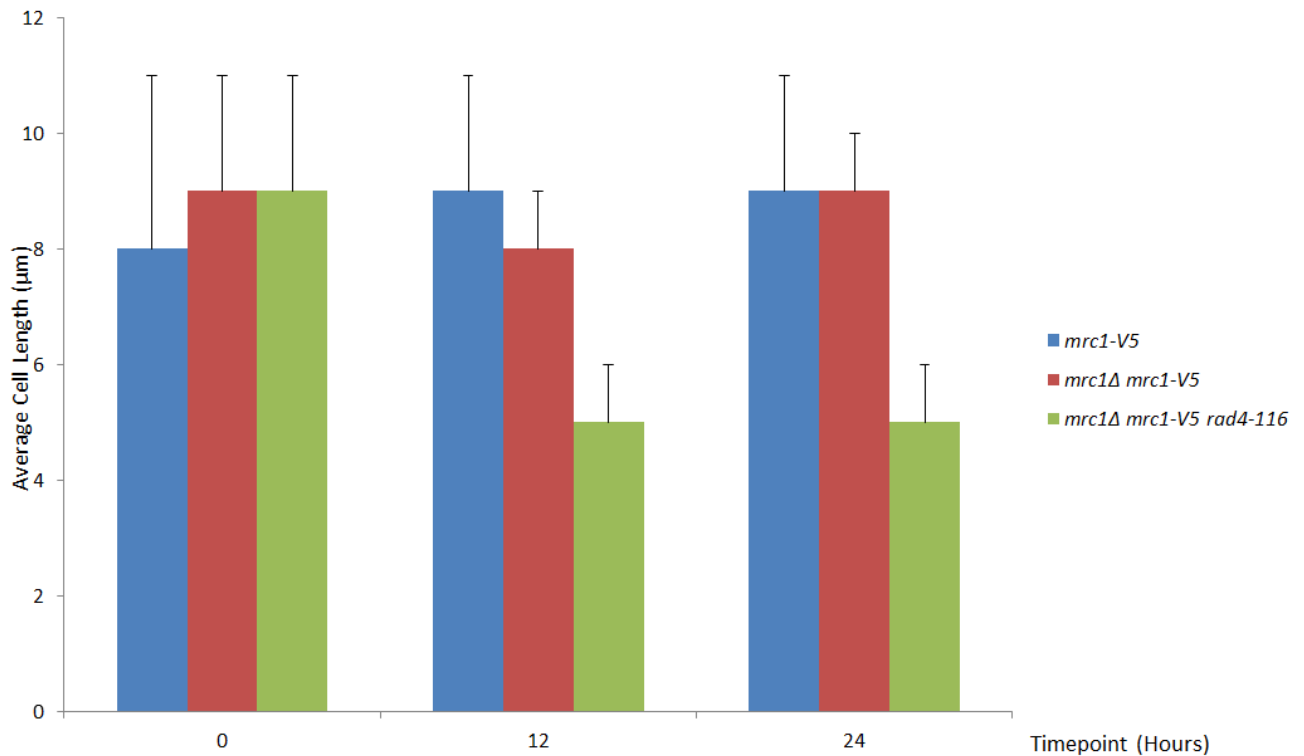


Figure 5-18. The average cell length of the strains carrying the *mrc1-V5* allele. The figure shows the graphical representation of the comparison of average cell length between the base *mrc1-V5* strain, the *mrc1-V5 mrc1Δ* strain and the *mrc1-V5 mrc1Δ rad4-116* strain. No significant change in average cell length occurred in both the base *mrc1-V5* strain and the *mrc1-V5 mrc1Δ* strain as the value is between 8 and 9µm between the 0 hour to 24 hours after thiamine addition. As for the *mrc1-V5 mrc1Δ rad4-116* strain, the initial average cell length at 0 is similar to the other two strains, but then a significant decrease occurs from 9 µm to 5µm at both 12 hours and 24 hours after the addition of thiamine.

As observed in Figure 5-10 for QPCR and Figures 5-12, 5-13, 5-14 for western blotting, the expression of the RNA product and protein for Mrc1-V5 were successfully depleted after 24 hours of incubation in media with thiamine. The adjusted relative quantity for the *mrc1-V5* RNA expression reached 0.356 for the *mrc1-V5* strain in Figure 5-7, 0.308 for the *mrc1Δ mrc1-V5* strain in Figure 5-8 and 0.324 for the *mrc1Δ mrc1-V5 rad4-116* strain in Figure 5-9. The adjusted relative quantity for all the *mrc1-V5* strains across the 24 hour timecourse is summarised in Figure 5-10. The preliminary experiment in Figure 5-11 using the *mrc1-V5* strain (SPSC1114), showed that the signal present using the anti-V5 antibody, was abolished completely following 16 hour incubation with thiamine. The Mrc1-V5 protein signal was present at timepoints 0 and 4 hours in all the three strains SPSC 1114, SPSC 1115 and SPSC 1116 as observed in Figure 5-12, Figure 5-13 and Figure 5-14 respectively. A very faint signal was observed at 8 hours after thiamine induction using SPSC 1116 in Figure 5-14. In all 3 figures, the signal was abolished below the detectable level from 12 hours after thiamine addition onwards. The level of expression of the control α -Tubulin for all three strains across all the timepoints did not show any change.

Indeed, the levels of RNA expression did not reach 0 as seen in Figure 5-10, yet, those levels were sufficient to lead to an abolishment of Mrc1-V5 protein expression below detectable levels as observed in the western blots. The depletion of RNA expression and protein signals also caused a decrease in viability, as seen in Figure 5-19, consistent with the time and level of abolishment of the V5-tagged protein in the *mrc1Δ mrc1-V5 rad4-116* strain but not in any of the other strains. The *mrc1Δ mrc1-V5 rad4-116* strain showed a gradual loss of viability dropping from 95% viability at 0 timepoint to 28% after 12 hours, then to 4% viability at 24 hours. The

decrease in viability at timepoints 12 and 24 was statistically significant at $p \leq 0.01$ with values of 28% and 4% respectively compared to the 0 hour timepoint which is consistent with the depletion of V5 protein signal. However, the presence of viable cells indicated that the level of depletion per cell in the culture population is not equal. This is also reflected in the presence of 0.324 adjusted relative quantity value of V5 RNA for the *mrc1* Δ *mrc1-V5* *rad4-116* strain as represented in Figure 5-9.

In terms of cell morphology, as observed in Figure 5-15 and Figure 5-16, the cell size and length and nuclear integrity of SPSC 1114 (*mrc1-V5*) and SPSC 1115 (*mrc1* Δ *mrc1-V5*) respectively did not show any change across the 24 hour timecourse. However, as seen in Figure 5-17, the *mrc1* Δ *mrc1-V5* *rad4-116* strain SPSC 1116, showed a distinct phenotype in terms of cell size. The phenotype shown was shorter of less than 6 μm with irregular nuclear size and shape with some nuclei being fragmented or compacted. Those changes were detectable after 12 hours of thiamine incubation and more pronounced at the 24 hour timepoint. The changes in average cell length for SPSC 1116 was compared at the 0, 12 and 24 hours timepoints to the SPSC 1114 (*mrc1-V5*) and SPSC 1115 (*mrc1* Δ *mrc1-V5*) strains and summarised in Figure 5-18.

5.3.5 The viability profile of *mrc1Δ mrc1-V5 rad4-116*

The paired Student T-test was performed to compare the viability of each *mrc1-V5* strain at each timepoints 4, 8, 12 and 24 hours after the addition of thiamine to the media to the starting 0 hour viability value. Each value of viable cells was obtained from an average of a triplicate separate cultures of strain at each timepoint at which a triplicate of EMM+ uracil+ leucine+ thiamine plates were used to grow 100 colonies. After 3 days of incubation at 26 °C, the number of viable colonies on each plate was counted and recorded and the average calculated for the *mrc1Δ* strain and compared to the *rad4⁺* strain at its corresponding timepoint. The variance for both samples were similar allowing the use of the 2-tailed Student T-test. The degree of freedom for each sample used at each timepoint was 2 and the critical value over which the difference is significant is 9.925 at $p \leq 0.01$. $p \leq 0.01$ was chosen over the standard $p \leq 0.05$ as the critical values, calculated and determined to be significant at $p \leq 0.05$, were also significant at $p \leq 0.01$. For the *mrc1-V5* and *mrc1Δ mrc1-V5*, there was no significant difference the viability counts observed across all the timepoints recorded from 0 to 24 hours. However, for *mrc1Δ mrc1-V5 rad4-116* strain, timepoints 12 and 24 showed a significant decrease in viability at $p \leq 0.01$ with values of 28% and 4% respectively compared to the 0 hour timepoint.

Viability Comparison of *mrc1-V5* strains

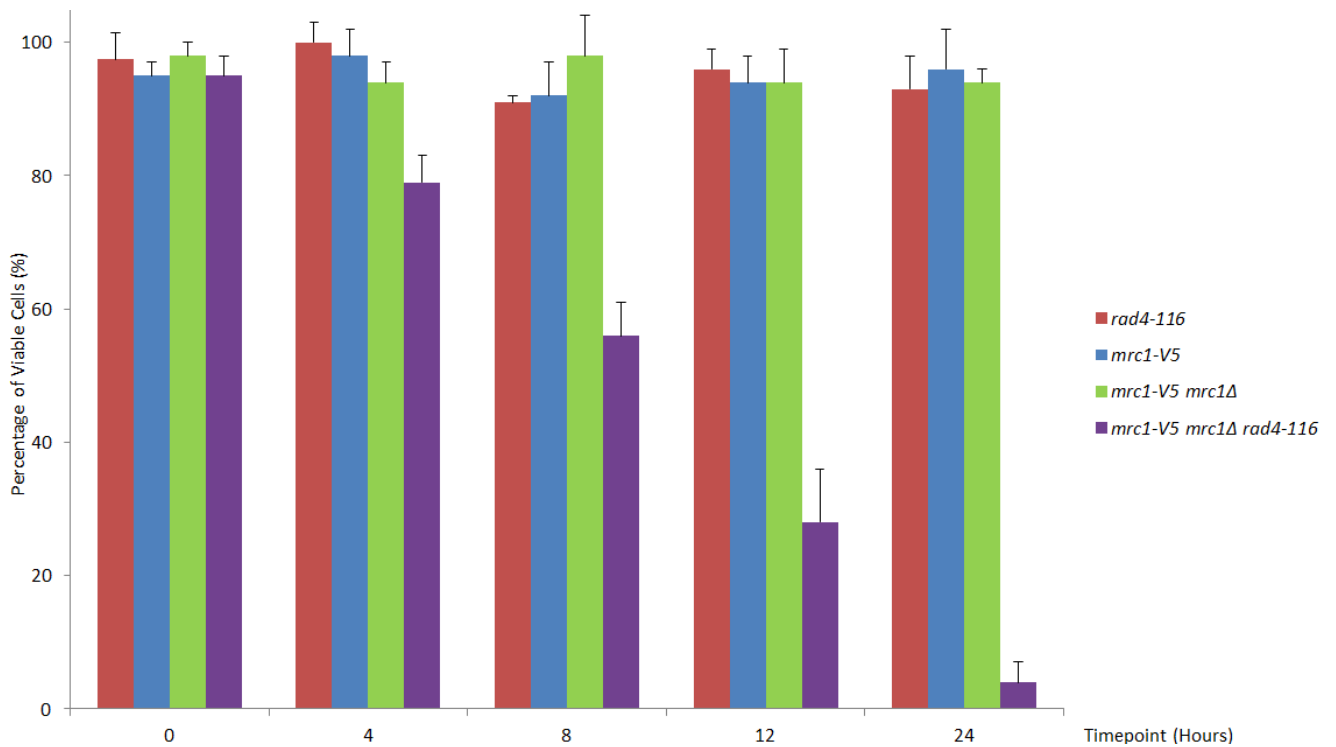


Figure 5-19. The viability comparison of strains carrying the *mrc1-V5* allele against the control *rad4-116* strain. The figure shows the graphical representation of the comparison of viability between the *Mrc1-V5* strains and the *Rad4-116* strain across the 24 hour timecourse after the addition of thiamine to the media. Only SPSC 1116 showed a gradual loss of viability dropping from 95% viability at 0 timepoint to 28% after 12 hours, then to 4% viability at 24 hours. All the other strains represented showed no significant loss of viability across the 24 hour timecourse ranging from 100% to 91% viability.

5.3.6 Phenotypic Characterisation of *mrc1-V5* strains by FACS

The FACS method and analysis were carried out as detailed in Section 3.3.6.

Phenotypic Characterisation of *mrc1-V5* (SPSC 1114) and *mrc1Δ mrc1-V5* (SPSC 1115) strains by FACS

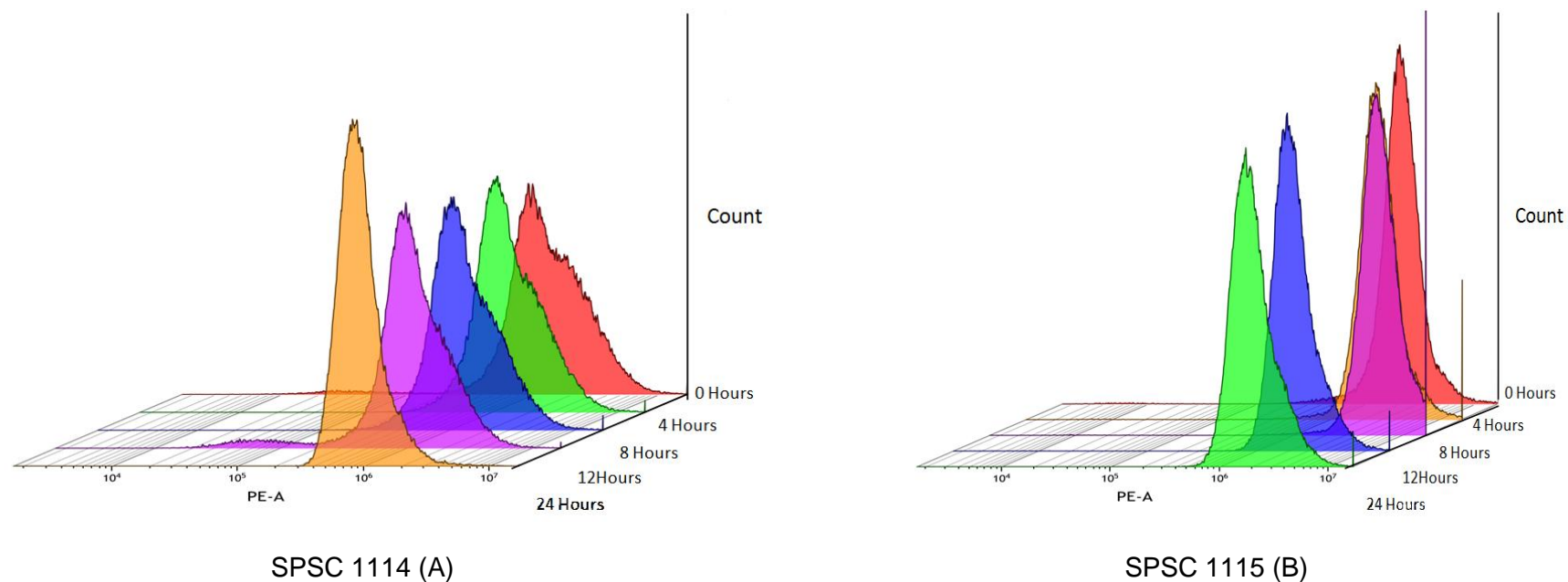


Figure 5-20. Cell population as investigated through FACS. The figure shows the analysis of the populations of SPSC 1114(A) and SPSC 1115 (B) as representation of count (y-axis) against the phycoerythrin channel PE-A (x-axis) across 24 hours with 0 hour being the furthest along the z-axis followed by 4, 8, 12 and finally, 24 hours being the nearest along the z-axis. For (A) SPSC 1114, no change in staining occurred or shift in peaks across the 24 hours with only the 24 hour sample showing a increased peak level with a sharper peak. For (B) SPSC 1115, no change in staining occurred or shift in peaks across the 24 hours with only the 24 hour sample showing a decreased peak level.

Phenotypic Characterisation of *rad4-116 mrc1Δ mrc1-V5* strain SPSC 1116 by FACS

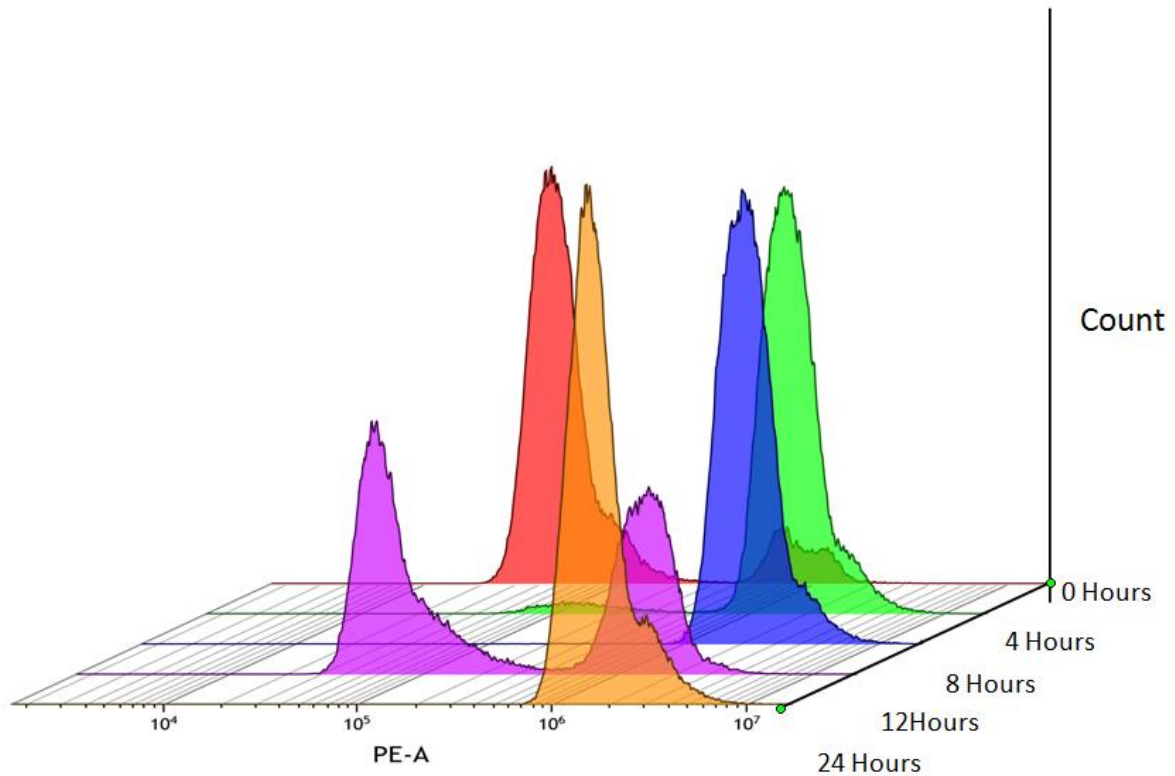


Figure 5-21. Cell population as investigated through FACS. The figure shows the analysis of the population of SPSC 1116 as representation of count (y-axis) against the phycoerythrin channel PE-A (x-axis) across 24 hours with 0 hour being the furthest along the z-axis followed by 4, 8, 12 and finally, 24 hours being the nearest along the z-axis. Initially, at timepoint 0, 2 peaks are present with a sharp peak at 10^4 and a minor peak at 10^6 . A shift in peak occurred from 0 to 4 hours, as the 10^4 is no longer observed and a sharp lone peak is present at 10^6 . No change occurred from timepoint 4 to 8 hours. However, at 12 hours, two peaks are visible at 10^4 and 10^6 , with neither of them being strong signals as the previous peaks observed at 4 and 8 hours. Finally, at 24 hours, a sharp peak is observed at 10^6 with a much weaker peak between the 10^6 and 10^7 marks.

5.4 Characterisation of the *rad4-116 mrc1Δ mrc1-V5 rad52-GFP* strain

The aim of this experiment was to observe DNA stalled replication profile, in terms of accumulation and resolution of DNA forks, of the *rad4-116 mrc1Δ mrc1-V5 rad52-GFP* after the depletion of *mrc1-V5* from the cells. This ability to assess and monitor such profile would be achieved by utilising Rad52-GFP which is recruited to repair and aid the progress of stalled replication forks. The strains were constructed by mating *rad4-116 mrc1Δ mrc1-V5* with *rad4-116 rad52-GFP* and selecting NAT and G418 resistant 2:2 patterns on agar plates after segregation with the micromanipulator. All the strains were grown into cultures up to 0.8 OD overnight at 26 °C in EMM+uracil+leucine (no thiamine) then inoculated into a total volume of 200 ml EMM+uracil+leucine+ 50 µg/ml thiamine. The cultures were then incubated at 26 °C in a shaking incubator. The cell nuclei were assessed in two ways; the first being the percentage and number of nuclei that carry GFP fluorescent foci spanning the 24 hours compared to the starting time point (0) of the thiamine addition, and the second by assessing the number of foci per nucleus and arranging them in categories. The foci were assessed using the Softworx program by taking a 3D reconstruction of the cells to be able to assess if the foci observed were nuclear foci to be counted. The viability of each strain was tested at each timepoint by plating 100 cells on EMM+uracil+leucine+50 µg/ml thiamine agar plates in triplicates. Cell pellets for protein extraction were collected at 0, 12 and 24 hours and were snap-frozen in liquid nitrogen and stored at -80 °C. Cell pellets for FACS analysis were collected at 0, 12 and 24 hours and were fixed for PI staining.

Strains for *swi1Δ swi1-V5 rad4-116 rad52-GFP* , *swi3Δ swi3-V5 rad4-116 rad52-GFP* , *hip1Δ hip1-V5* and *rad4-116 rad52-GFP* were also constructed and tested

using the same techniques. All of them showed viability and V5 protein signal depletion patterns as their corresponding strains without Rad52-GFP. However, none of them developed visible Rad52-GFP nuclear foci across the 24 hour timecourse.

5.4.1 The depletion of *mrc1-V5* expression by RT-QPCR

RT-QPCR was used to be able to assess the depletion of the transcript of *mrc1-V5* in the *mrc1-V5 mrc1Δ rad4-116* strain carrying Rad52-GFP SPSC 1117. The RT-QPCR method and analysis were carried out as detailed in Section 3.3.1.

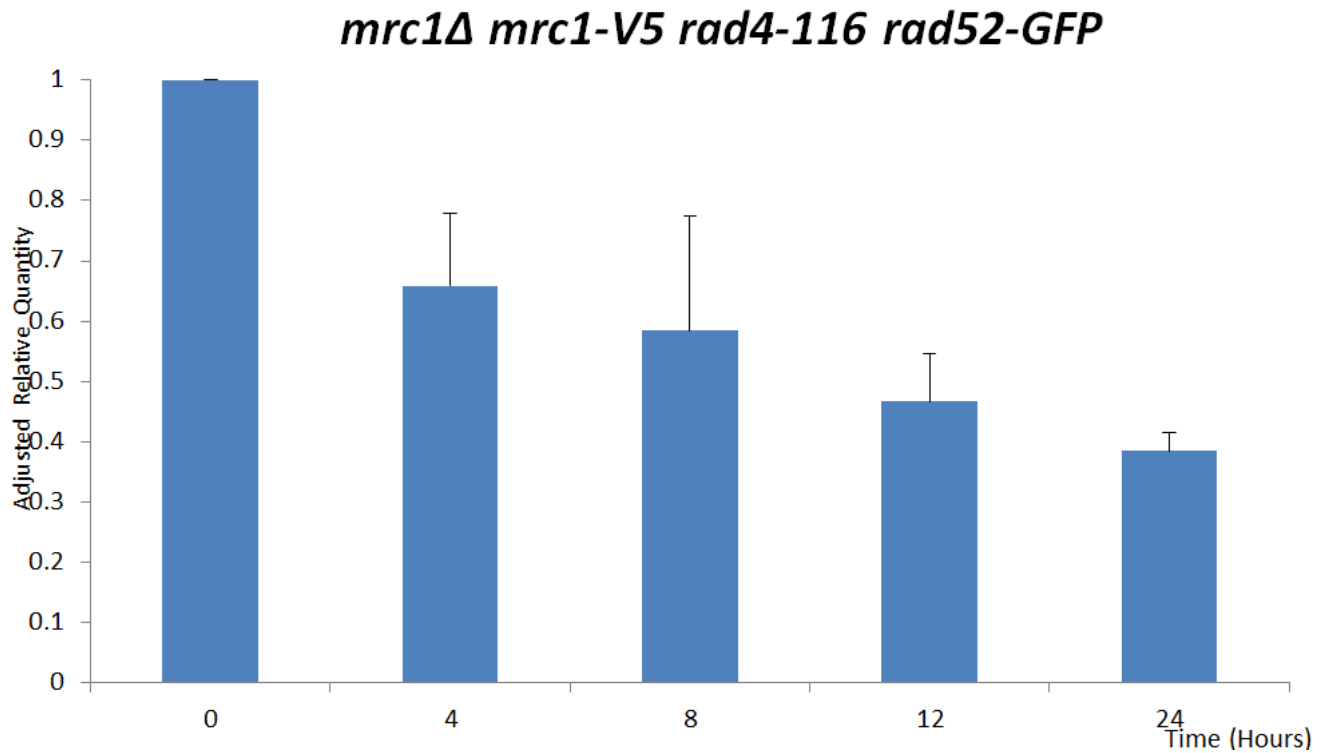


Figure 5-22. The adjusted relative quantity of RNA measured by RT-QPCR for the *mrc1Δ mrc1-V5 rad4-116 rad52-GFP* strain SPSC 1117. The figure shows the adjusted relative quantity of the RT-QPCR SPSC 1117 culture across 24 hours of incubation with thiamine added.

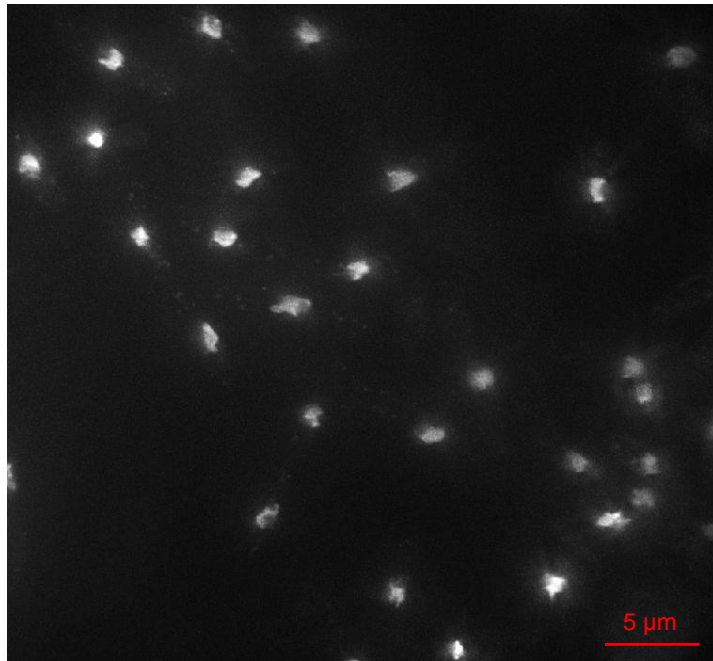
5.4.2 The depletion of *mrc1-V5* expression by western blotting

Western blotting was used to be able to assess the depletion of the Mrc1-V5 protein in the *mrc1-V5 mrc1Δ rad4-116* strain carrying Rad52-GFP SPSC 1117 (Figure 5-23). The western blotting method and analysis were carried out as detailed in Section 3.3.2.

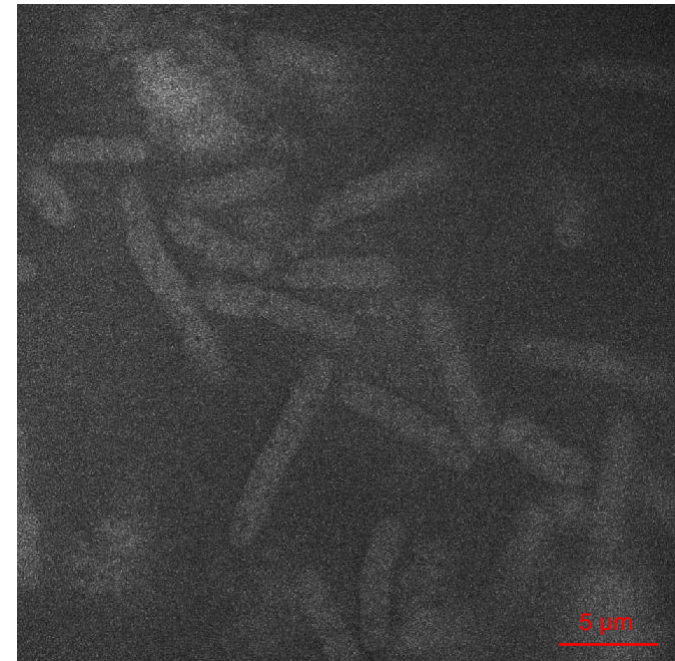


Figure 5-23. Depletion of V5 tag in the *mrc1-V5 mrc1Δ rad4-116* strain carrying Rad52-GFP SPSC 1117 after the addition of thiamine. Protein samples were taken from SPSC 1117 incubated for 24 hours in EMM+uracil+leucine with the addition of thiamine to the media. The protein samples were taken from 0, the time of addition of thiamine to the 0.5 OD culture, 12 hours and 24 hours. The western blot shown represents the samples after being probed with anti-V5 (top signal). The 0 hour sample strongly expresses the V5 tag, a weaker signal at the 12 hour mark and very faint signal after 24 hours of thiamine induction displaying a V5 signal depletion of the Mrc1-V5 protein.

5.4.3 The effect of thiamine addition on the *rad4-116 mrc1Δ mrc1-V5 rad52-GFP* strain morphology



(A) (*mrc1-V5 mrc1Δ rad4-116 rad52-GFP* DAPI)



(B) (*mrc1-V5 mrc1Δ rad4-116 rad52-GFP* GFP)

Figure 5-24. Rad52-GFP foci of the *mrc1-V5 mrc1Δ rad4-116 rad52-GFP* strain at 100X at timepoint 0. The figure shows the cells of the SPSC 1117 strain stained with (A) DAPI to show the nuclei and (B) anti-GFP to show the Rad52-GFP foci. The cells were reconstructed into 3D using the Softworx program to identify nuclear foci. No nuclei contained nuclear Rad52-GFP foci.

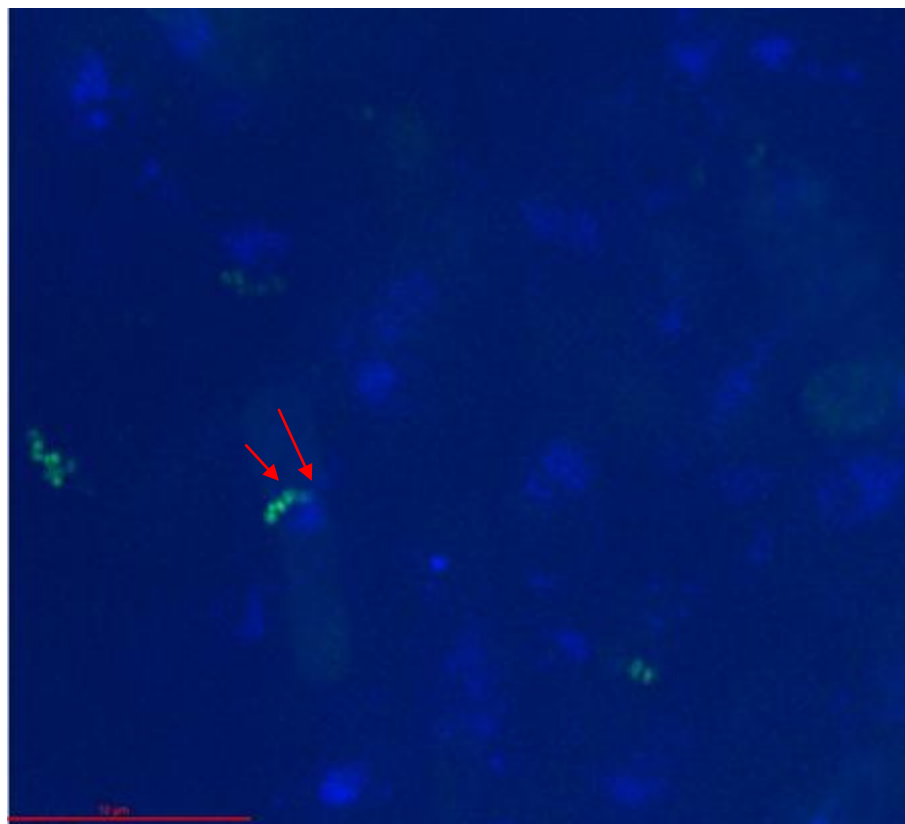
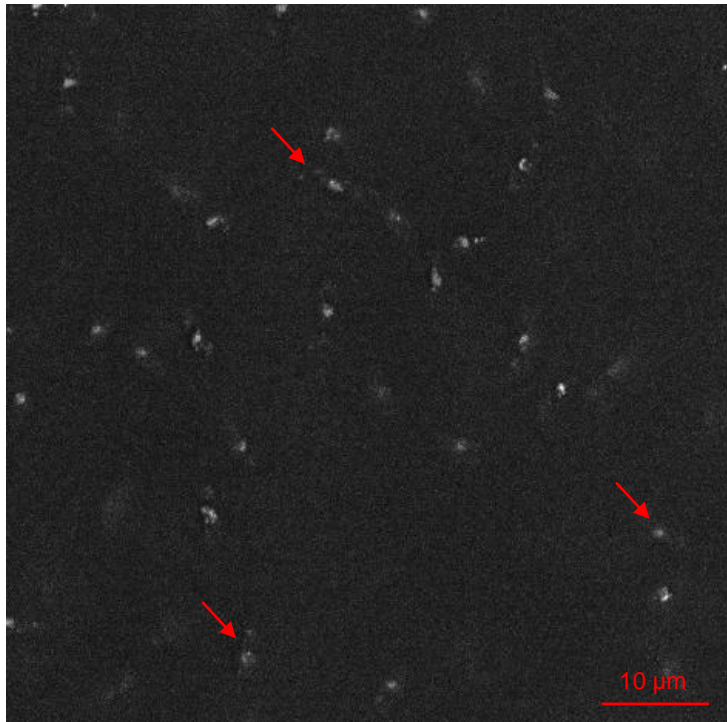
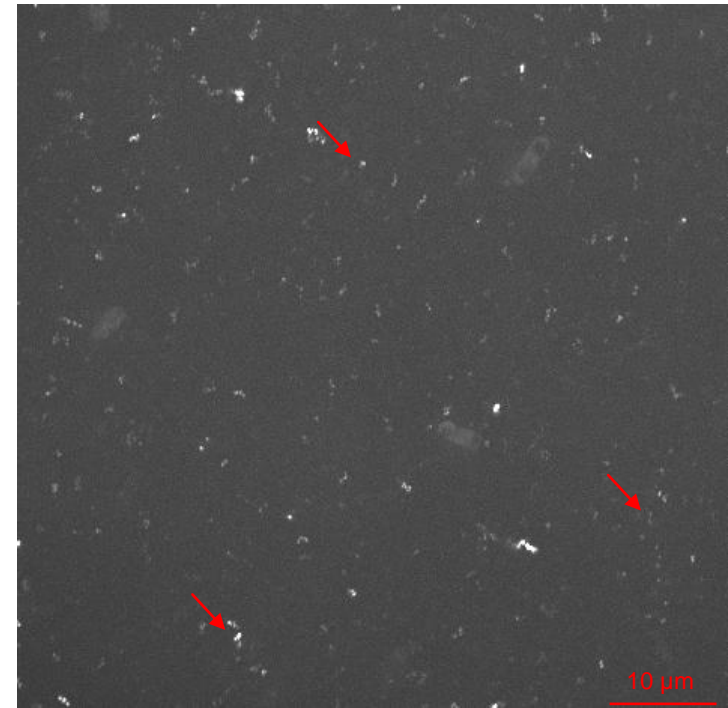


Figure 5-25. A merged image of *mrc1-V5 mrc1Δ rad4-116 rad52-GFP* cells after 4 hours of thiamine addition. The nucleus (blue) highlighted by the arrow contains multiple GFP signals (bright green). The cells were reconstructed into 3D using the Softworx program to reensure that the foci seen are indeed nuclear foci. The presence of multiple foci per nucleus is common in *mrc1-V5 mrc1Δ rad4-116 rad52-GFP* cells and the frequency of occurrence increases with incubation time after thiamine addition.



(A) (*mrc1-V5 mrc1Δ rad4-116 rad52-GFP DAPI*)



(B) (*mrc1-V5 mrc1Δ rad4-116 rad52-GFP GFP*)

Figure 5-26. Rad52-GFP foci of the *mrc1-V5 mrc1Δ rad4-116 rad52-GFP* strain at 60X magnification at timepoint 24. The figure shows the cells of the *SPSC 1117* strain stained with (A) DAPI to show the nuclei and (B) anti-GFP to show the Rad52-GFP foci. The cells were reconstructed into 3D using the Softworx program to identify nuclear foci. After 24 hours of incubation with thiamine, 82% of nuclei contained nuclear Rad52-GFP foci. Most of the nuclei appeared fragmented and compacted. Some nuclei contained multiple foci per nucleus. The red arrows point to some nuclei with Rad52-GFP foci.

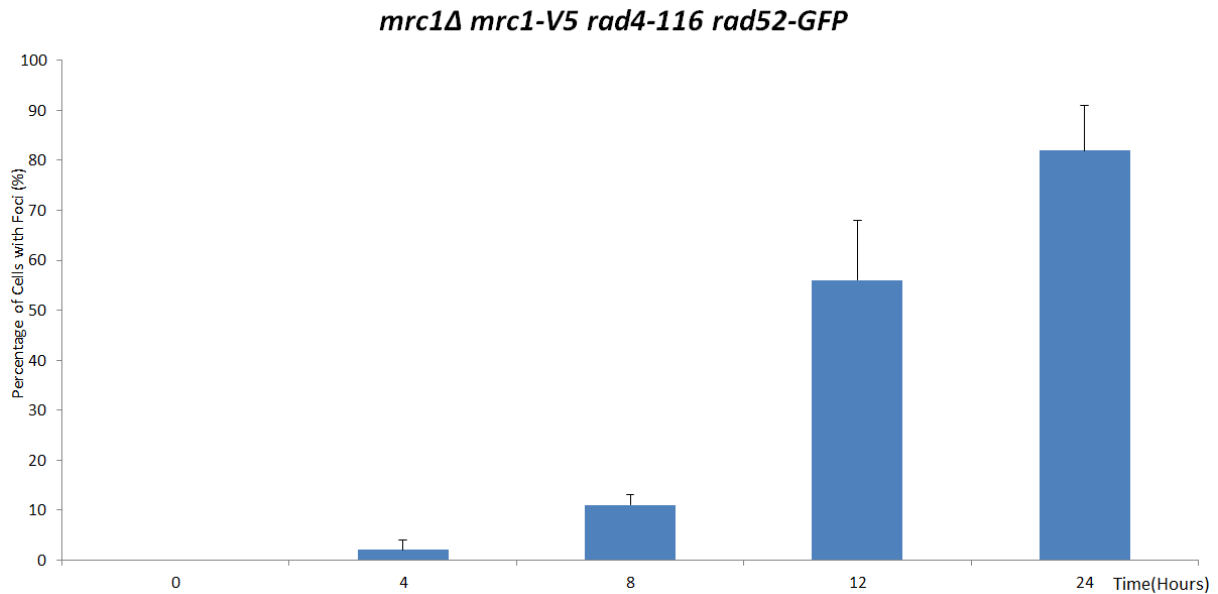


Figure 5-27. The Rad52-GFP profile of SPSC 1117 across the 24 hour timepoint. The figure shows graphical representation of the accumulation of Rad52-GFP foci in the *mrc1-V5 mrc1Δ rad4-116 rad52-GFP* strain. A gradual increase in the level of Rad52-GFP was observed across the 24 hour timecourse. An increase in the percentage of nuclei with Rad52-GFP foci was observed from no foci at 0 hour to 2% at 4 hours to 11% at 8 hours. A steep increase occurred from 11% at 8 hours to 56% at 12 hours. A final level of 82% was recorded at 24 hours.

5.4.4 The effect of thiamine addition on the *rad4-116 mrc1Δ mrc1-V5 rad52-GFP* viability

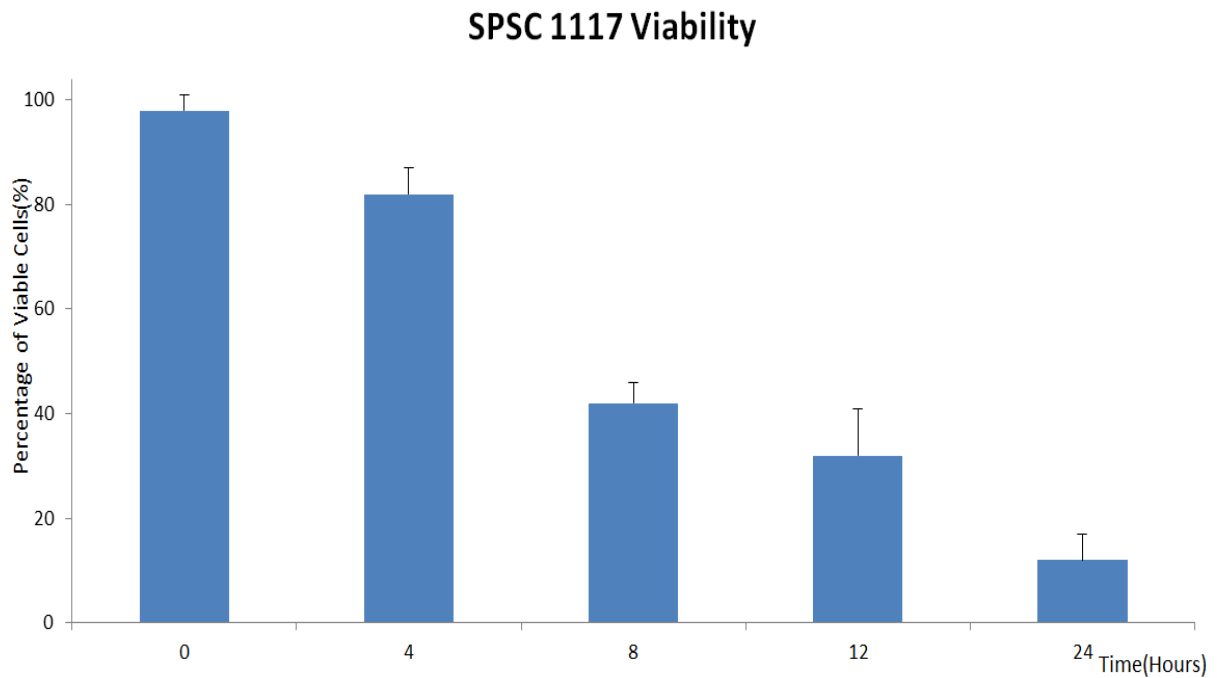


Figure 5-28. The viability change in SPSC 1117 across the 24 hour timepoint. The figure shows graphical representation of the viability of *mrc1-V5 mrc1Δ rad4-116 rad52-GFP* strain across the 24 hour timecourse. A gradual decrease in viability occurred dropping from 98% viability at 0 timepoint to 32% after 12 hours, then to 12% viability at 24 hours.

5.4.5 Phenotypic Characterisation of *rad4-116 mrc1Δ mrc1-V5 rad52-GFP* strain SPSC 1117 by FACS

The FACS method and analysis were carried out as detailed in Section 3.3.6.

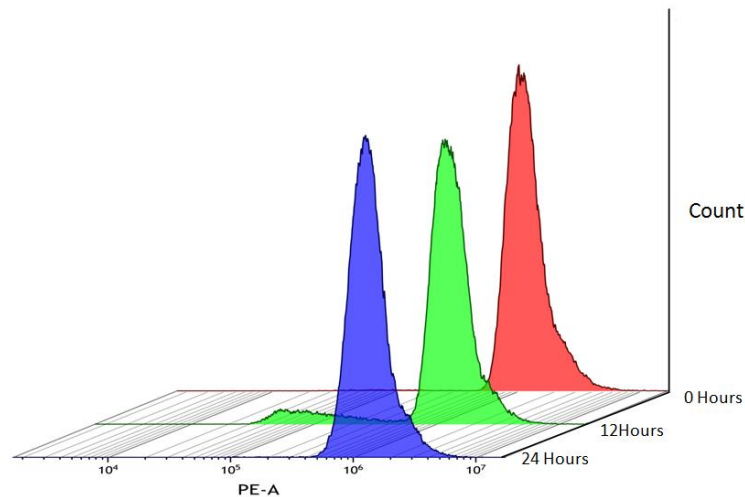


Figure 5-29. Cell population as investigated through FACS. The figure shows the analysis of the population of SPSC 1117 as representation of count (y-axis) against the phycoerythrin channel PE-A (x-axis) across 24 hours with 0 hour being the furthest along the z-axis followed by 4, 8, 12 and finally, 24 hours being the nearest along the z-axis. There was no change in staining or shift in peaks across the 24 hours except a very weak signal at 10^5 appearing at 12 hours then disappearing at 24 hours.

As observed in Figure 5-22 for QPCR and Figure 5-23 for western blotting, the expression of the RNA product and protein for Mrc1-V5 in SPSC 1117 were successfully depleted after 24 hours of incubation in media with thiamine. The adjusted relative quantity for the *mrc1-V5* RNA expression reached 0.3842 for the *mrc1Δ mrc1-V5 rad4-116 rad52-GFP* strain in Figure 5-23. The Mrc1-V5 protein signal was present at timepoints 0 with a weak signal was observed at 12 hours after and no signal at 24 hours as observed in Figure 5-23. In terms of FACS analysis, there was no change in staining or shift in peaks across the 24 hours except a very weak signal at 10^5 appearing at 12 hours then disappearing at 24 hours as seen in Figure 5-29.

The depletion of RNA expression and protein signals also caused a decrease in viability, as seen in Figure 5-28, consistent with the time and level of abolishment of the V5-tagged protein. The *mrc1Δ mrc1-V5 rad4-116 rad52-GFP* strain showed a gradual loss of viability dropping from 98% viability at 0 timepoint to 32% after 12 hours, then to 12% viability at 24 hours. The decrease in viability at timepoints 4, 8, 12 and 24 was statistically significant at $p \leq 0.01$ with values of 74%, 51%, 32% and 12% respectively compared to the 0 hour timepoint which is consistent with the depletion of V5 protein signal.

In terms of cell morphology, as observed in Figure 5-24 and Figure 5-26, the *mrc1Δ mrc1-V5 rad4-116 rad52-GFP* strain SPSC 1117, showed a distinct phenotype in terms of cell size. The phenotype shown was shorter of less than 6 μm with irregular nuclear size and shape with some nuclei being fragmented or compacted. Those changes were detectable after 12 hours of thiamine incubation and more pronounced at the 24 hour timepoint. Furthermore, an increase level of Rad52-GFP accumulation, as observed using anti-GFP antibody, was observed from 8 hours

after thiamine addition onwards. An increase in the percentage of nuclei with Rad52-GFP foci was observed from no foci at 0 hour to 2% at 4 hours to 11% at 8 hours to 56% at 12 hours to 82% at 24 hours as observed in Figure 5-27. This is consistent with both Figure 5-22 and Figure 5-23 for RNA level and V5-tagged protein level depletion respectively.

5.5 Mrc1 Chapter Discussion

By mapping the spores from crossing the *rad4-116* strain with the *mrc1Δ* strain in Figure 5-1 and tabulating 180 valid spores in total in Table 5-A, the χ^2 value was calculated at 12.8. The χ^2 value was significant to prove that the results obtained in terms of synthetic lethality of combining *rad4-116* and *mrc1Δ* was not due to chance but due to the interference occurring in one or more biological pathways. In this case, the interaction of *rad4-116* and *mrc1* in the stabilisation of stalled replication forks.

The comparison of DNA damage profiles of *rad4-116* and *mrc1Δ* strains after incubation with HU using Rad52-GFP foci was carried out using the aspects detailed in the previous chapters. The cells were stained for DAPI to show nuclei and anti-GFP to show foci as presented in Figure 5-3 for the *mrc1Δ* strain. The combination of both DAPI and GFP staining, concentrating on a single nucleus with multiple bright green GFP foci highlighted by red arrows, can be seen in Figure 5-2. It should be noted that the *rad4-116*, *rad4⁺* and *mrc1Δ* strains did not show a significant change in viability across the timecourse of the experiment as presented in the graph of Figure 5-4.

In terms of the number of foci per nucleus present, *rad4-116* cells and *mrc1Δ* cells both showed multiple foci per nucleus, in contrast to *rad4⁺* cells. It should be noted that only *rad4-116* cells and *mrc1Δ* cells showed multiple foci per nucleus, also in contrast to the *hip1Δ*, *swi1Δ* and *swi3Δ* strains. This can be easily observed in Figure 5-2 for *mrc1Δ* cells, Figure 3-8 for *rad4-116* cells and Figure 3-6 for *rad4⁺* cells.

The second aspect was the percentage of nuclei containing foci as a section of all the population of nuclei counted at the starting point, timepoint 0, of the experiment. The starting percentage was similar in *mrc1Δ* cells and *rad4-116* cells at 27% , as presented in Figure 5-5, and 26%, as presented in Figure 3-7, respectively. This was in contrast to the much lower value of 6% for *rad4⁺* cells at timepoint 0 as shown in Figure 3-9. To reiterate, these results highlight the function that of *rad4* and *mrc1* carry out in the stabilisation of stalled replication forks

Another aspect was the peak of the percentage of nuclei with GFP foci as a section of the total population of nuclei across the duration of the experiment, 210 minutes. The peak values of each of the strains did not match each other in terms of time reached or the level of accumulation of foci. For the *mrc1Δ* strain, the peak was reached at 30 minutes for a value of 40% as seen in Figure 5-5. For the *rad4⁺* strain, the peak was reached at 120 minutes for a value of 27% as observed in Figure 3-7. For the *rad4-116* strain, the peak was reached at 150 minutes for a value of 49% as seen in Figure 3-9. In both the *mrc1Δ* strain and the *rad4-116* strain, the shape of the graph was similar with sudden increase occurring after 30 minutes and maintaining a steady plateau level till 120 minutes. Then, a gradual decrease occurs in the *mrc1Δ* strain from 39% at 90 minutes till reaching to 24% at 210 minutes as seen in Figure 5-5. This is in contrast to the *rad4-116* strain where the decrease occurs only at the 210 minute timepoint as seen in Figure 3-9. It should be noted that the end point readings for both the *mrc1Δ* strain and the *rad4-116* strain were similar at 24% and 21% respectively.

The final aspect was the final reading of nuclei with foci and the comparison between the starting and final timepoints for each strain. For both the *mrc1Δ* strain and the

rad4-116 strain, the final readings were similar at 24% and 21% respectively and are quite near to the starting values of 27% and 26% as observed in Figure 5-5 and Figure 3-9 respectively. This differed from the *rad4⁺* strain, which reached a final reading of 3% compared to the already low initial reading of 6% as observed in Figure 3-7. In the case of the *mrc1Δ* strain, the final reading was only 3% lower than the initial reading. The initial values, peak values and final readings for all three strains are summarised in Figure 5-6 to further highlight the recovery patterns of all three strains. In contrast to the *rad4⁺* strain, the *mrc1Δ* strain and the *rad4-116* strain failed to recover from the incubation with HU as cells accumulated stalled, and possibly collapsed, DNA replication forks without resolution. Furthermore, both strains kept a steady level of nuclei with multiple foci as time increased fluctuating between 9% and 5% for the *rad4-116* strain and 5% to 2% of all nuclei counted for the *mrc1Δ* strain.

By constructing strains carrying the repressible *mrc1-V5* allele in the presence of *rad4-116*, it was possible to observe the behaviour of cells during cell death as the V5-tagged Mrc1 activity was abolished. By using RT-QPCR, it was confirmed that a gradual decrease in the relative quantity of RNA encoding *mrc1-V5* in all the strains tested as observed in Figure 5-10. Evidence of Mrc1-V5 depletion was confirmed using western blotting using the V5 antibody, alongside TAT1 as a control, for the strains carrying *mrc1-V5*. By observing Figures 5-12, 5-13 and 5-14, all three *mrc1-V5* strains showed total abolishment of the Mrc1-V5 signal, at the 114 kDa mark, after 8 to 12 hours of the addition of thiamine to the media.

The depletion of the RNA signal and tagged protein product did not cause a visible change in cell morphology in both the *mrc1-V5* and *mrc1Δ mrc1-V5* strains across

the 24 hour time course as observed in Figure 5-15 and Figure 5-16 respectively. However, the cell morphology began to change significantly in the *mrc1Δ mrc1-V5 rad4-116* in response to the depletion of the RNA signal and Mrc1-V5 as observed in Figure 5-17. The correlation in the time of decrease of RNA product leading to the decrease in protein product appeared as change in cell morphology and length as soon as 8 hours after thiamine addition. A significant change was observed after 12 hours, as seen in Figure 5-17(B), as well as a more pronounced change after 24 hours, as seen in Figure 5-17(C).

There are several changes that occur in the cell morphology of the *mrc1Δ mrc1-V5 rad4-116* strain in terms of nuclear integrity, cellular shape and cell length and. In Figure 5-17(B), most of the cells develop compact nuclei observed as soon as 12 hours after thiamine addition. This escalates into further decrease in nuclear area stained with DAPI with a low degree of nuclear fragmentation, as seen in Figure 5-17(C), 24 hours after thiamine addition. The change in nuclear composition was not expected as *mrc1* does not play a role in the maintenance of nuclear integrity but could be related to the additional roles of *rad4*.

The more important aspect of change in cellular morphology of the *mrc1Δ mrc1-V5 rad4-116* strain, was the gradual in cell length in Figure 5-18 compared to the *mrc1-V5* and *mrc1Δ mrc1-V5* strains did not show a significant change in cell length across the 24 hour time course. The starting timepoint 0 showed a similar cell length distribution to the *mrc1-V5* and *mrc1Δ mrc1-V5* strains. In contrast, the *mrc1Δ mrc1-V5 rad4-116* strain began to decrease in cell length in a gradual manner. By the 24 hour timepoint, cells could be seen as short as 4μm with a round, nearly spherical, shape and highly compact, nearly dot-shaped, nuclei. As seen in Figure 5-19, only

the *mrc1Δ mrc1-V5 rad4-116* strain showed a gradual cell death whilst no cell death occurred in other two strains carrying *mrc1-V5* or the control strain carrying *rad4-116* with a wildtype *mrc1* allele. The loss of viability corresponded to the depletion of RNA and protein product of *mrc1-V5*.

Finally, in terms of using PI to investigate the nuclear content of the cells across the 24 hour timecourse after thiamine addition, no conclusion could be reached. For the *mrc1-V5* and *mrc1Δ mrc1-V5* strains, Figure 5-20 (A) and (B) show that no significant change occurred across the 24 hours. However, as seen in Figure 5-21, the *mrc1Δ mrc1-V5 rad4-116* strain showed a shift in peak position and the sharpness of each peak. The only comparable shift in peaks occurred in an experiment carried out by Sabatinos and coworkers on a *mrc1Δ rad52-GFP* strain following HU strain(Sabatinos *et al.*, 2012). This experiment could be carried out such that samples would be taken in an hourly manner instead of each 4 hours and that could possibly provide a clearer pattern to the change occurring.

To able to assess the accumulation of Rad52-GFP foci during the 24-hour timecourse, after the addition of thiamine to the media, the *mrc1Δ mrc1-V5 rad4-116 rad52-GFP* strain was constructed. The strain showed nearly identical results in terms of RNA depletion and V5 signal abolishment as observed in Figure 5-22 and Figure 5-23 respectively. The loss of viability was also similar in pattern to *mrc1Δ mrc1-V5 rad4-116* reaching 12% after 24 hours as seen in Figure 5-28.

The *mrc1Δ mrc1-V5 rad4-116 rad52-GFP* strain started similar in length to the other *mrc1-V5*, as seen in Figure 5-24, but followed the pattern of *mrc1Δ mrc1-V5 rad4-116* strain in terms of gradual decrease in length, as seen in Figure 5-26. The cells developed more compacted nuclei and nuclear fragmentation was visible after 24

hours as seen in Figure 5-26. Furthermore, there was a steady accumulation of Rad52-GFP foci from the 0 hour to 24 hour timepoint as shown in Figure 5-27. True to the comparison with the *mrc1Δ mrc1-V5 rad4-116* strain, SPSC 1117 showed multiple foci per nucleus as soon as 4 hours after thiamine addition, as seen in Figure 5-25. However, unlike the *mrc1Δ mrc1-V5 rad4-116* strain, FACS analysis for the SPSC 1117 showed no change from the 0 to 12 to 24 hour timepoints as seen in Figure 5-29. As previously mentioned, the hourly sampling could possibly provide a clearer pattern to the change occurring.

Chapter 6: Final Discussion

The synthetic lethality data obtained by crossing *rad4-116* and *hip1Δ*, *swi1Δ*, *swi3Δ* and *mrc1Δ* separately provided confirmation of the preliminary SGAA screen. As observed in Tables 3-A, 4-A, 4-B and 5-A, all the crosses produced statistically significant synthetically lethal phenotypes. This further proves the synthetically interaction between *rad4-116* on one side and *hip1Δ*, *swi1Δ*, *swi3Δ* and *mrc1Δ* separately on the other side. The synthetic lethality profiles of *swi1Δ* and *swi3Δ* are nearly identical to each other in terms of the χ^2 values being 23.4 and 22.5. The synthetic lethality profile of *hip1Δ* was also similar to *swi1Δ* and *swi3Δ* profiles with a χ^2 value of 27.7. However, surprisingly, the synthetic lethality profile of *mrc1Δ* was not as similar to *hip1Δ*, *swi1Δ* and *swi3Δ* profiles in terms of χ^2 value as the χ^2 value was 12.8. Indeed, all the χ^2 values were statistically significant showing lethality. The difference of synthetic lethality profiles is interesting given that Swi1, Swi3 and Mrc1 act to stabilise stalled replication forks (Shimmoto *et al.*, 2009; Tanaka *et al.*, 2010). However, it should be noted that the Swi1-Swi3 complex recruits Mrc1 onto the replication fork (Tanaka *et al.*, 2010).

In terms of the DNA replication stalled fork profiles, a similar pattern was observed. The *hip1Δ*, *swi1Δ* and *swi3Δ* DNA replication stalled fork recovery profiles are similar in terms of peak value of nuclei and recovery with Rad52-GFP foci as observed in Figure 3-5, Figure 4-5 and Figure 4-26 respectively. The DNA replication stalled fork recovery profiles of *swi1Δ* and *swi3Δ* were less similar than their synthetic lethality profiles with the *swi3Δ* strain showing a very low accumulation of Rad52-GFP foci even when compared to the *rad4⁺* strain as observed in Figure 4-26 and Figure 4-27. Furthermore, a strong similarity was observed between the *rad4-116* and *mrc1Δ* DNA replication stalled fork profiles as observed in Figure 5-6. The full profiles

across the full 210 minute timecourse showed the same pattern in terms of starting level of percentage of cells with Rad52-GFP foci, the increase up to a similar peak level, maintenance of a steady level of foci and final level observed at 210 minutes as illustrated in Figure 3-9 for *rad4-116* and Figure 5-5 for *mrc1Δ*. These findings for *mrc1Δ* are consistent with those presented previously in *S.cerevisiae* (Katou *et al.*, 2003). The *rad4-116* and *mrc1Δ* strains are the only two strains that do not recover below the starting level of Rad52-GFP foci as observed in Figure 3-9 and Figure 5-5 respectively. The accumulation of Rad52-GFP in *swi1Δ* and *swi3Δ* strains were similar, albeit not reaching the same level of accumulation, as those noted in previous studies in *S.cerevisiae* (Noguuchi *et al.*, 2003 a; b). It is important to note that none of the strains with Rad52-GFP showed a decrease in viability across the 210 minute timecourse.

With regards to the depletion phenotypes of strains with *rad4-116* backgrounds, the viability profiles for Swi1 and Swi3 were most similar as observed in Figure 4-19 and Figure 4-45 respectively. All the strains carrying the gene deletion, the V5-tagged allele of the same gene and the *rad4-116* gene showed a gradual decrease in viability from timepoint 0 to timepoint 24 hours. Strains with either the gene deletion (*hip1Δ*, *swi1Δ*, *swi3Δ*, *mrc1Δ*) and/or the V5-tagged allele (*hip1-V5*, *swi1-V5*, *swi3-V5*, *mrc1-V5*) and *rad4⁺* showed no decrease in viability from timepoint 0 across the 24 hours timecourse after thiamine addition as observed in Figure 3-28, Figure 4-19, Figure 4-45 and Figure 5-19 respectively. All the mentioned figures also contained a *rad4-116* control with no gene mutations or V5-tagged alleles that did not show any decrease in viability and was repeated every time a strain was sampled. The strain that showed the highest level of viability loss was the *mrc1Δ mrc1-V5 rad4-116* dropping from 95% at timepoint 0 to 4% after 24 hours for a total loss of 91% as

observed in Figure 5-19. In one repetition of *mrc1Δ mrc1-V5 rad4-116* sampling, the three EMM agar plates showed no colonies growing with the expectancy of 100 viable colonies of each in case of 100% viability.

In terms of V5 RNA and protein expression, all the strains with V5-tagged genes (*hip1-V5*, *swi1-V5*, *swi3-V5*, *mrc1-V5*) showed a gradual decrease across the 24 hours after thiamine addition. Generally, using western blotting, the V5 signal is abolished at the 8 or 12 hour timepoint with a strong signal observed at the initial timepoint 0 and a weaker signal observed at timepoint 4 hours with no change observed in the α -Tubulin control protein expression. The decrease and eventual abolishment of detectable V5-tagged protein signal is consistent with the decrease in V5 transcription of each gene. In addition, in the strains carrying the gene deletion, the V5-tagged allele of the same gene and the *rad4-116* gene, the depletion of V5 RNA and protein signals was consistent with the development of cellular phenotypes in terms of cell length, nuclear integrity and size, typically present at 12 hours and more pronounced at 24 hours.

In the experiment with *hip1Δ hip1-V5 rad4-116* strain SPSC 1103, two distinct phenotypes were observed at timepoints 12 and 24 hours. The more common phenotype being longer of more than 10 μm in length and the less common phenotype being a shorter cell of less than 7 μm in length as observed in Figure 3-20. Both phenotypes show irregular nuclear size and shape with some nuclei being elongated and others fragmented or compacted. The fragmented nuclei, as observed in Figures 3-21 and 3-27, were to be expected as the HIRA proteins, including Hip1, have been proven to be integral in histone modification and chromatin structure protection (Prochasson *et al.*, 2005; Anderson *et al.*, 2009).

In the *swi1Δ swi1-V5 rad4-116* strain SPSC 1099, a single phenotype was observed at timepoints 12 and 24 hours as seen in Figure 4-17. A significant increase occurs from 6 μm to 9 μm at 12 hours before reaching 11 μm at 24 hours after the addition of thiamine as shown graphically in Figure 4-18. The cells also show multiple cellular polarisation with a common phenotype being 3 cytoplasmic ends. The increase in cell length was accompanied by a fragmentation of nuclei and the emergence of compact nuclei and occasionally cells showing no DAPI staining indicating uneven nuclear division. This is consistent with the role of Swi1 (Tof1) in terms of function in paused fork resolution and for stable association of replisome components with sites of DNA synthesis in the presence of hydroxyurea (Katou *et al.*, 2003; Calzada *et al.*, 2005; Lambert *et al.*, 2005; 2007). This may also indicate additional roles of Swi1 in terms of chromatin structure maintenance that may be affected by Rad4.

With regards to the *swi3-V5 swi3Δ rad4-116* strain SPSC1102, two distinct phenotypes were observed at timepoints 12 and 24 hours as seen in Figure 4-38. The more common phenotype being shorter of less than 5 μm in length and the less common phenotype being a longer cell of more than 5 μm in length as observed in Figure 4-38. Both phenotypes show irregular nuclear size and shape with some nuclei being elongated or compacted. It should be noted that nuclear fragmentation was not observed unlike those observed in the *swi1Δ swi1-V5 rad4-116* and *hip1Δ hip1-V5 rad4-116* strains. The appearance of the shorter length phenotype not seen in the *swi1Δ swi1-V5 rad4-116* strain was interesting, indicating a function exclusive to Swi3 not present in Swi1. The difference in phenotypes between *swi1Δ swi1-V5 rad4-116* and *swi3-V5 swi3Δ rad4-116* was also interesting given that Swi1 and Swi3 act to stabilise stalled replication forks as the same complex (Shimmoto *et al.*, 2009; Tanaka *et al.*, 2010).

As for the *mrc1-V5 mrc1Δ rad4-116* strain SPSC 1116, the cells show a distinct phenotype, that develop at timepoint 12 and 24 hours as seen in Figure 5-17. The initial average cell length at 0 is similar to the other two *mrc1-V5* strains, but then a significant decrease occurs from 9 μm to 5μm at both 12 hours and 24 hours after the addition of thiamine as observed in Figure 5-18. The decrease in cell length was accompanied by a fragmentation and compaction of nuclei with the shape of the nuclei similar to those seen in *swi1Δ swi1-V5 rad4-116* and *hip1Δ hip1-V5 rad4-116* strains. The phenotype in the *mrc1-V5 mrc1Δ rad4-116* strain was similar to the shorter phenotype of the *swi3-V5 swi3Δ rad4-116* strain in terms of cell length. This is consistent with the role of Mrc1 as a conserved replication fork factor and its interaction with Swi1-Swi3 complex (Tanaka *et al.*, 2007; Hayano *et al.*, 2011). It is important to note the similarity in phenotype between the shorter phenotype of the *swi3-V5 swi3Δ rad4-116* strain and *mrc1-V5 mrc1Δ rad4-116* strain on one hand and the similarity between longer phenotype of the *swi3-V5 swi3Δ rad4-116* and *hip1Δ hip1-V5 rad4-116* strain in terms of cell length.

In terms of FACS analysis, the most interesting result was for the *mrc1-V5 mrc1Δ rad4-116* strain which showed a shift in the strength and position of the peaks observed in terms of DNA content as shown in Figure 5-21. The results were similar to the FACS results obtained in *mrc1Δ* mutants when subjected to HU in terms of shift in DNA content, albeit the results presented here showing the change over a longer period of time, 24 hours instead of 90 minutes, in a synthetically lethal interaction (Sabatinos *et al.*, 2012). The fact that little change was observed in the *swi1Δ swi1-V5 rad4-116*, *swi3-V5 swi3Δ rad4-116* and *hip1Δ hip1-V5 rad4-116* strains could be due to the lack of separation of signals based on the different cell populations to show an whole population instead. This is especially true for the *swi3-*

V5 *swi3Δ rad4-116* and *hip1Δ hip1-V5 rad4-116* strains and this required further analysis. The conclusion that can be drawn here, is that based on the FACS data as well as the depletion phenotypes observed, is that the *swi1Δ swi1-V5 rad4-116*, *swi3-V5 swi3Δ rad4-116* and *hip1Δ hip1-V5 rad4-116* fail to initiate or reinitiate replication once the non-essential gene is depleted. This is especially true given that none of the strain versions with the *rad52-GFP* allele showed any accumulation of Rad52-GFP foci indicating the lack of recruitment of Rad52-GFP onto the stalled fork sites. Future FACS analysis of the strains needs to include a correlation to cellular size, nuclear size and nuclear integrity.

It should be noted that the *rad4-116* interaction with the gene deletions (*hip1Δ*, *swi1Δ*, *swi3Δ*, *mrc1Δ*) was most likely due to the development of stalled replication forks, with eventual fork collapse, and double strand breaks as the *rad4-116* allele mimics conditions of replication stress in the absence of checkpoint function (McFarlane *et al.*, 1997). However, that does not rule out additional interactions based on the other roles of Rad4 which led to the development of different and distinct phenotypes as the V5-tagged genes were deleted in the presence of *rad4-116* leading to eventual cell death.

Strains for *swi1Δ swi1-V5 rad4-116 rad52-GFP*, *swi3Δ swi3-V5 rad4-116 rad52-GFP*, *hip1Δ hip1-V5* and *rad4-116 rad52-GFP* and *rad52-GFP mrc1-V5 mrc1Δ rad4-116* were all constructed to be able to build profiles for the accumulation of Rad52-GFP foci during the depletion of the V5-tagged proteins using thiamine. All of these strains showed a depletion of V5-tagged gene expression using QPCR and V5-tagged protein expression using western blotting, similar to those shown in their corresponding strains without the *rad52-GFP* gene. The results for them were not

shown, except for *rad52-GFP mrc1-V5 mrc1Δ rad4-116*, as they did not develop any Rad52-GFP foci even after the 24 hour period. It should be noted that a loss of viability was observed for all of these similar to their corresponding strains without the *rad52-GFP* gene. The development of Rad52-GFP foci in the *rad52-GFP mrc1-V5 mrc1Δ rad4-116* after the depletion of Mrc1-V5 showed an increase in fork stalling and eventual collapse with no recovery as the level of nuclei carrying GFP foci increased up to 82% after 24 hours of incubation with thiamine. This is consistent with the profile observed in this study with the *mrc1Δ rad52-GFP* strain in response to HU incubation and previous studies as well (Sabatinos *et al.*, 2012).

This project identified that the non-essential genes *mrc1*, *swi1*, *swi3* and *hip1* are required for survival under replication stress. The role these genes play in the resolution of DNA replication forks in combination with the loss of function from the hypomorphic *rad4-116*, appears to be the driving cause of the synthetic lethality of the double mutant strains. The inability of cells to recover from the fork stalling, and subsequent collapse caused cells to die during the depletion of the tested gene .

Further experiments need to be undertaken using the genes presented in this thesis to be able to further clarify their roles and interaction with *rad4*. For example, DNA replication at centromeres, telomeres and known early origins of replication could be monitored in synchronized cultures using BrdU incorporation combined with ChIP (Chromatin Immunoprecipitation). The analysis and mapping of replication origin firing, in terms of frequency and position could establish distinct profiles for each null mutant and could be used in depletion experiments, of the non-essential genes, combined with *rad4-116* to investigate and clarify the exact pathway or interaction leading to the lethality observed. The phenotypic characterisation in this thesis could

be used in terms of strain construction, experimentation and analysis techniques to investigate more genes that have been identified using the SGAA screen. The interaction between *rad4-116* and chromatin remodelling genes such as *swi6* could be useful in mapping and confirming the results obtained with *hip1* (Grewal and Jia 2007). Obviously, an interesting gene would be *rad52* itself and it would be important to observe the genetic interaction between *rad4-116* and *rad52*, given the modifications needed for strain construction and experimental analysis required. Another gene would be *abo1/2 (yta71)* which is involved in transcriptional regulation and histone modification (Gradolatto *et al.*, 2008; Fillingham *et al.*, 2009).

The eventual aim of the research using TopBP1 and its homologs, is to be able to map the interactions of TopBP1 such that comprehensive network of interaction is completed. The importance of TopBP1 in pathogenesis, especially tumourigenesis, makes it an important target for drug targeting. However, due to its extensive network of its interactions and due to the sheer sophistication of genetic machinery and cancer cell development, targeting TopBP1 alone would not be sufficient. A comprehensive strategic plan of targeting TopBP1 as well as specific proteins within its network needs to be undertaken depending on the genetic profile of the tumour and the pharmacogenetic profile of the patient. As with the case of most cancers, the ultimate goal is to be able to provide a personalised approach of treatment selection to target the specifically disrupted pathways causing the disease. This would potentially provide a treatment strategy which is efficient in both drug activity and cost with the least adverse side-effects from off-target toxicity, thereby improving patient quality of life and median survival rate.

In summary, this thesis provides the phenotypic analysis of strains to be able to identify non-essential genes required for survival under conditions of DNA stress. The work carried out in *S. pombe* could be built upon in higher eukaryotes to be able to map the interactions of TopBP1.

Bibliography:

- Adachi Y, Usukura J, Yanagida M. A globular complex formation by Nda1 and the other five members of the MCM protein family in fission yeast. *Genes Cells.* 1997 Jul;2(7):467-79.
- Adhikary S, Eilers M. Transcriptional regulation and transformation by Myc proteins. *Nat Rev Mol Cell Biol.* 2005 Aug;6(8):635-45. Review.
- al-Khodairy F, Carr AM. DNA repair mutants defining G2 checkpoint pathways in *Schizosaccharomyces pombe*. *EMBO J.* 1992 Apr;11(4):1343-50
- Alcasabas AA, Osborn AJ, Bachant J, Hu F, Werler PJ, Bousset K, Furuya K, Diffley JF, Carr AM, Elledge SJ. Mrc1 transduces signals of DNA replication stress to activate Rad53. *Nat Cell Biol.* 2001 Nov;3(11):958-65.
- Amin AD, Vishnoi N, Prochasson P. A global requirement for the HIR complex in the assembly of chromatin. *Biochim Biophys Acta.* 2013 Mar-Apr;1819(3-4):264-76. Review.
- Anderson HE, Wardle J, Korkut SV, Murton HE, López-Maury L, Bähler J, Whitehall SK. The fission yeast HIRA histone chaperone is required for promoter silencing and the suppression of cryptic antisense transcripts. *Mol Cell Biol.* 2009 Sep;29(18):5158-67.
- Aparicio OM, Stout AM, Bell SP. Differential assembly of Cdc45p and DNA polymerases at early and late origins of DNA replication. *Proc Natl Acad Sci U S A.* 1999 Aug 3;96(16):9130-5.
- Araki H. Initiation of chromosomal DNA replication in eukaryotic cells; contribution of yeast genetics to the elucidation. *Genes Genet Syst.* 2011;86(3):141-9. Review.

- Araki H, Leem SH, Phongdara A, Sugino A. Dpb11, which interacts with DNA polymerase II(epsilon) in *Saccharomyces cerevisiae*, has a dual role in S-phase progression and at a cell cycle checkpoint. *Proc Natl Acad Sci U S A*. 1995 Dec 5;92(25):11791-5.
- Avvakumov N, Nourani A, Côté J. Histone chaperones: modulators of chromatin marks. *Mol Cell*. 2011 Mar 4;41(5):502-14. Review.
- Ball HL, Ehrhardt MR, Mordes DA, Glick GG, Chazin WJ, Cortez D. Function of a conserved checkpoint recruitment domain in ATRIP proteins. *Mol Cell Biol*. 2007 May;27(9):3367-77.
- Ball HL, Myers JS, Cortez D. ATRIP binding to replication protein A-single-stranded DNA promotes ATR-ATRIP localization but is dispensable for Chk1 phosphorylation. *Mol Biol Cell*. 2005 May;16(5):2372-81.
- Bardin AJ, Amon A. Men and sin: what's the difference? *Nat Rev Mol Cell Biol*. 2001 Nov;2(11):815-26. Review.
- Bartek J, Bartkova J, Lukas J. DNA damage signalling guards against activated oncogenes and tumour progression. *Oncogene*. 2007 Dec 10;26(56):7773-9. Review.
- Bartkova J, Horejsí Z, Koed K, Krämer A, Tort F, Zieger K, Guldberg P, Sehested M, Nesland JM, Lukas C, Ørntoft T, Lukas J, Bartek J. DNA damage response as a candidate anti-cancer barrier in early human tumorigenesis. *Nature*. 2005 Apr 14;434(7035):864-70.
- Bell SP, Dutta A. DNA replication in eukaryotic cells. *Annu Rev Biochem*. 2002;71:333-74. Epub 2001 Nov 9. Review.

- Bentley NJ, Holtzman DA, Flaggs G, Keegan KS, DeMaggio A, Ford JC, Hoekstra M, Carr AM. The Schizosaccharomyces pombe rad3 checkpoint gene. EMBO J. 1996 Dec 2;15(23):6641-51.
- Bermudez VP, Lindsey-Boltz LA, Cesare AJ, Maniwa Y, Griffith JD, Hurwitz J, Sancar A. Loading of the human 9-1-1 checkpoint complex onto DNA by the checkpoint clamp loader hRad17-replication factor C complex in vitro. Proc Natl Acad Sci U S A. 2003 Feb 18;100(4):1633-8.
- Blackwell C, Martin KA, Greenall A, Pidoux A, Allshire RC, Whitehall SK. The Schizosaccharomyces pombe HIRA-like protein Hip1 is required for the periodic expression of histone genes and contributes to the function of complex centromeres. Mol Cell Biol. 2004 May;24(10):4309-20.
- Blattner FR, Plunkett G 3rd, Bloch CA, Perna NT, Burland V, Riley M, Collado-Vides J, Glasner JD, Rode CK, Mayhew GF, Gregor J, Davis NW, Kirkpatrick HA, Goeden MA, Rose DJ, Mau B, Shao Y. The complete genome sequence of Escherichia coli K-12. Science. 1997 Sep 5;277(5331):1453-62.
- Blaut MA, Bogdanova NV, Bremer M, Karstens JH, Hillemanns P, Dörk T. TOPBP1 missense variant Arg309Cys and breast cancer in a German hospital-based case-control study. J Negat Results Biomed. 2010 Nov 25;9:9.
- Boddy MN, Russell P. DNA replication checkpoint. Curr Biol. 2001 Nov 27;11(23):R953-6.
- Boner W, Morgan IM. Novel cellular interacting partners of the human papillomavirus 16 transcription/replication factor E2. Virus Res. 2002 Dec;90(1-2):113-8.
- Boner W, Taylor ER, Tsimonaki E, Yamane K, Campo MS, Morgan IM. A Functional interaction between the human papillomavirus 16

transcription/replication factor E2 and the DNA damage response protein TopBP1. *J Biol Chem.* 2002 Jun 21;277(25):22297-303.

- Booher RN, Alfa CE, Hyams JS, Beach DH. The fission yeast *cdc2/cdc13/suc1* protein kinase: regulation of catalytic activity and nuclear localization. *Cell.* 1989 Aug 11;58(3):485-97.
- Boone C, Bussey H, Andrews BJ. Exploring genetic interactions and networks with yeast. *Nat Rev Genet.* 2007 Jun;8(6):437-49. Review.
- Boos D, Frigola J, Diffley JF. Activation of the replicative DNA helicase: breaking up is hard to do. *Curr Opin Cell Biol.* 2012 Jun;24(3):423-30..
- Boos D, Sanchez-Pulido L, Rappas M, Pearl LH, Oliver AW, Ponting CP, Diffley JF. Regulation of DNA replication through Sld3-Dpb11 interaction is conserved from yeast to humans. *Curr Biol.* 2011 Jul 12;21(13):1152-7.
- Brewer BJ, Chlebowicz-Sledziewska E, Fangman WL. Cell cycle phases in the unequal mother/daughter cell cycles of *Saccharomyces cerevisiae*. *Mol Cell Biol.* 1984 Nov;4(11):2529-31.
- Brewer, B.J. and Fangman, W.L., 1993. Initiation at closely spaced replication origins in a yeast chromosome. *Science-AAAS-Weekly Paper Edition-including Guide to Scientific Information*, 262(5140), pp.1728-1730.
- Bruck I, Kanter DM, Kaplan DL. Enabling association of the GINS protein tetramer with the mini chromosome maintenance (Mcm)2-7 protein complex by phosphorylated Sld2 protein and single-stranded origin DNA. *J Biol Chem.* 2011 Oct 21;286(42):36414-26.
- Bruck I, Kaplan DL. Origin single-stranded DNA releases Sld3 protein from the Mcm2-7 complex, allowing the GINS tetramer to bind the Mcm2-7 complex. *J Biol Chem.* 2011 May 27;286(21):18602-13. doi:

10.1074/jbc.M111.226332. Epub 2011 Apr 1. Erratum in: J Biol Chem. 2017 Jun 16;292(24):10318.

- Burgess RJ, Zhang Z. Histone chaperones in nucleosome assembly and human disease. *Nat Struct Mol Biol* 2013; 20:14-22; PMID:23288364; <http://dx.doi.org/10.1038/nsmb.2461>
- Burnette WN. "Western blotting": electrophoretic transfer of proteins from sodium dodecyl sulfate--polyacrylamide gels to unmodified nitrocellulose and radiographic detection with antibody and radioiodinated protein A. *Anal Biochem.* 1981 Apr;112(2):195-203.
- Burrows AE, Elledge SJ. How ATR turns on: TopBP1 goes on ATRIP with ATR. *Genes Dev.* 2008 Jun 1;22(11):1416-21.
- Byun TS, Pacek M, Yee MC, Walter JC, Cimprich KA. Functional uncoupling of MCM helicase and DNA polymerase activities activates the ATR-dependent checkpoint. *Genes Dev.* 2005 May 1;19(9):1040-52.
- Caetano C, Klier S, de Bruin RA. Phosphorylation of the MBF repressor Yox1p by the DNA replication checkpoint keeps the G1/S cell-cycle transcriptional program active. *PLoS One.* 2011 Feb 16;6(2):e17211.
- Carr AM. DNA structure dependent checkpoints as regulators of DNA repair. *DNA Repair (Amst).* 2002 Dec 5;1(12):983-94. Review.
- Carr AM, Moudjou M, Bentley NJ, Hagan IM. The chk1 pathway is required to prevent mitosis following cell-cycle arrest at 'start'. *Curr Biol.* 1995 Oct 1;5(10):1179-90.
- Calzada A, Hodgson B, Kanemaki M, Bueno A, Labib K. Molecular anatomy and regulation of a stable replisome at a paused eukaryotic DNA replication fork. *Genes Dev.* 2005 Aug 15;19(16):1905-19.

- Caspari T, Carr AM. DNA structure checkpoint pathways in *Schizosaccharomyces pombe*. *Biochimie*. 1999 Jan-Feb;81(1-2):173-81. Review.
- Cayrou, C., Coulombe, P., Vigneron, A., Stanojckik, S., Ganier, O., Rivals, E., Puy, A., Laurent-Chabalier, S., Desprat, R. and Mechali, M., 2011. Genome-scale analysis of metazoan replication origins reveals their organization in specific but flexible sites defined by conserved features. *Genome Research*, pp.gr-121830.
- Cavero S, Limbo O, Russell P. Critical functions of Rpa3/Ssb3 in S-phase DNA damage responses in fission yeast. *PLoS Genet*. 2010 Sep 23;6(9):e1001138.
- Cescutti R, Negrini S, Kohzaki M, Halazonetis TD. TopBP1 functions with 53BP1 in the G1 DNA damage checkpoint. *EMBO J*. 2010 Nov 3;29(21):3723-32.
- Chagin, V.O., Casas-Delucchi, C.S., Reinhart, M., Schermelleh, L., Markaki, Y., Maiser, A., Bolius, J.J., Bensimon, A., Fillies, M., Domaing, P. and Rozanov, Y.M., 2016. 4D Visualization of replication foci in mammalian cells corresponding to individual replicons. *Nature Communications*, 7, 11231.
- Chapman CR, Evans ST, Carr AM, Enoch T. Requirement of sequences outside the conserved kinase domain of fission yeast Rad3p for checkpoint control. *Mol Biol Cell*. 1999 Oct;10(10):3223-38.
- Chen Y, Sanchez Y. Chk1 in the DNA damage response: conserved roles from yeasts to mammals. *DNA Repair (Amst)*. 2004 Aug-Sep;3(8-9):1025-32. Review.

- Chini CC, Chen J. Human claspin is required for replication checkpoint control. *J Biol Chem.* 2003 Aug 8;278(32):30057-62.
- Choi JH, Lindsey-Boltz LA, Sancar A. Reconstitution of a human ATR-mediated checkpoint response to damaged DNA. *Proc Natl Acad Sci U S A.* 2007 Aug 14;104(33):13301-6.
- Choi JH, Lindsey-Boltz LA, Sancar A. Cooperative activation of the ATR checkpoint kinase by TopBP1 and damaged DNA. *Nucleic Acids Res.* 2009 Apr;37(5):1501-9.
- Chu Z, Eshaghi M, Poon SY, Liu J. A Cds1-mediated checkpoint protects the MBF activator Rep2 from ubiquitination by anaphase-promoting complex/cyclosome-Ste9 at S-phase arrest in fission yeast. *Mol Cell Biol.* 2009 Sep;29(18):4959-70.
- Chujo M, Tarumoto Y, Miyatake K, Nishida E, Ishikawa F. HIRA, a conserved histone chaperone, plays an essential role in low-dose stress response via transcriptional stimulation in fission yeast. *J Biol Chem.* 2012 Jul 6;287(28):23440-50.
- Ciccia A, Elledge SJ. The DNA damage response: making it safe to play with knives. *Mol Cell.* 2010 Oct 22;40(2):179-204. doi: 10.1016/j.molcel.2010.09.019. Review.
- Cimprich KA. Fragile sites: breaking up over a slowdown. *Curr Biol.* 2003 Mar 18;13(6):R231-3.
- Cimprich KA, Cortez D. ATR: an essential regulator of genome integrity. *Nat Rev Mol Cell Biol.* 2008 Aug;9(8):616-27. doi: 10.1038/nrm2450. Epub 2008 Jul 2. Review.

- Clyne RK, Kelly TJ. Genetic analysis of an ARS element from the fission yeast *Schizosaccharomyces pombe*. *EMBO J.* 1995 Dec 15;14(24):6348-57.
- Cortez D, Guntuku S, Qin J, Elledge SJ. ATR and ATRIP: partners in checkpoint signaling. *Science.* 2001 Nov 23;294(5547):1713-6.
- Connolly T, Beach D. Interaction between the Cig1 and Cig2 B-type cyclins in the fission yeast cell cycle. *Mol Cell Biol.* 1994 Jan;14(1):768-76.
- Coverley, D., Laman, H. and Laskey, R.A., 2002. Distinct roles for cyclins E and A during DNA replication complex assembly and activation. *Nature Cell Biology*, 4(7), pp.523-528.
- Croce, C.M., 2008. Oncogenes and cancer. *New England Journal of Medicine*, 358(5), pp.502-511.
- Dalgaard JZ, Klar AJ. *swi1* and *swi3* perform imprinting, pausing, and termination of DNA replication in *S. pombe*. *Cell.* 2000 Sep 15;102(6):745-51.
- de Bruin RA, Kalashnikova TI, Aslanian A, Wohlschlegel J, Chahwan C, Yates JR 3rd, Russell P, Wittenberg C. DNA replication checkpoint promotes G1-S transcription by inactivating the MBF repressor Nrm1. *Proc Natl Acad Sci U S A.* 2008 Aug 12;105(32):11230-5.
- de Bruin RA, Wittenberg C. All eukaryotes: before turning off G1-S transcription, please check your DNA. *Cell Cycle.* 2009 Jan 15;8(2):214-7. Review.
- Delacroix S, Wagner JM, Kobayashi M, Yamamoto K, Karnitz LM. The Rad9-Hus1-Rad1 (9-1-1) clamp activates checkpoint signaling via TopBP1. *Genes Dev.* 2007 Jun 15;21(12):1472-7.

- Delgado, S., Gómez, M., Bird, A. and Antequera, F., 1998. Initiation of DNA replication at CpG islands in mammalian chromosomes. *The EMBO Journal*, 17(8), pp.2426-2435.
- den Elzen NR, O'Connell MJ. Recovery from DNA damage checkpoint arrest by PP1-mediated inhibition of Chk1. *EMBO J.* 2004 Feb 25;23(4):908-18.
- Dhar SK, Delmolino L, Dutta A. Architecture of the human origin recognition complex. *J Biol Chem.* 2001 Aug 3;276(31):29067-71.
- Diffley JF, Labib K. The chromosome replication cycle. *J Cell Sci.* 2002 Mar 1;115(Pt 5):869-72. Review
- Dolan WP, Sherman DA, Forsburg SL. Schizosaccharomyces pombe replication protein Cdc45/Sna41 requires Hsk1/Cdc7 and Rad4/Cut5 for chromatin binding. *Chromosoma.* 2004 Sep;113(3):145-56.
- Donaldson AD, Blow JJ. DNA replication: stable driving prevents fatal smashes. *Curr Biol.* 2001 Nov 27;11(23):R979-82. Review.
- Douglas, M.E. and Diffley, J.F., 2016. Recruitment of Mcm10 to sites of replication initiation requires direct binding to the minichromosome maintenance (Mcm) complex. *Journal of Biological Chemistry*, 291(11), pp.5879-5888.
- Drlica, K. and Zhao, X., 1997. DNA gyrase, topoisomerase IV, and the 4-quinolones. *Microbiology and Molecular Biology Reviews*, 61(3), pp.377-392.
- Du LL, Nakamura TM, Russell P. Histone modification-dependent and -independent pathways for recruitment of checkpoint protein Crb2 to double-strand breaks. *Genes Dev.* 2006 Jun 15;20(12):1583-96.

- Duck P, Nasim A, James AP. Temperature-sensitive mutant of *Schizosaccharomyces pombe* exhibiting enhanced radiation sensitivity. *J Bacteriol.* 1976 Nov;128(2):536-9.
- Dunaway S, Liu HY, Walworth NC. Interaction of 14-3-3 protein with Chk1 affects localization and checkpoint function. *J Cell Sci.* 2005 Jan 1;118(Pt 1):39-50.
- Duronio RJ, Xiong Y. Signaling pathways that control cell proliferation. *Cold Spring Harb Perspect Biol.* 2013 Mar 1;5(3):a008904. doi: 10.1101/cshperspect.a008904. Review.
- Dutta C, Patel PK, Rosebrock A, Oliva A, Leatherwood J, Rhind N. The DNA replication checkpoint directly regulates MBF-dependent G1/S transcription. *Mol Cell Biol.* 2008 Oct;28(19):5977-85.
- Egel R. Fission yeast on the brink of meiosis. *Bioessays.* 2000 Sep;22(9):854-60.
- Enoch T, Carr AM, Nurse P. Fission yeast genes involved in coupling mitosis to completion of DNA replication. *Genes Dev.* 1992 Nov;6(11):2035-46.
- Enoch T, Nurse P. Mutation of fission yeast cell cycle control genes abolishes dependence of mitosis on DNA replication. *Cell.* 1990 Feb 23;60(4):665-73.
- Enoch T, Nurse P. Coupling M phase and S phase: controls maintaining the dependence of mitosis on chromosome replication. *Cell.* 1991 Jun 14;65(6):921-3. Review.
- Evrin, C., Clarke, P., Zech, J., Lurz, R., Sun, J., Uhle, S., Li, H., Stillman, B. and Speck, C., 2009. A double-hexameric MCM2-7 complex is loaded onto origin DNA during licensing of eukaryotic DNA replication. *Proceedings of the National Academy of Sciences*, 106(48), pp.20240-20245.

- Ewers E, Yoda K, Hamid AB, Weise A, Manvelyan M, Liehr T. Centromere activity in dicentric small supernumerary marker chromosomes. *Chromosome Res.* 2010 Jul;18(5):555-62.
- Eyfjord JE, Bodvarsdottir SK. Genomic instability and cancer: networks involved in response to DNA damage. *Mutat Res.* 2005 Dec 30;592(1-2):18-28. Epub 2005 Jul 5. Review.
- Fenech M, Carr AM, Murray J, Watts FZ, Lehmann AR. Cloning and characterization of the rad4 gene of *Schizosaccharomyces pombe*; a gene showing short regions of sequence similarity to the human XRCC1 gene. *Nucleic Acids Res.* 1991 Dec 25;19(24):6737-41.
- Feng YQ, Seibler J, Alami R, Eisen A, Westerman KA, Leboulch P, Fiering S, Bouhassira EE. Site-specific chromosomal integration in mammalian cells: highly efficient CRE recombinase-mediated cassette exchange. *J Mol Biol.* 1999 Oct 1;292(4):779-85.
- Fennessy D, Grallert A, Krapp A, Cokoja A, Bridge AJ, Petersen J, Patel A, Tallada VA, Boke E, Hodgson B, Simanis V, Hagan IM. Extending the *Schizosaccharomyces pombe* molecular genetic toolbox. *PLoS One.* 2014 May 21;9(5):e97683.
- Field SJ, Tsai FY, Kuo F, Zubiaga AM, Kaelin WG Jr, Livingston DM, Orkin SH, Greenberg ME. E2F-1 functions in mice to promote apoptosis and suppress proliferation. *Cell.* 1996 May 17;85(4):549-61.
- Fillingham J, Kainth P, Lambert JP, van Bakel H, Tsui K, Peña-Castillo L, Nislow C, Figeys D, Hughes TR, Greenblatt J, Andrews BJ. Two-color cell array screen reveals interdependent roles for histone chaperones and a

chromatin boundary regulator in histone gene repression. *Mol Cell*. 2009 Aug 14;35(3):340-51.

- Fisher DL, Nurse P. A single fission yeast mitotic cyclin B p34cdc2 kinase promotes both S-phase and mitosis in the absence of G1 cyclins. *EMBO J*. 1996 Feb 15;15(4):850-60.
- Forma E, Krzeslak A, Bernaciak M, Romanowicz-Makowska H, Brys M. Expression of TopBP1 in hereditary breast cancer. *Mol Biol Rep*. 2012 Jul;39(7):7795-804.
- Forsburg SL. The art and design of genetic screens: yeast. *Nat Rev Genet*. 2001 Sep;2(9):659-68. Review.
- Forsburg SL. Overview of *Schizosaccharomyces pombe*. *Curr Protoc Mol Biol*. 2003 Nov;Chapter 13:Unit 13.14.
- Forsburg SL, Nurse P. Cell cycle regulation in the yeasts *Saccharomyces cerevisiae* and *Schizosaccharomyces pombe*. *Annu Rev Cell Biol*. 1991;7:227-56. Review.
- Forsburg SL, Nurse P. Analysis of the *Schizosaccharomyces pombe* cyclin *puc1*: evidence for a role in cell cycle exit. *J Cell Sci*. 1994 Mar;107 (Pt 3):601-13.
- Forsburg SL, Rhind N. Basic methods for fission yeast. *Yeast*. 2006 Feb;23(3):173-83. Review.
- Foss EJ. Top1p regulates DNA damage responses during S phase in *Saccharomyces cerevisiae*. *Genetics*. 2001 Feb;157(2):567-77.
- Fragkos, M., Ganier, O., Coulombe, P. and Méchali, M., 2015. DNA replication origin activation in space and time. *Nature Reviews Molecular Cell Biology*, 16(6), pp.360-374.

- Fukuura M, Nagao K, Obuse C, Takahashi TS, Nakagawa T, Masukata H. CDK promotes interactions of Sld3 and Drc1 with Cut5 for initiation of DNA replication in fission yeast. *Mol Biol Cell*. 2011 Jul 15;22(14):2620-33.
- Furuya K, Carr AM. DNA checkpoints in fission yeast. *J Cell Sci*. 2003 Oct 1;116(Pt 19):3847-8. Review.
- Furuya K, Poitelea M, Guo L, Caspari T, Carr AM. Chk1 activation requires Rad9 S/TQ-site phosphorylation to promote association with C-terminal BRCT domains of Rad4TOPBP1. *Genes Dev*. 2004 May 15;18(10):1154-64.
- Gaillard H, García-Muse T, Aguilera A. Replication stress and cancer. *Nat Rev Cancer*. 2015 May;15(5):276-89. doi: 10.1038/nrc3916. Review.
- Gal C, Moore KM, Paszkiewicz K, Kent NA, Whitehall SK. The impact of the HIRA histone chaperone upon global nucleosome architecture. *Cell Cycle*. 2015;14(1):123-34.
- Garcia V, Furuya K, Carr AM. Identification and functional analysis of TopBP1 and its homologs. *DNA Repair (Amst)*. 2005 Nov 21;4(11):1227-39. Review.
- Ge, X. Q., Blow, J. Julian. Conserved steps in Eukaryotic DNA replication. In *Molecular themes in DNA replication*, 2009 (ed. L. Cox), pp. 1-21. Cambridge: Royal Society of Chemistry.
- Ge, X.Q., Jackson, D.A. and Blow, J.J., 2007. Dormant origins licensed by excess Mcm2–7 are required for human cells to survive replicative stress. *Genes & Development*, 21(24), pp.3331-3341.
- Germann SM, Oestergaard VH, Haas C, Salis P, Motegi A, Lisby M. Dpb11/TopBP1 plays distinct roles in DNA replication, checkpoint response and homologous recombination. *DNA Repair (Amst)*. 2011 Feb 7;10(2):210-24.

- Going JJ, Nixon C, Dornan ES, Boner W, Donaldson MM, Morgan IM. Aberrant expression of TopBP1 in breast cancer. *Histopathology*. 2007 Mar;50(4):418-24.
- Gómez EB, Forsburg SL. Analysis of the fission yeast *Schizosaccharomyces pombe* cell cycle. *Methods Mol Biol*. 2004;241:93-111.
- Gong Z, Kim JE, Leung CC, Glover JN, Chen J. BACH1/FANCI acts with TopBP1 and participates early in DNA replication checkpoint control. *Mol Cell*. 2010 Feb 12;37(3):438-46.
- González-Aguilera C, Tous C, Gómez-González B, Huertas P, Luna R, Aguilera A. The THP1-SAC3-SUS1-CDC31 complex works in transcription elongation mRNA export preventing RNA-mediated genome instability. *Mol Biol Cell*. 2008 Oct;19(10):4310-8.
- Gorgoulis VG, Vassiliou LV, Karakaidos P, Zacharatos P, Kotsinas A, Liloglou T, Venere M, Ditullio RA Jr, Kastrinakis NG, Levy B, Kletsas D, Yoneta A, Herlyn M, Kittas C, Halazonetis TD. Activation of the DNA damage checkpoint and genomic instability in human precancerous lesions. *Nature*. 2005 Apr 14;434(7035):907-13.
- Gradolatto A, Rogers RS, Lavender H, Taverna SD, Allis CD, Aitchison JD, Tackett AJ. *Saccharomyces cerevisiae* Yta7 regulates histone gene expression. *Genetics*. 2008 May;179(1):291-304. Greer DA, Besley BD, Kennedy KB, Davey S. hRad9 rapidly binds DNA containing double-strand breaks and is required for damage-dependent topoisomerase II beta binding protein 1 focus formation. *Cancer Res*. 2003 Aug 15;63(16):4829-35
- Greenall A, Williams ES, Martin KA, Palmer JM, Gray J, Liu C, Whitehall SK. Hip3 interacts with the HIRA proteins Hip1 and SIm9 and is required for

transcriptional silencing and accurate chromosome segregation. *J Biol Chem.* 2006 Mar 31;281(13):8732-9.

- Greenfeder SA, Newlon CS. Replication forks pause at yeast centromeres. *Mol Cell Biol.* 1992 Sep;12(9):4056-66.
- Greer DA, Besley BD, Kennedy KB, Davey S. hRad9 rapidly binds DNA containing double-strand breaks and is required for damage-dependent topoisomerase II beta binding protein 1 focus formation. *Cancer Res.* 2003 Aug 15;63(16):4829-35.
- Grewal SI, Jia S. Heterochromatin revisited. *Nat Rev Genet.* 2007 Jan;8(1):35-46. Review.
- Guarente L. Synthetic enhancement in gene interaction: a genetic tool come of age. *Trends Genet.* 1993 Oct;9(10):362-6. Review.
- Hagan IM, Hyams JS. The use of cell division cycle mutants to investigate the control of microtubule distribution in the fission yeast *Schizosaccharomyces pombe*. *J Cell Sci.* 1988 Mar;89 (Pt 3):343-57.
- Haggard HW. The Conception of Cancer Before and After Johannes Müller. *Bull N Y Acad Med.* 1938 Apr;14(4):183-97.
- Handa T, Kanke M, Takahashi TS, Nakagawa T, Masukata H. DNA polymerization-independent functions of DNA polymerase epsilon in assembly and progression of the replisome in fission yeast. *Mol Biol Cell.* 2012 Aug;23(16):3240-53.
- Harris S, Kemplen C, Caspari T, Chan C, Lindsay HD, Poitelea M, Carr AM, Price C. Delineating the position of rad4+/cut5+ within the DNA-structure checkpoint pathways in *Schizosaccharomyces pombe*. *J Cell Sci.* 2003 Sep 1;116(Pt 17):3519-29.

- Hartman JL 4th, Garvik B, Hartwell L. Principles for the buffering of genetic variation. *Science*. 2001 Feb 9;291(5506):1001-4. Review.
- Hartwell LH. Nobel Lecture. Yeast and cancer. *Biosci Rep*. 2002 Jun-Aug;22(3-4):373-94.
- Harvey SL, Kellogg DR. Conservation of mechanisms controlling entry into mitosis: budding yeast wee1 delays entry into mitosis and is required for cell size control. *Curr Biol*. 2003 Feb 18;13(4):264-75.
- Hashimoto Y, Takisawa H. Xenopus Cut5 is essential for a CDK-dependent process in the initiation of DNA replication. *EMBO J*. 2003 May 15;22(10):2526-35.
- Hashimoto Y, Tsujimura T, Sugino A, Takisawa H. The phosphorylated C-terminal domain of Xenopus Cut5 directly mediates ATR-dependent activation of Chk1. *Genes Cells*. 2006 Sep;11(9):993-1007.
- Hayano M, Kanoh Y, Matsumoto S, Masai H. Mrc1 marks early-firing origins and coordinates timing and efficiency of initiation in fission yeast. *Mol Cell Biol*. 2011 Jun;31(12):2380-91.
- Hayashi MT, Takahashi TS, Nakagawa T, Nakayama J, Masukata H. The heterochromatin protein Swi6/HP1 activates replication origins at the pericentromeric region and silent mating-type locus. *Nat Cell Biol*. 2009 Mar;11(3):357-62.
- Hayles J, Nurse P. Genetics of the fission yeast *Schizosaccharomyces pombe*. *Annu Rev Genet*. 1992;26:373-402. Review.
- Heichinger C, Penkett CJ, Bähler J, Nurse P. Genome-wide characterization of fission yeast DNA replication origins. *EMBO J*. 2006 Nov 1;25(21):5171-9.

- Helleday T, Petermann E, Lundin C, Hodgson B, Sharma RA. DNA repair pathways as targets for cancer therapy. *Nat Rev Cancer*. 2008 Mar;8(3):193-204.
- Heller RC, Kang S, Lam WM, Chen S, Chan CS, Bell SP. Eukaryotic origin-dependent DNA replication in vitro reveals sequential action of DDK and S-CDK kinases. *Cell*. 2011 Jul 8;146(1):80-91.
- Herold S, Wanzel M, Beuger V, Frohme C, Beul D, Hillukkala T, Syvaioja J, Saluz HP, Haenel F, Eilers M. Negative regulation of the mammalian UV response by Myc through association with Miz-1. *Mol Cell*. 2002 Sep;10(3):509-21.
- Hicks WM, Yamaguchi M, Haber JE. Real-time analysis of double-strand DNA break repair by homologous recombination. *Proc Natl Acad Sci U S A*. 2011 Feb 22;108(8):3108-15.
- Hirano T, Funahashi S, Uemura T, Yanagida M. Isolation and characterization of *Schizosaccharomyces pombe* cutmutants that block nuclear division but not cytokinesis. *EMBO J*. 1986 Nov;5(11):2973-9.
- Hodgson B, Calzada A, Labib K. Mrc1 and Tof1 regulate DNA replication forks in different ways during normal S phase. *Mol Biol Cell*. 2007 Oct;18(10):3894-902.
- Hoess RH, Abremski K. Mechanism of strand cleavage and exchange in the Cre-lox site-specific recombination system. *J Mol Biol*. 1985 Feb 5;181(3):351-62.
- Hook SS, Lin JJ, Dutta A. Mechanisms to control rereplication and implications for cancer. *Curr Opin Cell Biol*. 2007 Dec;19(6):663-71. Epub 2007 Nov 28. Review.

- Horn C, Handler AM. Site-specific genomic targeting in *Drosophila*. *Proc Natl Acad Sci U S A*. 2005 Aug 30;102(35):12483-8.
- Ivessa AS, Lenzmeier BA, Bessler JB, Goudsouzian LK, Schnakenberg SL, Zakian VA. The *Saccharomyces cerevisiae* helicase Rrm3p facilitates replication past nonhistone protein-DNA complexes. *Mol Cell*. 2003 Dec;12(6):1525-36.
- Jallepalli PV, Brown GW, Muzi-Falconi M, Tien D, Kelly TJ. Regulation of the replication initiator protein p65cdc18 by CDK phosphorylation. *Genes Dev*. 1997 Nov 1;11(21):2767-79.
- Jeon Y, Lee KY, Ko MJ, Lee YS, Kang S, Hwang DS. Human TopBP1 participates in cyclin E/CDK2 activation and preinitiation complex assembly during G1/S transition. *J Biol Chem*. 2007 May 18;282(20):14882-90.
- Jeon Y, Ko E, Lee KY, Ko MJ, Park SY, Kang J, Jeon CH, Lee H, Hwang DS. TopBP1 deficiency causes an early embryonic lethality and induces cellular senescence in primary cells. *J Biol Chem*. 2011 Feb 18;286(7):5414-22.
- Kaguni, J.M., 2011. Replication initiation at the *Escherichia coli* chromosomal origin. *Current Opinion in Chemical Biology*, 15(5), pp.606-613.
- Kai M, Boddy MN, Russell P, Wang TS. Replication checkpoint kinase Cds1 regulates Mus81 to preserve genome integrity during replication stress. *Genes Dev*. 2005 Apr 15;19(8):919-32.
- Kamimura Y, Masumoto H, Sugino A, Araki H. Sld2, which interacts with Dpb11 in *Saccharomyces cerevisiae*, is required for chromosomal DNA replication. *Mol Cell Biol*. 1998 Oct;18(10):6102-9.

- Kamimura Y, Tak YS, Sugino A, Araki H. Sld3, which interacts with Cdc45 (Sld4), functions for chromosomal DNA replication in *Saccharomyces cerevisiae*. *EMBO J.* 2001 Apr 17;20(8):2097-107.
- Kanke M, Kodama Y, Takahashi TS, Nakagawa T, Masukata H. Mcm10 plays an essential role in origin DNA unwinding after loading of the CMG components. *EMBO J.* 2012 May 2;31(9):2182-94.
- Kanoh J, Russell P. Sln9, a novel nuclear protein involved in mitotic control in fission yeast. *Genetics.* 2000 Jun;155(2):623-31.
- Karppinen SM, Erkkö H, Reini K, Pospiech H, Heikkinen K, Rapakko K, Syväoja JE, Winqvist R. Identification of a common polymorphism in the TopBP1 gene associated with hereditary susceptibility to breast and ovarian cancer. *Eur J Cancer.* 2006 Oct;42(15):2647-52.
- Katou Y, Kanoh Y, Bando M, Noguchi H, Tanaka H, Ashikari T, Sugimoto K, Shirahige K. S-phase checkpoint proteins Tof1 and Mrc1 form a stable replication-pausing complex. *Nature.* 2003 Aug 28;424(6952):1078-83.
- Kelley R, Ideker T. Systematic interpretation of genetic interactions using protein networks. *Nat Biotechnol.* 2005 May;23(5):561-6.
- Kelman, Z., 1997. PCNA: structure, functions and interactions. *Oncogene*, 14(6).
- Kim DU, Hayles J, Kim D, Wood V, Park HO, Won M, Yoo HS, Duhig T, Nam M, Palmer G, Han S, Jeffery L, Baek ST, Lee H, Shim YS, Lee M, Kim L, Heo KS, Noh EJ, Lee AR, Jang YJ, Chung KS, Choi SJ, Park JY, Park Y, Kim HM, Park SK, Park HJ, Kang EJ, Kim HB, Kang HS, Park HM, Kim K, Song K, Song KB, Nurse P, Hoe KL. Analysis of a genome-wide set of gene deletions

in the fission yeast *Schizosaccharomyces pombe*. *Nat Biotechnol.* 2010 Jun;28(6):617-23.

- Kim JE, McAvoy SA, Smith DI, Chen J. Human TopBP1 ensures genome integrity during normal S phase. *Mol Cell Biol.* 2005 Dec;25(24):10907-15.
- Kim SM, Huberman JA. Regulation of replication timing in fission yeast. *EMBO J.* 2001 Nov 1;20(21):6115-26.
- Knudson AG Jr. Mutation and cancer: statistical study of retinoblastoma. *Proc Natl Acad Sci U S A.* 1971 Apr;68(4):820-3.
- Krings G, Bastia D. swi1- and swi3-dependent and independent replication fork arrest at the ribosomal DNA of *Schizosaccharomyces pombe*. *Proc Natl Acad Sci U S A.* 2004 Sep 28;101(39):14085-90.
- Kumagai A, Dunphy WG. Claspin, a novel protein required for the activation of Chk1 during a DNA replication checkpoint response in *Xenopus* egg extracts. *Mol Cell.* 2000 Oct;6(4):839-49.
- Kumagai A, Lee J, Yoo HY, Dunphy WG. TopBP1 activates the ATR-ATRIP complex. *Cell.* 2006 Mar 10;124(5):943-55.
- Kuntz K, O'Connell MJ. The G(2) DNA damage checkpoint: could this ancient regulator be the Achilles heel of cancer? *Cancer Biol Ther.* 2009 Aug;8(15):1433-9. Epub 2009 Aug 22. Review.
- Lee J, Kumagai A, Dunphy WG. The Rad9-Hus1-Rad1 checkpoint clamp regulates interaction of TopBP1 with ATR. *J Biol Chem.* 2007 Sep 21;282(38):28036-44.
- Labib K, Gambus A. A key role for the GINS complex at DNA replication forks. *Trends Cell Biol.* 2007 Jun;17(6):271-8. Review.

- Lambert S, Froget B, Carr AM. Arrested replication fork processing: interplay between checkpoints and recombination. *DNA Repair (Amst)*. 2007 Jul 1;6(7):1042-61.
- Lambert S, Watson A, Sheedy DM, Martin B, Carr AM. Gross chromosomal rearrangements and elevated recombination at an inducible site-specific replication fork barrier. *Cell*. 2005 Jun 3;121(5):689-702.
- Lamour V, Lécluse Y, Desmaze C, Spector M, Bodescot M, Aurias A, Osley MA, Lipinski M. A human homolog of the *S. cerevisiae* HIR1 and HIR2 transcriptional repressors cloned from the DiGeorge syndrome critical region. *Hum Mol Genet*. 1995 May;4(5):791-9.
- Langer SJ, Ghafoori AP, Byrd M, Leinwand L. A genetic screen identifies novel non-compatible loxP sites. *Nucleic Acids Res*. 2002 Jul 15;30(14):3067-77.
- Larimer FW, Perry JR, Hardigree AA. The REV1 gene of *Saccharomyces cerevisiae*: isolation, sequence, and functional analysis. *J Bacteriol*. 1989 Jan;171(1):230-7.
- Larner JM, Lee H, Little RD, Dijkwel PA, Schildkraut CL, Hamlin JL. Radiation down-regulates replication origin activity throughout the S phase in mammalian cells. *Nucleic Acids Res*. 1999 Feb 1;27(3):803-9.
- Lebofsky, R., Heilig, R., Sonnleitner, M., Weissenbach, J. and Bensimon, A., 2006. DNA replication origin interference increases the spacing between initiation events in human cells. *Molecular Biology of the Cell*, 17(12), pp.5337-5345.

- Lee BS, Grewal SI, Klar AJ. Biochemical interactions between proteins and mat1 cis-acting sequences required for imprinting in fission yeast. *Mol Cell Biol.* 2004 Nov;24(22):9813-22.
- Lee, Y.M. and Sicinski, P., 2006. Targeting cyclins and cyclin-dependent kinases in cancer: lessons from mice, hopes for therapeutic applications in humans. *Cell Cycle*, 5(18), pp.2110-2114.
- Legouras I, Xouri G, Dimopoulos S, Lygeros J, Lygerou Z. DNA replication in the fission yeast: robustness in the face of uncertainty. *Yeast.* 2006 Oct 15;23(13):951-62. Review.
- Leonard, A.C. and Méchali, M., 2013. DNA replication origins. *Cold Spring Harbor Perspectives in Biology*, 5(10), p.a010116.
- Leung CC, Sun L, Gong Z, Burkat M, Edwards R, Assmus M, Chen J, Glover JN. Structural insights into recognition of MDC1 by TopBP1 in DNA replication checkpoint control. *Structure.* 2013 Aug 6;21(8):1450-9.
- Li F, Martienssen R, Cande WZ. Coordination of DNA replication and histone modification by the Rik1-Dos2 complex. *Nature.* 2011 Jul 3;475(7355):244-8.
- Liachko, I. and Dunham, M.J., 2014. An autonomously replicating sequence for use in a wide range of budding yeasts. *FEMS Yeast Research*, 14(2), pp.364-367.
- Lin SJ, Wardlaw CP, Morishita T, Miyabe I, Chahwan C, Caspari T, Schmidt U, Carr AM, Garcia V. The Rad4(TopBP1) ATR-activation domain functions in G1/S phase in a chromatin-dependent manner. *PLoS Genet.* 2012 Jun;8(6):e1002801.

- Lin WC, Lin FT, Nevins JR. Selective induction of E2F1 in response to DNA damage, mediated by ATM-dependent phosphorylation. *Genes Dev.* 2001 Jul 15;15(14):1833-44.
- Lindahl T. Instability and decay of the primary structure of DNA. *Nature.* 1993 Apr 22;362(6422):709-15. Review.
- Lindsay HD, Griffiths DJ, Edwards RJ, Christensen PU, Murray JM, Osman F, Walworth N, Carr AM. S-phase-specific activation of Cds1 kinase defines a subpathway of the checkpoint response in *Schizosaccharomyces pombe*. *Genes Dev.* 1998 Feb 1;12(3):382-95.
- Lindsey-Boltz LA, Sancar A. Tethering DNA damage checkpoint mediator proteins topoisomerase IIbeta-binding protein 1 (TopBP1) and Claspin to DNA activates ataxia-telangiectasia mutated and RAD3-related (ATR) phosphorylation of checkpoint kinase 1 (Chk1). *J Biol Chem.* 2011 Jun 3;286(22):19229-36.
- Liu K, Bellam N, Lin HY, Wang B, Stockard CR, Grizzle WE, Lin WC. Regulation of p53 by TopBP1: a potential mechanism for p53 inactivation in cancer. *Mol Cell Biol.* 2009 May;29(10):2673-93.
- Liu K, Lin FT, Ruppert JM, Lin WC. Regulation of E2F1 by BRCT domain-containing protein TopBP1. *Mol Cell Biol.* 2003 May;23(9):3287-304.
- Liu K, Luo Y, Lin FT, Lin WC. TopBP1 recruits Brg1/Brm to repress E2F1-induced apoptosis, a novel pRb-independent and E2F1-specific control for cell survival. *Genes Dev.* 2004 Mar 15;18(6):673-86.
- Liu K, Paik JC, Wang B, Lin FT, Lin WC. Regulation of TopBP1 oligomerization by Akt/PKB for cell survival. *EMBO J.* 2006 Oct 18;25(20):4795-807.

- Liu S, Shiotani B, Lahiri M, Maréchal A, Tse A, Leung CC, Glover JN, Yang XH, Zou L. ATR autophosphorylation as a molecular switch for checkpoint activation. *Mol Cell*. 2011 Jul 22;43(2):192-202.
- Lopez-Girona A, Mondesert O, Leatherwood J, Russell P. Negative regulation of Cdc18 DNA replication protein by Cdc2. *Mol Biol Cell*. 1998 Jan;9(1):63-73.
- Lopez-Girona A, Tanaka K, Chen XB, Baber BA, McGowan CH, Russell P. Serine-345 is required for Rad3-dependent phosphorylation and function of checkpoint kinase Chk1 in fission yeast. *Proc Natl Acad Sci U S A*. 2001 Sep 25;98(20):11289-94.
- Lopez-Mosqueda J, Maas NL, Jonsson ZO, Defazio-Eli LG, Wohlschlegel J, Toczyski DP. Damage-induced phosphorylation of Sld3 is important to block late origin firing. *Nature*. 2010 Sep 23;467(7314):479-83.
- Lou H, Komata M, Katou Y, Guan Z, Reis CC, Budd M, Shirahige K, Campbell JL. Mrc1 and DNA polymerase epsilon function together in linking DNA replication and the S phase checkpoint. *Mol Cell*. 2008 Oct 10;32(1):106-17.
- Lucas I, Germe T, Chevrier-Miller M, Hyrien O. Topoisomerase II can unlink replicating DNA by precatenane removal. *EMBO J*. 2001 Nov 15;20(22):6509-19.
- Lygerou Z, Nurse P. The fission yeast origin recognition complex is constitutively associated with chromatin and is differentially modified through the cell cycle. *J Cell Sci*. 1999 Nov;112 (Pt 21):3703-12.
- Macheret M, Halazonetis TD. DNA replication stress as a hallmark of cancer. *Annu Rev Pathol*. 2015;10:425-48. doi: 10.1146/annurev-pathol-012414-040424. Review.
- Malumbres, M., 2014. Cyclin-dependent kinases. *Genome Biology*, 15(6), p.1.

- Malumbres M, Barbacid M. Cell cycle, CDKs and cancer: a changing paradigm. *Nat Rev Cancer*. 2009 Mar;9(3):153-66. doi: 10.1038/nrc2602. Review.
- Mantiero D, Mackenzie A, Donaldson A, Zegerman P. Limiting replication initiation factors execute the temporal programme of origin firing in budding yeast. *EMBO J*. 2011 Nov 11;30(23):4805-14.
- Mäkinen M, Hillukkala T, Tuusa J, Reini K, Vaara M, Huang D, Pospiech H, Majuri I, Westerling T, Mäkelä TP, Syväoja JE. BRCT domain-containing protein TopBP1 functions in DNA replication and damage response. *J Biol Chem*. 2001 Aug 10;276(32):30399-406.
- Maric C, Prioleau MN. Interplay between DNA replication and gene expression: a harmonious coexistence. *Curr Opin Cell Biol*. 2010 Jun;22(3):277-83.
- Martín-Castellanos C, Blanco MA, de Prada JM, Moreno S. The puc1 cyclin regulates the G1 phase of the fission yeast cell cycle in response to cell size. *Mol Biol Cell*. 2000 Feb;11(2):543-54.
- Masumoto H, Muramatsu S, Kamimura Y, Araki H. S-Cdk-dependent phosphorylation of Sld2 essential for chromosomal DNA replication in budding yeast. *Nature*. 2002 Feb 7;415(6872):651-5.
- Masumoto H, Sugino A, Araki H. Dpb11 controls the association between DNA polymerases alpha and epsilon and the autonomously replicating sequence region of budding yeast. *Mol Cell Biol*. 2000 Apr;20(8):2809-17.
- Maya-Mendoza, A., Ostrakova, J., Kosar, M., Hall, A., Duskova, P., Mistrik, M., Merchut-Maya, J.M., Hodny, Z., Bartkova, J., Christensen, C. and Bartek, J., 2015. Myc and Ras oncogenes engage different energy metabolism

programs and evoke distinct patterns of oxidative and DNA replication stress. *Molecular Oncology*, 9(3), pp.601-616.

- McFarlane RJ, Mian S, Dalgaard JZ. The many facets of the Tim-Tipin protein families' roles in chromosome biology. *Cell Cycle*. 2010 Feb 15;9(4):700-5.
- McIntosh, D. and Blow, J.J., 2012. Dormant origins, the licensing checkpoint, and the response to replicative stresses. *Cold Spring Harbor Perspectives in Biology*, 4(10), p.a012955.
- Mehanna A, Diffley JF. Pre-replicative complex assembly with purified proteins. *Methods*. 2012 Jun;57(2):222-6.
- Miki T, Smith CL, Long JE, Eva A, Fleming TP. Oncogene *ect2* is related to regulators of small GTP-binding proteins. *Nature*. 1993 Apr 1;362(6419):462-5. Erratum in: *Nature* 1993 Aug 19;364(6439):737.
- Mimura S, Takisawa H. *Xenopus* Cdc45-dependent loading of DNA polymerase alpha onto chromatin under the control of S-phase Cdk. *EMBO J*. 1998 Oct 1;17(19):5699-707.
- Mizuki F, Tanaka A, Hirose Y, Ohkuma Y. The HIRA complex subunit Hip3 plays important roles in the silencing of meiosis-specific genes in *Schizosaccharomyces pombe*. *PLoS One*. 2011 Apr 29;6(4):e19442.
- Mondesert O, McGowan CH, Russell P. Cig2, a B-type cyclin, promotes the onset of S in *Schizosaccharomyces pombe*. *Mol Cell Biol*. 1996 Apr;16(4):1527-33.
- Mordes DA, Glick GG, Zhao R, Cortez D. TopBP1 activates ATR through ATRIP and a PIKK regulatory domain. *Genes Dev*. 2008 Jun 1;22(11):1478-89.(A)

- Mordes DA, Nam EA, Cortez D. Dpb11 activates the Mec1-Ddc2 complex. *Proc Natl Acad Sci U S A.* 2008 Dec 2;105(48):18730-4 (B)
- Morgan, D. *The cell cycle: principles of control*: Oxford University Press. 2007
- Moreno S, Klar A, Nurse P. Molecular genetic analysis of fission yeast *Schizosaccharomyces pombe*. *Methods Enzymol.* 1991;194:795-823.
- Morishima K, Sakamoto S, Kobayashi J, Izumi H, Suda T, Matsumoto Y, Tauchi H, Ide H, Komatsu K, Matsuura S. TopBP1 associates with NBS1 and is involved in homologous recombination repair. *Biochem Biophys Res Commun.* 2007 Nov 3;362(4):872-9.
- Moser BA, Russell P. Cell cycle regulation in *Schizosaccharomyces pombe*. *Curr Opin Microbiol.* 2000 Dec;3(6):631-6. Review.
- Moyer SE, Lewis PW, Botchan MR. Isolation of the Cdc45/Mcm2-7/GINS (CMG) complex, a candidate for the eukaryotic DNA replication fork helicase. *Proc Natl Acad Sci U S A.* 2006 Jul 5;103(27):10236-41.
- Müller, C.A., Hawkins, M., Retkute, R., Malla, S., Wilson, R., Blythe, M.J., Nakato, R., Komata, M., Shirahige, K., de Moura, A.P. and Nieduszynski, C.A., 2013. The dynamics of genome replication using deep sequencing. *Nucleic Acids Research*, 42(1), e3.
- Muraki K, Nyhan K, Han L, Murnane JP. Mechanisms of telomere loss and their consequences for chromosome instability. *Front Oncol.* 2012 Oct 4;2:135.
- Musgrove EA, Caldon CE, Barraclough J, Stone A, Sutherland RL. Cyclin D as a therapeutic target in cancer. *Nat Rev Cancer.* 2011 Jul 7;11(8):558-72. doi: 10.1038/nrc3090. Review.

- Namiki Y, Zou L. ATRIP associates with replication protein A-coated ssDNA multiple interactions. *Proc Natl Acad Sci U S A*. 2006 Jan 17;103(3):580-5.
- Navadgi-Patil VM, Burgers PM. Yeast DNA replication protein Dpb11 activates the Mec1/ATR checkpoint kinase. *J Biol Chem*. 2008 Dec 19;283(51):35853-9.
- Navadgi-Patil VM, Kumar S, Burgers PM. The unstructured C-terminal tail of yeast Dpb11 (human TopBP1) protein is dispensable for DNA replication and the S phase checkpoint but required for the G2/M checkpoint. *J Biol Chem*. 2011 Nov 25;286(47):40999-1007.
- Negrini S, Gorgoulis VG, Halazonetis TD. Genomic instability--an evolving hallmark of cancer. *Nat Rev Mol Cell Biol*. 2010 Mar;11(3):220-8. doi: 10.1038/nrm2858. Review.
- Nevins JR. The Rb/E2F pathway and cancer. *Hum Mol Genet*. 2001 Apr;10(7):699-703. Review.
- Nieduszynski, C.A., Knox, Y. and Donaldson, A.D., 2006. Genome-wide identification of replication origins in yeast by comparative genomics. *Genes & Development*, 20(14), pp.1874-1879.
- Noguchi E, Noguchi C, Du LL, Russell P. Swi1 prevents replication fork collapse and controls checkpoint kinase Cds1. *Mol Cell Biol*. 2003 Nov;23(21):7861-74.
- Noguchi E, Noguchi C, McDonald WH, Yates JR 3rd, Russell P. Swi1 and Swi3 are components of a replication fork protection complex in fission yeast. *Mol Cell Biol*. 2004 Oct;24(19):8342-55.

- Noguchi C, Rapp JB, Skorobogatko YV, Bailey LD, Noguchi E. Swi1 associates with chromatin through the DDT domain and recruits Swi3 to preserve genomic integrity. *PLoS One*. 2012;7(8):e43988.
- Noguchi E, Shanahan P, Noguchi C, Russell P. CDK phosphorylation of Drc1 regulates DNA replication in fission yeast. *Curr Biol*. 2002 Apr 2;12(7):599-605.
- Nurse P, Masui Y, Hartwell L. Understanding the cell cycle. *Nat Med*. 1998 Oct;4(10):1103-6.
- Nurse P, Thuriaux P, Nasmyth K. Genetic control of the cell division cycle in the fission yeast *Schizosaccharomyces pombe*. *Mol Gen Genet*. 1976 Jul 23;146(2):167-78.
- Ogiwara H, Ui A, Onoda F, Tada S, Enomoto T, Seki M. Dpb11, the budding yeast homolog of TopBP1, functions with the checkpoint clamp in recombination repair. *Nucleic Acids Res*. 2006 Jul 13;34(11):3389-98.
- Okazaki K, Okazaki N, Kume K, Jinno S, Tanaka K, Okayama H. High-frequency transformation method and library transducing vectors for cloning mammalian cDNAs by trans-complementation of *Schizosaccharomyces pombe*. *Nucleic Acids Res*. 1990 Nov 25;18(22):6485-9.
- Ostermann K, Lorentz A, Schmidt H. The fission yeast *rad22* gene, having a function in mating-type switching and repair of DNA damages, encodes a protein homolog to Rad52 of *Saccharomyces cerevisiae*. *Nucleic Acids Res*. 1993 Dec 25;21(25):5940-4.
- Paixão S, Colaluca IN, Cubells M, Peverali FA, Destro A, Giadrossi S, Giacca M, Falaschi A, Riva S, Biamonti G. Modular structure of the human lamin B2 replicator. *Mol Cell Biol*. 2004 Apr;24(7):2958-67.

- Pan X, Ye P, Yuan DS, Wang X, Bader JS, Boeke JD. A DNA integrity network in the yeast *Saccharomyces cerevisiae*. *Cell*. 2006 Mar 10;124(5):1069-81. Epub 2006 Feb 16. Erratum in: *Cell*. 2013 May 23;153(5):1165.
- Park YJ, Luger K. Histone chaperones in nucleosome eviction and histone exchange. *Curr Opin Struct Biol* 2008; 18:282-9;
- Parrilla-Castellar ER, Arlander SJ, Karnitz L. Dial 9-1-1 for DNA damage: the Rad9-Hus1-Rad1 (9-1-1) clamp complex. *DNA Repair (Amst)*. 2004 Aug-Sep;3(8-9):1009-14. Review.
- Paulsen RD, Cimprich KA. The ATR pathway: fine-tuning the fork. *DNA Repair (Amst)*. 2007 Jul 1;6(7):953-66. Review.
- Petermann E, Helleday T, Caldecott KW. Claspin promotes normal replication fork rates in human cells. *Mol Biol Cell*. 2008 Jun;19(6):2373-8.
- Pfander B, Diffley JF. Dpb11 coordinates Mec1 kinase activation with cell cycle-regulated Rad9 recruitment. *EMBO J*. 2011 Sep 23;30(24):4897-907.
- Prochasson P, Florens L, Swanson SK, Washburn MP, Workman JL. The HIR corepressor complex binds to nucleosomes generating a distinct protein/DNA complex resistant to remodeling by SWI/SNF. *Genes Dev*. 2005 Nov 1;19(21):2534-9.
- Puddu F, Granata M, Di Nola L, Balestrini A, Piergiovanni G, Lazzaro F, Giannattasio M, Plevani P, Muzi-Falconi M. Phosphorylation of the budding yeast 9-1-1 complex is required for Dpb11 function in the full activation of the UV-induced DNA damage checkpoint. *Mol Cell Biol*. 2008 Aug;28(15):4782-93.

- Qu M, Rappas M, Wardlaw CP, Garcia V, Ren JY, Day M, Carr AM, Oliver AW, Du LL, Pearl LH. Phosphorylation-dependent assembly and coordination of the DNA damage checkpoint apparatus by Rad4(TopBP1). *Mol Cell*. 2013 Sep 26;51(6):723-736.
- Qu M, Yang B, Tao L, Yates JR 3rd, Russell P, Dong MQ, Du LL. Phosphorylation-dependent interactions between Crb2 and Chk1 are essential for DNA damage checkpoint. *PLoS Genet*. 2012 Jul;8(7):e1002817.
- Qin XQ, Livingston DM, Kaelin WG Jr, Adams PD. Deregulated transcription factor E2F-1 expression leads to S-phase entry and p53-mediated apoptosis. *Proc Natl Acad Sci U S A*. 1994 Nov 8;91(23):10918-22.
- Raghuraman MK, Brewer BJ, Fangman WL. Cell cycle-dependent establishment of a late replication program. *Science*. 1997 May 2;276(5313):806-9.
- Raghuraman, M.K., Winzeler, E.A., Collingwood, D., Hunt, S., Wodicka, L., Conway, A., Lockhart, D.J., Davis, R.W., Brewer, B.J. and Fangman, W.L., 2001. Replication dynamics of the yeast genome. *Science*, 294(5540), pp.115-121.
- Ralph E, Boye E, Kearsey SE. DNA damage induces Cdt1 proteolysis in fission yeast through a pathway dependent on Cdt2 and Ddb1. *EMBO Rep*. 2006 Nov;7(11):1134-9. Epub 2006 Oct 13. Erratum in: *EMBO Rep*. 2007 Feb;8(2):200.
- Ransom M, Dennehey BK, Tyler JK. Chaperoning histones during DNA replication and repair. *Cell* 2010; 140:183-95;
- Rapp JB, Noguchi C, Das MM, Wong LK, Ansbach AB, Holmes AM, Arcangioli B, Noguchi E. Checkpoint-dependent and -independent roles of

Swi3 in replication fork recovery and sister chromatid cohesion in fission yeast. *PLoS One*. 2010 Oct 12;5(10):e13379

- Rappas M, Oliver AW, Pearl LH. Structure and function of the Rad9-binding region of the DNA-damage checkpoint adaptor TopBP1. *Nucleic Acids Res*. 2011 Jan;39(1):313-24. doi: 10.1093/nar/gkq743. Epub 2010 Aug 19. Erratum in: *Nucleic Acids Res*. 2013 Apr;41(8):4741.
- Rebbeck TR, Mitra N, Domchek SM, Wan F, Chuai S, Friebel TM, Panossian S, Spurdle A, Chenevix-Trench G; kConFab, Singer CF, Pfeiler G, Neuhausen SL, Lynch HT, Garber JE, Weitzel JN, Isaacs C, Couch F, Narod SA, Rubinstein WS, Tomlinson GE, Ganz PA, Olopade OI, Tung N, Blum JL, Greenberg R, Nathanson KL, Daly MB. Modification of ovarian cancer risk by BRCA1/2-interacting genes in a multicenter cohort of BRCA1/2 mutation carriers. *Cancer Res*. 2009 Jul 15;69(14):5801-10.
- Ren B, Cam H, Takahashi Y, Volkert T, Terragni J, Young RA, Dynlacht BD. E2F integrates cell cycle progression with DNA repair, replication, and G(2)/M checkpoints. *Genes Dev*. 2002 Jan 15;16(2):245-56.
- Rhind N, Russell P. Tyrosine phosphorylation of cdc2 is required for the replication checkpoint in *Schizosaccharomyces pombe*. *Mol Cell Biol*. 1998 Jul;18(7):3782-7.
- Rhind N, Russell P. Chk1 and Cds1: linchpins of the DNA damage and replication checkpoint pathways. *J Cell Sci*. 2000 Nov;113 (Pt 22):3889-96. Review.
- Rhind N, Russell P. Roles of the mitotic inhibitors Wee1 and Mik1 in the G(2)DNA damage and replication checkpoints. *Mol Cell Biol*. 2001 Mar;21(5):1499-508.

- Robinson, A. and van Oijen, A.M., 2013. Bacterial replication, transcription and translation: mechanistic insights from single-molecule biochemical studies. *Nature Reviews Microbiology*, 11(5), pp.303-315.
- Roos-Mattjus P, Hopkins KM, Oestreich AJ, Vroman BT, Johnson KL, Naylor S, Lieberman HB, Karnitz LM. Phosphorylation of human Rad9 is required for genotoxin-activated checkpoint signaling. *J Biol Chem*. 2003 Jul 4;278(27):24428-37.
- Sabatinos SA, Green MD, Forsburg SL. Continued DNA synthesis in replication checkpoint mutants leads to fork collapse. *Mol Cell Biol*. 2012 Dec;32(24):4986-97.
- Saka Y, Esashi F, Matsusaka T, Mochida S, Yanagida M. Damage and replication checkpoint control in fission yeast is ensured by interactions of Crb2, a protein with BRCT motif, with Cut5 and Chk1. *Genes Dev*. 1997 Dec 15;11(24):3387-400.
- Saka Y, Fantes P, Sutani T, McInerney C, Creanor J, Yanagida M. Fission yeast cut5 links nuclear chromatin and M phase regulator in the replication checkpoint control. *EMBO J*. 1994 Nov 15;13(22):5319-29.
- Saka Y, Yanagida M. Fission yeast cut5+, required for S phase onset and M phase restraint, is identical to the radiation-damage repair gene rad4+. *Cell*. 1993 Jul 30;74(2):383-93.
- Samejima I, Matsumoto T, Nakaseko Y, Beach D, Yanagida M. Identification of seven new cut genes involved in *Schizosaccharomyces pombe* mitosis. *J Cell Sci*. 1993 May;105 (Pt 1):135-43.
- Sanjiv K, Hagenkort A, Calderón-Montaña JM, Koolmeister T, Reaper PM, Mortusewicz O, Jacques SA, Kuiper RV, Schultz N, Scobie M, Charlton PA,

Pollard JR, Berglund UW, Altun M, Helleday T. Cancer-Specific Synthetic Lethality between ATR and CHK1 Kinase Activities. *Cell Rep.* 2016 Jan 12;14(2):298-309.

- Santocanale C, Diffley JF. A Mec1- and Rad53-dependent checkpoint controls late-firing origins of DNA replication. *Nature.* 1998 Oct 8;395(6702):615-8.
- Schafer KA. The cell cycle: a review. *Vet Pathol.* 1998 Nov;35(6):461-78. Review.
- Schmidt U, Wollmann Y, Franke C, Grosse F, Saluz HP, Hänel F. Characterization of the interaction between the human DNA topoisomerase IIbeta-binding protein 1 (TopBP1) and the cell division cycle 45 (Cdc45) protein. *Biochem J.* 2008 Jan 1;409(1):169-77.
- Schüpbach M. The isolation and genetic classification of UV-sensitive mutants of *Schizosaccharomyces pombe*. *Mutat Res.* 1971 Apr;11(4):361-71.
- Sclafani RA, Holzen TM. Cell cycle regulation of DNA replication. *Annu Rev Genet.* 2007;41:237-80. Review.
- Segurado M, de Luis A, Antequera F. Genome-wide distribution of DNA replication origins at A+T-rich islands in *Schizosaccharomyces pombe*. *EMBO Rep.* 2003 Nov;4(11):1048-53.
- Seibler J, Zevnik B, Küter-Luks B, Andreas S, Kern H, Hennek T, Rode A, Heimann C, Faust N, Kauselmann G, Schoor M, Jaenisch R, Rajewsky K, Kühn R, Schwenk F. Rapid generation of inducible mouse mutants. *Nucleic Acids Res.* 2003 Feb 15;31(4):e12.
- Seol HJ, Yoo HY, Jin J, Joo KM, Kim HS, Yoon SJ, Choi SH, Kim Y, Pyo HR, Lim DH, Kim W, Um HD, Kim JH, Lee JI, Nam DH. The expression of DNA

damage checkpoint proteins and prognostic implication in metastatic brain tumors. *Oncol Res.* 2011;19(8-9):381-90.(A)

- Seol HJ, Yoo HY, Jin J, Joo KM, Kong DS, Yoon SJ, Yang H, Kang W, Lim DH, Park K, Kim JH, Lee JI, Nam DH. Prognostic implications of the DNA damage response pathway in glioblastoma. *Oncol Rep.* 2011 Aug;26(2):423-30. (B)
- Shackleton, N.J. and Peltier, W.R., 1992. ATP-dependent recognition of eukaryotic origins of DNA replication by a multiprotein complex. *Nature*, 357.
- Sheldrick KS, Carr AM. Feedback controls and G2 checkpoints: fission yeast as a model system. *Bioessays.* 1993 Dec;15(12):775-82. Review.
- Shimamoto M, Matsumoto S, Odagiri Y, Noguchi E, Russell P, Masai H. Interactions between Swi1-Swi3, Mrc1 and S phase kinase, Hsk1 may regulate cellular responses to stalled replication forks in fission yeast. *Genes Cells.* 2009 Jun;14(6):669-82. doi: 10.1111/j.1365-2443.2009.01300.x. Epub 2009 Apr 30. Erratum in: *Genes Cells.* 2010 Mar;15(3):313.
- Shirahige K, Hori Y, Shiraishi K, Yamashita M, Takahashi K, Obuse C, Tsurimoto T, Yoshikawa H. Regulation of DNA-replication origins during cell-cycle progression. *Nature.* 1998 Oct 8;395(6702):618-21.
- Simanis V, Carr AM, Goss M, Lee MG, MacNeill SA, Nurse P. Cell cycle regulation in yeasts and man: towards a unifying mechanism. *Antonie Van Leeuwenhoek.* 1987;53(5):319-23. Review.
- Simanis V, Hayles J, Nurse P. Control over the onset of DNA synthesis in fission yeast. *Philos Trans R Soc Lond B Biol Sci.* 1987 Dec 15;317(1187):507-16. Review.

- Sipiczki M. Where does fission yeast sit on the tree of life? *Genome Biol.* 2000;1(2):REVIEWS1011. Epub 2000 Aug 4. Review.
- Spector MS, Raff A, DeSilva H, Lee K, Osley MA. Hir1p and Hir2p function as transcriptional corepressors to regulate histone gene transcription in the *Saccharomyces cerevisiae* cell cycle. *Mol Cell Biol.* 1997 Feb;17(2):545-52.
- St Onge RP, Besley BD, Pelley JL, Davey S. A role for the phosphorylation of hRad9 in checkpoint signaling. *J Biol Chem.* 2003 Jul 18;278(29):26620-8.
- Stevens C, La Thangue NB. The emerging role of E2F-1 in the DNA damage response and checkpoint control. *DNA Repair (Amst).* 2004 Aug-Sep;3(8-9):1071-9. Review.
- Stiff T, Walker SA, Cerosaletti K, Goodarzi AA, Petermann E, Concannon P, O'Driscoll M, Jeggo PA. ATR-dependent phosphorylation and activation of ATM in response to UV treatment or replication fork stalling. *EMBO J.* 2006 Dec 13;25(24):5775-82.
- Sun, W. and Yang, J., 2010. Functional mechanisms for human tumor suppressors. *Journal of Cancer*, 1, pp.136-140.
- Sung MK, Huh WK. Bimolecular fluorescence complementation analysis system for in vivo detection of protein-protein interaction in *Saccharomyces cerevisiae*. *Yeast.* 2007 Sep;24(9):767-75.
- Syljuåsen RG, Sørensen CS, Hansen LT, Fugger K, Lundin C, Johansson F, Helleday T, Sehested M, Lukas J, Bartek J. Inhibition of human Chk1 causes increased initiation of DNA replication, phosphorylation of ATR targets, and DNA breakage. *Mol Cell Biol.* 2005 May;25(9):3553-62.

- Szyjka SJ, Viggiani CJ, Aparicio OM. Mrc1 is required for normal progression of replication forks throughout chromatin in *S. cerevisiae*. *Mol Cell*. 2005 Sep 2;19(5):691-7.
- Tak YS, Tanaka Y, Endo S, Kamimura Y, Araki H. A CDK-catalysed regulatory phosphorylation for formation of the DNA replication complex Sld2-Dpb11. *EMBO J*. 2006 May 3;25(9):1987-96.
- Takayama Y, Kamimura Y, Okawa M, Muramatsu S, Sugino A, Araki H. GINS, a novel multiprotein complex required for chromosomal DNA replication in budding yeast. *Genes Dev*. 2003 May 1;17(9):1153-65.
- Takeda, D.Y. and Dutta, A., 2005. DNA replication and progression through S phase. *Oncogene*, 24(17), pp.2827-2843.
- Tanaka K, Russell P. Mrc1 channels the DNA replication arrest signal to checkpoint kinase Cds1. *Nat Cell Biol*. 2001 Nov;3(11):966-72.
- Tanaka S, Araki H. Regulation of the initiation step of DNA replication by cyclin-dependent kinases. *Chromosoma*. 2010 Dec;119(6):565-74.
- Tanaka S, Tak YS, Araki H. The role of CDK in the initiation step of DNA replication in eukaryotes. *Cell Div*. 2007 Jun 5;2:16.
- Tanaka S, Umemori T, Hirai K, Muramatsu S, Kamimura Y, Araki H. CDK-dependent phosphorylation of Sld2 and Sld3 initiates DNA replication in budding yeast. *Nature*. 2007 Jan 18;445(7125):328-32.
- Tanaka T, Yokoyama M, Matsumoto S, Fukatsu R, You Z, Masai H. Fission yeast Swi1-Swi3 complex facilitates DNA binding of Mrc1. *J Biol Chem*. 2010 Dec 17;285(51):39609-22.

- Taricani L, Wang TS. Rad4TopBP1, a scaffold protein, plays separate roles in DNA damage and replication checkpoints and DNA replication. *Mol Biol Cell*. 2006 Aug;17(8):3456-68.
- Taylor M, Moore K, Murray J, Aves SJ, Price C. Mcm10 interacts with Rad4/Cut5(TopBP1) and its association with origins of DNA replication is dependent on Rad4/Cut5(TopBP1). *DNA Repair (Amst)*. 2011 Nov 10;10(11):1154-63.
- Tercero JA, Labib K, Diffley JF. DNA synthesis at individual replication forks requires the essential initiation factor Cdc45p. *EMBO J*. 2000 May 2;19(9):2082-93.
- Tercero JA, Longhese MP, Diffley JF. A central role for DNA replication forks in checkpoint activation and response. *Mol Cell*. 2003 May;11(5):1323-36.
- "The Nobel Prize in Physiology or Medicine 2001". Nobelprize.org. 3 Jul 2012 http://www.nobelprize.org/nobel_prizes/medicine/laureates/2001/
- Thompson LH, Brookman KW, Jones NJ, Allen SA, Carrano AV. Molecular cloning of the human XRCC1 gene, which corrects defective DNA strand break repair and sister chromatid exchange. *Mol Cell Biol*. 1990 Dec;10(12):6160-71.
- Ticau, S., Friedman, L.J., Ivica, N.A., Gelles, J. and Bell, S.P., 2015. Single-molecule studies of origin licensing reveal mechanisms ensuring bidirectional helicase loading. *Cell*, 161(3), pp.513-525.
- Tong AH, Evangelista M, Parsons AB, Xu H, Bader GD, Pagé N, Robinson M, Raghibizadeh S, Hogue CW, Bussey H, Andrews B, Tyers M, Boone C. Systematic genetic analysis with ordered arrays of yeast deletion mutants. *Science*. 2001 Dec 14;294(5550):2364-8.

- Tourrière H, Versini G, Cordon-Preciado V, Alabert C, Pasero P. Mrc1 and Tof1 promote replication fork progression and recovery independently of Rad53. *Mol Cell*. 2005 Sep 2;19(5):699-706.
- Truong LN, Wu X. Prevention of DNA re-replication in eukaryotic cells. *J Mol Cell Biol*. 2011 Feb;3(1):13-22. doi: 10.1093/jmcb/mjq052. Review.
- Tuduri, S., Tourrière, H. and Pasero, P., 2010. Defining replication origin efficiency using DNA fiber assays. *Chromosome Research*, 18(1), pp.91-102.
- Tyson JJ, Novak B. Temporal organization of the cell cycle. *Curr Biol*. 2008 Sep 9;18(17):R759-R768. doi: 10.1016/j.cub.2008.07.001. Review.
- Unsal-Kaçmaz K, Sancar A. Quaternary structure of ATR and effects of ATRIP and replication protein A on its DNA binding and kinase activities. *Mol Cell Biol*. 2004 Feb;24(3):1292-300.
- Van C, Yan S, Michael WM, Waga S, Cimprich KA. Continued primer synthesis at stalled replication forks contributes to checkpoint activation. *J Cell Biol*. 2010 Apr 19;189(2):233-46.
- Wang H, Elledge SJ. DRC1, DNA replication and checkpoint protein 1, functions with DPB11 to control DNA replication and the S-phase checkpoint in *Saccharomyces cerevisiae*. *Proc Natl Acad Sci U S A*. 1999 Mar 30;96(7):3824-9.
- Wang H, Elledge SJ. Genetic and physical interactions between DPB11 and DDC1 in the yeast DNA damage response pathway. *Genetics*. 2002 Apr;160(4):1295-304.
- Wang J, Gong Z, Chen J. MDC1 collaborates with TopBP1 in DNA replication checkpoint control. *J Cell Biol*. 2011 Apr 18;193(2):267-73.

- Ward IM, Chen J. Histone H2AX is phosphorylated in an ATR-dependent manner in response to replicational stress. *J Biol Chem*. 2001 Dec 21;276(51):47759-62.
- Warmerdam DO, Kanaar R. Dealing with DNA damage: relationships between checkpoint and repair pathways. *Mutat Res*. 2010 Apr-Jun;704(1-3):2-11. doi: 10.1016/j.mrrev.2009.12.001. Epub 2009 Dec 16. Review.
- Watson AT, Garcia V, Bone N, Carr AM, Armstrong J. Gene tagging and gene replacement using recombinase-mediated cassette exchange in *Schizosaccharomyces pombe*. *Gene*. 2008 Jan 15;407(1-2):63-74.
- Watson AT, Werler P, Carr AM. Regulation of gene expression at the fission yeast *Schizosaccharomyces pombe* *urg1* locus. *Gene*. 2011 Sep 15;484(1-2):75-85.
- WATSON JD, CRICK FH. Molecular structure of nucleic acids; a structure for deoxyribose nucleic acid. *Nature*. 1953 Apr 25;171(4356):737-8.
- Watt S, Mata J, López-Maury L, Marguerat S, Burns G, Bähler J. *urg1*: a uracil-regulatable promoter system for fission yeast with short induction and repression times. *PLoS One*. 2008 Jan 16;3(1):e1428.
- Wolkow TD, Enoch T. Fission yeast Rad26 is a regulatory subunit of the Rad3 checkpoint kinase. *Mol Biol Cell*. 2002 Feb;13(2):480-92.
- Wollmann Y, Schmidt U, Wieland GD, Zipfel PF, Saluz HP, Hänel F. The DNA topoisomerase IIbeta binding protein 1 (TopBP1) interacts with poly (ADP-ribose) polymerase (PARP-1). *J Cell Biochem*. 2007 Sep 1;102(1):171-82.
- Wood V, Gwilliam R, Rajandream MA, Lyne M, Lyne R, Stewart A, Sgouros J, Peat N, Hayles J, Baker S, Basham D, Bowman S, Brooks K, Brown D, Brown S, Chillingworth T, Churcher C, Collins M, Connor R, Cronin A, Davis P,

Feltwell T, Fraser A, Gentles S, Goble A, Hamlin N, Harris D, Hidalgo J, Hodgson G, Holroyd S, Hornsby T, Howarth S, Huckle EJ, Hunt S, Jagels K, James K, Jones L, Jones M, Leather S, McDonald S, McLean J, Mooney P, Moule S, Mungall K, Murphy L, Niblett D, Odell C, Oliver K, O'Neil S, Pearson D, Quail MA, Rabinowitsch E, Rutherford K, Rutter S, Saunders D, Seeger K, Sharp S, Skelton J, Simmonds M, Squares R, Squares S, Stevens K, Taylor K, Taylor RG, Tivey A, Walsh S, Warren T, Whitehead S, Woodward J, Volckaert G, Aert R, Robben J, Grymonprez B, Weltjens I, Vanstreels E, Rieger M, Schäfer M, Müller-Auer S, Gabel C, Fuchs M, Düsterhöft A, Fritzc C, Holzer E, Moestl D, Hilbert H, Borzym K, Langer I, Beck A, Lehrach H, Reinhardt R, Pohl TM, Eger P, Zimmermann W, Wedler H, Wambutt R, Purnelle B, Goffeau A, Cadieu E, Dréano S, Gloux S, Lelaure V, Mottier S, Galibert F, Aves SJ, Xiang Z, Hunt C, Moore K, Hurst SM, Lucas M, Rochet M, Gaillardin C, Tallada VA, Garzon A, Thode G, Daga RR, Cruzado L, Jimenez J, Sánchez M, del Rey F, Benito J, Domínguez A, Revuelta JL, Moreno S, Armstrong J, Forsburg SL, Cerutti L, Lowe T, McCombie WR, Paulsen I, Potashkin J, Shpakovski GV, Ussery D, Barrell BG, Nurse P. The genome sequence of *Schizosaccharomyces pombe*. *Nature*. 2002 Feb 21;415(6874):871-80. Erratum in: *Nature* 2003 Jan 2;421(6918):94.

- Wright RH, Dornan ES, Donaldson MM, Morgan IM. TopBP1 contains a transcriptional activation domain suppressed by two adjacent BRCT domains. *Biochem J*. 2006 Dec 15;400(3):573-82.
- Xu YJ, Davenport M, Kelly TJ. Two-stage mechanism for activation of the DNA replication checkpoint kinase Cds1 in fission yeast. *Genes Dev*. 2006 Apr 15;20(8):990-1003.

- Yabuuchi H, Yamada Y, Uchida T, Sunathvanichkul T, Nakagawa T, Masukata H. Ordered assembly of Sld3, GINS and Cdc45 is distinctly regulated by DDK and CDK for activation of replication origins. *EMBO J.* 2006 Oct 4;25(19):4663-74.
- Yamane K, Mizuguchi T, Cui B, Zofall M, Noma K, Grewal SI. Asf1/HIRA facilitate global histone deacetylation and associate with HP1 to promote nucleosome occupancy at heterochromatic loci. *Mol Cell.* 2011 Jan 7;41(1):56-66.
- Yamane K, Wu X, Chen J. A DNA damage-regulated BRCT-containing protein, TopBP1, is required for cell survival. *Mol Cell Biol.* 2002 Jan;22(2):555-66.
- Yamamoto RR, Axton JM, Yamamoto Y, Saunders RD, Glover DM, Henderson DS. The *Drosophila* mus101 gene, which links DNA repair, replication and condensation of heterochromatin in mitosis, encodes a protein with seven BRCA1 C-terminus domains. *Genetics.* 2000 Oct;156(2):711-21.
- Yan S, Lindsay HD, Michael WM. Direct requirement for Xmus101 in ATR-mediated phosphorylation of Claspin bound Chk1 during checkpoint signaling. *J Cell Biol.* 2006 Apr 24;173(2):181-6.
- Yan S, Michael WM. TopBP1 and DNA polymerase alpha-mediated recruitment of the 9-1-1 complex to stalled replication forks: implications for a replication restart-based mechanism for ATR checkpoint activation. *Cell Cycle.* 2009 Sep 15;8(18):2877-84. Epub 2009 Sep 9. Review.
- Yan S, Willis J. WD40-repeat protein WDR18 collaborates with TopBP1 to facilitate DNA damage checkpoint signaling. *Biochem Biophys Res Commun.* 2013 Feb 15;431(3):466-71.

- Yeeles, J.T., Deegan, T.D., Janska, A., Early, A. and Diffley, J.F., 2015. Regulated eukaryotic DNA replication origin firing with purified proteins. *Nature*, 519(7544), pp.431-435.
- Yeeles, J.T., Janska, A., Early, A. and Diffley, J.F., 2016. How the Eukaryotic Replisome Achieves Rapid and Efficient DNA Replication. *Molecular Cell*. 65(1), pp105-116.
- Yekezare, M., Gómez-González, B. and Diffley, J.F., 2013. Controlling DNA replication origins in response to DNA damage—inhibit globally, activate locally. *Journal of Cell Science*, 126(6), pp.1297-1306.
- Yoo HY, Kumagai A, Shevchenko A, Shevchenko A, Dunphy WG. Ataxia-telangiectasia mutated (ATM)-dependent activation of ATR occurs through phosphorylation of TopBP1 by ATM. *J Biol Chem*. 2007 Jun 15;282(24):17501-6.
- Yoo HY, Kumagai A, Shevchenko A, Shevchenko A, Dunphy WG. The Mre11-Rad50-Nbs1 complex mediates activation of TopBP1 by ATM. *Mol Biol Cell*. 2009 May;20(9):2351-60.
- You Z, Komamura Y, Ishimi Y. Biochemical analysis of the intrinsic Mcm4-Mcm6-mcm7 DNA helicase activity. *Mol Cell Biol*. 1999 Dec;19(12):8003-15.
- Yu X, Chini CC, He M, Mer G, Chen J. The BRCT domain is a phospho-protein binding domain. *Science*. 2003 Oct 24;302(5645):639-42.
- Yue M, Singh A, Wang Z, Xu YJ. The phosphorylation network for efficient activation of the DNA replication checkpoint in fission yeast. *J Biol Chem*. 2011 Jul 1;286(26):22864-74.
- Zegerman P, Diffley JF. Lessons in how to hold a fork. *Nat Struct Biol*. 2003 Oct;10(10):778-9.

- Zegerman P, Diffley JF. Phosphorylation of Sld2 and Sld3 by cyclin-dependent kinases promotes DNA replication in budding yeast. *Nature*. 2007 Jan 18;445(7125):281-5.
- Zegerman P, Diffley JF. DNA replication as a target of the DNA damage checkpoint. *DNA Repair (Amst)*. 2009 Sep 2;8(9):1077-88. doi: 10.1016/j.dnarep.2009.04.023.
- Zegerman P, Diffley JF. Checkpoint-dependent inhibition of DNA replication initiation by Sld3 and Dbf4 phosphorylation. *Nature*. 2010 Sep 23;467(7314):474-8.
- Zeng Y, Piwnica-Worms H. DNA damage and replication checkpoints in fission yeast require nuclear exclusion of the Cdc25 phosphatase via 14-3-3 binding. *Mol Cell Biol*. 1999 Nov;19(11):7410-9.
- Zhang YW, Hunter T, Abraham RT. Turning the replication checkpoint on and off. *Cell Cycle*. 2006 Jan;5(2):125-8.
- Zhao H, Russell P. DNA binding domain in the replication checkpoint protein Mrc1 of *Schizosaccharomyces pombe*. *J Biol Chem*. 2004 Dec 17;279(51):53023-7.
- Zhivotovsky B, Orrenius S. Cell cycle and cell death in disease: past, present and future. *J Intern Med*. 2010 Nov;268(5):395-409.
- Zou L, Elledge SJ. Sensing DNA damage through ATRIP recognition of RPA-ssDNA complexes. *Science*. 2003 Jun 6;300(5625):1542-8.
- Zou L, Stillman B. Assembly of a complex containing Cdc45p, replication protein A, and Mcm2p at replication origins controlled by S-phase cyclin-dependent kinases and Cdc7p-Dbf4p kinase. *Mol Cell Biol*. 2000 May;20(9):3086-96.